



UNIVERSITAT
POLITÈCNICA
DE VALÈNCIA

Departamento de Máquinas y Motores Térmicos

DOCTORAL THESIS:

**“Engineering Large Eddy
Simulation of diesel sprays”**

Presented by: D. JUAN MANUEL MOMPÓ LABORDA
Supervised by: DR. D. SERGIO HOYAS CALVO

in fulfillment of the requisites for the degree of

Doctor of Philosophy

March 26, 2014

PhD. Thesis

“Engineering Large Eddy Simulation of diesel sprays”

AUTHORS

Presented by: D. JUAN MANUEL MOMPÓ LABORDA
Supervised by: DR. D. SERGIO HOYAS CALVO

DEFENSE COMMITTEE

Chairman: DR. D.
Secretary: DR. D.
Members: DR. D.
DR. D.
DR. D.

Valencia, March 26, 2014

Abstract

The main objective of this PhD thesis is the study of Diesel sprays under evaporative conditions by means of Large Eddy Simulations (LES) techniques. This study has been performed implementing a precise, low-demanding LES model in the free, full-purpose Computational Fluid Dynamics (CFD) code OpenFOAM.

The starting point was a careful and exhaustive review of the physical processes involved in sprays. An emphasis in CFD methodology, particularly for LES methods, was essential for the thesis, as we were able to find the possible problems and limitations of our approximation. Moreover, as the most widely used techniques for the industrial simulation of sprays are based on the Reynolds-Averaged Navier-Stokes models, we have highlighted the many advantages of LES modeling. As the latter are, by definition, more computationally expensive than RANS, we made an optimal configuration that, while it is able to recover accurately the experimental results, its characteristic time is in the same order of magnitude that RANS ones. As applicability is a must in this thesis, we use the surname “Engineering” LES.

One of the key points of the thesis has been the correct configuration of the flow turbulent conditions on the inlet. In order to get accurate results, the turbulent structures coming from this inlet need to be time- and space-coherent. An adequate calibration of this conditions is needed to perform any spray simulation.

Last but not least, all the simulations performed were validated against experiments, obtaining a very good agreement even close to the nozzle.

Resumen

El objetivo principal de esta tesis es el estudio del modelado numérico de chorros diesel evaporativos mediante la técnica de la simulación de grandes remolinos (LES por sus siglas en inglés). Este estudio se ha realizado mediante la implementación de un modelo LES de altas prestaciones y poco consumo informático en el código libre de dinámica de fluidos computacional (CFD) OpenFOAM.

El trabajo de esta tesis ha partido de una revisión exhaustiva de los procesos físicos que tienen lugar en el chorro desde la perspectiva del modelado CFD en general y LES en particular. Esta revisión nos ha permitido identificar los problemas y limitaciones de nuestro planteamiento. Además, dado que la principal técnica CFD usada para el modelado de chorro diesel en procesos industriales son los modelos basados en las ecuaciones promediadas de Reynolds (RANS), se ha incidido en la tesis sobre las ventajas del modelado LES. Dado que estas técnicas son inherentemente más caras que los métodos RANS, se ha hecho hincapié en conseguir una configuración óptima que, siendo lo más fiel posible a los resultados experimentales, esté cercana a los tiempos propios de las técnicas RANS. Entendiendo que se quiere hacer énfasis en la aplicabilidad del modelo, se habla de “Engineering” LES.

Uno de los puntos claves de la tesis es la adecuada configuración de las condiciones de contorno turbulentas a la entrada de la tobera, que necesitan ser coherentes tanto en espacio como en tiempo. La calibración adecuada de estas condiciones es clave para una correcta simulación del chorro.

Por último, todas las simulaciones realizadas han sido validadas contra resultados experimentales, obteniendo un muy aceptable comportamiento de nuestro modelo incluso cerca de la tobera.

Resum

L'objectiu principal d'aquesta tesi és l'estudi del modelatge numèric de esprais dièsel evaporatius mitjançant la tècnica de simulació de grans remolins (LES per les sigles en anglès). Aquest estudi s'ha realitzat mitjançant la implementació d'un model LES d'altres prestacions i reduït consum informàtic en el codi lliure de dinàmica de fluids computacional (CFD) OpenFOAM.

El treball d'aquesta tesi ha partit d'una revisió exhaustiva dels processos físics que tenen lloc en l'esprai des de la perspectiva del modelatge CFD en general i LES en particular. Aquesta revisió ens ha permès identificar els problemes i limitacions del nostre plantejament. A més, com que la principal tècnica CFD per a la modelització de esprais dièsel en processos industrials són els models basats en les equacions mitjanades de Reynolds (RANS), s'ha incidit sobre els avantatges del modelatge LES. Com aquestes tècniques són inherentment més cares que els mètodes RANS, s'ha posat l'accent en aconseguir una configuració òptima que, sent el més fidel possible als resultats experimentals, està propera als temps propis de les tècniques RANS. Per emfatitzar l'aplicabilitat del model, es parla de "Engineering" LES.

Un dels punts claus de la tesi és l'adequada configuració de les condicions de contorn turbulentes a l'entrada de la tovera. Per tal d'obtenir resultats precisos, les estructures turbulentes procedents d'aquesta entrada han de ser coherents en temps i espai. El calibratge adequat d'aquestes condicions és clau per a una correcta simulació de l'esprai. Finalment, totes les simulacions realitzades han estat validades contra resultats experimentals, obtenint un comportament molt acceptable del nostre model fins i tot prop de la tovera.

Acknowledgments

I would like to thank everyone who has helped me in one way or another to be successful in this project.

Valencia, March 2014.

“Ehara koe i a ia!”

Contents

1	Introduction	1
1.1	Introduction	2
1.1.1	CFD codes	7
1.2	Objectives	9
1.3	Methodology	11
1.4	Outline of the thesis	16
	Chapter 1 bibliography	17
2	Spray Fundamentals and CFD spray modeling	19
2.1	Introduction	20
2.2	Spray characterization	22
2.3	Turbulent approaches to simulate diesel sprays	31
2.3.1	Direct Numerical Simulation	31
2.3.2	Reynolds-averaged Navier-stokes	32
2.3.3	Large-Eddy Simulation	35
2.4	Interface and particle tracking	45
2.5	Phenomenological spray models	49
2.5.1	Spray injection	50
2.5.2	Atomization and Break-up	52
2.5.3	Collision and coalescence	58
2.5.4	Momentum transfer	60
2.5.5	Evaporation	63
2.5.6	Turbulent dispersion	67
	Chapter 2 bibliography	70
3	Numerical set-up	91
3.1	Introduction	92
3.2	Diesel-like gas jet	92
3.2.1	Injection rate	92

3.2.2	Mesh domain	93
3.2.3	Turbulent modelling	99
3.3	Non-evaporative case	100
3.3.1	Injection	100
3.3.2	Atomization	101
3.3.3	Collision	102
3.3.4	Momentum transfer	102
3.3.5	Turbulent dispersion	105
3.4	Evaporative case (<i>Spray-A</i>)	107
3.4.1	Injection rate	107
	Chapter 3 bibliography	109
4	Results and Discussion	113
4.1	Introduction	114
4.2	LES of diesel-like gas jets	114
4.2.1	Mesh size and temporal schemes independency	114
4.2.2	Boundary conditions sensitivity	134
4.3	Non-evaporating diesel sprays	161
4.3.1	Mesh size and temporal schemes independency	161
4.3.2	Injection profile sensitivity	164
4.3.3	Particle-gas phase interaction	167
4.3.4	Comparison with E-E equivalent gas jet.	168
4.4	Evaporating diesel sprays	173
	Chapter 4 bibliography	178
5	Conclusions and future works	179
5.1	Conclusions	180
5.2	Future works	182
	Chapter 5 Bibliography	183
	Global bibliography	185

List of Figures

1.1	Precedent of actual ICEs	4
2.1	Spray dynamics within ICEs. Adapted from [Lip+05]	20
2.2	Gas jet phenomenological models [Pas+08; Hir+83]	21
2.3	Visualization of a spray taken at 825 μs after the start of the injection ($P_{inj} = 80 MPa$, $d_0 = 0.14 \mu m$, and $\rho_{cha} = 20 kg/m^3$) [Des+07]	23
2.4	Macroscopic parameters of spray.	25
2.5	Average velocity profiles. Adapted from [Cha13]	29
2.6	Main achievements in the DNS of jets and sprays.	32
2.7	DNS simulation of diesel spray. Computational domain is (0.3 x 0.3 x 2.2)mm, grid size is 128 x 128 x 896, $d_0 = 100 \mu m$, $U = 100$ m/s, $\rho_{inj} = 696 kg/m^3$, $\rho_{cha} = 50 kg/m^3$, computing time 10,000 h on 14 processors (Lebas et al., 2009 [Leb+09])	33
2.8	Scheme showing treatment of droplets (Adapted from Vujanovic et al. 2009 [Vuj+09])	48
2.9	Diesel flow characteristics under different cavitation stages (Adapted from Park et al. 2008 [Par+08])	51
2.10	Discrete number probability function, its corresponding continuous number PDF, $f_0(D)$, and its corresponding continuous volume PDF, $f_3(D)$ [Asg11])	52
2.11	Atomization mechanisms at the nozzle exit [Bau06]	53
2.12	Atomization regimes. B ($Re_l = 790$, $We_g = 0.06$); C ($Re_l = 5500$, $We_g = 2.7$); D ($Re_l = 16500$, $We_g = 24$); E ($Re_l = 28000$, $We_g = 70$) [Dum08])	55
2.13	Break-up modes [Wie90]	56
2.14	Schematic illustration of the KH and RT models	57
2.15	Combined blob-KH/RT model [Bau06]	58
2.16	Coalescence regimes.	59
2.17	Collision requirements	60

2.18	Possible drop trajectories in a turbulent flow field [Cro+88] . . .	69
3.1	Injection rate measurements. Nozzle 634 ($p_{inj} - p_a \approx (800 - 35)bar$) [Gim08].	93
3.2	Meshing procedure for gas jet calculations. From top to bottom. Right column: Original mesh cells=(1 × 1 × 1)mm, first refinement step (Z direction.), second refinement step (XY direcc.) Left column: Detail of refinements.	94
3.3	Mesh shape effect on E-E DS spray evolution ($\Delta z = 0.25mm$).	96
3.4	Structured 3D growth rate meshing procedure. Left image: detail of inlet BC	97
3.5	Axial cut plane colored by cell volume ($\Delta z \approx 0.0625mm$ at inlet).	98
3.6	Injection blob-method (adapted from [Bau06])	101
3.7	Momentum terms contribution [$kg/(m^2s^2)$] (RANS k- ε , $\Delta z \approx 0.5mm$, $t = 0.0015s$ ASOI, red dots are parcels).	103
3.8	Momentum contribution along the spray axis (RANS k- ε , $\Delta z \approx 0.5mm$, $t = 0.0015s$ ASOI	104
3.9	Momentum contribution along the spray axis (LES, $\Delta z \approx 0.5mm$, $t = 0.0015s$ ASOI).	104
3.10	Turbulent dispersion magnitude compared to relative velocity (DS, $\Delta z \approx 0.5mm$, $C_k = 0.3$ and $C_\varepsilon = 0.05$, $t = 0.003s$ ASOI).	106
3.11	Spray-A injection rate.	108
4.1	Turbulent model penetration comparison (vanDriest filter, improved mesh. \perp Experimental results, $-\cdot-$ Sm, $---$ SA, $+$ OEE, \times DS, $---$ k - ε (RANS)	115
4.2	Iso-surface of $Y_{fuel} = 0.01$ colored by velocity magnitude (t = 3ms ASOI)	116
4.3	Mesh size independence study. \perp Experimental results, $-\cdot-$ $\Delta z = 1mm$, $---$ $\Delta z = 0.5mm$, $---$ $\Delta z = 0.25mm$, $-\circ-$ $\Delta z = 0.125mm$	116
4.4	Gas jet axis velocity decay ($\bar{U}_0 = 373.27m/s$, $t = 3ms$ ASOI, first ddt). $---$ Theoretical decay, $---$ k - ε (RANS), $---$ OEE, $\cdot\cdot\cdot$ DS, $-\cdot-$ k - ε (RANS $\Delta z = 0.0625mm$)	117
4.5	Time step and temporal scheme effect on penetration ($\Delta z = 0.25mm$, reference mesh). \perp Experimental results, $---$ k - ε (RANS), $---$ $1^{st} ddt$ CFL = 0.5, $-\circ-$ $1^{st} ddt$ CFL = 0.125, $+$ $2^{nd} ddt$ CFL = 0.125	119

4.6	Contour plots of velocity magnitude (Reference mesh, $\Delta z = 0.25\text{mm}$; $t=0.003\text{s}$ ASOI). Left column: One equation eddy. Right column: Dynamic structure.	120
4.7	Gas jet first instants. Isosurface $Y_{fuel} = 0.01$ colored by velocity (DS, $\Delta z = 0.25\text{ mm}$, reference mesh)	121
4.8	Mesh shape and filter effect on gas jet ($\Delta z = 0.25\text{mm}$, filter maxDelta). —Round inlet, -·- Improved mesh, --- Reference mesh	122
4.9	Temporal evolution of velocity decay (DS, $\Delta z = 0.25\text{mm}$, filter maxDelta) ---Theoretical decay.	123
4.10	Average velocity decay ($\Delta z = 0.25\text{mm}$). I Round inlet, I Reference mesh.	123
4.11	Mesh shape effect on E-E gas jet (DS, $\Delta z = 0.25\text{mm}$).	124
4.12	Mesh shape and filter effect on gas jet spreading angle ($\Delta z = 0.25\text{mm}$, $t=0.003\text{s}$ ASOI). Left column: vanDriest filter. Right column: maxDelta filter.	126
4.13	Mesh topology effect on averaged gas jet (DS, $\Delta z = 0.25\text{mm}$).	127
4.14	Mesh topology and filter effect on OEE gas jet ($\Delta z = 0.25\text{mm}$, $t=0.003\text{s}$ ASOI).	129
4.15	Mesh shape effect on E-E OEE spray evolution (DS, $\Delta z = 0.25\text{mm}$, $t=0.003\text{s}$ ASOI). From left to right: reference mesh, improved mesh and round inlet.	130
4.16	Mesh topology effect on averaged OEE gas jet ($\Delta z = 0.25\text{mm}$, maxDelta).	131
4.17	Axis velocity probes ($\Delta z = 0.25\text{mm}$, roundInlet, maxDelta filter) Ordinate range in zoom region is the same as the originating graph.	132
4.18	Penetration ($\Delta z = 0.0625\text{mm}$). I Experimental data, — Improved mesh, --- Grading mesh.	133
4.19	Gas jet axis velocity decay ($\bar{U}_0 = 373.27\text{m/s}$, $\Delta z = 0.0625\text{mm}$, $t = 3\text{ms}$ ASOI). — Theoretical decay, — $k - \varepsilon$ (RANS), ··· Improved mesh, ---Grading mesh.	134
4.20	Gas jet shape as a function of inlet BC type (OEE, $t=3\text{ms}$ ASOI)	135
4.21	Evolution of the inlet BC	136
4.22	Penetration. Effect of consistent turbulence. (vanDriest, roundInlet mesh). — <i>turbulentInlet</i> , -·- mapped (5mm probe), --- OEE $c_\varepsilon = 0.916$, $c_k = 0.067$ (mapped from 5mm probe),	137

4.23	Velocity decay. Effect of consistent turbulence. (vanDriest, roundInlet mesh). — <i>turbulentInlet</i> , \cdots mapped (5mm probe), - - - OEE $c_\varepsilon = 0.916$, $c_k = 0.067$ (mapped from 5mm probe).	138
4.24	Average velocity decay. Effect of consistent turbulence. (DS, vanDriest, roundInlet mesh). \perp <i>turbulentInlet</i> , \perp mapped (5mm probe), — <i>turbulentInlet</i> (3ms ASOI), - - - mapped (3ms ASOI).	138
4.25	Effect of probe location (vanDriest, roundInlet mesh). Left column: OEE, right column: DS. — <i>turbulentInlet</i> , - - - mapped (4mm probe), - \cdot - mapped (5mm probe).	140
4.26	Average velocity decay. Effect of inlet turbulent content. (DS, vanDriest, roundInlet mesh). \perp <i>turbulentInlet</i> , \perp mapped, — <i>turbulentInlet</i> (3ms ASOI), - \cdot - mapped (3ms ASOI)	141
4.27	Average velocity decay. Effect of consistent turbulence on LES model. (vanDriest, roundInlet mesh, mapped from 4mm probe). \perp DS, \perp OEE, —DS (3ms ASOI), - \cdot - OEE (3ms ASOI)	142
4.28	Velocity decay. Extended averaging time and instant values. (OEE, vanDriest, roundInlet mesh). \perp 6ms averaged, \perp 3ms averaged, - - - 3ms ASOI, + \cdot + 5ms ASOI, \cdots 6ms ASOI, - \cdot - 7ms ASOI, - \times - 9ms ASOI.	142
4.29	Axis probes. (3ms average window, vanDriest, roundInlet mesh). Left column: OEE. Right column DS.	144
4.30	Inlet turbulent content effect on gas jet velocity field ($\Delta z = 0.25mm$, $t=0.003s$ ASOI). Left column: OEE. Right column: DS.	145
4.31	Inlet turbulent content effect on averaged DS gas jet. $Y_{fuel} = 0.01$, colored by U ($\Delta z = 0.25mm$, $t=3ms$ ASOI).	146
4.32	Temporal scheme effect on DS gas jet. $Y_{fuel} = 0.01$, colored by U (backward scheme, $\Delta z = 0.25mm$, $t=3ms$ ASOI).	147
4.33	Inlet turbulent content effect on averaged OEE gas jet. $Y_{fuel} = 0.01$, colored by U ($\Delta z = 0.25mm$, $t=3ms$ ASOI).	148
4.34	Initial deviation from experimental results (vanDriest, roundInlet mesh).	149
4.35	Effect of experimental injection rate (vanDriest, roundInlet mesh). Left column: OEE, right column: DS. \perp Experimental data, — <i>turbulentInlet</i> , - \cdot - mapped (4mm probe), - - - turbulent experimental rate.	150
4.36	Inlet turbulent content effect on gas jet velocity field ($\Delta z = 0.25mm$, $t=0.003s$ ASOI). Left column: OEE. Right column: DS.	151

4.37	Effect of experimental injection rate (vanDriest, grading mesh). Left column: OEE, right column: DS. \perp Experimental data, — theoretical decay, —grading mesh (<i>turbulentInlet</i>), - · - grading mesh (turbulent experimental rate), --- roundInlet mesh ($\Delta z = 0.25mm$, turbulent experimental rate).	152
4.38	Average velocity decay (vanDriest). \perp 4mm mapped (roundInlet, $\Delta z = 0.25mm$), \perp turbulent experimental rate (gradMesh, $\Delta z = 0.0625mm$),	153
4.39	Average velocity decay (vanDriest, grading mesh). \perp OEE, \perp DS.	154
4.40	Turbulent experimental rate impact on gas jet velocity contours ($t=0.003s$ ASOI). Left column: OEE. Right column: DS. . . .	155
4.41	Turbulent model effect on averaged gas jet. $Y_{fuel} = 0.01$, colored by U (grading mesh, turbulent experimental rate, $\Delta z = 0.0625mm$, $t=3ms$ ASOI).	156
4.42	Radial profiles of axial velocity (DS, grading mesh, turbulent experimental rate, $\Delta z = 0.0625mm$). Left column: 0° radius. Right column: 45° radius. \perp 50mm, \perp 40mm, \perp 35mm, \perp 30mm, \perp 25mm, symbols: experimental measurements coincide with locations color code.	157
4.43	Radial profiles of axial velocity (OEE, grading mesh, turbu- lent experimental rate, $\Delta z = 0.0625mm$). \perp 50mm, \perp 40mm, \perp 35mm, \perp 30mm, \perp 25mm, symbols: experimental measure- ments coincide with locations color code.	157
4.44	Energy content of inlet BC turbulent scales (roundInlet mesh, time window 3-6ms ASOI). Left column: OEE. Right column: DS. — $-5/3$ slope.	158
4.45	Energy content of turbulent scales (time window 3-6ms ASOI). First column: OEE roundInlet. Second column: OEE grad- ing mesh. Third column: DS roundInlet. Fourth column: DS grading mesh. — $-5/3$ slope.	160
4.46	Energy content of turbulent scales (time window 3-6ms ASOI). First column: OEE roundInlet. Second column: OEE grad- ing mesh. Third column: DS roundInlet. Fourth column: DS grading mesh. — $-5/3$ slope.	161
4.47	Turbulent model dependency on mesh refinement. \perp Experi- mental data, — $k - \varepsilon$ (RANS), - · - 0.5 mm mesh, --- 0.025 mm mesh.	162

4.48	Effect of temporal scheme and δt on DS spray behavior (experimental injection profile) \perp Experimental data, — $k - \varepsilon$ (RANS), — first order ddt, - · - second order ddt, --- 0.125 CFL.	163
4.49	Improved turbulent coefficients for t=3ms ASOI ($\Delta z = 0.25mm$) \perp Experimental data, — $k - \varepsilon$ (RANS), - · - OEE ($c_k = 0.6$, $c_\varepsilon = 0.05$), --- DS ($c_k = 0.05$, $c_\varepsilon = 0.3$).	164
4.50	Parcels shadow (t=3ms ASOI)	165
4.51	Penetration ($\Delta z = 0.25mm$). \perp Experimental data, — $k - \varepsilon$ (RANS), - · - Experimental injection profile, --- Average injection profile.	166
4.52	Axis velocity decay. ($U_0=373.27m/s$, t=3ms ASOI, first ddt). Top: parcel scaled with droplet diameter. Bottom: fixed size.	167
4.53	Turbulent dispersion sensitivity. (t=3ms ASOI). Upper row: No dispersion velocity. Lower row: Dispersion velocity.	168
4.54	Axis velocity decay. ($U_0=373.27m/s$, t=3ms ASOI, first ddt). Left column: $\Delta x = 0.5mm$. Right column: $\Delta x = 0.25mm$	169
4.55	Contour plot of $U_y(\pm 5m/s)$ ($\Delta z = 0.25mm$; t=3ms ASOI)	171
4.56	Comparison with shadowgraph pictures (t = 0.9 ms ASOI, $\Delta z = 0.25mm$)	172
4.57	Penetration and LL for LES of sprayA for t=3ms ASOI ($\Delta z = 0.25mm$), \perp Vapor penetration, — LL, - · - OEE ($c_k = 0.4$, $c_\varepsilon = 0.05$), --- DS.	173
4.58	Axis velocity decay of evaporative cases ($\Delta x = 0.25mm$). Left column: OEE. Right column: DS. — Theoretical decay, \perp liquid phase (parcels), - · - gas phase.	174
4.59	Turbulent development of evaporative cases ($\Delta x = 0.25mm$, gas jet limit: $Y_{fuel} = 0.01$, t=1.4ms ASOI). Left column: OEE. Right column: DS.	176
4.60	Spray temporal evolution. (t=1-9ms). Left column: OEE. Right column: DS.	177

List of Symbols

ρ	Gas phase density	22
(x, y, z)	Cartesian coordinates	21
(x, r, θ)	Cylindrical coordinates	21
p	Pressure	22
Γ_{ij}	Viscous stress tensor	22
τ_{ij}	Reynolds stresses	22
h_s	Sensible entalpy	22
Y_k	Species mass fraction	22
u_i	Velocity components	22
D_k	Species diffusivity coefficient	22
α	Thermal diffusivity	22
d_0	Nozzle diameter	24
ρ_a	Ambient gas density	24
θ	Spray angle	24
P_{inj}	Injection pressure	25
U_0	Centerline velocity	26
$r_{1/2}$	Jet's half width	26
d_{eq}	Equivalent diameter	27
\dot{m}_0	Fuel mass flow rate	27
Sc	Schmidt number	28
d_{ab}	Droplet diameter	30
$N_{d,p}$	Statistical number of droplets inside the parcel	31
μ_t	Turbulent viscosity	33
\tilde{S}_{ij}	rate-of-strain tensor	33
k	Turbulent kinetic energy	33
ε	Turbulent dissipation	33
C_s	Smagorinsky constant	36

Δ	Filter length	36
C_{ij}	DS tensor coefficient	41
L_{ij}	Modified Leonard tensor	41
\mathbf{U}_{rel}	Relative velocity between the liquid droplet and gas	42
S_k	Source term for sub-grid turbulent kinetic energy	42
C_d	Discharge coefficient	50
L_{bu}	Liquid core length	54
F_d	Drag force	60
Re_p	Reynolds numbers of the droplets	61
C_D	Drag coefficient	61
$S_{M,i}$	Momentum source term	62
\wp	Characteristic time ratio	62
D_k	Mass diffusivity	65
Sh	Sherwood number	65
St	Stokes number	68

List of Acronyms

<i>CFD</i>	COmputational Fluid Dynamics	2
<i>RANS</i>	Reynolds-Averaged Navier-Stokes	2
<i>LES</i>	Large Eddy Simulation	2
<i>ICE</i>	Internal Combustion Engine	3
<i>NO_x</i>	Nitrogen Oxides	4
<i>ECN</i>	Engine Combustion Network	13
<i>BC</i>	Boundary Conditions	13
<i>LL</i>	Liquid Length	23
<i>SMD</i>	Sauter Mean Diameter	30
<i>DNS</i>	Direct Numerical Simulation	31
<i>PDF</i>	Probability density function	33
<i>OEE</i>	One equation eddy	40
<i>DS</i>	Dynamic structure	41
<i>L – E</i>	Lagrangian-Eulerian framework	45
<i>E – E</i>	Eulerian-Eulerian framework	45
<i>DDM</i>	Discrete Droplet Method	45
<i>VoF</i>	Volume of Fluid	48
<i>LS</i>	Level set methods	48
<i>KH</i>	Kelvin-Helmholtz model	55
<i>RT</i>	Rayleigh-Taylor model	56
<i>TKE</i>	Turbulent Kinetic Energy	56
<i>L</i>	Characteristic Length	67
<i>ASOI</i>	After Start Of Injection	103

Chapter 1

Introduction

Contents

1.1	Introduction	2
1.2	Objectives	9
1.3	Methodology	11
1.4	Outline of the thesis	16
	Chapter 1 bibliography	17

1.1 Introduction



BEAUTY is the glow of the true and the good that radiates from every ordered state of being (Joseph Pieper). This thought which I found within some reflections to the letter to all artists by H.H. Pope John Paul II should be the basis of any honest research (specially those using computational fluid dynamics (CFD) simulations). There is a common feeling of excitement in the very moment we understand something. At the instant when one apprehends reality, that glow of grasped truth (which has always been there for us) produces a powerful joy students and researchers (lucky longterm students) experience every now and then.

Far from being a vague introduction to a thesis titled *Engineering LES of diesel sprays*, the beauty definition sets its framework. Why do we do CFD? Because it is beautiful and consequently useful. Because when properly performed, CFD is able to show (in detail) realistic evolution of complex systems involving transport of mass and energy within a fluid. And why do we do LES¹ (i.e. instead of RANS²)? Because it is even more beautiful. We are able to see more of that truth about the studied phenomena (which entails a higher degree of use)³.

The underlying hypothesis here is that complete understanding of the studied phenomena has not been achieved and cumulative previous knowledge helps us discover more about it. However, that is not enough to inspire and promote neither research nor even study. In fact, there is also some commitment involved: *“The objectivity required by science rightly rejects all ideological neutrality, all ambiguity, all conformism, all cowardliness: love for the truth involves the life and entire work of the scientist”* (St. Josemaria, address at honorary doctoral degree conferral ceremony by the University of Navarra, 9 May 1974.)

One of the aspects of the commitment to truth is the contribution to the common good. The truth that we come to know from studied systems, brings goods that can be *managed* and put into the service of mankind. And has

¹Large Eddy Simulation

²Reynolds-Averaged Navier-Stokes

³RANS and LES are two different ways of turbulent modeling. For the sake of argument let just say LES has a higher potential of physical description. A detailed explanation is provided at section 2.3

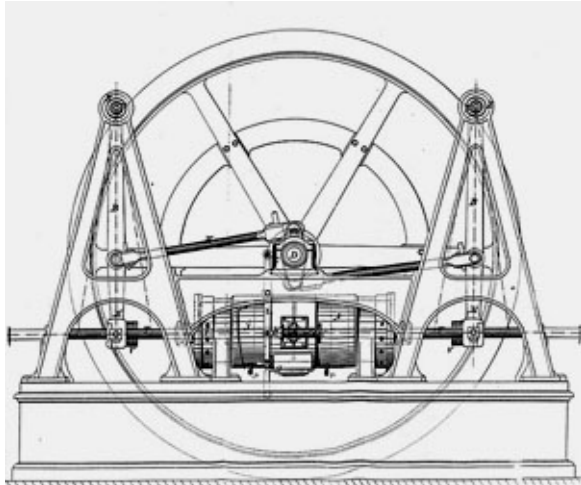
anything ever had a greater impact than engines on people's daily life? The reasons and history are beyond (and the cause of) well-worn statistics⁴. From the historical point of view -apart from its ancestor, the steam engine- we will just cite a few milestones in the early timeline of internal combustion engines (ICE from now on). A complete synopsis can be consulted in the first chapter of [PD11] (also, further information can be found at the references included here [Ame08; Cum89; Cum93; NS80; SAE97; Suz97]). One has to look back to 1854-57 to find an ICE-like machine that worked based on the combustion of a mixture of air and an inflammable gas. Eugenio Barsanti and Felice Matteucci had invented a device⁵ able to use the energy contained in nature to extend human will beyond its bodily power. Hence, a sufficient knowledge of the true and good from matter, available materials and constructive structures was brought into play in a unique form. In 1861 Alphonse Beau de Rochas patented the 4-cycle engine to hand on the invention. Coincidentally⁶, Nikolaus August Otto was the first one to build and sell an engine in less than a year, putting it in this way into the service of common good. However, more than 30 years had to pass (1893) before the pioneer on -back then- alternative fuels and combustion modes: Rudolf Diesel, driven by the ideal of high efficiency engines, based his own 4-cycle engine on the Carnot cycle (published in 1824).

Once today's most widespread cycles were set, more than three generations of passionate engineers trying to optimize this use of matter's energetic contents on daily basis, led us to the present transport situation and progress. In more than a hundred years of ICE history and technological evolution some improvements have been shared by both types of engines and some are specific for each cycle. Regarding the first ones, some noteworthy advances are: forced induction, position and number of valves, electronic control and advances in lubrication, materials and manufacturing technologies. These last three confer one of the highest levels of mechanical reliability on current engines. Ignition and mixture formation are key advances to Otto engines as injection systems to diesel engines. Although injection is being used for both types of engines, it had a specific evolution for each of them. The same can be applied to emis-

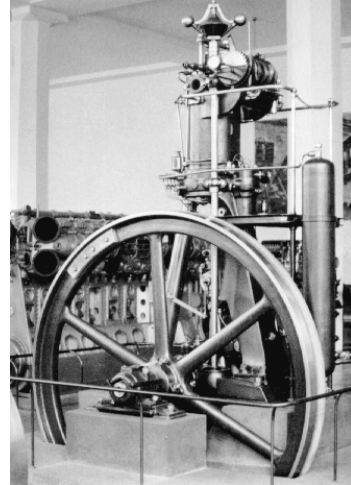
⁴Transport currently accounts for half of global oil consumption and nearly 20% of world energy use, of which approximately 40% is used in urban transport alone. The IEA expects urban transport energy consumption to double by 2050, despite ongoing vehicle technology and fuel-economy improvements.(2013 IEA report)

⁵The request bears the no.700 of Volume VII of the Patent Office of the Reign of Piedmont. There is no text of the patent request, but a photo of the table which contains a drawing of the engine. Fondazione Barsanti&Matteucci (<http://www.barsantiatteucci.it>)

⁶They did not know each others work



(a) Sketch from the 1861 Barsanti & Matteucci patent



(b) First operational engine designed by Diesel (1897)

Figure 1.1: Precedent of actual ICEs

sion control technologies which have played an important role in the last three decades of ICE evolution.

Consequently, any effort to better understand the processes involved in ICEs may have a great impact on the environment due to their widespread use. Also it will help move forward to the future combustion concepts diversifying the technologies for a more sustainable transport.

Although optimization processes are part of the personal commitment with a responsible management of natural resources; pollutant restrictions imposed by legislation and the necessity to keep production costs bounded, encourage researchers with specific goals (ambitious) to optimize the efficiency of ICEs. Fuel sprays play a major role in achieving the required combustion characteristics and pollutant emissions' reduction on ICE, and therefore, an accurate prediction of spray's behavior is required to perform reliable engine combustion and pollutant simulations. In particular, diesel engines entail two problems: soot and NOx⁷. It is a well-known fact that there exists a direct relation between emissions and instantaneous values of both temperature

⁷NOx is a generic term for mono-nitrogen oxides NO and NO₂

and fuel concentration fields inside the engine [KB88]. Although the improvement of spray development and combustion has thoroughly been investigated (mainly by experimental means)⁸ it is still a challenging task nowadays due to the complex interrelated phenomena taking place, some of them still not fully understood. Moreover, several new systems have recently appeared in the field of ICE (i.e. direct injection spark ignited combustion, Homogeneous Combustion Compression Ignition systems (HCCI), urea injection systems associated with DeNO_x catalyst, Reactivity Controlled Compression Ignition (RCCI)). This great variety makes it even more challenging to accurately understand and predict the behavior of multiphase sprays, which -as already stated- is vital to successfully fulfill current restrictions imposed by legislation.

Nowadays, engine research has two complementary areas: experiments and simulation. Experimental research advanced along with the evolution of technology: continuous reduction of size and increasing range of temperature and pressure sensors, fuel rate indicator (1966), rapid compression machines (1974), pulsed shadowgraphy and double-pulsed holography along with fast high-resolution cameras, the use of laser diagnostics (droplet anemometry 1988 or Laser Doppler velocimetry (LDV) (1991) induced fluorescence (2002), phase-Doppler anemometry (PDA) (1998) transparent engines or x-ray absorption (2001) are some of the scientific advances that increased the precision and depth of the information acquired from ICEs.

Although the experimental research has prevailed over simulations, no matter how accurate the technique or small the sensors may be, the complexity of ICE makes the non-intrusive measurements in real conditions difficult. Hence, the alternative is clear: solve the equation system of the physics involved in that problem. Contrary to experiments, simulations of the fluid dynamics have access to any field at any time without affecting the flow itself⁹ and make it almost trivial to perform changes in the design and operation points. Mathematical equations governing the physics involved have been known for more than 140 years. However, it is also accepted that they are impossible to solve in case of any technological problem¹⁰. Researchers have adapted them to

⁸CMT-Motores Térmicos itself has since 2000 more than 50 publications in journals (39 on experimental research and 13 in simulations) and 24 PhD thesis

⁹Note we refer to both types of models to study ICE following Heywood's classification [Hey88]. Thermodynamic and fluid dynamic simulations will be explained afterwards [chapter 2].

¹⁰Moreover, the existence and uniqueness of the solution of Navier Stokes equations in a general 3D domain is still an open problem. It is one of the six problems of the Millenia for

the level of physical description required and -since the sixties of the previous century- to the computational power available over time. The consideration of restrictive hypothesis may even provide analytical solutions to simplified problems [Des+07], but to look for them in such a complex problem as the injection of fluid in a cylinder is considered an expensive waste of time nowadays. In order to get the level of physical description needed to move forward in the optimization of performance and fuel consumption, a compromise must be reached between the impossibility of solving the general Navier-Stokes equations and the excessively simplified models that provide an analytical solution. From the physics' point of view, probably one of the most difficult problems is turbulence. Therefore, in order to obtain results with the desired accuracy, we need to model turbulence. This is usually done in two ways: RANS (models every turbulent scale) and LES (models smaller turbulent scales). In this way, the proper use of simulations¹¹ has helped researchers in understanding the flow behavior and also in allowing predictions of the results of different configurations without the cost of testing them experimentally. For reasons such as the aforementioned, simulations have become an essential tool in helping both the analysis and design of many parts¹² of an ICE.

With time (and money), knowledge about nature increased and diversified into fields requiring more time and as a consequence people dedicated to, moving from the concept of wise men to experts and researchers of both pure and applied science as well as product developers. Historically engineers, have been filling the gap between the former ones putting the “new” knowledge into the service of mankind. Following that great tradition of continuous service in little things, this thesis aims to bring LES closer to (automotive) industry.

Finally, LES is not a matter of cultural/scientific fashion or current fads, nor a fulfillment of Parkinson's law to the increase of computational power. Beforehand examples of advanced combustion modes and emission control system require not only the accurate prediction of the temporal evolution of an ensemble average of the field but also the instant values and their standard deviation from the mean, which is key in understanding the actual evolution and its influence on e.g. the cycle to cycle variability [Vit+12].

the Clay institute of Mathematics, prized with 1 Million Dollars.

¹¹Provided that the simulation tools had been properly validated against experimental results

¹²Any related with a fluid motion such as, the intake and exhaust systems, injection system, piston bowl, lubrication and refrigeration, HVAC and external aerodynamics

1.1.1 CFD codes

The simulations mentioned previously are the result of the synergy between the current degree of mathematical description of the physics and computational capacity of solving non-linear problems. However, there is a difference (already established by Pope [Pop00]) between modelling and simulation. In the first case (i.e. modelling), the equations being solved are a suitable representation of a simplified reality that allows prediction of some mean quantities of the flow. Hence, models appear in response to lack of knowledge or computational power (or reasonable patience). By contrast, in a turbulent-flow simulation, governing equations are solved for a time-dependent velocity field that, to some extent, represents the actual¹³ velocity field for one realization of the turbulent flow. The distinction is required here because, as its name states, Large Eddy simulation (LES) solves the governing equations up to a certain scale, and models the influence of the smaller-scale motions. In addition, spray cases require models to describe the evolution of the liquid phase and its interaction with the gas phase.

Governing equations and models are implemented in CFD codes. The kernel of the most successful CFD codes (Ansys or CD adapco and the similar ones) is supported by a great number of experts and to create one of these codes from scratch is a totally unachievable task for an applied Engineer. Nonetheless, the CFD codes are used in a wide range of engineering applications. Regarding the degree of physical description, the most commonly used are the one-dimensional and the three dimensional CFD models¹⁴ whose use is constantly increasing. One-dimensional CFD codes allow us to understand global behavior of a flow system in terms of flow rates and pressure, having a good resolution in unsteady compressible problems. These codes solve a simplified version of the fluid flow governing equations in cases that have a dominant direction. Their main advantage is the low computational cost. However, if a good geometrical resolution or a more detailed flow field is needed, 3D simulations become essential. Three-dimensional CFD codes allow one to obtain an accurate solution of the flow field of the studied system, but with a higher computational cost, especially if non-steady simulations are considered.

¹³not averaged

¹⁴Note, “models” is used to refer to both simulations and to turbulence models, when the distinction is not needed

CMT-Motores Térmicos has developed a 1D CFD code, particularly designed for the calculation of gas jet evolution in a constant volume vessel under diesel-like conditions. DICOM is an open source one-dimensional gas dynamic model able to compute the evolution of the spray at the axis and infer from there the radial profiles of velocity and concentration of the equivalent gas jet under both inert [Pas+08] and reacting conditions [Des+08]. Thus, it is originally a 1D code extended to 2D. Its precedent [Des+07] calculates the analytical solution of the stationary, isothermal equivalent gas jet. The code is based on momentum flux conservation in the axial direction of the diesel spray and considers local density variations. Validation of such concepts is achieved by comparing model predictions with both CFD 3D gas jet simulations and experimental diesel spray measurements. Consequently, it has been used in the present work as a reference trend line, as well as to set up inlet B.C. (sections 3.2 and 4.2).

Dealing with three-dimensional computations, CMT-Motores Térmicos has experience with several commercial and open source codes. The main computational tool used in the current work is the OpenFOAM®software [Ope10]. OpenFOAM is a free, open source CFD software package providing an extensive range of libraries to solve anything from complex fluid flows involving chemical reactions, turbulence and heat transfer, to solid dynamics and electromagnetic. They provided an excellent framework to implement and modify the necessary models needed for the present study. In particular, the use of an open source code has the advantage of having full accessibility to the flow variables and to the code itself which facilitates intermediate steps and check points. To point out the main drawback, OpenFoam has the inconvenience of being far less user friendly and intuitive than other standard commercial codes. Although, the learning curve may be slightly longer, it can be argued that working directly with libraries of equations helps to become aware of the hypothesis and boundary conditions applied, as well as reinforces the physical meaning of each term.

Many CFD packages are available for spray modeling and simulation as shown in table 1.1. Standard CFD code can solve single-phase flows or multi-phase flows, and 2D or 3D problems. In addition, specific spray and turbulent sub-models for spray simulations are implemented in each computational code. As already stated, in our case the code chosen was OpenFOAM.

Software	Developer
Star-CD	CD-adapco
AVL Fire	AVL Advanced Simulation Technologies
ANSYSCFD/Fluent	ANSYS, INC
CONVERGE CFD	Convergent Science, Inc
KIVA	The Los Alamos National Labs, The Engine Research Center (UW - Madison)
OpenFOAM	ESI Group-OpenCFD Ltd
CT-FUEL	Gamma Technologies
CFDS-FLOW3D	Computational Fluid Dynamics Services, Inc.
PHOENICS	CHAM ltd
CFD-ACE+	ESI-Group
TransAT/ CMFD	ASCOMP GmbH
JETMIX/JETEVAP TESS TM	Southwest Research Institute (SwRI)
SURFER Code	Université Pierre et Marie Curie
Gerris Code	Stephane Popinet at NIWA, NZ

Table 1.1: CFD codes for spray modeling and simulation

1.2 Objectives

The present work aims to contribute to the effort of bringing the potential of LES close to the industry and more applied research. In this regard, this study focuses on the engineering LES of non-evaporating spray. The concept of *engineering LES* was introduced in 2011 by Rutland [Rut11] when applied to the study of applications and practical devices. Among Rutland's comments and suggestions regarding the use of engineering LES, the author would like to highlight one which states that it is up to the user to evaluate the suitability of the method as well as its relative impact on the results.

In order to keep the scope of the thesis at an affordable size, the objectives will focus at the first level on evaporating non-reacting multiphase jets. The extension to combustion sprays will be proposed in the scope of a continuation project as future work [section 5.2].

Thus, the main objective of the thesis is to develop and validate a CFD spray model based on LES methods for turbulence modeling at a reasonable computational cost (RANS-like). This main objective includes the implemen-

tation and development of the two-phase spray model on the open source CFD code OpenFOAM, the analysis of different turbulent models and their interaction with the phenomenological spray models, and the validation of the results compared to experimental data. In order to achieve the main goal, the following specific objectives have been proposed:

- Implement several LES methods for the simulation of two phase flows. Different LES subgrid models will be programmed into OpenFOAM code, and evaluated in order to select the most suitable for the flow characteristics found in sprays.
- Development of sub-models for spray atomization and disperse phase dynamics. This second objective will be dedicated to adapt available models, for spray atomization and droplet/particle-gas interactions within the framework of CFD-LES simulations. The main goal is to take advantage of the more accurate flow field predictions of LES methods, compared to RANS, on which standard spray atomization and dynamics sub-models were based.
- LES-spray vaporization model interaction. This objective concerns vaporizing liquid spray and aims to analyze a liquid evaporation model, which accounts for the different spray droplets conditions, from near nozzle field to diluted spray region. Although previous studies report a proper behavior of the phenomenological models beforehand mentioned they do not include the *dynamic structure* turbulent model implemented in the code. Therefore the analysis must be included for completion.
- Manipulation of LES fields to mimic experimental data base for spray modeling validation. The main advantage of the use of CFD is that the complete flow field can be analyzed, in contrast to the current experimental measurements, in which the data available is restricted to global variables or -at most- to a surface perpendicular to the measuring device. Therefore, there is an acknowledgeable effort performed by CFD researchers to resemble experimental data in order to be able to validate their results [Kem07]. Both macroscopic (spray penetration and dispersion) and microscopic (drop size and velocity) spray characterization measurements, already available in the research group, will be used for validation.

Since this is the first thesis at CMT-Motores Térmicos which has as a main core a CFD analysis of LES of sprays, a collateral objective is to develop a methodology to set up the cases and characterize the behavior of a diesel spray obtained by means of this type of simulations. Additionally, the methodology intends to optimize the use of the current computational resources available, obtaining enough resolution for practical purposes in a workday.

Finally, the advantage of CFD in terms of amount of data available, in contrast to experimental measurements, has already been exposed. The last objective is the use of this new information available to help increase related knowledge, particularly for the transient flow regime.

1.3 Methodology

As clearly stated, the objectives will focus firstly on evaporating non-reacting multiphase jets. In terms of computational difficulty (table 1.2) the spray is meant to finally be injected into the cylinder of a reciprocating engine (the most difficult). Hence, the complete characterization in a constant volume vessel is required in order to distinguish particular problems when simulated in an engine cylinder. Within this complex problem we can differentiate the contribution of three interrelated phenomena: gas-gas interaction, liquid-gas interaction and the phenomenological models regarding liquid evolution (i.e. injection, turbulent dispersion, breakup, atomization and evaporation) Following Leibniz method of complex problems approach which consists of a combination of simpler ones, the methodology of the thesis begins with a simplification of the problem and will successively eliminate restrictive hypothesis in order to study the diesel spray under evaporative conditions (in a constant volume vessel with an inert atmosphere). This procedure has been reflected in the outline of chapters 3 and 4.

First the study focuses on the gas-gas interaction. Experimental information [Pas+08] shows that diesel sprays under both non-vaporising and vaporising conditions can be described by a mixing-controlled approach, and thus

¹⁵number of directions of statistical inhomogeneity

¹⁶statistically stationary, boundary layer approximations apply

¹⁷e.g. plane jet: in similarity variables, turbulence-model equations for two dimensional self-similar free shear flows have a single independent variable

Dimension ¹⁵	Boundary layer ¹⁶	Statistically stationary	Not statistically stationary
0			Homogeneous shear flow
1		Fully developed channel flow; self-similar free shear flow ¹⁷	Temporal mixing layer
2	Jet in a co-flow	flow through a sudden expansion in a 2D duct	Flow over an oscillating cylinder
3	Boundary layer on a wing	Jet in a cross-flow	Flow in the cylinder of a reciprocating engine

Table 1.2: Adapted from [Pop00]. Examples of turbulent flow of various levels of computational difficulty (the difficulty increases downward and to the right)

they can be simplified to an equivalent gas-jet¹⁸. The approach of diesel-like gas jet has three clear advantages. Firstly, sensitivity and independency study (i.e. mesh procedure, temporal schemes, boundary conditions) are not influenced by spray phenomenological models. Therefore, the results will shed some light on the advantages and drawbacks of the specific LES turbulent models analyzed. Secondly, it offers a unique template where both the near nozzle and the disperse region of the spray can be compared. Consequently, the range of validity mixing-controlled approach can be delimited. Finally, depending on the temperature of the chamber, evaporative sprays evolve as gas-gas interaction downstream of the liquid length. Therefore, gas jet results in set up convergence may apply to this region and we can set these fields as a reference to the simulations of evaporated fields.

In the second phase, liquid is introduced by means of discrete blobs in a non-evaporative ambient. Special attention is given to the liquid-gas interaction on a sub-grid level and its influence on the LES turbulent models previously studied. The analysis will include both atomization and breakup

¹⁸Since fuel-air mixing process is significantly influenced by fuel atomization, breakup and collision this simplification is even more restrictive for LES due to its degree of physical description

models in an attempt to isolate their effect from the evaporation process.

Finally, the spray under the Engine Combustion Network (ECN) Spray-A conditions is simulated with LES models. CMT-Motores Térmicos is contributing to the ECN with experimental data and RANS simulations in this specific case. The analysis is focused on the effect of the evaporation model on the turbulent evolution of the spray. Also, the comparison with previous simplified simulations provides closure to the physical description of the diesel injection under evaporative conditions.

Once the main lines of the thesis' formal logic have been established, the particular methodology followed in each part (i.e. diesel-like gas jet, non-evaporative spray, Spray-A) is now described.

1. Mesh

The meshing process in a CFD simulation is fundamental in order to obtain accurate results. A good mesh can save a lot of time if adequately designed from the very beginning. Using a pure gas jet, our first studies will be about the meshes needed for the LES methods to work. Meshes made in the previous studies are modified in order to improve the results and limit the computational cost with the required accuracy. We are also interested in following droplets in the jet, so new studies about the meshes will be needed reaching a compromise in size and morphology in both cases (i.e. Eulerian-Eulerian and Lagrangian-Eulerian). In this way we avoid taking into account the mesh factor when comparing all three types of simulations. Having said that, for the diesel-like gas jet case, scientific type of meshes have been calculated as well. The purpose of this high definition (HD) simulations is double. On the one hand, they are used as a reference of how restrictive the engineering meshes are, not only in terms of the flow scales simulated but also the accuracy of the inlet boundary condition (BC) needed by the turbulent models. In this regard, the initial idea was that poor physical discretization may require poor turbulent description on the imposed inlet fields (e.g. not physically consistent random perturbations on the inlet). Note that, in the interest of time and simplicity the comparison was focused on the disperse part of the jet and the initial zone was omitted at the scientific meshes. On the other hand, we also wanted to check how restrictive inlet BC in the case of scientific mesh are, as a function of the type of LES turbulent model.

2. Models development and implementation

This is the most important task from the CFD point of view. This part gathers the study, implementation and validation of the models used in the thesis. Data provided by previous CMT experiments and those results from specialized literature are used.

Regarding LES models, as in the case of RANS ones, many of them have appeared in the literature since Smagorinsky first presented his own in a publication in 1963. Different LES methods can be found both in commercial and open codes. At first, implemented methods in OpenFOAM are evaluated for diesel-like gas jets. Afterwards, those found in the literature that showed a potential improvement are introduced in OpenFOAM. Although, dynamic structure was chosen for its special treatment of gas-liquid phase interaction, it has been included in the Eulerian-Eulerian study as well. Unlike already implemented LES models in OpenFOAM, dynamic structure is a non-viscous model¹⁹. Because of this interesting feature, the turbulent model was selected over other models proposed for future works.

Apart from LES turbulent models, Lagrangian-Eulerian spray simulation is characterized by the phenomenological models required to describe liquid evolution. In recent years there have been many studies about the mechanism that controls the primary and secondary atomization of a jet [Vil+04; Che+09; JL10; Koj+12], but due to the complexity of this phenomenon and the large amount of mechanisms involved in it, both experiments and CFD simulations are evolving and therefore the issue still remains an open problem. We observe both phenomena through the implementation of the last known methods and validate the results obtained. As with the following models, part of the challenge consist in the analysis of their interaction with LES methods and their adaptation if needed.

3. Particle Tracking and Clustering.

In this part of the study we are interested in the behavior of non-evaporative jets with droplets inside. It is necessary to evaluate and validate the sub-grid schemes for the movement of these particles. Also, it is complementary to the study of evaporation models in order to discern specific contribution from related effects. Moreover, one of the

¹⁹Difference that we will further discuss later on.

advantages of LES methods over RANS ones is its capacity to reproduce some of the turbulent scales and thus better recreate the structures of the flow. Hence, the different structures that the particles can adopt are analyzed.

4. Evaporation models

In many cases, as in the diesel sprays, the evaporation of the droplets is needed for the combustion. We use the model provided in OpenFOAM. By comparing the LES results with the RANS ones and the data obtained from the experiments we are able to measure the interaction with LES method and the improvement of the results.

5. Spray Boundaries and Final Integration

Here is where the LES methods show both their strengths and weaknesses. Compared to RANS, the use of low-cost LES is very recent and the results need a complete validation against experiments. LES can represent the boundaries of the spray better than RANS, but they require a detailed study of the boundary conditions and of the LES schemes used to represent accurately the behavior of the fluid, especially near the boundary.

Finally, the thesis has no interest in the development of all these codes to solve a theoretical problem, but as a tool for solving real life problems of great industrial interest. Consequently, a great effort is continuously made to achieve the minimum computational power needed to get reliable results and assess the degree of credibility. In this regard, there is an obvious danger to face. As in the case of new products or emerging technologies expected to meet and even surpass satisfaction levels of consolidated previous ones, LES results have to compete with more than 30 years of RANS validated calculations. At this point, it is important to establish some interrelated principles:

- **Subsidiarity.** Applied LES has its own market/scientific niche, which will be progressively defined along with LES growing experience. This idea lies behind the methodology proposed.
- **Patience.** Most of the validation process required for LES has been already established for RANS over the years. Skipping or underestimating the importance of this task for LES calculations may provide

a nice-looking²⁰ unfounded outcome which will generate a high level of expectations and the proportional disenchantment if the results do not match reality. In order to avoid the consequences of an unfortunate overreaction, the methodology proposed tries to contextualize obtained results.

1.4 Outline of the thesis

The thesis is structured as follows: A basic understanding and significance of the project's background, sources of motivation, as well as the aim and scope of the project have been explained in this chapter.

The state of the art about the spray modeling and the different theoretical approaches to the physics of sprays are briefly reported in chapter 2 together with the main governing equations of the model.

In chapter 3, the detailed description of the LES numerical set up, underlying principles and computational procedure are presented.

Chapter 4 firstly presents the outcomes of the LES of diesel-like gas jets, followed by non-evaporating diesel sprays and finally under evaporating conditions.

Chapter 5 presents the main conclusions of this job, together with the future work.

²⁰In contrast to beautiful

Chapter 1 bibliography

- [Ame08] R. Amengual. *Bielas y Álabes*. Oficina Española de Patentes y Marcas, 2008 (cit. on p. 3).
- [Che+09] J. Chesnel, J Reveillon, T Menard, M Doring, A Berlemont, and F X Demoulin. “LES of atomization: From the resolved liquid surface to the subgrid scale spray”. In: *ILASS* (2009) (cit. on p. 14).
- [Cum89] L Cummins. “Internal fire”. In: *SAE International* (1989) (cit. on p. 3).
- [Cum93] L Cummins. *Diesel’s Engine*. Carnot press, 1993 (cit. on p. 3).
- [Des+07] J M Desantes, R Payri, José M García-Oliver, and F J Salvador. “A contribution to the understanding of isothermal diesel spray dynamics”. In: *Fuel* 86.7-8 (2007), pp. 1093–1101. ISSN: 0016-2361. DOI: 10.1016/j.fuel.2006.10.011 (cit. on pp. 6, 8, 23, 28, 97, 102, 168).
- [Des+08] J M Desantes, J V Pastor, José M García-Oliver, and J M Pastor. “A 1D model for the description of mixing-controlled reacting diesel sprays”. In: *Combustion and Flame* 156.1 (2008), pp. 234–249. ISSN: 0010-2180. DOI: DOI : 10.1016/j.combustflame.2008.10.008 (cit. on p. 8).
- [Hey88] J B Heywood. *Internal combustion engine fundamentals*. McGraw-Hill, Inc., 1988. ISBN: 0-07-028637-X (cit. on pp. 5, 21, 45).
- [JL10] W P Jones and C Lettieri. “Large eddy simulation of spray atomization with stochastic modeling of breakup”. In: *Physics of Fluids* 22.11 (2010), p. 115106. ISSN: 10706631. DOI: 10.1063/1.3508353 (cit. on pp. 14, 58).
- [KB88] T Kamimoto and MH Bae. “High combustion temperature for the reduction of particulate in diesel engines”. In: *SAE Technical Paper 880423* (1988). DOI: 10.4271/880423. (cit. on p. 5).
- [Kem07] Andreas M. Kempf. “LES Validation from Experiments”. In: *Flow, Turbulence and Combustion* 80.3 (Dec. 2007), pp. 351–373. ISSN: 1386-6184. DOI: 10.1007/s10494-007-9128-9 (cit. on pp. 10, 35).
- [NS80] T Newcomb and R Spurr. *A Technical history of the motorcar*. 1980 (cit. on p. 3).

- [Pas+08] J M Pastor, J J Lopez, and José M García-Oliver. “A 1D model for the description of mixing-controlled inert diesel sprays”. In: *Fuel* 87.13-14 (2008), pp. 2871–2885. ISSN: 0016-2361. DOI: 10.1016/j.fuel.2008.04.017 (cit. on pp. 8, 11, 21).
- [PD11] F Payri and J M Desantes. *Motores de combustión interna alternativos*. Ed. by F Payri and J.M. Desantes. Ed. Reverté, 2011, p. 1002. ISBN: 978-84-291-4802-2 (cit. on p. 3).
- [Pop00] S Pope. *Turbulent Flows*. Cambridge University Press, 2000, p. 771. ISBN: 978-0-521-59886-6 (cit. on pp. 7, 12, 21, 26, 33, 36).
- [Rut11] Christopher J Rutland. “Large-eddy simulations for internal combustion engines - a review”. In: *International Journal of Engine Research* 12.5 (Aug. 2011), pp. 421–451. ISSN: 1468-0874. DOI: 10.1177/1468087411407248 (cit. on pp. 9, 35, 36).
- [SAE97] SAE. *The automobile. A century of progress*. 1997 (cit. on p. 3).
- [Suz97] T Suzuki. *The romance of engines*. 1997 (cit. on p. 3).
- [Vil+04] E de Villiers, A.D. Gosman, and H.G. Weller. “Large Eddy Simulation of Primary Diesel Spray Atomization”. In: *SAE Technical* (Mar. 2004). DOI: 10.4271/2004-01-0100 (cit. on pp. 14, 44, 49).
- [Vit+12] Oldrich Vitek, Jan Macek, Reinhard Tatschl, Zoran Pavlovic, and Peter Priesching. “LES Simulation of Direct Injection SI-Engine In-Cylinder Flow”. In: *SAE Technical Paper 2012-01-0138* (2012). DOI: 10.4271/2012-01-0138 (cit. on pp. 6, 58).
- [Koj+12] Koji Kitaguchi, Soichi Hatori, Tsukasa Hori, and Jiro Senda. “Optimization of breakup model using LES of diesel spray”. In: *Atomization and Sprays* 22.1 (2012), pp. 57–77 (cit. on pp. 14, 58).
- [Ope10] OpenCFD Limited. *OpenFOAM-The Open-source CFD toolbox*. 2010 (cit. on p. 8).


Chapter 2

Spray Fundamentals and CFD spray modeling

Contents

2.1	Introduction	20
2.2	Spray characterization	22
2.3	Turbulent approaches to simulate diesel sprays	31
2.4	Interface and particle tracking	45
2.5	Phenomenological spray models	49
	Chapter 2 bibliography	70

2.1 Introduction

 INSIGHT IN THE BEHAVIOR of an evaporating fuel spray is of great importance for engine designers. Improvements in injection systems reduce emissions and increase power by means of a more effective combustion process. Therefore, a deep understanding of the physics of diesel spray provides some fundamental knowledge for the design of more efficient, less consuming, and cleaner engines. Nowadays -more than ever- experimental research relies on spray simulation in order to help engine optimization, development, and design.

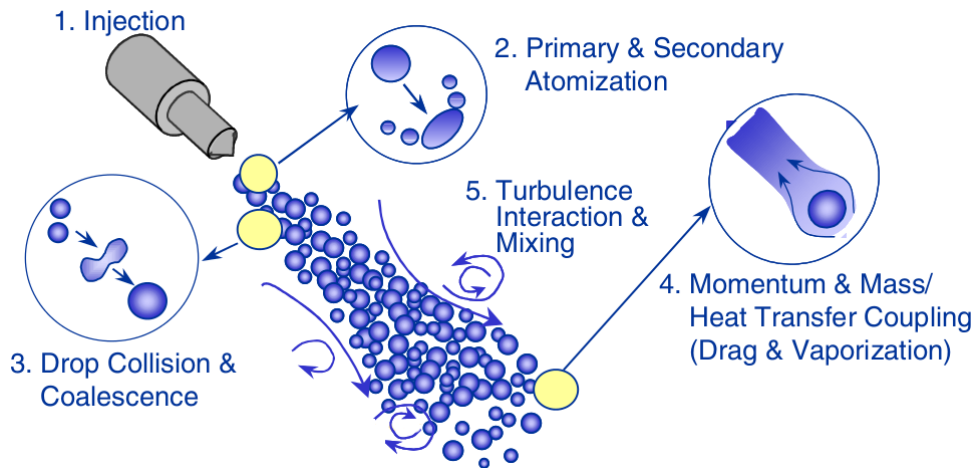


Figure 2.1: Spray dynamics within ICEs. Adapted from [Lip+05]

In this chapter, diesel spray physical description and related models are presented. Methodologies of spray simulation as well as key physical processes in liquid-fuel spray mixture with air (Figure 2.1) are reviewed. Note Figure 2.1 omits combustion and wall impingement¹ processes because they are out of the scope of the present thesis.

In summary, the physics of the spray can be described as follows: after start of injection, the spray increases turbulent level, liquid core is dispersed into blobs and droplets and flow decelerates along with air entrainment as a result of processes depicted at Figure 2.1(i.e. Atomization, coalescence, momentum transfer, turbulence interaction and evaporation).

¹Splashing and deposition, film transport and spread, film vaporization.

Spray simulation models may inherit the more general classification proposed by Heywood for ICEs [Hey88]: thermodynamic and fluid dynamic models:

- Thermodynamic models, based on conservation mass and thermodynamics' first law, can be zero-dimensional or phenomenological, depending on whether they include geometric characteristics of the flow movement (i.e. spreading rate, radial velocity distribution...) (Figure 2.2)

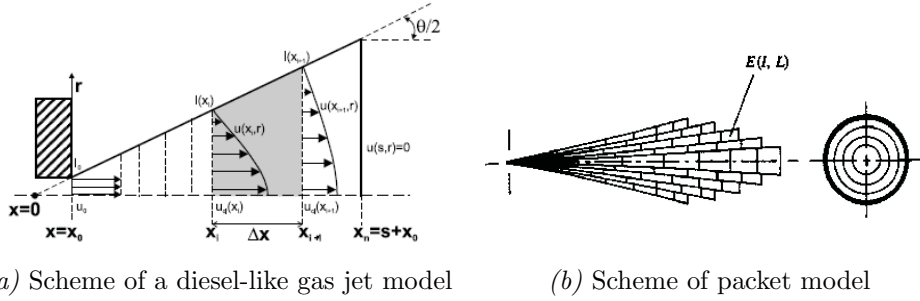


Figure 2.2: Gas jet phenomenological models [Pas+08; Hir+83]

- Fluid dynamic models are based on the governing equations coming from continuity, momentum and energy. Versteeg et al [VM95] and Pope [Pop00] give an excellent introduction at their books.

Two different coordinate systems can (and will) be used². Taking cylindrical coordinates, the circumferential coordinate will be denoted by ϕ and the radial by r . In the case of using cartesian coordinates, the spanwise ones will be denoted by $(x, y, z) = (x_1, x_2, x_3)$. Using the latter, the final form³ of the evolution equations applied to a compressible⁴ multiphase spray are cast here as follows:

$$\frac{\partial \rho}{\partial t} + \frac{\partial(\rho u_j)}{\partial x_j} = S_m, \quad (2.1)$$

²Let x be the axial coordinate.

³As they are implemented at the OpenFOAM solver used for the present work

⁴Newtonian fluid

$$\frac{\partial \rho u_i}{\partial t} + \frac{\partial \rho u_i u_j}{\partial x_j} = -\frac{\partial p}{\partial x_i} + \frac{\partial \rho \Gamma_{ij}}{\partial x_j} - \frac{\partial \rho \tau_{ij}}{\partial x_j} - \rho g + S_{M,i}, \quad (2.2)$$

$$\frac{\partial \rho h_s}{\partial t} + \frac{\partial \rho u_j h_s}{\partial x_j} - \frac{\partial^2 (\alpha h_s)}{\partial x_j^2} = \frac{Dp}{Dt} + S_h, \quad (2.3)$$

$$\frac{\partial \rho Y_k}{\partial t} + \frac{\partial \rho u_j Y_k}{\partial x_j} = \rho D_k \frac{\partial Y_k}{\partial x_j} + S_{Y,k}, \quad (2.4)$$

where ρ , p , Γ_{ij} , τ_{ij} , h_s , Y_k and u_i , are gas phase density, pressure, viscous stress tensor, Reynolds stresses⁵, sensible enthalpy, species mass fraction, and velocity, respectively. In eq. 2.4, D_k is the species diffusivity coefficient, and in eq. 2.3, α is the thermal diffusivity of the gas. The effect of liquid phase (droplets or parcels) can be treated as source terms for mass, momentum, energy and mass fraction in the gas phase governing equations⁶. The spray source terms in eqs. 2.1 - 2.4 (S_m , $S_{M,i}$, S_h , $S_{Y,k}$) are defined at section 2.5.

2.2 Spray characterization

Generally speaking experimental research is previous to CFD, and its benchmark in terms of validation and comparison. As a consequence, physical characterization of the simulated processes tend to emulate experimental derived variables and visualization methods. Typically, spray characteristics are classified into two sub groups, macroscopic and microscopic (Table 2.1).

Macroscopic characteristics	Microscopic characteristics
Spray tip penetration	Velocity and concentration distribution
Liquid length ⁷	Droplet size (D_{10} , D_{32} ⁸)
Spray cone angle / Spreading rate	
Entrainment	

Table 2.1: Macroscopic and microscopic spray characteristics.

⁵In LES it denotes the sub-grid stresses

⁶Assuming that the characteristic dimension of each droplet/parcel is much smaller than the surrounding discretized gas

In order to help explaining in detail spray characteristics, a general (classic) spray description⁹ must be provided: two different sub-regions are present at Diesel sprays ([HA90; Des+06] and [Des+07]). First, the so-called steady region, which is a region located inside a conical-sharp of spray starting from the nozzle exit to approximately 60%-70% of the farthest distance of the whole spray. The temporal average shown in the results of this thesis is delimited to the steady region of the spray at the time the average was initiated. The rest of the spray is defined as the unsteady or transient region as shown in Figure 2.3. This region is also referred to as the plume.

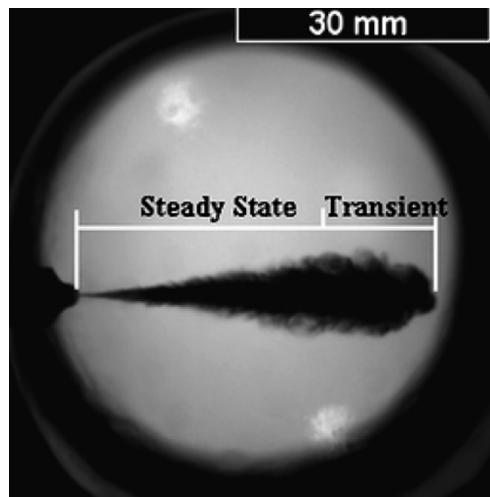


Figure 2.3: Visualization of a spray taken at $825 \mu s$ after the start of the injection ($P_{inj} = 80 MPa$, $d_0 = 0.14 \mu m$, and $\rho_{cha} = 20 kg/m^3$) [Des+07]

Macroscopic description pays attention to spray basic geometric characteristics such as penetration, liquid penetration, known as liquid length (LL), spray cone angle or entrainment. On the other hand, microscopic description looks over the internal structure of the spray. The parameters analyzed are the distribution of velocity and concentration (for both liquid and gas phase) and the droplet size.

- Penetration.

⁷Liquid spray only

⁸Representative diameters of the spray droplets see 2.14

⁹It applies for gas jet and liquid spray under both non-evaporating and evaporating conditions.

Spray tip penetration (or simply called spray penetration) is defined as the axial distance from the nozzle exit to the spray front. This macroscopic parameter is an important mixing process indicator. Particularly, knowing this length is crucial to predict when the spray impinges on the wall which greatly affects combustion and soot formation.

Desantes et al. [Des+06] relate the penetration of a non-evaporative spray, $S(T)$ with nozzle diameter d_0 , and pressure drop between the injector and the chamber and as inversely proportional to ambient gas density ρ_a and spray angle, θ , as follows:

$$S(t) \propto \rho_a^{-0.25} \Delta P^{0.25} D_{ef}^{0.5} \tan^{-0.5}(\theta/2) t^{0.5} \quad (2.5)$$

Under evaporative conditions, Naber and Siebers [NS96] observed a reduction of penetration up to a 20% due to the increase of the mixture density (ambient gas and fuel vapor). The change on density is caused by the temperature decrease due to the evaporation process. For the same reason (i.e. temperature effect on density) penetration increases under reactive conditions.

Note how, the phase that determines penetration differs from evaporative to non-evaporative conditions. In this sense, spray penetration and liquid penetration coincide for non-evaporative cases. However, spray penetration under evaporative conditions is delimited by the gas phase. In this case LL stabilizes at a certain value while vapor penetration keeps increasing with time. In the present work, vapor penetration is defined as the farthest location of a cell containing more than 1% of mass fraction of fuel vapor where LL is the length including 99% of the liquid mass in the chamber.

- Spray cone angle / Spreading rate

Along with penetration, spray cone angle is commonly used for spray characterization. There are different definitions of the spray cone angle in literature. Bae et al. [Bae+02] set the spray angle as the angle between two lines connecting the nozzle tip and the spray boundary at 50% of the spray penetration. Other authors obtain this value at 60% of spray tip penetration [Lef89], [Pay+08b]. Despite the reference (i.e. 50% or 60%) or the technique used, spray angle depends on the air-fuel density ratio [NS96; Ran58; RB79; Wu+84; Del+05; Des+05] (see eq. 2.6). Under non-evaporative conditions the range of the density ratio

exponent varies from 0.2 to 0.5, although for Naber and Siebers [NS96], 0.19 is the exponent that better fits experimental measurements.

$$\tan^{-0.5}(\theta/2) \propto \left(\frac{\rho_a}{\rho_l}\right)^{0.19}. \quad (2.6)$$

Regarding present results, experimental reference angle is 21.6° [Pay+08c] (N1 nozzle, $P_{inj} = 80\text{MPa}$, $\rho_a = 40\text{kg/m}^3$) for the non evaporative case. Also, in order to be consistent with penetration measurements, gas jet limit is defined by a $Y_f = 0.01$ isosurface.

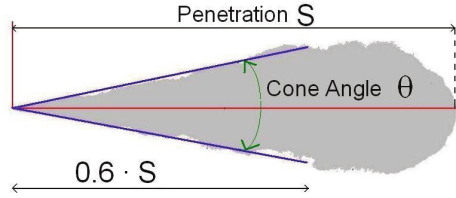


Figure 2.4: Macroscopic parameters of spray.

Consistently with penetration, spray angle changes under evaporative and reactive conditions. Under evaporative conditions, spray angle suffers a contraction. Conversely, the increase of temperature due to exothermic reaction increases the angle.

A consideration must be done about spray angle and spreading rate. From an experimental point of view, spray angle is based on opacity differences with the background due to fuel concentration and density variations. Therefore, the spray contour is defined by the concentration threshold recognized by the post-processing tool¹⁰ which CFD fields must mimic to quantitatively compare simulated injections. The predicament relies on the comparison of pictures¹¹ -where 3D experimental information has been collapsed into a 2D image- with pure 2D cut planes of the simulated field (e.g. contour plots of Y_f)

In contrast, spreading rate is defined by velocity field. The advantage is that the field can be directly compared with measurements from different experimental techniques. In terms of the mean axial velocity field, \equiv

¹⁰Shadowgraphy like images or X-ray radiography measurements [Yue+01; Kas+09]

¹¹or numerical data extracted from pictures (i.e. angles)

$\langle U(x, r, \phi) \rangle$, which is independent of ϕ , the centerline velocity is defined as

$$U_0(x) \equiv \langle U(x, 0, 0) \rangle, \quad (2.7)$$

and the jet's half width as

$$\frac{1}{2}U_0(x) \equiv \langle U(x, r_{1/2}(x), 0) \rangle. \quad (2.8)$$

The spreading rate is thus defined as the rate of change of jet's half width along x , i.e., $S = \frac{\partial r_{1/2}}{\partial x}$ for round jets. In the case of plane jets an equivalent definition is obtained by means of a variable change $y = r$, $S = \frac{\partial y_{1/2}}{\partial x}$.

In this way, the definition of spreading rate is applicable to both round and plane jets. Therefore, spreading rate is preferred from a turbulence point of view, since axis velocity reference (U_0) makes self-similar treatment easier.

Measurements of velocity field by means of LDA (Laser Doppler anemometers), hot-wire and velocity probes are point source that can be extended to a line, a surface or a volume by moving the sensor. Therefore, one can achieve same dimension (e.g. 2D in space) of information than cut planes of simulated velocity fields. In this case, simulations can be directly compared with experimental measurements. In the case of PIV images, comparison must be done with caution since the 3D to 2D collapse of information previously related is inherent to the experimental technique.

Finally, note how axis velocity is the reference to locate spreading rate. Although different average velocity decay law rules round jet ($U_0 \sim x^{-1}$) and plane jet ($U_0 \sim x^{-1/2}$), both present the same spreading rate ($S \approx 0.1$) [Pop00]. Consequently, conclusions from turbulent model validation of plane jets' spreading rate should be of general application¹² and therefore valid for round jets (i.e. diesel-like gas jets). Quantitative comparison with S is restricted to temporal average of the stationary part of the spray¹³.

¹²Under similar spatial discretization

¹³The ensemble average of distinct simulations under the same BC is valid as well.

- Entrainment.

Air entrained volume allows to quantify fuel-air mixing process. It gives an idea of the overall fuel concentration and it is a parameter to take into account when analyzing spray evaporation process. There are two entrainment functions to quantify such process: mixture rate and entrainment coefficient.

López [Lop05] evaluates entrainment based on the evolution of the mass fraction on the spray axis. Hence, mixture rate is defined as

$$MR(x) = d_{eq} \frac{\partial(1/Y_{f,cl}(x))}{\partial x}, \quad (2.9)$$

where equivalent diameter (d_{eq}) is defined as follows:

$$d_{eq} = d_0 \sqrt{\frac{\rho_f}{\rho_a}}. \quad (2.10)$$

In his work, López deduced a universal¹⁴ evolution of this expression as a function of x/d_{eq} , approaching a constant value ($MR \cong 0.2045$). Although the conclusion was achieved with non-isodense isothermal spray simulations, a review on experimental investigation confirms a range between 0.194 and 0.230 for the same relation [HO99]. In addition, gas jet simulations produced values between 0.18 and 0.19 for the stabilized zone [GO06].

Regarding entrainment coefficient (C_e), Ricou and Spalding [RS61] and Han and Mugal [HM01], experimentally measured the entrainment in turbulent round jets under no iso-dense conditions, defined as follows,

$$C_e(x) = \frac{d_{eq}}{\dot{m}_0} \frac{\partial \dot{m}(x)}{\partial x}, \quad (2.11)$$

where \dot{m}_0 is mass flow rate of fuel at the nozzle exit . The entrainment coefficient was determined to be 0.32 for the steady part of the jet¹⁵. This value agrees with measurements on iso-dense cases [Hil72]. Hence, both parameters are useful not only during the validation of simulations, but for the methodology to determine the turbulent model coefficients.

¹⁴Independent of density, injection velocity and nozzle diameter

¹⁵Depending on the velocity profile at the nozzle exit, initial evolution of C_e may differ.

Note, equivalent diameter (d_{eq}) has been included in eq. 2.9 and eq. 2.11. Therefore both iso-dense and non iso-dense cases are taken into consideration.

- Velocity and concentration distribution.

Velocity and concentration distribution can be addressed from a spatial point of view (i.e. axial and radial directions of the spray) and attending to the phase (i.e. gas phase and liquid phase)

Axial characterization of velocity and concentration has been modeled for diesel-like gas jet under stationary conditions [Des+07]. Tendencies and magnitude of the model have proven suitable for the disperse part of the diesel spray. Consequently, the model has been used as a reference for both instantaneous and average simulated fields. In order to be consistent with the model, only the axial component velocity is taken into account for the averaged axis velocity decay of the simulations. In fact at this particular location, averaged perpendicular components are order of magnitudes smaller than the axial one. Otherwise the result would be overestimated. The axis velocity of liquid phase is extracted from the axial component of the parcels located inside the cells surrounding the center line (i.e. $|x| < 0.5mm$ and $|y| < 0.5mm$)

As for axial decay, radial distribution of velocity and concentration averaged profiles show isomorphism within the self-similar region. Both exhibit a Gaussian-like shape that can be modeled by exponential expressions [Des+06]:

$$u(x, r) = u_0(x) \exp\left(-\alpha_s \left(\frac{r}{R(x)}\right)^2\right), \quad (2.12)$$

$$Y(x, r) = Y_{f_0}(x) \exp\left(-\alpha_s Sc \left(\frac{r}{R(x)}\right)^2\right), \quad (2.13)$$

where Sc is the Schmidt number¹⁶, R the cone radius that limits the spray, and α_s the shape factor of the Gaussian distribution ($\alpha_s = 4.6$). These are the functions that better fit the available experimental data in the literature [PM96; Hin75; Pas+00].

¹⁶Schmidt number (Sc) represents the relative rate of momentum and mass transport

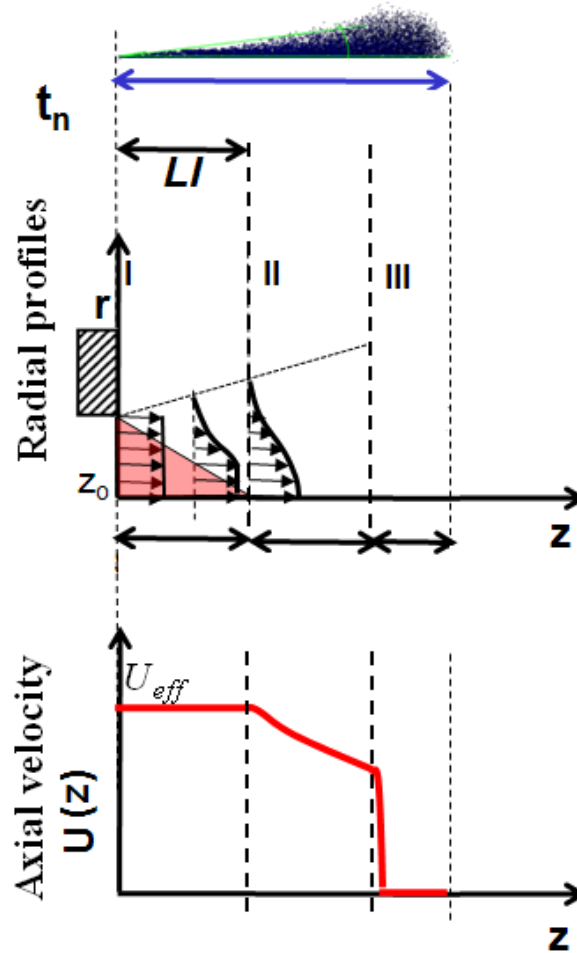


Figure 2.5: Average velocity profiles. Adapted from [Cha13]

Again, these models for the developed region in the spray are used as a reference of the velocity fields and the droplet concentration coming from LES.

Figure 2.5 outlines the averaged radial and axial velocity profiles previously described. There are three different regions. Region II (self-similar) and III (spray plume) have been already discussed. Within the steady state part of the spray, there is a certain distance where the in-

jected gas, located at the jet axis, does not interact with the surrounding phase (i.e. region I). Therefore, the gas remains at the same velocity as it was injected in what is known as the *non-perturbed zone* where the transition between top hat like velocity profile and Gaussian profile of eq. 2.12 takes place.

There are several reasons to highlight this region. Firstly, it plays an important role in the boundary conditions setup and the domain delimitation of present simulations, as explained in the following chapter. Secondly, there is a parallelism with the liquid-core length (L_{bu}) that will be discussed in detail at the atomization model section.

- Droplet size.

The degree of spray atomization can be defined by the droplet diameter, d_{ab} . Since, droplet diameter varies with time and space, Mugele and Evans [ME51], proposed an expression to get a diameter representative of the whole spray:

$$d_{ab} = \left(\frac{\sum_{i=1}^N N_i d_i^a}{\sum_{i=1}^N N_i d_i^b} \right)^{\frac{1}{a-b}}, \quad (2.14)$$

where d_i is the droplet diameter and N_i the total number of droplets with that diameter. Depending on the values assigned for a and b , different characteristic diameter can be obtained. In our case, arithmetic diameter ($a = 1, b = 0$) and Sauter Mean Diameter (SMD) ($a = 3, b = 2$) are the most commonly used for diesel spray characterization. In particular, SMD represent the droplet diameter of a monodisperse spray equivalent (i.e. same volume-surface ratio) to our polydisperse¹⁷ diesel spray. Hence, the lower the SMD the higher the surface of the droplet (in relation to the volume) and thus increasing the efficiency of both mixing and evaporation processes. Note, liquid phase is discretized by parcels instead of droplets and SMD can be written as:

$$d_{32} = \frac{\sum N_{d,p} d_p^3}{\sum N_{d,p} d_p^2}, \quad (2.15)$$

¹⁷I.e, non-uniform

where $N_{d,p}$ is the statistical¹⁸ number of droplets gather by the parcel and d_p is the diameter they have in common. SMD temporal evolution takes into account every parcel in the domain at a given time step. Radial distribution at different spray sections is also analyzed.

2.3 Turbulent approaches to simulate diesel sprays

There are three distinct streams of numerical solution techniques: finite difference, finite element and spectral methods. Here we are solely concerned with the finite volume method, a special finite difference formulation that is central to OpenFOAM as well as to the most well-established CFD codes (i.e. *ANSYS*, *Star-CD*...)

Regarding two phase flows, CFD models can be classified as a function of the type of conservation equations used: Navier-Stokes, Laplace, Lattice-Boltzmann. Navier-Stokes equations are the most commonly used¹⁹. At the same time, CFD models can be classified depending on the degree of turbulent resolution of the continuous phase in: DNS, LES and RANS. The extent of the field resolved by the governing equations (2.1 - 2.4), i.e. only average, large scales or direct and complete resolution depends on the turbulent approach as is further expounded on this section.

2.3.1 Direct Numerical Simulation

As its name states, DNS directly²⁰ solves the conservation equations for the instantaneous flow, and consequently, all the relevant turbulent scales. Although results obtained by means of DNS have the same validity as experiments [Jim03], their prohibitive computational cost²¹ restricts DNS to fundamental research.

Since DNS provides the highest spatial discretization²², the highly non-

¹⁸It does not have to be a natural number.

¹⁹By the aforementioned CFD codes

²⁰Without further approximation or modeling

²¹Since the smallest structures of the flow have to be solved, the computational cost increases as $Re^{9/4}$ and the resources required for most practical cases are above current computer hardware limitations (and will probably be in the next 20 year [Jim03; HJ06])

²²Turbulence-wise.

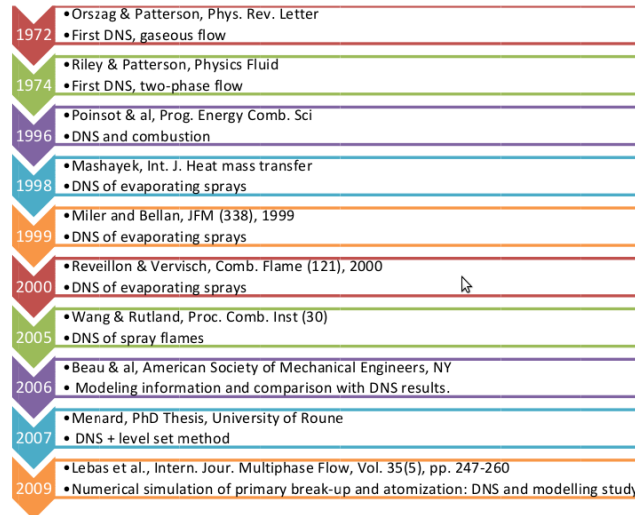


Figure 2.6: Main achievements in the DNS of jets and sprays.

linear phenomena controlling fuel liquid breakup process, surface break-up, and turbulent multi-phase mixture can be better captured by this approach. As a consequence, DNS of primary breakup for diesel spray has garnered the attention of the scientific community [M+06; Leb+09]. Note, the spatial resolution required by the surface of two-phase flows may be greater than the limit imposed by turbulence. Also, the underlying physics of fuel sprays and two-phase flows are not well understood to perform DNS. Hence, we need to rely on sub-grid scale models developed based on experimental evidence. A review of DNS approach applied to multi-phase modeling and fuel spray is listed in chronological order in Figure 2.6.

2.3.2 Reynolds-averaged Navier-stokes

Contrary to DNS, RANS approach has the highest level of modeling and it can be seen as a successful interpolation between experimental data sets. Hence, without a careful check of the results against experiments, little can be said.

Regarding diesel spray injection, the most commonly used codes in the automotive industry -up to now- are based on the RANS approach because of their reasonably accurate results and relatively lower computational cost.

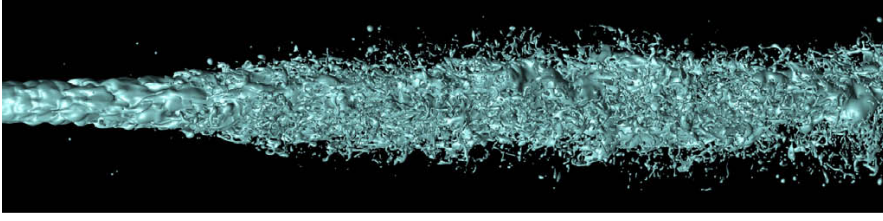


Figure 2.7: DNS simulation of diesel spray. Computational domain is $(0.3 \times 0.3 \times 2.2)$ mm, grid size is $128 \times 128 \times 896$, $d_0 = 100\mu\text{m}$, $U = 100$ m/s, $\rho_{inj} = 696\text{kg}/\text{m}^3$, $\rho_{cha} = 50\text{kg}/\text{m}^3$, computing time 10,000 h on 14 processors (Lebas et al., 2009 [Leb+09])

In addition, coupled to probability density functions (PDF) RANS is able to overcome combustion simulations with similar computational requirements [Saf+10] to inert ones.

There has been a continuous work in this field since the first RANS models were developed in the earlier '60s. We will describe briefly the $k - \varepsilon$ turbulent model used in this work. A detailed description of this and other models can be found in [Pop00; VM95; ET83; YO86; LS74].

The main difference between RANS models is the calculation of τ_{ij} (Reynolds stresses term) from eq. 2.2. The most common form of turbulence modeling involves the use of turbulent viscosity, μ_t . Using the Boussinesq [Sch07] or mean-gradient assumption gives the following traditional model

$$\tau_{ij}^r = -2\mu_t \tilde{S}_{ij}, \quad (2.16)$$

where τ_{ij}^r is the anisotropic portion of τ_{ij} (e.g. see Pope [Pop00]) and \tilde{S}_{ij} is the rate-of-strain tensor

$$\tilde{S}_{ij} = \frac{1}{2} \left(\frac{\partial \tilde{u}_i}{\partial x_j} + \frac{\partial \tilde{u}_j}{\partial x_i} \right). \quad (2.17)$$

From equation 2.16, the turbulence model requires an expression for μ_t . Usually, $k - \varepsilon$ -like models represent μ_t as a function of turbulent kinetic energy (k) and other quantity to obtain velocity and length scales. In the case of $k - \varepsilon$ the other quantity is the turbulent dissipation (ε) obtaining the turbulent

viscosity as

$$\mu_t = C_\mu \frac{k^2}{\varepsilon}, \quad (2.18)$$

where $C_\mu \simeq 0.09$. In the case of the $k - \omega$ methods, quite popular also, the inverse of dissipation (ω) is used instead of ε . The transport equation for k comes directly from Navier-Stokes and energy conservation equations, while the equation for the other variable is more or less constructed by means of dimensional analysis. In particular, standard $k - \varepsilon$ turbulent model obtains these terms from additional transport equations as follows:

$$\frac{\partial \bar{\rho} k}{\partial t} + \frac{\partial \bar{\rho} k \tilde{u}_j}{\partial x_j} - \left(\mu + \frac{\mu_t}{\sigma_\mu} \right) \frac{\partial^2 k}{\partial x_j^2} = G - \frac{2}{3} \bar{\rho} k \frac{\partial \tilde{u}_j}{\partial x_j} - \bar{\rho} \varepsilon, \quad (2.19)$$

$$\begin{aligned} \frac{\partial \bar{\rho} \varepsilon}{\partial t} + \frac{\partial \bar{\rho} \varepsilon \tilde{u}_j}{\partial x_j} - \left(\mu + \frac{\mu_t}{\sigma_\varepsilon} \right) \frac{\partial^2 \varepsilon}{\partial x_j^2} = & C_{1\varepsilon} \left(G \frac{\varepsilon}{k} - \frac{2}{3} \bar{\rho} \varepsilon \frac{\partial \tilde{u}_j}{\partial x_j} \right) \\ & - C_{2\varepsilon} \bar{\rho} \frac{\varepsilon^2}{k} - C_{3\varepsilon} \bar{\rho} \varepsilon \frac{\partial \tilde{u}_j}{\partial x_j}. \end{aligned} \quad (2.20)$$

Note μ_t equation and k and ε transport equations have been written here as they are coded by default in OpenFOAM. Also, the tilde over u_i means velocity field has been Favre-averaged,

$$\tilde{\Phi} \equiv \frac{\overline{\rho \Phi}}{\bar{\rho}}. \quad (2.21)$$

The only modification on the model has been applied to the value of $C_{1\varepsilon}$ in order to avoid an elevated dispersion of the jet [JP82; Dal98; Nin07; Cha13]. Janicka et al. [JP82] and Dally et al. [Dal98] recommend values of $C_{1\varepsilon}$ 1.52 and 1.60, respectively. In a recent thesis, Chavez [Cha13] confirmed the values proposed for $C_{1\varepsilon}$ comparing the entrainment of both diesel-like gas jets and diesel spray calculations with the constant found by Ricou and Spalding (i.e. $C_e = 0.32$). In the present calculations, $C_{1\varepsilon} = 1.60$ have proven a good agreement with experimental penetration 4.3(a).

In the interest of completeness in the physical understanding of the model, it is useful to rewrite the model (eq.2.18) based on a physical interpretation using a velocity and length scale

$$\mu_t = u' \ell, \quad (2.22)$$

then k and ε provide a turbulent velocity scale $u' \sim \sqrt{k}$ and a turbulent length scale of $\ell \sim k^{1.5}/\varepsilon$. In this interpretation, the length scale is thought of as the integral scale of the turbulence even though the flow is not homogeneous.

2.3.3 Large-Eddy Simulation

Although a brief introduction on RANS models have been provided in the previous section here we go back to the main subject of this thesis, and LES methodology is introduced. The parallelism established between RANS and LES models is a pedagogic device emulated from Rutland's general review on LES for ICE [Rut11]²³.

RANS velocity field is decomposed in two components: averaged and fluctuating. In the case of LES the decomposition divides the field into spatial filtered $\tilde{\mathbf{u}}$ and sub-grid scale \mathbf{u}' .

$$\mathbf{u} = \tilde{\mathbf{u}} + \mathbf{u}'. \quad (2.23)$$

Note, we intentionally keep the same notation for both turbulent approaches. The operation that produces the tilde²⁴ and the prime²⁵ are purely conceptual and, as a consequence, they are not explicitly formulated in CFD codes. The final choice of the turbulent model²⁶ specifies the actual formulation of those operators. As a filtering operator the tilde ($\tilde{}$) filters some of the scales for LES where it filters all of them for RANS. Consequently, LES puts higher demands on the validation process than RANS [Kem07] due to the higher physical description of turbulence and its newness when applied to some fields of research.

In the same way, τ_{ij} is never calculated in the code but modeled by the specific turbulent model. Here, not only the name of the variable (i.e. *sub-grid stresses* instead of *Reynolds stresses*) but the model used sets the first actual

²³In addition, the author of the thesis highly recommends the reading of the review.

²⁴Ensemble averaging in RANS or spatial filtering in LES

²⁵Fluctuating in RANS or sub-grid in LES

²⁶Note the distinction between turbulent model (e.g. $k - \varepsilon$ (RANS), Smagorinsky (LES), One equation eddy (LES)...) and the turbulent approach (i.e. RANS, LES, DNS)

difference between LES and RANS. Therefore, *at the equation level, the similarity is clear and it is probably best to view LES as an evolving development of turbulence modeling rather than a completely new approach distinct from RANS* [Rut11].

Following, we present the differences on the turbulence modeling of the term τ_{ij} for the models used in the present thesis. The selection of the models is focused on those commonly found in engine applications. Besides basic turbulence modeling equations, specific formulation to address particular turbulent-related problems (e.g. spray liquid-gas interaction) will be included.

2.3.3.1 No sub-grid scale model.

In this case the modeling relies on the numerical dissipation related to the methods selected, and no further modeling is done. Hence, the cell size must be restricted so that numerical dissipation is equivalent to the one generated by the eddies contained within the cell (i.e. viscosity of modeled eddies). This “*equilibrium*” can be achieved by means of very dissipative numerical methods [Bor+92] or a very refined mesh. This last option can be seen as a LES approaching DNS spatial discretization or a low resolution DNS. However, both situations and the lack of control of μ_t prevent from using this approach for practical engine application, as already discussed.

2.3.3.2 Smagorinsky.

The Smagorinsky turbulence model was the first applied to LES [Sma63]. The model obtains the sub-grid stress term (τ_{ij} at eq. 2.2) as a function of turbulent viscosity and the strain rate. Back to eq.2.16, the turbulent viscosity is algebraically modeled without extra transport equation as

$$\mu_t = \bar{\rho}(C_S\Delta)^2|\tilde{S}_{ij}|, \quad (2.24)$$

where C_S is the Smagorinsky constant. This constant has a theoretical value in the range [0.1-0.2] [Pop00]. Δ is the filter length, and $|\tilde{S}_{ij}|$ measures the magnitude of the resolved strain rate²⁷. The filter length (Δ) is a measure

²⁷Frobenious norm: $|\tilde{S}_{ij}| = \sqrt{2\tilde{S}_{ij}\tilde{S}_{ij}}$

of the actual cell size: cube root of the cell volume, maximum length of the cell edges, maximum distance between cell center and cell faces, etc. Hence Δ filters flow scales that can not be captured by the spatial discretization providing a distribution of the sub-grid scale characteristic lengths (similar to Figure 3.5). Following previous analogy of μ_t as the product of velocity and length scale, $u' \sim \Delta|\tilde{S}|$ and $\ell \sim \Delta$.

The Smagorinsky constant varies with both aspect ratio [Sco+93] and the mean shear [Hor93; Yak+89]. Although some dynamic implementation of the Smagorinsky model allow to determine C_S as a function of time and position [Ger+91], some studies show little to be gained in the case of high Reynolds number free flows of the type considered [Jon+10]. Moreover, despite the improvements achieved by an automatic algorithm to set the turbulent coefficient, inherent drawbacks from viscous formulation remain unsolved. Fundamentally²⁸, Boussinesq assumption expressed in eq. 2.16 is known to be incorrect (i.e. principle directions of τ_{ij} do not align with \tilde{S}_{ij})²⁹ [Cla+79].

Finally, a note on the actual implementation of the model in OpenFOAM. In order to keep an uniform structure within the viscous models, C_S does not appear explicitly but as a function of two different constants, C_k and C_ε . In the specific case of incompressible flows C_S can be obtained as follows:

$$C_S = \frac{C_k^{\frac{3}{4}}}{C_\varepsilon^{\frac{1}{4}}}, \quad (2.25)$$

and the sub-grid scale turbulent kinetic energy is coded as follows:

$$k = 2 \frac{C_k}{C_\varepsilon} \Delta^2 |\tilde{S}|^2, \quad (2.26)$$

which allows to obtain characteristic sub-grid velocity³⁰ $u' \sim \Delta|\tilde{S}|$ from the sub-grid scale field for k generated by OpenFOAM as $u' \sim \sqrt{k}$.

²⁸ There are other drawbacks, the model provides dissipation over a wide range of length scales instead of being focused at the small scales (dense grid required), and the lack of an specific equation for sub-grid kinetic energy (required for combustion and spray models) but the main restriction of the model is the Boussinesq assumption.

²⁹ Principle directions of τ_{ij} do not align with \tilde{S}_{ij}

³⁰ Needed, for example, to complete radial distribution of Reynolds stresses

2.3.3.3 Spalart-Allmaras.

Compared with Smagorinsky model, the Spalart-Allmaras one [SA94] introduces an extra transport equation. Here, μ_t is calculated by multiplying the transported variable $\tilde{\nu}$ (modified turbulent kinematic viscosity) by a function (f_{v1}):

$$\mu_t = \bar{\rho}\tilde{\nu}f_{v1}, \quad (2.27)$$

where

$$f_{v1} = \frac{\chi^3}{\chi^3 + c_{v1}^3}, \quad (2.28)$$

$$\chi = \frac{\bar{\rho}\tilde{\nu}}{\mu}, \quad (2.29)$$

and the one-equation model is given by:

$$\frac{\partial \bar{\rho}\tilde{\nu}}{\partial t} + \frac{\partial \bar{\rho}\tilde{\nu}\tilde{u}_j}{\partial x_j} - \frac{\partial}{\partial u_j} \left[\left(\bar{\rho}\tilde{\nu} + \frac{\mu}{\sigma} \right) \frac{\partial \tilde{\nu}}{\partial x_j} \right] \quad (2.30)$$

$$- \frac{\bar{\rho}c_{b2}}{\sigma} \left| \frac{\partial \tilde{\nu}}{\partial x_i} \right|^2 = \bar{\rho}c_{b1}\tilde{S}\tilde{\nu} - \bar{\rho}c_{w1}f_w \left(\frac{\tilde{\nu}}{\tilde{d}} \right)^2. \quad (2.31)$$

Additional definitions are given by the following equations:

$$\tilde{S} = f_{v3}\sqrt{2}|\nabla \times \tilde{\mathbf{u}}| + f_{v2}\frac{\tilde{\nu}}{\kappa^2\tilde{d}^2}, \quad (2.32)$$

where the first term of the right hand side is proportional to the supposed-to-be magnitude of the vorticity. \tilde{d} takes into account not only the filter size, but the distance from the field point to the nearest wall ($\tilde{d} = \min(c_{des}\Delta, y_{wall})$), and

$$f_{v2} = \frac{1}{\left(1 + \frac{\bar{\rho}\tilde{\nu}}{\mu c_{v2}}\right)^3}, \quad (2.33)$$

$$f_{v3} = \frac{(1 + f_{v1})}{c_{v2}} \frac{3 \left(1 + \chi/c_{v2} + (\chi/c_{v2})^2 \right)}{(1 + \chi/c_{v2})^3}, \quad (2.34)$$

$$f_w = g \left[\frac{1 + c_{w3}^6}{g^6 + c_{w3}^6} \right]^{1/6}, \quad (2.35)$$

$$g = r + c_{w2} (r^6 - r), \quad (2.36)$$

$$r = \min \left[\frac{\check{\nu}}{\tilde{S} \kappa^2 \check{d}^2}, 10 \right]. \quad (2.37)$$

The constants in the previous formulas are given at Table 2.2.

σ	c_{b1}	c_{b2}	c_{v1}	c_{v2}	c_{des}	κ	c_{w1}	c_{w2}	c_{w3}
2/3	0.1355	0.622	7.1	5.0	0.65	0.41	$c_{w1} = \frac{c_{b1}}{\kappa^2} + \frac{1+c_{b2}}{\sigma}$	0.3	2.0

Table 2.2: Spalart-Allmaras model constants (compressible flow)

The original Spalart-Allmaras model (1994) is a one equation model developed for aerodynamics applications including boundary layer separation [SA94]. The model as it appears coded for compressible flows in OpenFOAM does not fully match with any of the fourteen versions found in literature. However, this compressible form has certain changes that appeared at the *SA-salsa*³¹ version [Run+03]

Finally, compared with Smagorinsky model (zero-equation model) the extra computational effort of the transport equation must to be compensated by an improvement in the results. Note, regardless of the complexity of the model (i.e. ten model constants) it still inherits the drawbacks of the eq. 2.16 viscosity models previously addressed.

³¹Primarily developed to extend the predictive capability of the model for non-equilibrium conditions.

2.3.3.4 One equation eddy (OEE).

OEE turbulent model [YH85] is a viscous model, like Smagorinsky and Spalart-Allmaras ones. As Spalart-Allmaras does, it introduces an extra transport equation, but for the sub-grid turbulent kinetic energy (k). Consequently, it is also known as a k -equation model where the sub-grid turbulent viscosity (μ_t) from eq. 2.16 is modeled as a function of k as follows:

$$\mu_t = C_k \bar{\rho} \Delta \sqrt{k}. \quad (2.38)$$

For compressible flows, the transport equation for k is implemented in OpenFOAM as

$$\frac{\partial \bar{\rho} k}{\partial t} + \frac{\partial \bar{\rho} k \tilde{u}_j}{\partial x_j} - (\mu + \mu_t) \frac{\partial^2 k}{\partial x_j^2} = G - \frac{2}{3} \bar{\rho} k \frac{\partial \tilde{u}_j}{\partial x_j} - C_\varepsilon \bar{\rho} \frac{k^{3/2}}{\Delta}, \quad (2.39)$$

with $C_k = 0.094$ and $C_\varepsilon = 1.048$ as default turbulent coefficients. The last term of the right hand side is known as the sub-grid dissipation source term (ε). The other two terms are known as the sub-grid production source term. Note, from eq. (2.38) that sub-grid turbulent velocity $u' \sim \sqrt{k}$ and length scale $\ell \sim \Delta$. Hence, ε is not used to obtain length scales or time scales as it is in RANS modeling. Thus, dissipation modeling is much less critical, and simple models seem to work reasonable well.

This one-equation may allow the use of coarser grids than no-model or a zero-equation model because it considers additional processes at a sub-grid level (i.e. convection, dissipation and production of sub-grid kinetic energy). Also, as the Smagorinsky model, there is a formulation to compute turbulent coefficients for any cell at any time step [KM95]. Although already implemented in OpenFoam for incompressible and compressible flows, this advanced formulation is not tested since this feature has not been developed for the dynamic structure model. In this way all models are equally treated.

Finally, some implementations of the model include a source term to account for the effect interaction between the gas phase and the liquid on the sub-grid kinetic energy. Again, spray cases within this thesis has been calculated with the model as implemented by default in OpenFOAM (i.e. no source

term on the k -equation). The influence of gas-liquid interaction on k has been addressed for the dynamic structure turbulent model.

2.3.3.5 Dynamic structure (DS)

Contrary to the models previously presented, the dynamic structure model, developed by Pomraning and Rutland [PR02] does not use the turbulent viscosity approach. The model was implemented in OpenFOAM as it appears in a work of Bharadwaj and Rutland [BR10a]. In his work, Bharadwaj presents a complete derivation of the DS model as well as LES continuity equations for Lagrangian-Eulerian simulations of two phase flows. The following is a brief presentation of the model to show the actual implementation and highlight the main differences with viscous models. The model obtains the sub-grid stress term, τ_{ij} as a function of a tensor coefficient, C_{ij} and the sub-grid turbulent kinetic energy k ,

$$\tau_{ij} = \bar{\rho} C_{ij} k, \quad (2.40)$$

where k is obtained from a transport equation

$$\frac{\partial \bar{\rho} k}{\partial t} + \frac{\partial \bar{\rho} k \tilde{u}_j}{\partial x_j} - \mu_t \frac{\partial^2 k}{\partial x_j^2} = \underbrace{-\bar{\rho} \tau_{ij} \frac{\partial \tilde{u}_j}{\partial x_j}}_{\text{Production}} - \underbrace{C_\varepsilon \bar{\rho} \frac{k^{3/2}}{\Delta}}_{\text{Dissipation}} + S_k, \quad (2.41)$$

and the tensor coefficient comes from the dynamic approach [Ger+91]

$$C_{ij} = 2 \frac{L_{ij}}{L_{kk}}, \quad (2.42)$$

where L_{ij} is the modified Leonard stress tensor given by

$$L_{ij} = \widehat{\tilde{u}_i \tilde{u}_j} - \widehat{\tilde{u}_i} \widehat{\tilde{u}_j}. \quad (2.43)$$

This quantity is known in the sense that it can be calculated from the grid level velocities. Here $(\widehat{\quad})$ indicates the test-level filter, which is larger than the grid-level filter.

Regarding gas-particle interaction, a general review on the effect on the turbulence of the gas phase as well as a specific study on the influence on the sub-grid part of the flow can be found at Bharadwaj's thesis [BR10a]. In eq. 2.41, S_k is the spray source/sink term which models the effect of droplet-gas ambient interaction on the sub-grid turbulent kinetic energy as a dot product of the filtered drag and the gas phase sub-grid velocity.

$$S_k = -F_i u'_i, \quad (2.44)$$

where F_i is the summation of parcel drag within the cell

$$F_i = \left(\sum_p F_{i,p} \right) / V_{cell}, \quad (2.45)$$

and the sub-grid gas velocity u'_i is modeled as ³²

$$u'_i = 2\tilde{u}_i - 3\tilde{\tilde{u}}_i + \tilde{\tilde{\tilde{u}}}_i. \quad (2.46)$$

Hence, spray source term for sub-grid turbulent kinetic energy, S_k can be written as

$$S_k = -\frac{3}{4} \frac{C_D}{V_{cell}} \sum_p \left\{ \frac{m_p \bar{\rho} |\mathbf{U}_{rel}|}{d_p \bar{\rho}_l} (\mathbf{U}_{rel}) \left(2\tilde{u}_i - 3\tilde{\tilde{u}}_i + \tilde{\tilde{\tilde{u}}}_i \right) \right\}, \quad (2.47)$$

where C_D is the parcel drag coefficient, V_{cell} is the cell volume and $|\mathbf{U}_{rel}|$ is the magnitude of the relative velocity between the liquid droplet and gas³³,

$$\mathbf{U}_{rel} = \underbrace{u_{p,i}}_{u_{parcel}} - \underbrace{(\tilde{u}_i + u_{d,i})}_{u_{gas}}. \quad (2.48)$$

³²Obtained after applying an approximate deconvolution on the filtered gas velocity [Sho+07]. The extra tilde operations ($\tilde{\tilde{\cdot}}$) in this equation imply additional filtering applied through a test filter formed by an extra cell layer around the cell being filtered [BR10b].

³³Note the sign of equations 2.44 2.47 is opposite to the original papers because the definition of \mathbf{U}_{rel} .

Here, $u_{d,i}$ is the turbulent dispersion velocity as explained in section 2.5.6 and $u_{p,i}$ the parcel velocity. Note, S_k is included here because it is specific of DS turbulent model. The rest of source terms for the continuity equations (eqs. 2.1 to 2.4) can be found at its particular section within the phenomenological spray models 2.5.

Through τ_{ij} , a budget of turbulent kinetic energy is maintained between the grid scale velocity (eq. 2.2) field and the sub-grid k-equation. Note how Leonard stress tensor re-shapes k to provide a higher momentum to those directions of higher filtered velocity. Also, the word “dynamic ” refers to this feature of the turbulent model but has no relation with the automatic estimation of the turbulent coefficients as it is understood for other turbulent models.

Besides already mentioned engine applications of LES models, the following review is focused on the state of the art of LES of the spray. Part of it have been covered with the exposition of the previous basic model.

As with the approach of the present thesis, the studies on jet flows are the precursor of spray simulations and diesel spray in particular. Regarding the “simpler” model, back in 1992 Boris et al. [Bor+92] already reviewed mesh convergence of LES for a jet flow³⁴. The equilibrium happens when the residual numerical diffusion present is smaller than eddy diffusivity of the turbulent flow. From the pure description of the phenomena the delicacy of the balance reveals its instability (e.g unsuited for engine conditions). That said, some studies have used this approach for diesel applications with fine meshes [Vuo+08].

Others include this model as a reference to compare with. This is the case of [Xue+13] where the results with no sub-grid scale model are checked against Smagorinsky (viscous, zero-equation model) and Dynamic Structure (non-viscous, one-equation model).

Smagorinsky model has been used for direct injection gasoline sprays: with RANS correlations [Ara+07], with the VOF method to simulate internal and near-nozzle flow [Bia+07] or to examine cycle-to-cycle variations [Ado+07; Gra+12]. Regarding diesel sprays, some of the most recent work has been carried out by a group at Argonne National Lab. (ANL) in Chicago. Som et al.

³⁴Due to the trade off between the smaller simulated eddies and the numerical diffusion of the method.

[Som+12] showed that a Smagorinsky-based LES model captured the instantaneous equivalence ratio and soot contours more accurately than a RANS-based model. This model has been used as well to better understand HCCI [Yu+07; Joe+08; Vre+08].

Another zero-equation model is the *scale similarity*. This is not a viscosity model nor uses an energy budget to track the sub-grid kinetic energy. Instead, it assumes that unresolved sub-grid scales can be approximated by the smallest resolved scales. Hence the concept supposed a break through when proposed by Bardina et al. in 1980 [Bar+80]. Despite its initial instability, studies of HCCI combustion with diesel fuel have been successfully carried out [Yu+06; Yu+08].

OEE and DS represent a higher order of turbulence model (i.e. an extra transport equation) Regarding the viscous OEE, comparisons with RANS model for direct injection diesel engines have been reported [Kaa+03]. Here, the turbulence model was coupled with advanced combustion models (i.e. Magnusson Time-scale model) for which the extra transport equation term is used. Afterwards deVillers et al. [Vil+04] coupled the turbulent model with VOF to study near-nozzle flow and primary breakup in a diesel spray. More recent studies on the coupling of this turbulent model with classic spray models belong to a group at Doshisha University [Hor+06; Hor+07; Hor+08; Fuj+09].

Short after its implementation, DS had been already used to better understand advanced combustion strategies with the “Engineering LES” spirit followed by this thesis. In this regard, studies by Jhavar et al. report the mixing effects on HCCI [JR06] and the combustion modeling on PPC [Hu+07].

The proven robustness and flexibility of DS has encourage researchers to implement the model into open-source as well as commercial codes. In this regard it is worthy to mention a recent investigation on grid convergence under diesel spray conditions [Sen+13a]. The study is carried out with CONVERGE® where calculations are performed with AMR, drawing similar conclusions than unvaried meshes from the present thesis.

2.4 Interface and particle tracking

Besides the type of governing equations used and the turbulent modeling, two phase flow simulations can be classified depending on the approach to resolve the liquid phase. As a consequence, specific methods to follow the liquid-gas interface evolution may be needed.

Liquid phase can be addressed from a Lagrangian or a Eulerian frame of reference. Given that the gas phase is solved with an Eulerian reference frame, the two basic approaches are the Lagrangian-Eulerian (L-E) and the Eulerian-Eulerian (E-E)³⁵. L-E combines two numerical approaches:

- Gas phase is solved by Navier-Stokes equations applied to each of the cell volumes defining the mesh which is known as the *Eulerian* description
- Liquid phase is discretized into small amount of fluid such as droplets or *parcels*. A parcels gathers a statistical number of droplets with the same characteristics (i.e. diameter, mass, velocity, temperature, ...). Fluid units are labeled and followed through space and time in a Lagrangian reference frame. Temporal evolution of the liquid position and characteristics [Wil85] are modeled by phenomenological spray models of injection, atomization and break-up, collision, coalescence and evaporation (Section 2.5)

The statistical approach originally proposed by Dukowicz [Duk80] is known as the *Discrete Droplets Model* (DDM). In this method, liquid fluid is discretized in parcels. Note droplets within a parcel do not interplay with each other [Hey88]. Also, the liquid spray equation is solved by means of Monte-Carlo method. Compared with *Continuum Droplets Model* (CDM) -where each single droplet is represented- it has a lower computational cost and it can be controlled in the first place by the number of parcels being injected.

Since the singular interface droplet-gas can not be extended to the whole spray due to computational restrictions (as it happens with turbulent scale resolution) the flow processes must be addressed on a greater scale than the

³⁵Here, nomenclature designs first liquid phase and then gas phase. This is not the traditional way, but we choose this in order to better distinguish from advanced atomization models ELSA as we will see later on

droplet diameter [Sti03]. In this regard, phenomenological spray models take into account the gas phase flow to calculate each parcel evolution and at the same time they collect the changes for all of them (i.e. the entire spray) on the spray source terms. To close, gas-liquid interaction is fulfilled by including those spray source terms at the continuity equations (eq. 2.1 to 2.4).

L-E model was initially developed for disperse sprays. Void fraction³⁶ limit on CFD codes to ensure the proper coupling between gas and liquid equations³⁷ is low (~ 0.1). However, L-E method has been extended to simulate dense sprays due to the simplicity and reasonable efficiency to track liquid position and evolution. Depending on the flow regime, Diesel spray presents a liquid core near the nozzle (i.e. Parcels with diameter about the nozzle diameter $d_p \sim d_0$). Hence, some practical considerations restrain the use of L-E method for Diesel spray simulations:

- Near the nozzle exit, the void fraction limits the minimum size of the cells. It is clear to see how if there are cells within the nozzle orifice, in those cells the void fraction is 1.0, violating model hypothesis. In this regard, Abraham [Abr97] showed that $d_0/2$ is the minimum resolution to model a turbulent gas jet with RANS³⁸. Hence, we reach a implicit contradiction that prevents from having enough spatial discretization near the nozzle. This lack of mesh resolution affects phase interaction such as break-up and coalescence as well as momentum transfer as displayed in section 4.3.

In order to overcome this limitation different strategies have been used over the years:

- Avoid the trouble spot [Vuo+08; Vuo10]. Here the inlet BC is not place at the nozzle exit but several diameters far. At the inlet, gas velocity and droplet velocities are specified in addition to the initial size distribution of droplets. Similar strategy has been used by Martinez et al. for the E-E method [Mar+10; Til+13]
- Place the injector at the intersection of four cells. Note how the injector location in relation to the grid can be arranged in two possible ways (i.e. in one cell or at the intersection of four cells).

³⁶Ratio between gas volume and liquid volume

³⁷Note, liquid and gas phase equations are artificially linked up

³⁸ $d_0/4$ is the minimum recommended

As shown by Fabian Peng Kärholm et al. [Fab+08] this has an effect on the penetration, even if both grids have the same cell sizes.

- Adaptive mesh refinement (AMR) [Sen+13b] can include a void fraction limit. However, Xue et al. [Xue+13] have recently shown how this approach maintains stability for large liquid volume fractions such that cell sizes below the nozzle diameter can be explored.
- Mesh independent 1D models [Yan+00; Cha13] have overcome L-E model limitations for near-nozzle dense flow region modeling, where model basic hypothesis are not longer valid. In this regard, Chavez [Cha13] developed an approach combining Eulerian 1-D spray model based on turbulent jet theory and L-E 3D-CFD. The 1D phenomenological model was used to determine the gas-phase velocity along the spray axis and modify the relative velocity between the gas and liquid phases within the vicinity of the nozzle (five times the non-perturbed zone). Although applied to RANS simulations, LES present the same limitations and the solution may improve them as well.

Finally, the following three remarks are proposed by Stiesch [Sti03] to ensure a proper simulation of L-E sprays.

- Limitations to the integral scale: within the spray region, the turbulent scales are restricted to the spray diameter.
- Mesh conformed to the spray: the mesh set-up is adjusted to the spray orientation
- Avoid spray where droplets are modeled in great detail: spray sub-models including droplet interaction (e.g. coalescence) complicate statistical convergence. Also, O'Rourke's collision model is inherently grid dependent³⁹ [SR00].

As L-E is recommended for the disperse part of the sprays, E-E model provides a better prediction for the internal nozzle flow, the atomization region, and the zones with high concentration of droplets (e.g. dense zone of the Diesel spray). There are two approaches to differentiate between phases. Note, here

³⁹Its use may disguise the influence of the turbulent model within the refinement process

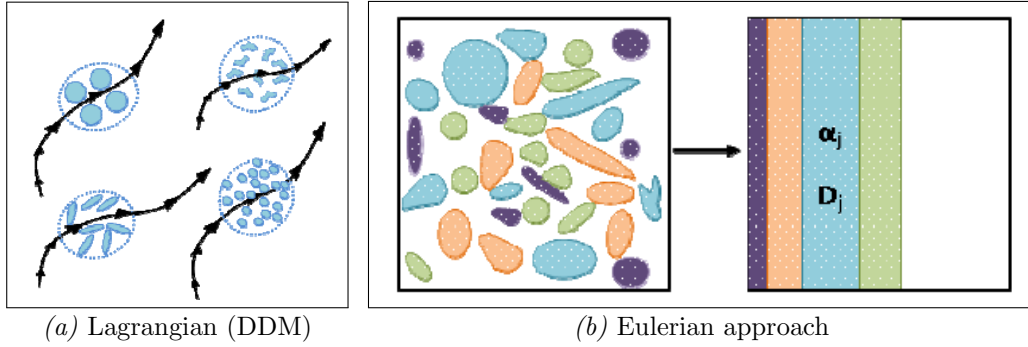


Figure 2.8: Scheme showing treatment of droplets (Adapted from Vujanovic et al. 2009 [Vuj+09])

we refer to flow phases with different state of the matter (i.e. liquid-gas) but same state mixtures may be resolved as well (i.e. liquid-liquid and gas-gas):

- Two-fluid model provide a group of continuity equations for each fluid. Those models are usually distinguished based on the method to track the interface. There are basically two groups of methods: sharp interface and diffuse interface. The diffuse interface is tracked by means of an extra surface density equation [Ish75]. Among sharp interface models two must be highlighted for their characteristics and applicability to Diesel spray simulations.

On one hand, *Volume of fluid* (VoF) [HN81] models small-scale topology fragmentation, hence, it is very suitable for Diesel sprays. The work of Deshpande et al. [Des+12] assessing the validity of a modified VoF approach included in OpenFOAM (interFoam) is of special interest. Simulations of capillary flows relevant to atomization resulted in good agreement with the results from literature. However, more than 20 years after the model was proposed, they found certain lack of superficial quality: a not inconsiderable ($\sim 10\%$) scope for improvement for the curvatures computed.

VoF model remains expensive in computing time since mesh requirement depends on the interface resolution required which implies simulations closer to DNS.

On the other hand, Level set method (LS) [Set99; SP00; SS03], solves a

hyperbolic equation for the topology to track the interface. For the fuel injection modeling, the LS method captures the liquid and gas interface, and follows it in time describing the liquid surface. Of special interest is the work of Anumolu et al. [AT13] where they address the well-known issue of volume loss. With the current implementation, the problem is solved even for objects that are of the size of one grid cell, and whose local radius of curvature falls below the local grid size. Hence, this powerful technique allows a detailed localization of the interface for coarse meshes.

- Single-fluid model provides NS equations for a single fluid of variable properties depending on the proportion of each of the phases. Sharp tracking interface models (LES-VOF [Vil+04]) as well as diffuse interface (ELSA [Val+01] and Sigma-Y [Nin07]) are used.
- Other methods applied to the computation of multiphase flow are: the Ghost Fluid Method (GFM)[Fed+99], the front tracking method [Try+01; Du+06], and Lattice-Boltzmann Method [San+99; Tak+00; Ina+04]. All these methods are mentioned here for the sake of completeness but their use is out of the scope of the present thesis.

In the present work diesel-like gas jets have been modeled with the “single fluid” approach (i.e. one phase -gas- compound of the same specie with two different names) and the liquid diesel spray with the L-E method. This modeling strategy has several advantages: it offers a good efficiency for RANS as well as for LES⁴⁰ when a good prediction of macroscopic variables are achieved. Also, it has been proved to successfully include any of the processes taking place inside a the ICE combustion chamber. Finally, as we have seen, the L-E approach has a inherent mesh limit where alternative E-E approaches need higher mesh refinements. Since one of the main goals is to keep the computational cost limited, it is important to maintain liquid-gas modeling requirements and turbulent modeling cost in the same order of magnitude.

2.5 Phenomenological spray models

In this section a brief introduction of the physics depicted at Figure 2.1 along with related phenomenological models for L-E DDM Diesel spray simulations

⁴⁰A priori same computational cost for both turbulent approaches

is presented.

2.5.1 Spray injection

Injection systems have been already mentioned (section 1.1). A critical part of the injector system is the nozzle, which channels the fuel to the combustion chamber, by means of the important pressure drop existing between the chamber and the injection. Chamber pressures are about 5–15MPa where the range of injection pressures are 10–200MPa. Such pressure differences are the key for the fuel to break up into small droplets, which enhances vaporization and air mixture.

The present work is focused on the air-fuel mixture after the nozzle. Hence, the characteristics of the previous wall bounded flow is not analyzed. However, the flow at the nozzle exit sets the inlet boundary conditions for the spray simulations, which implies a minimum knowledge of the basic parameters determining the initial spray structure. Following, some of the parameters needed: the values of discharge coefficient (C_d)⁴¹, theoretical mass flow rate⁴², mass flow rate (\dot{m})⁴³, total mass injected, and temperature. Geometric characteristics and the injector topology (e.g. single orifice axisymmetric) are necessary as well. Amongst geometric parameters, nozzle diameter (d_0), characteristic length (L_0), and curvature radius (r) warn about the presence and intensity of cavitation. Several investigations confirm the influence of cavitation, not only on the injection area and effective velocity, but on the atomization, the spray shape and mixture process [Sal03; Gim08; Mor11; Par+08] (Figure 2.9). Hence, if present, cavitation has to be taken into account both on the injection and the atomization models.

As it has been mentioned, spray simulated under the L-E DDM approach is injected into the domain on specific point(s)⁴⁴ that can be located anywhere in the domain. An injection point can be placed on a cell vertex or cell centre [Fab+08] or multiple points can be randomly distributed following a certain topological restriction [Xue+13; Vuo10]. In any case, it is necessary to provide initial velocity, angle, diameter, mass and temperature as well as fuel

⁴¹Ratio between measured and theoretical mass flow rate.

⁴²Obtained through Bernoulli equation.

⁴³Or momentum flux \dot{M} .

⁴⁴An entity that has a location in space or on a plane, but has no extent.

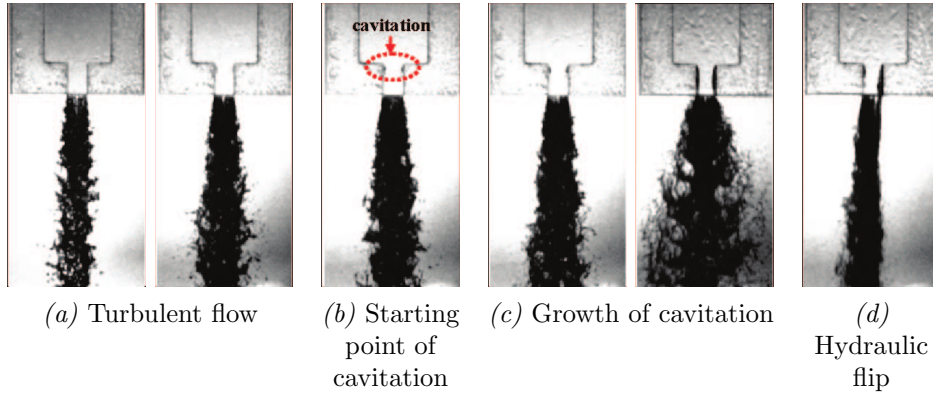


Figure 2.9: Diesel flow characteristics under different cavitation stages (Adapted from Park et al. 2008 [Par+08])

composition of the parcel injected.

Nozzle empiric sub-models determine injection velocity and effective area. Depending on geometric parameters, flow regime and in-cylinder conditions, these sub-models take into account the effect of cavitation inception and development as well as flow detachment inside the nozzle. Some models implemented in CFD codes are the Max Plank Institute model (MPI) developed by Obermeier [Obe91] (*Star-CD*) and Sarre et al. [von+99] (KIVA). Primary atomization models are applied to the injected parcels to generate the initial droplet population as explained in the following section. However, parcels may be injected with a certain size distribution (in contrast to $d_{\text{parcel}} \sim d_0$) replacing the effect of primary atomization. In order to model statistical distribution of droplet sizes a characteristic average diameter has to be known beforehand. Moreover, a previous evaluation of different functions is required in order to find the one matching experimental distribution [Lef89]. Amongst these functions⁴⁵ Rosin-Rammler one [RR33] is the most widely used for Diesel spray simulations. As an example, the expression is included here:

$$Q = 1 - e^{-\left(\frac{D_d}{X}\right)^q}, \quad (2.49)$$

where X and q are constants⁴⁶ and Q is the fraction of total volume taken by

⁴⁵Normal, Log-Normal, Nukiyama-Tanasawa [NT39].

⁴⁶The higher the exponent q , greater the homogeneity of the spray. Usual values are within

droplets smaller than D .

These functions modeling the statistical distribution of droplet sizes are commonly used to initialize parcels in combination with empiric sub-models [BR10a]. With those, the only parameter missing is the direction of injection.

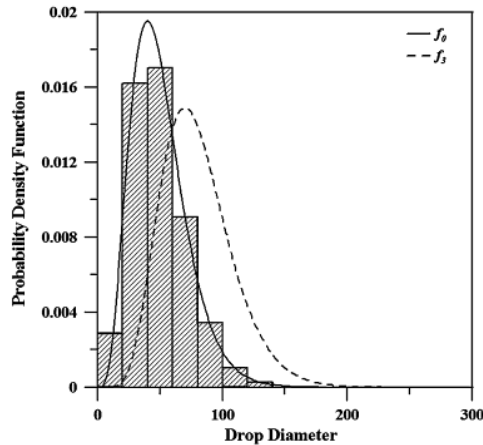


Figure 2.10: Discrete number probability function, its corresponding continuous number PDF, $f_0(D)$, and its corresponding continuous volume PDF, $f_3(D)$ [Asg11]

2.5.2 Atomization and Break-up

Generally speaking, atomization is the physical process in which the kernel of a liquid jet is broken up into droplets. As a consequence, the liquid surface area seen by the gas phase increases, enhancing subsequent processes such as vaporization or momentum transfer. Applied to Diesel sprays, it is usually divided into two stages:

1. Atomization: liquid core first break up into blobs or droplets due to internal forces such as liquid turbulence; inertial or jet velocity profile rearrangement effects, liquid supply pressure oscillations, and cavitation (figure 2.11) in competition with surface tension (which competes against the others drawing the liquid core together)

1.5 and 4.

2. Break-up: affects big blobs and droplets generated on the atomization⁴⁷ and generate smaller droplets. Both internal and aerodynamic forces are taken into account.

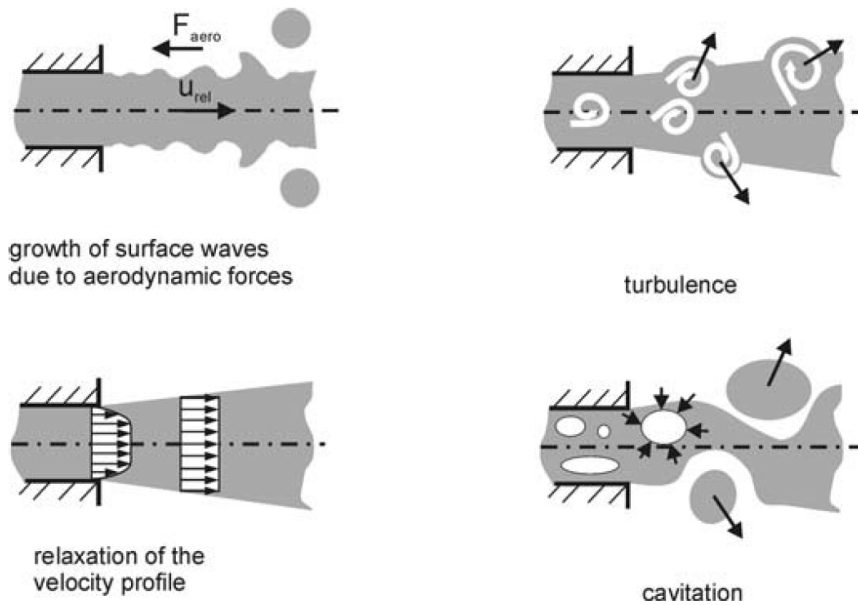


Figure 2.11: Atomization mechanisms at the nozzle exit [Bau06])

In his book, Lefebvre [Lef89] write down an excellent historical review on atomization. Just to cite some names, we can say that about 150 years ago, Lord Rayleigh [Ray78] presented a theory on jets instability. In his work, non viscous liquids are injected at low velocities and atomization occurs when surface tension is exceeded. Weber [Web31] extended Rayleigh's theory to viscous liquids and the effects of aerodynamic interaction when injection velocity increases. Reitz & Bracco [RB82] proposed the following atomization regimes as a function of increasing injection velocity:

1. Rayleigh mechanism of breakup (B): At low velocities, axisymmetric oscillations growing on the surface due to surface tension cause the jet to

⁴⁷Or previous break-up stages, provided that the droplet diameter is bigger than a critic diameter.

disintegrate into drops of fairly uniform size. Drop size is proportional to liquid viscosity and inversely proportional to jet velocity. Drop diameter is higher than jet diameter.

2. First regime due to aerodynamic interaction (C): At higher velocities, the break up into drops is caused by the growth of small oscillations on the surface (e.g. smaller than at the previous mode). Hence, breakup is caused by oscillations of the jet as a whole with respect to the jet axis so that the jet has a sinuous appearance. Drop diameter is similar to jet diameter
3. Second regime due to aerodynamic interaction (D): As jet velocity increases, the surface forces due to the relative velocity with air are greater. Hence, smaller waves on the surface become detached from the jet surface to form ligaments. Drops generated from the ligaments are much smaller than the initial jet diameter.
4. Atomization (E): At very high relative velocities atomization is complete within a short distance from the nozzle. A wide range of drop sizes is produced, the mean drop diameter being considerably less than the initial jet diameter.

These atomization regimes can be seen in figure 2.12 along with the stability curve where the liquid core length (L_{bu}) is related to injection velocity. Note, dripping (A regime) has not been mentioned.⁴⁸

Arrègle [Arr97] states that under current operating conditions, Diesel spray is within the last two atomization regimes. At the last regime L_{bu} has no dependency on injection velocity or droplet size. There are few points of agreement about L_{bu} under in-cylinder conditions. At the least, L_{bu} depends on the geometry of that nozzle and the presence cavitation, and the density ratio between the liquid injected and the air [RB82; Cor98]. It is important to properly asses this length, since physics involved in atomization and break-up are different and so the models address one or the other.

Regarding the first stage, besides L_{bu} , by generating the first droplets around the jet, it sets the initial conditions for the disperse region of the spray and the break-up stage [Fae96]. Unfortunately, there are several circumstances that difficult the study of this first stage of atomization: visualization of the

⁴⁸It has no interest under actual Diesel spray conditions.

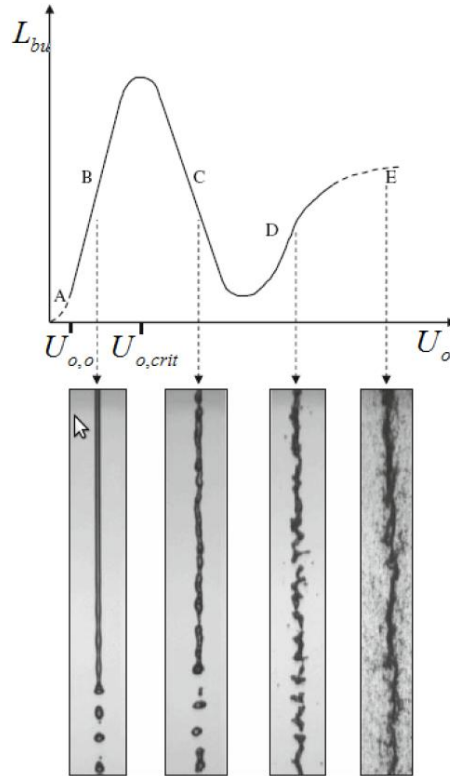


Figure 2.12: Atomization regimes. B ($Re_l = 790$, $We_g = 0.06$); C ($Re_l = 5500$, $We_g = 2.7$); D ($Re_l = 16500$, $We_g = 24$); E ($Re_l = 28000$, $We_g = 70$) [Dum08]

dense part of the spray and the almost immediately effect of break-up which modifies initial droplet population before experimental measurement can be performed.

Also, break-up and droplet distortion concur [Fae96]. Aerodynamic force distorts the droplet which eventually entails its break-up (if surface tension is exceeded). Moreover, distortion increases transport rate between phases and so affects mixture rate and at the same time break-up effect on droplet size affects mixture rate as well. Several break-up mechanism are represented in the figure 2.13 as a function of Weber number.

The atomization models commonly applied to diesel sprays are:

- Atomization sub-models: Kelvin-Helmholtz (KH) model (as outlined

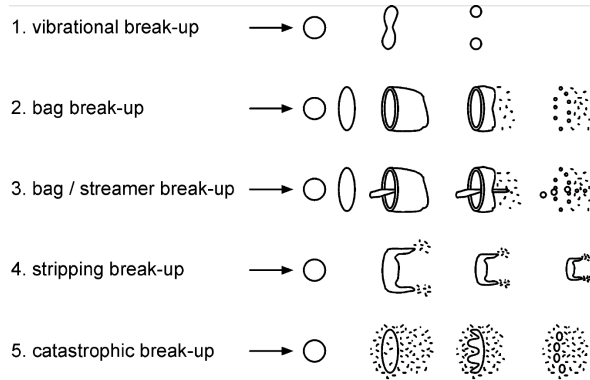


Figure 2.13: Break-up modes [Wie90]

by Reitz [Rei87]), Huh-Gosman (HG) model [HG91] and the more recent Kelvin Helmholtz-Aerodynamic Cavitation Turbulence (KH-ACT) model [SA10].

- Break-up sub-models: Reitz-Diwakar (RD) [RD87], Hsiang-Faeth (HF) [HF92a] and Rayleigh-Taylor (RT) models [Tay50].
- Break-up and droplet deformation sub-models: O'Rourke & Amsden [OA87] laied out a model based on Taylor's analogy (TAB) [Tay63]

Atomization sub-models can be arranged into two groups. The first group (e.g. HG, Nishimura et al. [NA00], KH-ACT) is based on the conservation of energy. Energy from the break up of cavitation bubbles or the wall friction is added to the turbulent kinetic energy (TKE) which adds a rupture force (additional to aerodynamic forces and surface tension). The second group (e.g. KH) was developed following the theory of liquid jet instabilities due to aerodynamic forces. Hence, the first group's formulation accounts for flow characteristics previous to the nozzle exit where the models of the second group do not consider such effects. These last models are purely based on the liquid core-gas aerodynamic interaction⁴⁹.

Sub-models usually describe different phenomena and they are usually combined to better model the different atomization mechanisms. As an ex-

⁴⁹In this regard, the second group provide simpler models. However, when different nozzle designs are simulated, the second group of models require an adjustment of the model constants to reproduce the differences at the initial jet conditions [Sti03]

ample, the combination of the models KH and RT is briefly introduced below. KH, also known as wave-breakup model, is based on the analysis of a Kelvin-Helmholtz instability growing on the surface of a cylindrical liquid jet. Due to the turbulence generated inside the nozzle, the jet surface is covered with a spectrum of sinusoidal waves with an infinitesimal axisymmetric displacement $\eta = \eta_0 \exp(\Omega t)$ (figure 2.14(a)). Gas-liquid interaction enhances wave amplitude (η) until stripped from the liquid core in form of a droplet. New droplet's diameter is a percentage⁵⁰ ($\sim 60\%$) of the faster growing wave (Λ). This instability is the only one applied to the injected blobs⁵¹ within the nozzle exit and the liquid core length (L_{bu}). Note, stripped parcels from the blobs are no longer part of the liquid core and are subject to both atomization and break-up models even if they are still located inside L_{bu} . As a consequence, KH model can be considered as a model for atomization and break-up, and RT only a break-up model

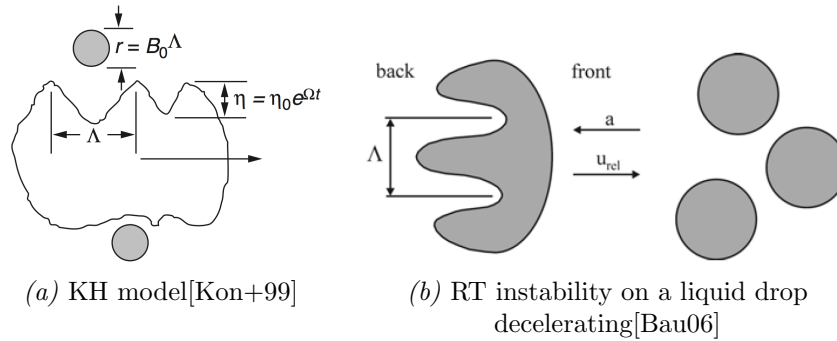


Figure 2.14: Schematic illustration of the KH and RT models

On the contrary, RT model is based the instability of the interface between two fluids of different densities in the case of an acceleration (or deceleration) normal to this interface. From figure 2.14(b), taking the droplet as a reference, the instabilities grow in the same direction as the acceleration (a) so instabilities grow at the back or the front of the droplet depending on the liquid-gas relative velocity. If Λ (remember, the fastest growing wave) is smaller than the droplet diameter new parcels are created with a similar diameter than Λ every characteristic rupture time.

⁵⁰Experimental results set the constant $B_0 \approx 0.6$.

⁵¹Blobs are parcels with the same diameter as the nozzle exit. This way to discretize the liquid core was introduced by Reitz and Diwakar [RD87]

The combination of KH and RT model has shown a better prediction of experimental distribution than KH model by itself [Su+96]. Diesel sprays are injected at high pressures, showing high velocity near the nozzle as well as a great deceleration. As it has been said, after L_{bu} (figure 2.15) there is a competition between the growth of instabilities from KH and RT (dominated by RT for the most part). Hence, by controlling L_{bu} controls droplet size distribution and related processes (e.g. the shorter L_{bu} , greater RT influence leading to smaller droplets and the consequent reduction in penetration, increase of evaporation, etc.)

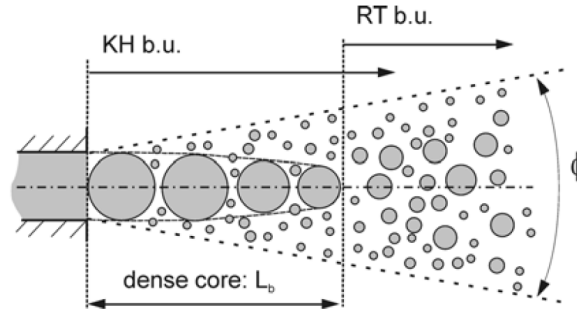


Figure 2.15: Combined blob-KH/RT model [Bau06]

Finally, the turbulent model has a direct influence on the atomization and break-up performance due to their use of relative velocity. As a consequence recent studies have revisited the historical combinations used for RANS, assessing their suitability combined with LES models [Apt+03; Hor+06; JL10; BR10a; Vit+12; Sen+13c; Xue+13; Sen+13a] and improving their performance [Koj+12]. One of the conclusions of this latter work is that as LES provide a better description of the physics and the turbulence, the modeling is improved in a global way.

2.5.3 Collision and coalescence

Coalescence is an antagonistic process to atomization [Arr97] where droplets join together making bigger ones. The probability of the process depends on the relative velocity of the droplets and the fuel concentration. Hence, collision frequency is higher in the vicinity of the nozzle (dense zone) and at the spray axis.

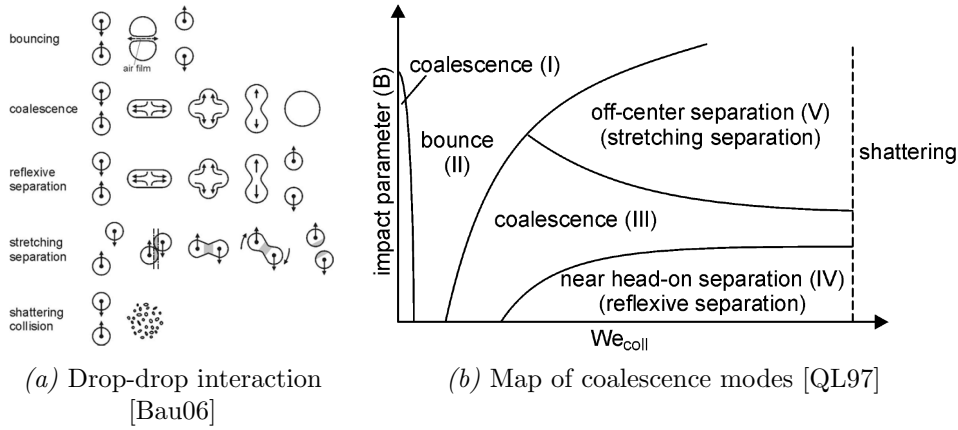


Figure 2.16: Coalescence regimes.

Collision mechanisms are complex. As seen in figure 2.16(a) several types of droplet-droplet interaction are possible and they may not end up in permanent coalescence. In this regard, researchers agree on the difficulty to measure droplet-air relative velocity and coalescence rate inside the dense region. There, spatial resolution is limited and the flow is opaque to optic diagnostic [Arr97; Fae87]. However, collision has a direct influence on the average diameter, dispersion and velocity of the droplets [PA02].

Regarding collision modeling, O'Rourke and Bracco [OB80], and Gavaises et al. [Gav+96] are the most used models. They are based on the experiments by Brazier-Smith et al. [BS+72] on water jets. Also, Post y Abraham [PA02] considered near nozzle conditions by including fuel density to the model proposed by O'Rourke.

Temporal and permanent collision are the only outcomes modeled by O'Rourke. For collision to happen two conditions must be fulfilled: parcels located at the same computational cell and collision probability been over a certain threshold. As pictured at figure 2.17(a) this model disregards parcel direction. This methodology has a strong mesh and time step dependence which can be resolved with adaptive mesh refinements⁵² [HS06] or simplifying characteristics length and time criteria⁵³ [PA02; GC97; MR07].

⁵²Refinements based on the parcel local density.

⁵³Distance between droplets subject to collision and average collision time.

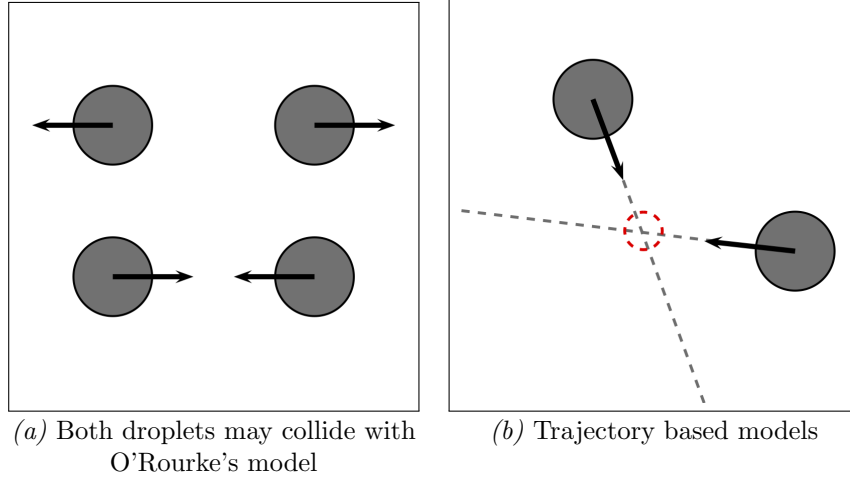


Figure 2.17: Collision requirements

2.5.4 Momentum transfer

Momentum transfer between droplets and surrounding gas can be described by Newton's law and aerodynamic drag:

$$F_d = \frac{\partial m_p \mathbf{u}_p}{\partial t}. \quad (2.50)$$

Note drag force is due to variations on velocity $m_p \partial \mathbf{u}_p / \partial t$. However parcels may change mass ($m^n \neq m^{n+1}$) under evaporative conditions, which affect the amount of momentum transferred. Although, eq. 2.50 compact formulation include both effects, only the change of velocity is covered at the present section. The change of mass due to evaporation is addressed at the following section (section 2.5.5). Behind the dense part of the spray, drag force (F_d) prevails over other forces such as the pressure gradient, Basset, Magnus, etc [Arc+97]. Air entrainment is related to the momentum transfer between liquid and gas phase. As a consequence, its simulation is very important, due to the fact that fuel-air mixture is key on the combustion process.

Basic fluid mechanics establish drag force over a sphere as a function of the shape and surface friction. The first is related to the pressure drop around the droplet, where the second is related to the shear stress generated by the

flow on the surface. In this regard, the sphere Reynolds number, Re_p , helps determine which effect controls drag force.

$$Re_p = \frac{\rho_g |\mathbf{U}_{\text{rel}}|^2 d_p}{2\mu_g}. \quad (2.51)$$

When Re_p is low, the drag coefficient (C_D) of a single solid sphere depends on the surface friction and can be modeled with Stokes' law. However, droplets at diesel sprays experience a high relative velocity ($\uparrow Re_p$) in which the flow is detached and the shape effect is greater than surface friction.

In addition, liquid droplets are far from behaving like perfect solid spheres [Ton+06]. Hence, several corrections must be applied to account for deviation from sphericity [HF92a; Liu+93], fuel density, the presence of other droplets [OB80; RI00], acceleration [Ing56], evaporation [Eis+67; Sir99], etc.

Regarding drag force modeling applied to L-E approach, the effect on the gas-liquid relative velocity affects break-up and coalescence models as well. Hence, drag force has an impact on both droplet size and distribution [Liu+93].

Drag force as seen by a single parcel can be modeled as

$$F_{i,p} = \frac{3}{4} \frac{\bar{\rho}}{\rho_l} \frac{m_d |\mathbf{U}_{\text{rel}}|}{d_p} \mathbf{U}_{\text{rel}} C_D, \quad (2.52)$$

where \mathbf{U}_{rel} has to be consistent with the definition provided at eq. 2.48.⁵⁴ In this way, liquid-gas interaction is included in the transfer between the energy related to the filtered velocity of the gas phase and the sub-grid scales.

Regarding C_D , there are several empiric correlations. As already mentioned, C_D varies as a function of Re_p so two regimes can be distinguished under high or low relative velocities (i.e. defined by whether the flow is detached from the droplet or not). From studies on a solid sphere with steady movement [Liu+93; Ams+89]⁵⁵:

⁵⁴In fact, as explained at eq. 2.44 the spray source term S_k at the sub-grid TKE is the dot product of the filtered drag and the gas phase sub-grid velocity.

⁵⁵A very similar expression was proposed by Reitz [Rei87]. Other interesting correlations may be found at Chen [YC76], Feng and Michaelides [FM01] and Clift et al. [Cli+78]

$$C_D = \begin{cases} \frac{24}{Re_p} \left(1 + \frac{1}{6} Re_p^{2/3}\right), & Re_p \leq 1000 \\ 0.44, & Re_p > 1000 \end{cases} \quad (2.53)$$

Several investigations proof how a droplet surrounded by others shows a lower C_D than a single one. In this regard O'Rourke and Bracco [OB80] and Rusche and Issa [RI00] propose expressions to include this behavior. Also, the correlation to account for spherical deviation of liquid droplets is based on the TAB break-up model [Liu+93]:

$$C_{D,dev} = C_D(1 + 2.632y_{dev}), \quad (2.54)$$

where y_{dev} is the deviation parameter. The final drag coefficient $C_{D,dev}$ is around 3.6 times greater than C_D when Re is high. Other researchers correct the drag following Hsiang y Faeth [HF92b] expressions⁵⁶.

Regarding the effect of evaporation on the droplet drag, Lefevbre [Lef89] mentions two factors: mass transfer, and the concentration and temperature gradients on the droplet surface⁵⁷.

Mass transfer reduces C_D as shown by Eisenklam et al. [Eis+67] on single droplets under vaporizing conditions⁵⁸. However, Yuen and Chen [YC76] state that the main difference on drag between evaporative and non evaporative conditions is produced by the changes of gas properties on the droplet surface (and transfer mass is reduced to a lesser extent). They suggest the use of previous correlations (eq. 2.53 and 2.54) with a correction on the viscosity used to calculate Re_p [Lef89].

Based on eq. 2.52, the actual implementation of the momentum source term, $S_{\dot{M},i}$ in OpenFOAM (as well as in most of similar codes) is as follows

$$S_{\dot{M},i} = \frac{\sum m^n u_{p,i}^n - m^{n+1} u_{p,i}^{n+1}}{\Delta t V_{cell}}. \quad (2.55)$$

⁵⁶As a function of Weber number and expressions for the characteristic time required to achieve the maximum deformation

⁵⁷Affects the relation between C_D and Re

⁵⁸Abramzon y Sirignano [AS89] suggest similar corrections to C_D .

Here, the change of velocity is based on a characteristic time ratio

$$\wp = \frac{dt}{\tau_{mom}} \quad (2.56)$$

where dt is the Lagrangian time step⁵⁹ and τ_{mom} has a distinct formulation depending on the Re :

$$\tau_{mom} = \begin{cases} \frac{\rho_l d^2}{18\rho\mu(1+2.632y_{dev})}, & Re_p \leq 0.1 \\ \frac{4\rho_l d}{3\rho C_D |\mathbf{U}_{rel}|}, & Re_p > 0.1 \end{cases} \quad (2.57)$$

$$\mathbf{u}_p^{n+1} = \frac{\mathbf{u}_p^n + \wp \mathbf{u}_{gas} + g dt}{1 + \wp}, \quad (2.58)$$

where g is the gravity, and the Lagrangian time step, dt , is defined as the minimum of the characteristic times modeling a given change of the parcel (i.e. velocity, mass, and temperature)

$$dt = \min(\tau_{mom}, \tau_{evap}, \tau_{boil}, \tau_{heat}), \quad (2.59)$$

and gas velocity, \mathbf{u}_{gas} includes filtered and dispersion components as specified at eq. 2.48. As already mentioned, changes in mass are explained at the following section. However, it is common practice to transfer to the gas phase, those parcels with a droplet radius lower than a certain threshold⁶⁰. The contribution to the gas phase momentum of this parcels is the total mass of the parcel multiplied by its velocity.

2.5.5 Evaporation

Once the fuel is atomized into droplets evaporation produces the air-fuel mixture that leads to the combustion process. Lefebvre [Lef89] explains how

⁵⁹At least half of the time step for the gas phase

⁶⁰A parcel can reach the critical size due to evaporation or after suffering an atomization event.

conduction and convection transfer vaporization enthalpy to the droplet surface increasing vapor pressure. Then, fuel vapor is transfer from the droplet boundary layer to the gas flow by means of convection and diffusion⁶¹.

Vaporization rate depends on gas properties (i.e. pressure, temperature and transport properties), liquid properties (i.e. temperature, volatility, droplet diameter), and the relative velocity between the gas and the droplet.

The study of vaporization at a droplet scale requires a multidisciplinary approach since involves mass and heat transport, fluid dynamics and chemical kinetics [Sir99]. A macroscopic point of view applied to diesel sprays under engine conditions simplifies the problem. In this regard, LL⁶² has become one of the most analyzed and useful parameters. For example, the fact that diesel spray is controlled by mixture was inferred from the LL dependence on injection conditions and fuel-gas thermodynamic characteristics.

Siebers [Sie99] shows how turbulent mixture has a greater influence than the diffusion of mass, momentum and energy between phases. Also, he illustrates the thermal equilibrium between species at a certain location under vaporizing conditions. In particular, the enthalpy required to evaporate the fuel comes from the entrained air. The liquid evaporates once a certain equivalence ratio is reached. This hypothesis allows researchers to study diesel spray under evaporative conditions as a gas jet [Sie99; GO06; Arc+89; Hir91].

The standard model of spray evaporation for a single droplet⁶³ involves the simultaneous resolution of both mass and heat transfer. The evaporation occurs in contact with an ideal gas, under quasi-stationary conditions (i.e. mass and heat transfer are slower for the gas than for the liquid phase)

The changes in mass are subject to a characteristic relaxation time (τ_{evap})⁶⁴ so that the parcel mass at the next time step can be calculated as follows:

$$m_p^{n+1} = \frac{m_p^n}{1 + fr}, \quad (2.60)$$

where fr accounts for the fraction of mass transferred within a specific period

⁶¹Usually, heat transfer due to radiation is negligible when compared with convection

⁶²Already introduced as part of spray characterization (section 2.2)

⁶³Single component, internal properties homogeneous and solely dependent with time

⁶⁴Boiling time is implemented following Rutland's flash boiling model [Zuo+00]

of time

$$fr = \frac{dt}{\tau_{Evaporation}}. \quad (2.61)$$

The calculation of the relaxation time follows the formulation proposed by Kralj [Kra95]:

$$\tau_{evap} = \frac{\rho_d d_p^2}{6D_k Sh \rho_v \ln \left(\frac{P - P_{v,\infty}}{P - P_{v,s}} \right)}, \quad (2.62)$$

where D_k is the mass diffusivity, Sh the Sherwood number, P the total pressure of gas mixture, and $P_{v,s}$ and $P_{v,\infty}$ stand for the partial fuel vapor pressure at the droplet surface and far from it, respectively. The fuel vapor density, ρ_v is evaluated from the ideal gas law. Note, τ_{evap} takes as a reference the droplet conditions but it is applicable to either a single droplet or a parcel.

The Sherwood number is calculated from the following correlation [RM52]:

$$Sh = 2 + 0.6\sqrt{Re_p} \sqrt[3]{Sc}. \quad (2.63)$$

Hence, the source term with which the spray locally contributes to the gas phase (eq. 2.1), changing the total mass and composition of the mixture is given by:

$$S_m = \frac{\sum_p \dot{m}_p}{\Delta t V_{cell}}, \quad (2.64)$$

where $\dot{m}_p = m_p^n - m_p^{n+1}$. As seen in the previous section, the momentum of the evaporated fuel contributes to the momentum content of the gas phase. In the case of a multicomponent fuel the previous set of equations is solved for each component, leaving the source term of eq. 2.4 as follows:

$$S_{Y,k} = \frac{\sum_p \dot{m}_{p,k}}{\Delta t V_{cell}}. \quad (2.65)$$

In addition to the modeling of mass loss, droplet change of temperature due to convection with surrounding air, and phase change has to be taken into account. Following previous methodology, a characteristic time controls the variations on temperature for a given time-frame [RM52]:

$$\tau_{heat} = \frac{\rho_l d_p^2 c_l}{6\kappa Nu}, \quad (2.66)$$

where κ is thermal conductivity, and Nu is the Nusselt number as defined in [RM52] for convection

$$Nu = 2 + 0.6\sqrt{Re_p} \sqrt[3]{Pr}. \quad (2.67)$$

Note how eq. 2.63 are exactly the same but substituting Sc by the Prandtl number, Pr . The characteristic time τ_{heat} appears at the correction factor, f_{corr} that controls the change of droplet temperature

$$T_p^{n+1} = \frac{T_p^n + dt \left(f_{corr} T_g - \left(\frac{h_v}{c_l \tau_{evap}} \right) \right)}{1 + dt f_{corr}}, \quad (2.68)$$

$$f_{corr} = \frac{f(z)}{\tau_{heat}} \quad (2.69)$$

where T_p is the parcel temperature, T_g is the gas phase temperature, h_v is the vaporization latent heat, and $f(z)$ a factor that corrects the effect of mass transfer on the heat transfer. The empiric correlation for $f(z)$ was proposed by El Wakil et al. [EW+54] as follows:

$$f_z = \frac{z}{e^z - 1}; z = \frac{C_{p,v} \tau_{heat}}{c_l \tau_{evap}}, \quad (2.70)$$

where $C_{p,v}$ is the specific heat capacity of the vapor fuel.

Regarding the spray source term for the equation 2.3, S_h gathers the energy exchanged with the gas phase (h_p) due to changes in the spray temperature, the evaporation, and work.

$$S_h = \frac{\sum h_p}{\Delta t V_{\text{cell}}}, \quad (2.71)$$

$$h_p = m_p^n \left((h_{s,p}^n - h_{v,p}^n) + \left(\frac{p - p_v}{\rho_l} \right)^n \right) \quad (2.72)$$

$$- m_p^{n+1} \left((h_{s,p}^{n+1} - h_{v,p}^{n+1}) + \left(\frac{p - p_v}{\rho_l} \right)^{n+1} \right), \quad (2.73)$$

where $h_{s,p}$ is the sensible enthalpy of the fuel. Note, if fuel has different components, $h_{s,p}$ stands for the combined sensible enthalpies of the liquid species. If that is the case, previous properties of the parcel related with the chemical composition are calculated based on the mass fraction of the different species in the liquid.

2.5.6 Turbulent dispersion

Under engine conditions, fuel air mixture occurs within a turbulent flow. This turbulence is often enhanced by piston or intake valves design. The constant volume vessel does not model such turbulence levels but provides a more controlled environment.

Regarding spray injection and combustion, large turbulent scales allow the chamber air to entrain till the spray core. Large scales are limited by the physical boundaries and the characteristic length of the flow, also known as the macro scale (L) [Tur00]. In the case of a spray, L can be taken as the spray diameter for a given axial distance.

The present section deals with the modeling of the interaction between the particles⁶⁵ and the turbulent structures of the continuous phase. In particular, It considers the possible generation or attenuation of the turbulence as a result of such interaction.

⁶⁵Generally speaking: solid or liquid particles and their representation into parcels or single droplets

Previous experiments include diversity of injected particles⁶⁶ as well as the background flow (e.g. water, air, SF_6). In this regard, Faeth [Fae87; Fae+95] review the three type of droplet-turbulence interaction:

1. Droplet dispersion, which is an effect of the turbulence on droplet properties.

Particles and eddies follow different trajectories and their interaction is limited in time. Hence the studies are focus on the variables controlling the characteristic interaction time: the eddy life time or the time needed to cross the eddy.

Turbulent dispersion and relative velocities are function of the droplet diameter. Turbulent dispersion has a reduced influence on big droplets. This may cause the higher average diameter of the spray axis, although some researches relate this trend with coalescence . As expected, turbulent dispersion effects have a lower impact under evaporation conditions.

2. Turbulent content alteration, as a consequence of the droplet movement.

This mechanism is a consequence of the direct action of particles on the turbulent properties of the gas phase, which may either increase or decrease turbulent levels as explained below.

One of the investigations referred by Faeth was carried by Gore and Crowe [GC89]. They conclude that small particles reduce turbulence levels and big particles increase their values. The transition between *small* and *big* particles occur at a 10% of the eddy characteristic length ($d_p/L \approx 0.1$). Faeth comments, this behavior is possible because small particles rapidly get the eddies local velocities, increasing the effects of turbulent modulation. In addition, small eddies have weak perturbations and particles lower the generation of turbulence. Both reasons apply the other way round in the case of big particles.

Recent studies referred by Bharadwaj and Rutland [BR10a], use Stokes number, St as a reference. This number is defined as $Stk = \frac{\tau U}{d}$, where τ is the relaxation time of the particle and d a characteristic length of the problem. Higher St reduce the turbulence of big eddies, increasing the energetic content of the smaller scales. However an increase of St can invert this behavior.

⁶⁶Monodisperse either small or big; high or low mass, different materials and phases (i.e. solid, liquid and gas bubbles).

Compared with single phase gas jets, turbulence modulation on sprays can be easily identified on the lower levels of anisotropy found at the velocity fluctuations. Regarding the turbulence on dense sprays, Faeth points out the role of the droplets to generate turbulence and its dissipation at the gas phase. Consequently, the turbulent patterns generated at the spray differ from those found on single phase gas jets ,

3. Change on the interphase transport rate, due to a combination of previous interactions.

This mechanism considers the increase on transport rate on sprays under evaporating conditions (i.e. mass transfer, heat and drag coefficients) as well as the enhance of combustion.

Unlike DNS, where any representative turbulent scale is simulated, RANS and LES model turbulent scales that are missed by the particles unless a specific interaction model is applied. For instance, in Figure 2.18 if the main flow direction happens to meet with the big parcel ($St \gg 1$) trajectory, any particle under a RANS calculation will follow their initial trajectory⁶⁷. Regarding LES, depending on the mesh resolution, vortex structure, l_e can be simulated and the turbulent dispersion for large and intermediate drops ($St \geq 1$) is carried out by momentum transfer. However, modeled scales affecting smaller droplets ($St \ll 1$) still need an interaction sub-model to achieve realistic particle distributions.

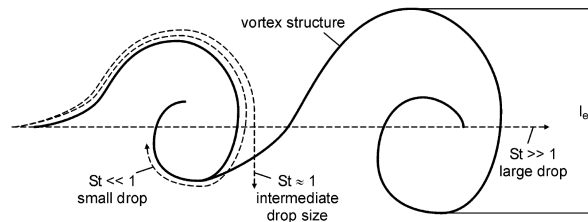


Figure 2.18: Possible drop trajectories in a turbulent flow field [Cro+88]

The three mechanisms described above⁶⁸ had been implemented for RANS turbulence models and naturally inherit by LES. A popular stochastic sub-model was suggested by Dukowicz [Duk80]. The version outlined by Gosman

⁶⁷Only a difference in velocity magnitude due to momentum transfer

⁶⁸Droplet dispersion, Eulerian turbulent content alteration and interphase transport rate enhancement

and Ioannides [GI83] is used in codes like *Star-CD* where the O'Rourke et al. [Ams+89] version is the one implemented in *KIVA* and *OpenFOAM*.

As shown in eq. 2.48, the gas turbulence velocity was included in the calculation of relative velocity between the parcels and the gas phase ($\mathbf{U}_{\text{rel}}(\mathbf{u}_{\mathbf{d}})$) [Ams+89]. Remember, for both RANS and LES follows the same formulation, and turbulence dispersion velocity u_d , is either the sub-grid velocity in LES or the fluctuating velocity in RANS. As proposed by Amsden et al. [Ams+89] turbulence velocity is directly proportional to turbulent kinetic energy within the cell

$$\mathbf{u}_{\mathbf{d}} = C_{\text{turb}} \sqrt{\frac{2}{3}k}, \quad (2.74)$$

where each component of the gas phase turbulence velocity is chosen randomly from a Gaussian distribution (i.e. C_{turb}). Note, k states for turbulent kinetic energy for RANS calculation, but only sub-grid scale turbulent kinetic energy for LES. Therefore, a smaller value of turbulent velocity is expected in LES.

At this point a clarification needs to be done. Although, *OpenFOAM* has the turbulence velocity field already implemented for RANS calculations, it had to be adapted by the authors for LES. Also, the addition of turbulence velocity is subject to a correlation time for RANS⁶⁹ that was not taken into account for LES due to the different nature of turbulent modeling (i.e. filtered VS ensemble averaged). As a consequence a new value of $\mathbf{u}_{\mathbf{d}}$ was modelled every Lagrangian time step (dt) for LES. The study of a correlation time in order to include $\mathbf{u}_{\mathbf{d}}$ to the calculation of relative velocity and the different types of Gaussian distributions to be used are out of the scope of the present study.

In our calculations, this relative gas velocity seen by a 'droplet' is used in the Lagrangian calculations of all the spray processes (i.e. drag, both primary and secondary break-up) and for k at the DS turbulent model.

⁶⁹The minimum value between the eddy life time and the parcel stay time.

Chapter 2 bibliography

- [Abr97] J Abraham. “What is adequate resolution in the numerical computations of transients jets?” In: *SAE paper 970051* 106 (1997), pp. 141–155 (cit. on pp. 46, 118).
- [Ado+07] P. Adomeit, O. Lang, S. Pischinger, R. Aymanns, M. Graf, and G. Stapf. “Analysis of cyclic fluctuations of charge motion and mixture formation in a DISI engine in stratified operation.” In: *SAE paper* 01 (2007), p. 1412 (cit. on p. 43).
- [Ams+89] Anthony A Amsden, Peter J O’Rourke, and D T Butler. “KIVA-II: A computer program for chemically reactive flows with sprays.” In: *LA-11560-MS, Los Alamos National Laboratory (T3 group internal report, approved for public release)* (1989) (cit. on pp. 61, 70).
- [Apt+03] Sourabh V Apte, M Gorokhovski, and P Moin. “LES of atomizing spray with stochastic modeling of secondary breakup”. In: *International Journal of Multiphase Flow* 29.9 (2003), pp. 1503–1522. ISSN: 0301-9322. DOI: 10.1016/S0301-9322(03)00111-3 (cit. on p. 58).
- [Ara+07] J. Arai, N. Oshima, M. Oshima, H. Ito, and M. Kubota. “Large eddy simulation of spray injection to turbulent flows from a slit nozzle.” In: *SAE paper 2007-01-1403* (2007) (cit. on p. 43).
- [Arc+89] C Arcoumanis, J.H. Whitelaw, and K.Y. Wong. “Gaseous Simulation of Diesel-Type Sprays in a Motored Engine”. In: *SAE paper 890793* (Feb. 1989). DOI: 10.4271/890793 (cit. on p. 64).
- [Arc+97] C Arcoumanis, M. Gavaises, and B. French. *Effect of Fuel Injection Processes on the Structure of Diesel Sprays*. Tech. rep. Feb. 1997. DOI: 10.4271/970799 (cit. on p. 60).
- [Arr97] J Arrègle. “Análisis de la estructura y dinámica interna de chorros Diesel”. PhD thesis. Valencia: E.T.S. Ingenieros Industriales. Universidad Politécnica de Valencia, 1997 (cit. on pp. 54, 58, 59).
- [AS89] B Abramzon and W A Sirignano. “Droplet vaporization model for spray combustion calculations”. In: *International Journal of Heat and Mass Transfer* 32.9 (Sept. 1989), pp. 1605–1618. ISSN: 00179310. DOI: 10.1016/0017-9310(89)90043-4 (cit. on p. 62).

- [Asg11] N Asgriz. *Handbook of Atomization and Sprays*. Ed. by Nasser Ashgriz. Boston, MA: Springer US, 2011. ISBN: 978-1-4419-7263-7. DOI: 10.1007/978-1-4419-7264-4 (cit. on p. 52).
- [AT13] Lakshman Anumolu and Mario F. Trujillo. “Gradient augmented reinitialization scheme for the level set method”. In: *International Journal for Numerical Methods in Fluids* 73.12 (Aug. 2013), pp. 1011–1041. ISSN: 02712091. DOI: 10.1002/fld.3834 (cit. on p. 49).
- [Bae+02] Choongsik Bae, Jun Yu, Jinsuk Kang, Jangsik Kong, Roy Cruenca, and Kyung Ook Lee. “The Influence of Injector Parameters on Diesel Spray”. In: (2002) (cit. on p. 24).
- [Bar+80] J. Bardina, J. H. Ferziger, and 1980 Reynolds W. C. 1980-1357. “Improved subgrid-scale models for large eddy simulation”. In: *AIAA paper* 1357 (1980), p. 0 (cit. on p. 44).
- [Bau06] C Baumgarten. *Mixture Formation in Internal Combustion Engines*. Ed. by D Mewes and F Mayinger. Springer, 2006, p. 311. ISBN: 978-3540308355 (cit. on pp. 53, 57–59, 101).
- [Bia+07] G. M Bianchi, F. Minelli, and 2007. Scardovelli R.. 2007-01-0244. “3D large scale simulation of the high-speed liquid jet atomization”. In: *SAE paper* 01 (2007), p. 0244 (cit. on p. 43).
- [Bor+92] J P Boris, F F Grinstein, E S Oran, and R L Kolbe. “New insights into large eddy simulation”. In: *Fluid Dynamics Research* 10.4-6 (Dec. 1992), pp. 199–228. ISSN: 0169-5983. DOI: 10.1016/0169-5983(92)90023-P (cit. on pp. 36, 43).
- [BR10a] Nidheesh Bharadwaj and Christopher J Rutland. “A Large-Eddy Simulation Study of Sub-Grid Two-Phase Interaction in Particle-Laden Flows and Diesel Engine Sprays”. In: *Atomization and Sprays* 20.8 (2010), pp. 673–695. ISSN: 1044-5110. DOI: 10.1615/AtomizSpr.v20.i8.20 (cit. on pp. 41, 42, 52, 58, 68).
- [BR10b] Nidheesh Bharadwaj and Christopher J Rutland. “Droplet-ambient sub-grid interaction modelling in large eddy simulation of diesel sprays”. In: May. Cincimmati, 2010 (cit. on pp. 42, 100).
- [BS+72] P. R. Brazier-Smith, S. G. Jennings, and J. Latham. “The Interaction of Falling Water Drops: Coalescence”. In: *Proceedings of the Royal Society A: Mathematical, Physical and Engineering Sciences* 326.1566 (Jan. 1972), pp. 393–408. ISSN: 1364-5021. DOI: 10.1098/rspa.1972.0016 (cit. on p. 59).

- [Cha13] Mariany de J. Chavez. “Modelado CFD Euleriano-Lagrangiano del Chorro Diesel y evaluacion de su combinacion con modelos fenomenologicos y unidimensionales.” PhD thesis. Universidad Politecnica de Valencia, 2013, p. 203 (cit. on pp. 29, 34, 47, 101).
- [Cla+79] R. A. Clark, J. H. Ferziger, and W. C. Reynolds. “Evaluations of subgrid-scale models using an accurately simulated turbulent flow.” In: *J. Fluid Mechanics* 91 (1979), pp. 1–16 (cit. on p. 37).
- [Cli+78] R Clift, J R Grace, and M E Weber. *Bubbles, Drops and Particles*. Academic Press, 1978, p. 394 (cit. on p. 61).
- [Cor98] D Correas. “Estudio teórico-experimental del chorro libre Diesel isoterma”. PhD thesis. Valencia: E.T.S. Ingenieros Industriales. Universidad Politécnica de Valencia, 1998 (cit. on pp. 54, 99).
- [Cro+88] C.T. Crowe, J.N. Chung, and T.R. Troutt. “Particle mixing in free shear flows”. In: *Progress in Energy and Combustion Science* 14.3 (Jan. 1988), pp. 171–194. ISSN: 03601285. DOI: 10.1016/0360-1285(88)90008-1 (cit. on p. 69).
- [Dal98] B B Dally. “Flow and mixing fields of turbulent bluff-body jets and flames”. In: *Combust. Theory Model.* 2 (1998), pp. 193–219 (cit. on p. 34).
- [Del+05] E Delacourt, B Desmet, and B Besson. “Characterisation of very high pressure diesel sprays using digital imaging techniques”. In: *Fuel* 84.7-8 (May 2005), pp. 859–867. ISSN: 00162361. DOI: 10.1016/j.fuel.2004.12.003 (cit. on p. 24).
- [Des+05] J M Desantes, J. V. Pastor, R Payri, and J. M. Pastor. “Experimental characterization of internal nozzle flow and Diesel spray behavior. Part II: Evaporative conditions”. In: *Atomization and Sprays* 15.5 (2005), pp. 517–544. ISSN: 1045-5110. DOI: 10.1615/AtomizSpr.v15.i5.30 (cit. on p. 24).
- [Des+06] J M Desantes, R Payri, F J Salvador, and A Gil. “Development and validation of a theoretical model for diesel spray penetration”. In: *Fuel* 85 (2006), pp. 910–917. ISSN: 0016-2361. DOI: 10.1016/j.fuel.2005.10.023 (cit. on pp. 23, 24, 28).

- [Des+07] J M Desantes, R Payri, José M García-Oliver, and F J Salvador. “A contribution to the understanding of isothermal diesel spray dynamics”. In: *Fuel* 86.7-8 (2007), pp. 1093–1101. ISSN: 0016-2361. DOI: 10.1016/j.fuel.2006.10.011 (cit. on pp. 6, 8, 23, 28, 97, 102, 168).
- [Des+12] Suraj S Deshpande, Lakshman Anumolu, and Mario F Trujillo. “Evaluating the performance of the two-phase flow solver interFoam”. In: *Computational Science & Discovery* 5.1 (Nov. 2012), p. 014016. ISSN: 1749-4699. DOI: 10.1088/1749-4699/5/1/014016 (cit. on p. 48).
- [Du+06] J. Du, B. Fix, J. Glimm, X. Jia, X. Li, Li Y., and L. Wu. “A simple package for front tracking.” In: *J. Comp. Phys.* 213 (2006.), pp. 613–628 (cit. on p. 49).
- [Duk80] John K Dukowicz. “A particle-fluid numerical model for liquid sprays”. In: *Journal of Computational Physics* 35.2 (Apr. 1980), pp. 229–253. ISSN: 00219991. DOI: 10.1016/0021-9991(80)90087-X (cit. on pp. 45, 69).
- [Dum08] Christophe Dumouchel. “On the experimental investigation on primary atomization of liquid streams”. In: *Experiments in Fluids* 45.3 (2008), pp. 371–422. ISSN: 0723-4864. DOI: 10.1007/s00348-008-0526-0 (cit. on p. 55).
- [Eis+67] P Eisenklam, S A Arunachlaman, and J A Weston. “Evaporation rates and drag resistances of burning drops”. In: *11th International Symposium on Combustion*. Pittsburgh, 1967, pp. 715–728 (cit. on pp. 61, 62).
- [ET83] S.H. El Tahry. “k-epsilon equation for compressible reciprocating engine flows”. In: *Journal of Energy* 7.4 (July 1983), pp. 345–353. ISSN: 0146-0412. DOI: 10.2514/3.48086 (cit. on p. 33).
- [EW+54] M.M. El Wakil, O.A. Uyehara, and P.S. Myers. “A theoretical investigation of the heating up period of injected fuel drops vaporizing in air”. In: *NACA* (1954), p. 3179 (cit. on p. 66).
- [Fae+95] G.M. Faeth, L.-P. Hsiang, and P.-K. Wu. “Structure and breakup properties of sprays”. In: *International Journal of Multiphase Flow* 21 (1995), pp. 99–127. ISSN: 0301-9322. DOI: 10.1016/0301-9322(95)00059-7 (cit. on p. 68).

- [Fae87] G M Faeth. “Mixing, transport and combustion in sprays”. In: *Prog. Energy and Combust. Sci.* 13 (1987), pp. 293–345 (cit. on pp. 59, 68).
- [Fae96] G M Faeth. “Spray combustion phenomena”. In: *Symposium (International) on Combustion* 26.1 (Jan. 1996), pp. 1593–1612. ISSN: 00820784. DOI: 10.1016/S0082-0784(96)80383-3 (cit. on pp. 54, 55).
- [Fed+99] R.P. Fedkiw, T. Aslam, B. Merriman, and S. Osher. “A non-oscillatory Eulerian approach to interfaces in multimaterial flows (the Ghost Fluid Method).” In: *J. Comput. Phys.* 152 (1999), pp. 457–492 (cit. on p. 49).
- [FM01] Zhi-Gang Feng and Efstathios E. Michaelides. “Drag Coefficients of Viscous Spheres at Intermediate and High Reynolds Numbers”. In: *Journal of Fluids Engineering* 123.4 (2001), p. 841. ISSN: 00982202. DOI: 10.1115/1.1412458 (cit. on p. 61).
- [Fuj+09] Hajime Fujimoto, Tsukasa Hori, and Jiro Senda. *Effect of Breakup Model on Diesel Spray Structure Simulated by Large Eddy Simulation*. Tech. rep. Sept. 2009. DOI: 10.4271/2009-24-0024 (cit. on pp. 44, 171).
- [Gav+96] M Gavaises, A Theodorakakos, G Bergeles, and G Brenn. “Evaluation of the effect of droplet collisions on spray mixing”. In: *ARCHIVE: Proceedings of the Institution of Mechanical Engineers, Part C: Journal of Mechanical Engineering Science 1989-1996 (vols 203-210)* 210.53 (June 1996), pp. 465–475. ISSN: 0954-4062. DOI: 10.1243/PIME\PROC\1996_210_220_02 (cit. on p. 59).
- [GC89] R.A. Gore and C.T. Crowe. “Effect of particle size on modulating turbulent intensity.” In: *Int. J. Multiphase Flow* 15 (1989), pp. 279–285. DOI: 10.1016/0301-9322(89)90076-1 (cit. on p. 68).
- [GC97] A D Gosman and D Clerides. “Diesel Spray Modelling: A Review”. In: *Proceedings of ILASS-Europe*. Florence, Italy, 1997. DOI: 10.1.1.45.6492 (cit. on p. 59).

- [Ger+91] Massimo Germano, Ugo Piomelli, Parviz Moin, and William H. Cabot. “A dynamic subgrid-scale eddy viscosity model”. In: *Physics of Fluids A: Fluid Dynamics* 3.7 (1991), p. 1760. ISSN: 08998213. DOI: 10.1063/1.857955 (cit. on pp. 37, 41).
- [GI83] A D Gosman and E Ioannides. “Aspects of computer simulation of liquid-fueled combustors”. In: *Journal Energy* (1983) (cit. on p. 70).
- [Gim08] J Gimeno. “Desarrollo y aplicación de la Medida del flujo de cantidad de movimiento de un chorro Diesel.” PhD thesis. Universidad Politécnica de Valencia, 2008 (cit. on pp. 50, 92, 93).
- [GO06] José M García-Oliver. *El proceso de combustión turbulenta de chorros diesel de inyección directa*. Editorial Reverté, S.A., 2006, p. 336. ISBN: 8429147098 (cit. on pp. 27, 64).
- [Gra+12] V Granet, O. Vermorel, C. Lacour, B. Enaux, V. Dugué, and T. Poinso. “Large-Eddy Simulation and experimental study of cycle-to-cycle variations of stable and unstable operating points in a spark ignition engine”. In: *Combustion and Flame* 159.4 (Apr. 2012), pp. 1562–1575. ISSN: 00102180. DOI: 10.1016/j.combustflame.2011.11.018 (cit. on p. 43).
- [HA90] H Hiroyasu and M Arai. “Structures of Fuel Sprays in Diesel Engines”. In: *SAE Technical Paper* (1990), p. 900475 (cit. on p. 23).
- [Hey88] J B Heywood. *Internal combustion engine fundamentals*. McGraw-Hill, Inc., 1988. ISBN: 0-07-028637-X (cit. on pp. 5, 21, 45).
- [HF92a] L-P Hsiang and G M Faeth. “Near-limit drop deformation and secondary breakup”. In: *International Journal of Multiphase Flow* 18.5 (Sept. 1992), pp. 635–652. ISSN: 03019322. DOI: 10.1016/0301-9322(92)90036-G (cit. on pp. 56, 61).
- [HF92b] L.-P. Hsiang and G.M. Faeth. “Near-limit drop deformation and secondary breakup”. In: *International Journal of Multiphase Flow* 18.5 (Sept. 1992), pp. 635–652. ISSN: 03019322. DOI: 10.1016/0301-9322(92)90036-G (cit. on p. 62).
- [HG91] K Y Huh and A D Gosman. “A phenomenological model of diesel sprays atomization”. In: *Proceedings of the International Conference on Multiphase Flows*. Tsukuba, Japan, 1991 (cit. on p. 56).

- [Hil72] B. J. Hill. “Measurement of local entrainment rate in the initial region of axisymmetric turbulent air jets”. In: *Journal of Fluid Mechanics* 51.04 (Mar. 1972), pp. 773–779. ISSN: 0022-1120. DOI: 10.1017/S0022112072001351 (cit. on p. 27).
- [Hin75] JO Hinze. *Turbulence*. McGraw-Hill, Inc., 1975. ISBN: 0-07-029037-7 (cit. on p. 28).
- [Hir+83] H Hiroyasu, T Kadota, and M Arai. “Development and use of spray combustion modelling to predict Diesel engine efficiency and pollutant emission”. In: *Bull. JSME* 26.214 (1983), pp. 569–575 (cit. on p. 21).
- [Hir91] H Hiroyasu. “Experimental and Theoretical studies on the structure of fuel sprays in Diesel engines”. In: *Proceedings of ICLASS-91*. Gaithersburg, MD, U.S.A, 1991 (cit. on p. 64).
- [HJ06] Sergio Hoyas and Javier Jiménez. “Scaling of the velocity fluctuations in turbulent channels up to $Re_{\tau}=2003$ ”. In: *Physics of Fluids* 18.1 (2006), p. 011702. ISSN: 10706631. DOI: 10.1063/1.2162185 (cit. on p. 31).
- [HM01] Donghee Han and M.G Mungal. “Direct measurement of entrainment in reacting/nonreacting turbulent jets”. In: *Combustion and Flame* 124.3 (Feb. 2001), pp. 370–386. ISSN: 00102180. DOI: 10.1016/S0010-2180(00)00211-X (cit. on p. 27).
- [HN81] C.W Hirt and B.D Nichols. “Volume of fluid (VOF) method for the dynamics of free boundaries”. In: *Journal of Computational Physics* 39.1 (Jan. 1981), pp. 201–225. ISSN: 00219991. DOI: 10.1016/0021-9991(81)90145-5 (cit. on p. 48).
- [HO99] Philip G. Hill and Patric Ouellette. “Transient Turbulent Gaseous Fuel Jets for Diesel Engines”. In: *Journal of Fluids Engineering* 121.1 (1999), p. 93. ISSN: 00982202. DOI: 10.1115/1.2822018 (cit. on p. 27).
- [Hor+06] Tsukasa Hori, Jiro Senda, Takahiro Kuge, and H. Gen Fujimoto. *Large Eddy Simulation of Non-Evaporative and Evaporative Diesel Spray in Constant Volume Vessel by Use of KIVALES*. Tech. rep. Oct. 2006. DOI: 10.4271/2006-01-3334 (cit. on pp. 44, 58).

- [Hor+07] Tsukasa Hori, Takahiro Kuge, Jiro Senda, and Hajime Fujimoto. *Large Eddy Simulation of Diesel Spray Combustion with Eddy-Dissipation Model and CIP Method by Use of KIVALES*. Tech. rep. Apr. 2007. DOI: 10.4271/2007-01-0247 (cit. on p. 44).
- [Hor+08] Tsukasa Hori, Takahiro Kuge, Jiro Senda, and Hajime Fujimoto. *Effect of Convective Schemes on LES of Fuel Spray by Use of KIVALES*. Tech. rep. Apr. 2008. DOI: 10.4271/2008-01-0930 (cit. on p. 44).
- [Hor93] Kiyosi Horiuti. “A proper velocity scale for modeling subgrid-scale eddy viscosities in large eddy simulation”. In: *Physics of Fluids A: Fluid Dynamics* 5.1 (1993), p. 146. ISSN: 08998213. DOI: 10.1063/1.858800 (cit. on p. 37).
- [HS06] Shuhai Hou and David P. Schmidt. “Adaptive collision meshing and satellite droplet formation in spray simulations”. In: *International Journal of Multiphase Flow* 32.8 (Aug. 2006), pp. 935–956. ISSN: 03019322. DOI: 10.1016/j.ijmultiphaseflow.2006.02.013 (cit. on p. 59).
- [Hu+07] B. Hu, R. Jhavar, S. Singh, and R. Reitz. “Combustion Modeling of Diesel Combustion with Partially Premixed Conditions”. In: *SAE Technical Paper* 01 (2007), p. 0163. DOI: doi:10.4271/2007-01-0163 (cit. on p. 44).
- [Ina+04] T. Inamuro, T. Ogata, S. Tajima, and N. Konishi. “A Lattice Boltzmann method for incompressible two-phase flows with large density differences”. In: *Journal of Computational Physics* 198 (2004), pp. 628–644 (cit. on p. 49).
- [Ing56] R.D. Ingebo. *Drag Coefficients for Droplets and Solid Spheres in Clouds Accelerating in Airstreams*. Tech. rep. National Advisory Committee for Aeronautics, Technical Note 3762, 1956 (cit. on p. 61).
- [Ish75] M. Ishii. *Thermo-Fluid Dynamic Theory*. Paris: Editorial Eyrolles, 1975 (cit. on p. 48).
- [Jim03] Javier Jiménez. “Computing high-Reynolds-number turbulence: will simulations ever replace experiments?” In: *Journal of Turbulence* 4.022 (June 2003). ISSN: 1468-5248. DOI: 10.1088/1468-5248/4/1/022 (cit. on p. 31).

- [JL10] W P Jones and C Lettieri. “Large eddy simulation of spray atomization with stochastic modeling of breakup”. In: *Physics of Fluids* 22.11 (2010), p. 115106. ISSN: 10706631. DOI: 10.1063/1.3508353 (cit. on pp. 14, 58).
- [Joe+08] T. Joelsson, R. Yu, X. S. Bai, A. Vressner, and 2008. Johansson B. 2008-01-1668. “Large eddy simulation and experiments of the auto-ignition process of lean ethanol/air mixture in HCCI engines.” In: *SAE paper* 01 (2008), p. 1668 (cit. on p. 44).
- [Jon+10] W P Jones, S. Lyra, and A.J. Marquis. “Large Eddy Simulation of evaporating kerosene and acetone sprays”. In: *International Journal of Heat and Mass Transfer* 53.11-12 (May 2010), pp. 2491–2505. ISSN: 00179310. DOI: 10.1016/j.ijheatmasstransfer.2010.01.028 (cit. on p. 37).
- [JP82] J Janicka and N Peters. “Prediction of turbulent jet diffusion flame lift-off using a PDF transport equation”. In: *Symposium International on Combustion* 19 (1982), pp. 367–374 (cit. on p. 34).
- [JR06] R. Jhavar and C. Rutland. “Using Large Eddy Simulations to Study Mixing Effects in Early Injection Diesel Engine Combustion”. In: *SAE Technical Paper* 01 (2006), p. 0871. DOI: doi:10.4271/2006-01-0871 (cit. on p. 44).
- [Kaa+03] Ossi Kaario, H Pokela, L Kjaldman, J Tiainen, and Martti Larmi. “LES and RNG turbulence modeling in DI diesel engines.” In: *SAE paper 2003-01-1069* (2003) (cit. on p. 44).
- [Kas+09] Alan L. Kastengren, Christopher F. Powell, Yujie Wang, Kyoung-Su Im, and Jin Wang. “X-ray radiography measurements of diesel spray structure at engine-like ambient density”. In: *Atomization and Sprays* 19.11 (2009), pp. 1031–1044. DOI: 10.1615/AtomizSpr.v19.i11.30 (cit. on p. 25).
- [Kem07] Andreas M. Kempf. “LES Validation from Experiments”. In: *Flow, Turbulence and Combustion* 80.3 (Dec. 2007), pp. 351–373. ISSN: 1386-6184. DOI: 10.1007/s10494-007-9128-9 (cit. on pp. 10, 35).

- [KM95] Won-Wook Kim and Suresh Menon. “A new dynamic one-equation subgrid-scale model for large eddy simulations”. In: *33rd Aerospace Sciences Meeting and Exhibit*. Reston, Virginia: American Institute of Aeronautics and Astronautics, Jan. 1995. DOI: 10.2514/6.1995-356 (cit. on p. 40).
- [Kon+99] S. C. Kong, P. K. Senecal, and Rolf D Reitz. “Developments in Spray Modeling in Diesel and Direct-Injection Gasoline Engines”. In: *Oil & Gas Science and Technology* 54.2 (Mar. 1999), pp. 197–204. ISSN: 1294-4475. DOI: 10.2516/ogst:1999015 (cit. on p. 57).
- [Kra95] Cedomir Kralj. “Numerical Simulation Of Diesel Spray Processes”. PhD thesis. Imperial College, 1995 (cit. on p. 65).
- [Leb+09] R Lebas, T Menard, P.A. Beau, A Berlemont, and F.X. Demoulin. “Numerical simulation of primary break-up and atomization: DNS and modelling study”. In: *International Journal of Multiphase Flow* 35.3 (Mar. 2009), pp. 247–260. ISSN: 03019322. DOI: 10.1016/j.ijmultiphaseflow.2008.11.005 (cit. on pp. 32, 33).
- [Lef89] A H Lefebvre. *Atomization and Sprays*. Hemisphere Publishing Corporation, 1989. ISBN: 0-89116-603-3 (cit. on pp. 24, 51, 53, 62, 63).
- [Lip+05] Andreas M Lippert, Shengming Chang, Sasanka Are, and David P. Schmidt. *Mesh Independence and Adaptive Mesh Refinement For Advanced Engine Spray Simulations*. Tech. rep. Apr. 2005. DOI: 10.4271/2005-01-0207 (cit. on p. 20).
- [Liu+93] Alex B. Liu, Daniel Mather, and Rolf D Reitz. *Modeling the Effects of Drop Drag and Breakup on Fuel Sprays*. Tech. rep. Mar. 1993. DOI: 10.4271/930072 (cit. on pp. 61, 62).
- [Lop05] J J Lopez. *Estudio teórico-experimental del chorro libre diesel no evaporativo y de su interacción con el movimiento del aire*. Reverté, S.A., 2005, p. 378. ISBN: 8429147039 (cit. on p. 27).
- [LS74] B E Launder and D B Spalding. “The numerical computation of turbulent flows”. In: *Computer Methods in Applied Mechanics and Engineering* 3.2 (1974), pp. 269–289. ISSN: 0045-7825. DOI: DOI:10.1016/0045-7825(74)90029-2 (cit. on p. 33).

- [M+06] T. Ménard, P. A. Beau, S. Tanguy, F. X. Demoulin, and A. Berlemont. “Numerical Jet Atomization: Part I â DNS Simulation of Primary Break Up”. In: *Volume 1: Symposia, Parts A and B*. Vol. 2006. ASME, 2006, pp. 547–554. ISBN: 0-7918-4750-0. DOI: 10.1115/FEDSM2006-98165 (cit. on p. 32).
- [Mar+10] Lionel Martinez, Adlene Benkenida, and Benedicte Cuenot. “A model for the injection boundary conditions in the context of 3D simulation of Diesel Spray: Methodology and validation”. In: *Fuel* 89.1 (2010), pp. 219–228. ISSN: 0016-2361. DOI: 10.1016/j.fuel.2009.06.012 (cit. on p. 46).
- [ME51] R. A. Mugele and H. D. Evans. “Droplet Size Distribution in Sprays”. In: *Industrial & Engineering Chemistry* 43.6 (June 1951), pp. 1317–1324. ISSN: 0019-7866. DOI: 10.1021/ie50498a023 (cit. on p. 30).
- [Mor11] J de la Morena. “Estudio de la influencia de las caractersticas del flujo interno en toberas sobre el proceso de inyección Diesel en el campo próximo”. PhD thesis. Universidad Politécnica de Valencia, 2011 (cit. on p. 50).
- [MR07] A Munnannur and Rolf D Reitz. “Droplet Collision Modeling in Multi-Dimensional Spray Computations”. In: *International Multidimensional Engine Modeling User’s Group Meeting at the SAE Congress*. Detroit, MI, 2007 (cit. on p. 59).
- [NA00] A Nishimura and Dennis N Assanis. “A Model for Primary Diesel Fuel Atomization Based on Cavitation Bubble Collapse Energy”. In: *ILASS*. 2000 (cit. on p. 56).
- [Nin07] Wei Ning. “Development of a Next-generation Spray and Atomization Model Using an Eulerian-Lagrangian Methodology”. PhD thesis. University of Wisconsin-Madison, 2007 (cit. on pp. 34, 49).
- [NS96] J D Naber and Dennis L Siebers. “Effects of gas density and vaporization on penetration and dispersion of Diesel sprays”. In: *SAE paper 960034* (1996) (cit. on pp. 24, 25).
- [NT39] S Nukiyama and Y Tanasawa. “Experiments on the atomization of liquids in an air stream, Report 3, On the droplet size distribution in an atomized jet”. In: *Trans. Soc. Mech. Eng. Jpn.* 5.18 (1939), pp. 62–67 (cit. on p. 51).

- [OA87] Peter J O'Rourke and Anthony A Amsden. *The Tab Method for Numerical Calculation of Spray Droplet Breakup*. Tech. rep. Nov. 1987. DOI: 10.4271/872089 (cit. on p. 56).
- [OB80] Peter J O'Rourke and F V Bracco. "Modeling of drop interactions in thick sprays and a comparison with experiments". In: *Proceedings of the Institution of Mechanical Engineers* 9 (1980), pp. 101–106 (cit. on pp. 59, 61, 62).
- [Obe91] F Obermeier. *Modeling of nozzle flow*. 1991 (cit. on p. 51).
- [PA02] Scott L Post and John Abraham. "Modeling the outcome of drop-drop collisions in Diesel sprays". In: *International Journal of Multiphase Flow* 28.6 (June 2002), pp. 997–1019. ISSN: 03019322. DOI: 10.1016/S0301-9322(02)00007-1 (cit. on p. 59).
- [Par+08] Su Han Park, Hyun Kyu Suh, and Chang Sik Lee. "Effect of Cavitating Flow on the Flow and Fuel Atomization Characteristics of Biodiesel and Diesel Fuels". In: *Energy & Fuels* 22.1 (2008), pp. 605–613. DOI: 10.1021/ef7003305 (cit. on pp. 50, 51).
- [Pas+00] J V Pastor, Emilio Encabo, and Santiago Ruiz. *New Modelling Approach For Fast Online Calculations In Sprays*. Tech. rep. Mar. 2000. DOI: 10.4271/2000-01-0287 (cit. on p. 28).
- [Pas+08] J M Pastor, J J Lopez, and José M García-Oliver. "A 1D model for the description of mixing-controlled inert diesel sprays". In: *Fuel* 87.13-14 (2008), pp. 2871–2885. ISSN: 0016-2361. DOI: 10.1016/j.fuel.2008.04.017 (cit. on pp. 8, 11, 21).
- [Pay+08b] R Payri, F J Salvador, J Gimeno, and J de la Morena. *Macroscopic Behavior of Diesel Sprays in the Near-Nozzle Field*. Tech. rep. 1. Apr. 2008, pp. 528–536. DOI: 10.4271/2008-01-0929 (cit. on p. 24).
- [Pay+08c] R Payri, B Tormos, F J Salvador, and L Araneo. "Spray droplet velocity characterization for convergent nozzles with three different diameters". In: *Fuel* 87.15-16 (Nov. 2008), pp. 3176–3182. ISSN: 00162361. DOI: 10.1016/j.fuel.2008.05.028 (cit. on pp. 25, 168).

- [PM96] U Petersen and S A MacGregor. “Jet mixing in a model direct injection Diesel engine with swirl”. In: *Journal of Mechanical Engineering Science, IME C07394* 210 (1996), pp. 69–78 (cit. on p. 28).
- [Pop00] S Pope. *Turbulent Flows*. Cambridge University Press, 2000, p. 771. ISBN: 978-0-521-59886-6 (cit. on pp. 7, 12, 21, 26, 33, 36).
- [PR02] Eric Pomraning and Christopher J Rutland. “Dynamic One-Equation Nonviscosity Large-Eddy Simulation Model”. In: *AIAA* 40.4 (2002) (cit. on pp. 41, 92).
- [QL97] J. Qian and C. K. Law. “Regimes of coalescence and separation in droplet collision”. In: *Journal of Fluid Mechanics* 331 (Jan. 1997), pp. 59–80. ISSN: 00221120. DOI: 10.1017/S0022112096003722 (cit. on p. 59).
- [Ran58] W E Ranz. “Some experiments on orifice sprays”. In: *The Canadian Journal of Chemical Engineering* (Aug. 1958), pp. 175–181 (cit. on p. 24).
- [Ray78] Lord Rayleigh. “On The Instability Of Jets”. In: *Proceedings of the London Mathematical Society* s1-10.1 (Nov. 1878), pp. 4–13. ISSN: 0024-6115. DOI: 10.1112/plms/s1-10.1.4 (cit. on p. 53).
- [RB79] Rolf D Reitz and F. B. Bracco. *On the Dependence of Spray Angle and Other Spray Parameters on Nozzle Design and Operating Conditions*. Tech. rep. Feb. 1979. DOI: 10.4271/790494 (cit. on p. 24).
- [RB82] Rolf D Reitz and F. B. Bracco. “Mechanism of atomization of a liquid jet”. In: *Physics of Fluids* 25.10 (1982), p. 1730. ISSN: 00319171. DOI: 10.1063/1.863650 (cit. on pp. 53, 54).
- [RD87] Rolf D Reitz and Ramachandra Diwakar. “Structure of High-Pressure Fuel Sprays”. In: *SAE Technical Paper 870598* 96 (1987), pp. 492–509. DOI: 10.4271/870598 (cit. on pp. 56, 57, 101, 102).
- [Rei87] Rolf D Reitz. “Modeling atomization processes in high-pressure vaporizing sprays.” In: *Atomization and Spray Technology* 3.4 (1987), pp. 309–337 (cit. on pp. 56, 61).
- [RI00] Henrik Rusche and R I Issa. “The Effect of Void age on the Drag Force on Particles, Droplets and Bubbles in Dispersed Two-Phase Flow.” In: *Japanese European Two-Phase Flow Meeting*. Tshkuba, Japan, 2000 (cit. on pp. 61, 62).

- [RM52] W.E. Ranz and W.R. Marshal. “Evaporation from drops”. In: *Chem. Eng. Prog.* 3 (1952), pp. 141–146 (cit. on pp. 65, 66).
- [RR33] P Rosin and E Rammler. “The laws governing the fineness of powdered coal”. In: *J. Inst. Fuel* 7.31 (1933), pp. 29–36 (cit. on p. 51).
- [RS61] F. P. Ricou and D. B. Spalding. “Measurements of entrainment by axisymmetrical turbulent jets”. In: *Journal of Fluid Mechanics* 11.1 (1961), pp. 21–32. ISSN: 0022-1120. DOI: 10.1017/S0022112061000834 (cit. on p. 27).
- [Run+03] T. Rung, U. Bunge, M. Schatz, and F. Thiele. “Restatement of the Spalart-Allmaras Eddy-Viscosity Model in Strain-Adaptive Formulation”. In: *AIAA Journal* 41.7 (July 2003), pp. 1396–1399. ISSN: 0001-1452. DOI: 10.2514/2.2089 (cit. on p. 39).
- [Rut11] Christopher J Rutland. “Large-eddy simulations for internal combustion engines - a review”. In: *International Journal of Engine Research* 12.5 (Aug. 2011), pp. 421–451. ISSN: 1468-0874. DOI: 10.1177/1468087411407248 (cit. on pp. 9, 35, 36).
- [SA10] Sibendu Som and Suresh K Aggarwal. “Effects of primary breakup modeling on spray and combustion characteristics of compression ignition engines”. In: *Combustion and Flame* 157.6 (June 2010), pp. 1179–1193. ISSN: 00102180. DOI: 10.1016/j.combustflame.2010.02.018 (cit. on pp. 56, 101).
- [SA94] P R Spalart and S R Almaras. “A one-equation turbulence model for aerodynamic flows”. In: *Recherche aerospaciale* 1 (1994), pp. 5–21 (cit. on pp. 38, 39).
- [Saf+10] Khadidja Safer, Abdelhamid Bounif, Mériem Safer, and Iskender Gökalp. “Free Turbulent Reacting Jet Simulation Based on Combination of Transport Equations and PDF”. In: *Engineering Applications of Computational Fluid Mechanics* 4.2 (2010), pp. 246–259 (cit. on p. 33).
- [Sal03] F J Salvador. “Estudio teorico experimental de la influencia de la geometria de toberas de inyeccion Diesel sobre las caracteristicas del flujo interno y del chorro.” PhD thesis. Universidad Politécnica de Valencia, 2003 (cit. on p. 50).

- [San+99] K. Sankaranarayanan, X. Shan, Kevrekidis I. G., and S. Sundaresan. “Bubble flow simulations with the Lattice Boltzmann method”. In: *Chemical Engineering Science* 54 (1999), pp. 4817–4823 (cit. on p. 49).
- [Sch07] François G. Schmitt. “About Boussinesq’s turbulent viscosity hypothesis: historical remarks and a direct evaluation of its validity”. In: *Comptes Rendus Mécanique* 335.9-10 (Sept. 2007), pp. 617–627. ISSN: 16310721. DOI: 10.1016/j.crme.2007.08.004 (cit. on p. 33).
- [Sco+93] Alberto Scotti, Charles Meneveau, and Douglas K. Lilly. “Generalized Smagorinsky model for anisotropic grids”. In: *Physics of Fluids A: Fluid Dynamics* 5.9 (1993), p. 2306. ISSN: 08998213. DOI: 10.1063/1.858537 (cit. on p. 37).
- [Sen+13a] P. K. Senecal, E. Pomraning, K. J. Richards, and Sibendu Som. *An Investigation of Grid Convergence for Spray Simulations using an LES Turbulence Model*. Tech. rep. Apr. 2013. DOI: 10.4271/2013-01-1083 (cit. on pp. 44, 58).
- [Sen+13b] P. K. Senecal, Eric Pomraning, K. J. Richards, and Sibendu Som. “Grid-Convergent Spray Models for Internal Combustion Engine Computational Fluid Dynamics Simulations”. In: *Journal of Energy Resources Technology* 136.1 (Sept. 2013), p. 012204. ISSN: 0195-0738. DOI: 10.1115/1.4024861 (cit. on p. 47).
- [Sen+13c] Peter K. Senecal, Eric Pomraning, Q Xue, Sibendu Som, Shidhartha Banerjee, B Hu, K Liu, and J M Deur. “Large eddy simulation of vaporizing sprays considering multi-injection averaging and grid-convergent mesh resolution”. In: *Proceedings of the ASME 2013 Internal Combustion Engine Division Fall Technical Conference* (2013) (cit. on p. 58).
- [Set99] J. A. Sethian. *Level set methods and fast marching methods*. second ed. Cambridge, U.K: Cambridge University Press, 1999. ISBN: 9780521645577 (cit. on p. 48).
- [Sho+07] Babak Shotorban, K.K.Q. Zhang, and Farzad Mashayek. “Improvement of particle concentration prediction in large-eddy simulation by defiltering”. In: *International Journal of Heat and Mass Transfer* 50.19-20 (Sept. 2007), pp. 3728–3739. ISSN: 00179310. DOI: 10.1016/j.ijheatmasstransfer.2007.02.033 (cit. on p. 42).

- [Sie99] Dennis L Siebers. “Scaling Liquid-Phase Fuel Penetration in Diesel Sprays Based on Mixing-Limited Vaporization”. In: *SAE paper 1999-01-0528* (Mar. 1999). DOI: 10.4271/1999-01-0528 (cit. on p. 64).
- [Sir99] W A Sirignano. *Fluid Dynamics and Transport of Droplets and Sprays*. Cambridge University Press, 1999 (cit. on pp. 61, 64).
- [Sma63] J Smagorinsky. “General circulation experiments with the primitive equations”. In: *Monthly Weather Review* 91.3 (1963), pp. 99–164. DOI: 10.1175/1520-0493(1963)091<0099:GCEWTP>2.3.CO;2 (cit. on p. 36).
- [Som+12] Sibendu Som, Douglas E. Longman, Zhaoyu Luo, Max Plomer, Tianfeng Lu, Peter K. Senecal, and Eric Pomraning. “Simulating Flame Lift-Off Characteristics of Diesel and Biodiesel Fuels Using Detailed Chemical-Kinetic Mechanisms and Large Eddy Simulation Turbulence Model”. In: *Journal of Energy Resources Technology* 134.3 (2012), p. 032204. ISSN: 01950738. DOI: 10.1115/1.4007216 (cit. on p. 44).
- [SP00] Mark Sussman and Elbridge Gerry Puckett. “A Coupled Level Set and Volume-of-Fluid Method for Computing 3D and Axisymmetric Incompressible Two-Phase Flows”. In: *Journal of Computational Physics* 162.2 (2000), pp. 301–337. ISSN: 0021-9991. DOI: 10.1006/jcph.2000.6537 (cit. on p. 48).
- [SR00] David P Schmidt and Christopher J Rutland. “A New Droplet Collision Algorithm”. In: *Journal of Computational Physics* 164.1 (2000), pp. 62–80. ISSN: 0021-9991. DOI: 10.1006/jcph.2000.6568 (cit. on pp. 47, 102).
- [SS03] J. A. Sethian and Peter Smereka. “Level set methods for fluid interfaces”. In: *Annual Review of Fluid Mechanics* 35.1 (Jan. 2003), pp. 341–372. ISSN: 0066-4189. DOI: 10.1146/annurev.fluid.35.101101.161105 (cit. on p. 48).
- [Sti03] Gunnar Stiesch. *Modeling Engine Spray and Combustion Processes*. Heat and Mass Transfer. Berlin, Heidelberg: Springer Berlin Heidelberg, 2003, p. 282. ISBN: 978-3-642-05629-1. DOI: 10.1007/978-3-662-08790-9 (cit. on pp. 46, 47, 56).

- [Su+96] T. F. Su, M. A. Patterson, Rolf D Reitz, and P. V. Farrell. *Experimental and Numerical Studies of High Pressure Multiple Injection Sprays*. Tech. rep. Feb. 1996. DOI: 10.4271/960861 (cit. on p. 58).
- [Tak+00] N. Takada, M. Misawa, A. Tomiyama, and Fujiwara. “Numerical simulation of two- and three-dimensional two-phase fluid motion by Lattice Boltzmann method”. In: *Computer Physics Communications* 129 (2000), pp. 233–246 (cit. on p. 49).
- [Tay50] G I Taylor. “The Instability of Liquid Surfaces when Accelerated in a Direction Perpendicular to their Planes. I”. In: *Proceedings of the Royal Society A: Mathematical, Physical and Engineering Sciences* 201.1065 (Mar. 1950), pp. 192–196. ISSN: 1364-5021. DOI: 10.1098/rspa.1950.0052 (cit. on p. 56).
- [Tay63] G I Taylor. *Generation of ripples by wind blowing over a viscous fluid*. 1963 (cit. on p. 56).
- [Til+13] J. Tillou, J.-B. Michel, C. Angelberger, C. Bekdemir, and D. Veynante. “Large-Eddy Simulation of Diesel Spray Combustion with Exhaust Gas Recirculation”. In: *Oil & Gas Science and Technology à Revue dâIFP Energies nouvelles* (Nov. 2013). ISSN: 1294-4475. DOI: 10.2516/ogst/2013139 (cit. on p. 46).
- [Ton+06] S Tonini, M Gavaises, C Arcoumanis, and A Theodorakakos. *Prediction of Liquid and Vapor Penetration of High Pressure Diesel Sprays*. Tech. rep. Apr. 2006. DOI: 10.4271/2006-01-0242 (cit. on p. 61).
- [Try+01] G. Tryggvason, B. Bunner, A. Esmaeeli, D. Juric, N. Al-Rawahi, W. Tauber, J. Han, S. Nas, and Y.J. Jan. “A front tracking method for the computations of multiphase flow.” In: *J. Comp. Phys.* 169 (2001.), pp. 708–759 (cit. on p. 49).
- [Tur00] S.R. Turns. *An introduction to combustion*. McGraw-Hill, 2000 (cit. on p. 67).
- [Val+01] Ariane Vallet, A A Burluka, and R Borghi. “Development of a Eulerian model for the atomization of a liquid jet”. In: *Atomization and sprays* 11 (2001), pp. 619–642 (cit. on p. 49).

- [Vil+04] E de Villiers, A.D. Gosman, and H.G. Weller. “Large Eddy Simulation of Primary Diesel Spray Atomization”. In: *SAE Technical* (Mar. 2004). DOI: 10.4271/2004-01-0100 (cit. on pp. 14, 44, 49).
- [Vit+12] Oldrich Vitek, Jan Macek, Reinhard Tatschl, Zoran Pavlovic, and Peter Priesching. “LES Simulation of Direct Injection SI-Engine In-Cylinder Flow”. In: *SAE Technical Paper 2012-01-0138* (2012). DOI: 10.4271/2012-01-0138 (cit. on pp. 6, 58).
- [VM95] H. K. Versteeg and W. Malalsekera. *An introduction to computational fluid dynamics - the finite volume method*. Longman Scientific and Technical, 1995, p. 267. ISBN: 978-0-13-127498-3 (cit. on pp. 21, 33).
- [Vre+08] A. Vressner, R. Egnell, and B.. Johansson. “Combustion chamber geometry effects on the performance of an ethanol fueled HCCI engine”. In: *SAE paper 1* (2008), p. 1656 (cit. on p. 44).
- [Vuj+09] M. Vujanovic, W. Edelbauer, E. von Berg, R. Tatschl, and N. Duic. “Numerical modeling of Diesel sprays with an Eulerian-Eulerian Approach”. In: *9th ERCOFTAC AHS Pilot Centre Meeting*. AVL List GmbH Austria, 2009 (cit. on p. 48).
- [Vuo+08] Ville Vuorinen, Martti Larimi, and Laszlo Fuchs. *Large-Eddy Simulation on the Effect of Droplet Size Distribution on Mixing of Passive Scalar in a Spray*. Tech. rep. Apr. 2008. DOI: 10.4271/2008-01-0933 (cit. on pp. 43, 46).
- [Vuo10] Ville Vuorinen. “LES of certain droplet size effects in fuel sprays”. PhD thesis. Aalto University, 2010 (cit. on pp. 46, 50).
- [Web31] Constantin Weber. “Zum Zerfall eines Flüssigkeitsstrahles (Disintegration of Liquid Jets)”. In: *ZAMM - Zeitschrift für Angewandte Mathematik und Mechanik* 11.2 (1931), pp. 136–154. ISSN: 00442267. DOI: 10.1002/zamm.19310110207 (cit. on p. 53).
- [Wie90] A. Wierzba. “Deformation and breakup of liquid drops in a gas stream at nearly critical Weber numbers”. In: *Experiments in Fluids* 9.1-2 (1990), pp. 59–64. ISSN: 0723-4864. DOI: 10.1007/BF00575336 (cit. on p. 56).
- [Wil85] F.A. Williams. *Combustion Theory*. Ed. by MA Reading. 2nd Editio. Addison-Wesley Publishing Co., 1985 (cit. on p. 45).

- [Wu+84] K Wu, C C Su, R L Steinberger, D Santavicca, and F V Bracco. “Measurements of the spray angle of atomizing jets”. In: *Journal of fluids engineering* 105.4 (1984), pp. 406–413 (cit. on p. 24).
- [Xue+13] Qingluan Xue, Sibendu Som, Peter Senecal, and Eric Pomraning. “Large Eddy Simulation of Fuel Spray under Non-reacting IC Engine Conditions”. In: *Atomization and Sprays* 23.10 (2013), pp. 925–955. ISSN: 1044-5110. DOI: 10.1615/AtomizSpr.2013008320 (cit. on pp. 43, 47, 50, 58).
- [Yak+89] A. Yakhot, S. A. Orszag, Victor Yakhot, and M. Israeli. “Renormalization group formulation of large-eddy simulations”. In: *Journal of Scientific Computing* 4.2 (June 1989), pp. 139–158. ISSN: 0885-7474. DOI: 10.1007/BF01061499 (cit. on p. 37).
- [Yan+00] Xiaofeng Yang, Yoshihisa Takamoto, and Atsushi Okajima. *Improvement of Three-Dimensional Diesel Spray Modeling in Near Region with Coarse Mesh*. Tech. rep. Mar. 2000. DOI: 10.4271/2000-01-0274 (cit. on p. 47).
- [YC76] M C Yuen and L W Chen. “On Drag of Evaporating Liquid Droplets”. In: *Combustion Science and Technology* 14.4-6 (Oct. 1976), pp. 147–154. ISSN: 0010-2202. DOI: 10.1080/00102207608547524 (cit. on pp. 61, 62).
- [YH85] Akira Yoshizawa and Kiyosi Horiuti. “A Statistically-Derived Subgrid-Scale Kinetic Energy Model for the Large-Eddy Simulation of Turbulent Flows”. In: *Journal of the Physics Society Japan* 54.8 (Aug. 1985), pp. 2834–2839. ISSN: 0031-9015. DOI: 10.1143/JPSJ.54.2834 (cit. on pp. 40, 100).
- [YO86] Victor Yakhot and Steven Orszag. “Renormalization-Group Analysis of Turbulence”. In: *Physical Review Letters* 57.14 (Oct. 1986), pp. 1722–1724. ISSN: 0031-9007. DOI: 10.1103/PhysRevLett.57.1722 (cit. on p. 33).
- [Yu+06] R. Yu, X. S. Bai, H. Lehtiniemi, S. S. Ahmed, F. Mauss, M. Richter, M. Alden, L. Hildings-son, B. Johansson, and A. Hultqvist. “Effect of turbulence and initial temperature inhomogeneity on homogeneous charge compression ignition combustion”. In: *SAE paper* 01 (2006), p. 3318 (cit. on p. 44).

- [Yu+07] R. Yu, X. S. Bai, A. Vressner, A. Hultqvist, B. Johansson, J. Olofsson, H. Seyfried, J. Sjöholm, M. Richter, and M. Alden. “Effect of turbulence on HCCI combustion. 2007- 01-0183”. In: *SAE paper* 01 (2007), p. 0183 (cit. on p. 44).
- [Yu+08] R. Yu, Bai X. S. Joelsson T., and B. Johansson. “Effect of temperature stratification on the auto- ignition of lean ethanol / air mixture in HCCI engine.” In: *SAE paper* 01 (2008), p. 1669 (cit. on p. 44).
- [Yue+01] Yong Yue, Christopher F. Powell, Ramesh Poola, Jinn Wang, and Johannes K. Schaller. “Quantitative measurements of diesel fuel spray characteristics in the near-nozzle region using x-ray absorption”. In: *Atomization and Sprays* 11.4 (2001), pp. 471–490 (cit. on p. 25).
- [Zuo+00] B. Zuo, A. M. Gomes, and C. J. Rutland. “Modelling superheated fuel sprays and vaporization”. In: *International Journal of Engine Research* 1 (2000), pp. 321–336. DOI: 10.1243/1468087001545218 (cit. on p. 64).
- [Fab+08] Fabian Peng Kärrholm, Feng Tao, and P A Niklas Nordin. “Three-Dimensional Simulation of Diesel Spray Ignition and Flame Lift-Off Using OpenFOAM and KIVA-3V CFD Codes.” In: *SAE paper 2008-01-0961* (2008). DOI: 10.4271/2008-01-0961 (cit. on pp. 47, 50).
- [Koj+12] Koji Kitaguchi, Soichi Hatori, Tsukasa Hori, and Jiro Senda. “Optimization of breakup model using LES of diesel spray”. In: *Atomization and Sprays* 22.1 (2012), pp. 57–77 (cit. on pp. 14, 58).
- [von+99] Christopher von Kuensberg Sarre, Song-Charng Kong, and Rolf D Reitz. *Modeling the Effects of Injector Nozzle Geometry on Diesel Sprays*. Tech. rep. Mar. 1999, pp. 1–14. DOI: 10.4271/1999-01-0912 (cit. on p. 51).

Chapter 3

Numerical set-up

Contents

3.1	Introduction	92
3.2	Diesel-like gas jet	92
3.3	Non-evaporative case	100
3.4	Evaporative case (<i>Spray-A</i>)	107
	Chapter 3 bibliography	109

3.1 Introduction



IN THE PREVIOUS CHAPTER we have reviewed the state-of-the art of the numerical simulation of sprays. Once the different ways of simulating sprays are stated, in this chapter we are going to focus in the set-up of a Diesel spray simulation. Using the configuration described here, we have performed all the simulations showed in the next chapter.

3.2 Diesel-like gas jet

The CFD code for E-E simulations used in this thesis is based on the rhoReactingFoam solver. Since there is no parcel-gas liquid interaction, only the part of the DS turbulent model published in 2002 was implemented [PR02]. Note the interface tracking is based on the VOF method.

Payri et al. [Pay+08a] ($\bar{M}_0 = 1.11N$)		
	Spray simulation	Gasjet simulation
Fuel	$C_{13}H_{28}$	N_2
Chamber	N_2	N_2
p_{inj} (MPa)	73.995	-
p_a (MPa)	3.5	3.5
$T_f = T_{ch}$ (k)	307.58	307.58
ρ_f/ρ_{ch}	21.26	1
$\bar{\mathbf{u}}_0$ (m/s)	373.27	373.27
d_{inlet} (μm)	112	516
d_{eq} (μm)	516	516

Table 3.1: Physical conditions of non-evaporative spray and gas jet simulations

3.2.1 Injection rate

Velocity profile can be explicitly calculated from the momentum flux or the mass flow rate. Figure 3.1 depicts the measurements from Gimeno [Gim08] used for the gas jet and the non-evaporative spray calculations. Momentum flux is achieved by measuring the impact force of the spray in a surface with

a piezo-electric sensor [Pay+05]. The improved methodology to get mass flow rate known as *Bosch method (log tube)*¹ is described by Payri et al. [Pay+08a].

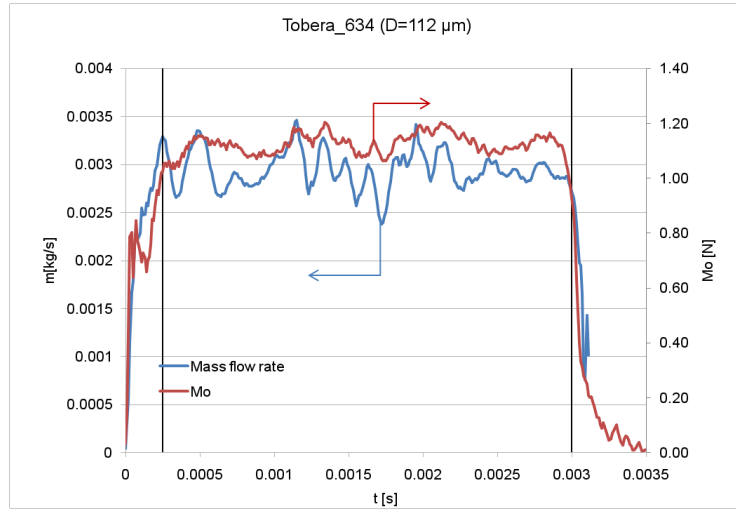


Figure 3.1: Injection rate measurements. Nozzle 634 ($p_{inj} - p_a \approx (800 - 35)bar$) [Gim08].

In accordance with ECN recommendations, the inlet BC is calculated from the mass flow rate measurements [Pay+08a]. Note a further improvement on the methodology has been recently reported by Pickett et al. [Pic+13]. This improved injection profile is used for the evaporative spray case². Bear in mind, mass flow rate is the average of a set of experiments. Therefore, turbulent fluctuations are erased by the average process and the fluctuations shown by the injection rate are due to the flow dynamics inside the nozzle. Since LES require a certain level of turbulence at the inlet BC different strategies have been tested.

3.2.2 Mesh domain

Two similar computational domains have been meshed with different approaches to study the influence of the cells shape and distribution on low-cost computational meshes: locally refined mesh and grading mesh.

¹From the pressure signal on an anechoic volume filled with the fuel injected.

²A virtual injection rate generator can be found at <http://www.cmt.upv.es/ECN03.aspx>.

Locally refined mesh

The first computational domain is a cylindrical constant volume vessel ($D = 40\text{mm}$, $L = 100\text{mm}$) that represents the shape of an injection test rig chamber. The meshing methodology is fairly the same for the gas jet and diesel spray calculations, with the same grid densities for both RANS and LES calculations. In the spray calculations there is no specific surface dedicated to the inlet BC (nozzle exit) and any external surface is defined as a wall.

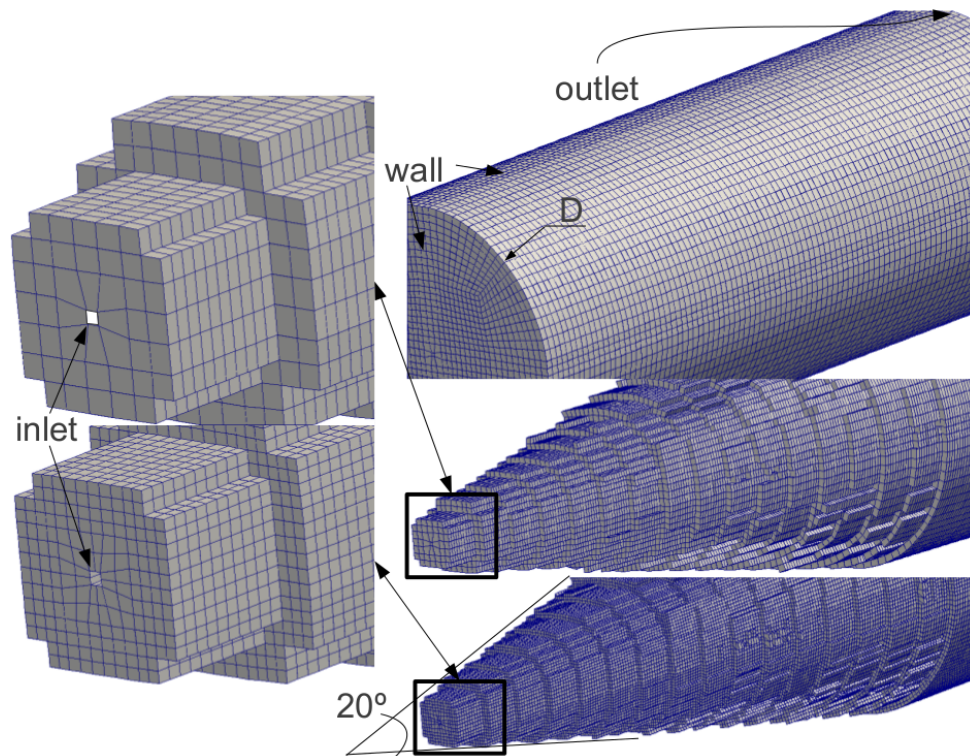


Figure 3.2: Meshing procedure for gas jet calculations. From top to bottom. Right column: Original mesh cells= $(1 \times 1 \times 1)\text{mm}$, first refinement step (Z direction.), second refinement step (XY direcc.) Left column: Detail of refinements.

The refinement process (Figure 3.2) is as follows: given the spray experimental angle (21.6°) [Pay+08a] and based on the $(1 \times 1 \times 1)\text{mm}$ cell mesh (coarse grid), the region within a 20° solid angle is refined. In a first step, cells are split in Z direction only. Afterwards, the same region but the core cells, is refined in XY direction. Core cells are not refined in XY direction because

inlet BC sides of the square have a length $l=457 \mu\text{m}$ according to the hydraulic equivalent diameter. Thus a $(0.5 \times 0.5 \times 0.5)\text{mm}$ cell mesh is confined to the region where the gas jet will develop (standard grid). Following refinements were performed in one step (i.e. X, Y, and Z directions at once) to get a finer grid $(0.25 \times 0.25 \times 0.25 \text{ mm})$. Note, $\Delta z = 0.25\text{mm}$ refinement step is performed only for the first 60mm, where penetration is expected by the end of the simulation.

Following refinements were done with the objective of keeping the max CFL number at the nozzle exit and improve there the physical description with the minimum increment in total cell number. In this way, $\Delta z = 0.125\text{mm}$ cells are located within the first 10mm, $\Delta z = 0.0625\text{mm}$ refinement goes until $Z = 7.5\text{mm}$ and $\Delta z = 0.03125\text{mm}$ refinement was applied for the first $Z = 5\text{mm}$ (table 3.2). Hence, up to five different meshes were tested at the mesh independency study were the difference between the most refined and the previous one is concentrated within the first 5mm. As explained in *full* refinements following $\Delta z = 0.25\text{mm}$ do not make a significative difference on RANS calculations, which sets the limit criteria for our engineering LES meshes. In addition, this methodology provides a mesh topology comparable to the grading mesh (Figure 3.5).

A biased shape of the gas jet case was detected which can be a consequence of mesh shape affecting resolved or sub-grid scales or the filter operation. In order to discern which one dominates, the study considers two different filter definitions (section 2.3.3.5) as well as variations on the morphology of the cells. First, *vanDriest* is the filter delta used for reference cases which calculates the characteristic length as the cube root of the cell volume. In this way, neighbor cells with half volume (i.e. the ones shown near the nozzle at Figure 3.3(a)) have half of the filter length.

In order to overcome the differences in filter length due to volume heterogeneity of neighbor cells, the so called *maxDelta* filter was used. This filter uses the maximum length between the cell centre and its faces as the filter length. Note, for a given perfect hexahedral cell, *maxDelta* filter length is half of the *vanDriest* one.

Regarding cells shape, three meshing procedures lead to the configurations shown at Figure 3.3. The reference mesh has a square inlet BC and both hanging nodes and a notable axial heterogeneity. For the improved mesh, inlet BC and hanging nodes are the same as the references but the cells are

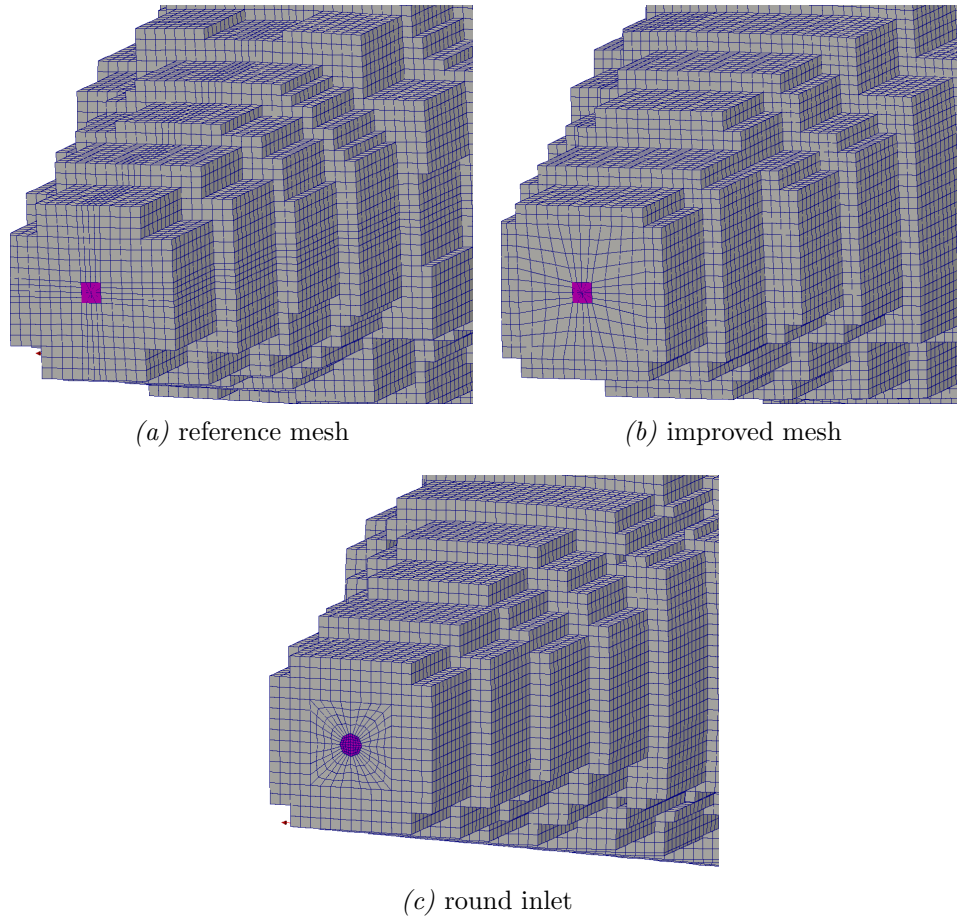


Figure 3.3: Mesh shape effect on E-E DS spray evolution ($\Delta z = 0.25\text{mm}$).

perfectly cubic, two hydraulic diameters from the inlet in the radial direction. Finally, a circular like inlet characterize the third mesh, were hanging nodes between axis and surrounding cells have been eliminated by means of a onetime refinement step. As a consequence, inlet and core cells in axial direction are smaller than the two previous meshes. In order to quantify, the improvement in roundness achieve by the circular like inlet boundary the ratio between the inlet perimeter an actual circle is provided:

$$\phi = \frac{\text{circle perimeter}}{\text{inlet perimeter}} \Big|_{\text{same area}}. \quad (3.1)$$

In the case of the square $\phi \approx 0.44$ where, for the octagon $\phi \approx 0.97$ being more than a 100% closer to a perfect circular inlet BC. In addition, note how every cell surrounding inlet BC share a face with inlet cells in contrast to previous meshes where corner cells have no connection.

Grading mesh

The second cylindrical domain (Figure 3.4) also represents the injection test rig chamber ($D = 40\text{mm}$, $L = 70\text{mm}$) but with two main differences: the mesh methodology and the beginning of the inlet BC. In this case, there is no local refinement, instead a growth ratio progressively increases the size of the cells downstream the inlet BC avoiding hanging nodes, filter size discontinuities and providing axial homogeneity (Figure 3.5). In addition, this mesh methodology is optimized for a cylinder shape. As a consequence, it offers a fine physical discretization at the inlet with a lower number of cells (i.e. $4.0 \cdot 10^5$ cells instead of $2.0 \cdot 10^6$ for $\Delta z \approx 0.0625\text{mm}$) (table 3.2). The square on Figure 3.5(a) depicts the extension and position of Figure 3.5(b).

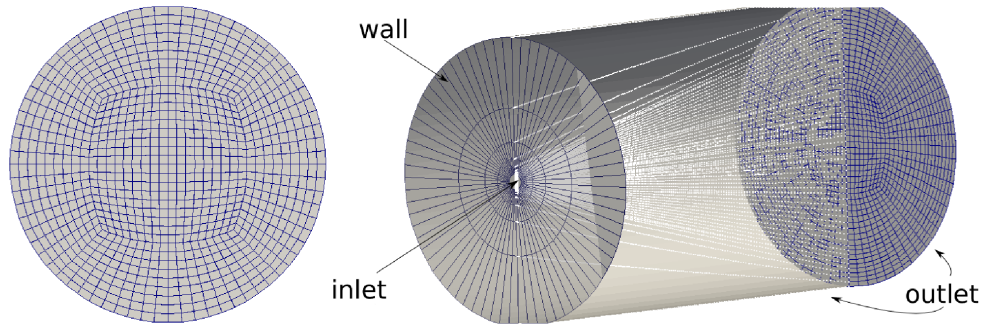
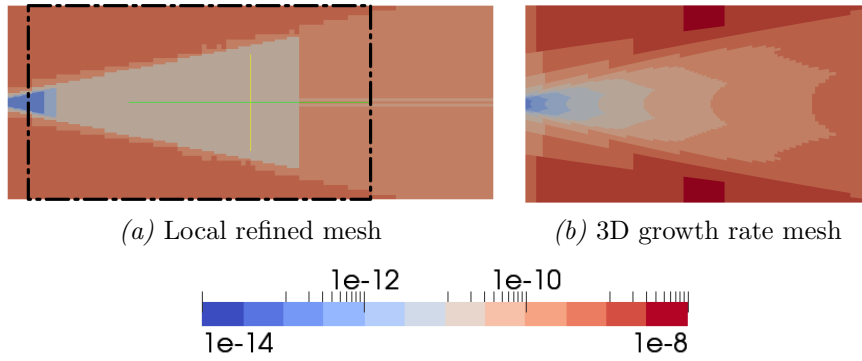


Figure 3.4: Structured 3D growth rate meshing procedure. Left image: detail of inlet BC

Regarding the location of the inlet BC, it is not located at the nozzle exit but at the average position of the non-perturbed zone for a stabilized gas jet. In order to determine the position as well as the fields to be set, the turbulent gas jet theory [Des+07] of a fully developed equivalent gas jet is applied as briefly presented below.

Δz_{inlet}	#cells (fully refined)	#cells (partially refined)	dt($CFL_{0.5}$)[s]
1mm	128100	128100	$1.2 \cdot 10^{-6}$
0.5mm(gasjet)	1024800	610997	$6.4 \cdot 10^{-7}$
0.5mm(spray)	897000	567160	$5.0 \cdot 10^{-7}$
0.25mm	8198400	1560617	$3 \cdot 10^{-7}$
0.125mm	65587200	1756743	$1.4 \cdot 10^{-7}$
0.0625mm	–	2072219	$7.7 \cdot 10^{-8}$
0.03125mm	–	2072219	$7.7 \cdot 10^{-8}$

Table 3.2: Mesh refinement

Figure 3.5: Axial cut plane colored by cell volume ($\Delta z \approx 0.0625\text{mm}$ at inlet).

Some studies referred at chapter 2 show how under certain conditions, momentum flux is conservative for any section perpendicular to the spray axis in the steady region of the gas jet or diesel spray, and thus equal to that existing at the nozzle exit [Des+03][Pay+05]. Therefore, a proper implementation of the inlet boundary condition would perform the same spray development independent of where it would be placed. Hence, the inlet boundary condition must be perpendicular to the spray axis, it has to contain the whole spray and -in order to ensure a more realistic development of the flow- the boundary inlet has to reproduce the same profile of the fields as in a steady spray. Since momentum flux can be obtained from experimental data, the unknown factors to set up the boundary condition can be identified by integrating momentum over the whole spray section:

$$\dot{M}_0 = \dot{M}(x) = \int_0^R 2\pi(x, r) \mathbf{u}(x, r) r \mathbf{u}(x, r) dr, \quad (3.2)$$

where subindex 0 identifies the fields at the inlet location, the x -coordinates coincides with the spray axis and the r is the radial coordinate, ρ is the local density in the diesel spray and once \mathbf{u} is integrated only the axial component (u_{axis}) is considered. Writing the density at an internal point of the spray in terms of local concentration and assuming a Gaussian radial profile [Cor98] for fuel concentration and axial velocity, Desantes et al, obtained the following expression for the spray momentum:

$$\dot{M}_0 = \frac{\pi}{2\alpha} \rho \tan^2(\theta_u) x^2 u_{axis}^2 \sum_{i=0}^{\infty} \frac{1}{(1 + i \frac{Sc}{2})} \left[\left(\frac{u_{axis}}{u_0} \right) \left(\frac{1 + Sc}{2} \right) \left(\frac{\rho_f - \rho_a}{\rho_f} \right) \right]^i, \quad (3.3)$$

here the Schmidt number (Sc) represents the relative rate of momentum and mass transport and θ_u is the spray cone angle. Note, theoretical velocity decay derived from eq. 3.3 will be used as a reference in future graphs. The inlet location is defined when $u_{axis} = u_0$. The gas jet injected under the physical conditions shown in Table 3.1 fixes the end of the non-perturbed zone for the isodense case at 4.073mm ($\sim 8d_{eq}$)³ from the nozzle exit. At this location, the gas jet diameter is 2.07mm which is set as the inlet BC diameter. Here, the velocity and concentration reference profiles follow equations 2.12 and 2.13. Since LES calculation requires perturbed inlet boundary conditions, the reference Gaussian profiles are randomly perturbed with a 10% turbulent intensity, as a first approximation (openFOAM's default *turbulentInlet* BC). In a further step, the fields from the locally refined mesh (Figure 3.5(a)) calculations are mapped at the inlet BC so the results from an average perturbed profile can be compared with the ones with actual simulated eddies.

3.2.3 Turbulent modelling

Turbulent models described in sections 2.3.2 and 2.3.3. Regarding LES models, the *no model* turbulent treatment was not utilized due to the mesh coarseness imposed by the thesis approach.

³Equivalent diameter, d_{eq} , was defined in 2.10.

Spalart-Allmaras and OEE turbulent coefficients can be found at related sections. Smagorinsky coefficient can be obtained as a combination of C_k and C_ε consistent with [YH85] (eq. 2.25). By default coefficients for incompressible flow are $C_k = 0.094$ and $C_\varepsilon = 1.048$ which provides the default constant recommended by Pope⁴ ($C_S = 0.167$). In the case of compressible flows, default values are $C_k = 0.02$ and $C_\varepsilon = 1.048$ because the formulation is slightly different⁵. Finally, DS turbulent coefficients are $C_k = 0.05$ and $C_\varepsilon = 0.3$ ⁶.

3.3 Non-evaporative case

For L-E spray simulations dieselFoam solver was modified by including the fully developed DS turbulent model. The detailed derivation of the model as well as the source term for parcel-gas phase sub-grid interaction can be found at the previous chapter (section 2.3.3.5) as well as at Bharadwaj's PhD thesis [BR10b].

As a result of the previous study of turbulent models, the study is focused on the effect of OEE and DS models on the L-E spray calculations under both evaporative and non-evaporative conditions. Mesh size effect is addressed with 0.5mm and 0.25mm cell size, and the topology used is the one known as *improved mesh* (Figure 3.3(b)). Following, the use of the phenomenological spray models described at section 2.5.

3.3.1 Injection

In contrast with E-E gas jet calculations, injection profile is defined by the mass flow rate instead of the velocity. In particular, the *constInjector* sub-model randomly distribute parcels in a solid cone⁷ where parcels injected within the same time step have the same mass. Additional parameters such total injected mass ($8.88 \cdot 10^{-6} kg$), nozzle diameter ($112 \mu m$), discharge coefficient ($C_d = 0.98$), temperature, number of parcels and the injection temporal evo-

⁴This constant can be 0.1 0.2 and using 0.2 can be cause of high diffusivity.

⁵In both cases formulation as well as turbulent coefficients were not modified.

⁶Note coefficients reported at Bharadwaj's thesis seems to be swapped by mistake.

⁷Experimental angle from [Pay+08a] (21.6°).

lution⁸ must be provided to the injection sub-model. Hence the experimental mass flow rate shown in figure 3.1 is directly used for this calculations. For statistical purposes a extended range of injection is obtained by concatenating the *stabilized* part of the signal (i.e. limited by vertical lines).

Regarding the number of parcels injected, this thesis follows a study published on a recent thesis of our department [Cha13]. In her work, Dr. Chavez concluded that, under actual conditions, the number of parcels injected can vary between $0.5 \cdot 10^7$ and $5 \cdot 10^7$. The number of parcels injected is within this range (i.e. 35.000 parcels).

Finally, injected parcels follow the blow method [RD87] where the detailed simulation is replaced by the injection of big spherical droplets with uniform size. The diameter of these blobs equals the nozzle hole diameter as depicted in Figure 3.6 which generates a region of large discrete liquid particles equivalent to a dense core. Right after injection, blobs are subject to KH atomization (section 2.5.2).

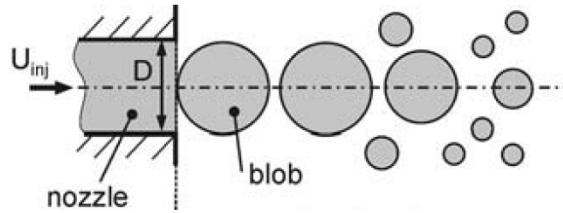


Figure 3.6: Injection blob-method (adapted from [Bau06])

3.3.2 Atomization

Advance recent models that account for cavitation KH-ACT [SA10] have proven its efficiency on LES of diesel spray. However, the injection is carried out by means of a non-cavitating nozzle which invites to select well-known KH-RT model.

Small modifications on KH-RT breakup model (including primary breakup) [BR99] were implemented. Standard KH-RT breakup model available in OpenFOAM limits child parcel's mass to a certain percentage of the average injected

⁸OpenFOAM automatically non-dimensionalize the profile in order to inject the total mass by the end of the injection event.

mass⁹. This limit was modified to take into account the actual mass of the parent parcel instead. For the atomization model, the condition of the liquid core was added to the modified break up model [RD87]:

$$L_{\text{core}} = C_{\text{BU}} d \sqrt{\frac{\rho_l}{\rho_g}}, \quad (3.4)$$

where L_{core} is the core length, C_{BU} is a constant between 7 and 15 (by default $C_{\text{BU}}=7$), d is the diameter of the nozzle exit and ρ_l and ρ_g are the density of the liquid and the gas respectively. Note, the liquid core length defined for L-E calculations has an equivalent portrayal to the non-perturbed zone of the gas jet analogy [Des+07] where local velocity of injected phase is not affected by the chamber gas, remaining at its injected velocity value a given times (i.e. C_{BU} times) the equivalent diameter. Consequently parcels belonging to the initial stream are not affected by drag (i.e. no momentum transfer with surrounding gas phase), within L_{core} . Note, this *drag-free* condition does not affect child parcels stripped from the injected ones as a consequence of the KH instability. Note, Weber number is limited to 6 instead of 12 as recommended by OpenFOAM.

3.3.3 Collision

Collision and coalescence in the diesel spray are not taken into account in this study due to numerical instabilities. Also, O'Rourke's collision model is inherently grid dependent [SR00] and its use may disguise the influence of the turbulent model within the refinement process.

3.3.4 Momentum transfer

Regarding drag calculation, the effect of droplet distortion on the parcel drag is taken into account by OpenFOAM's default formulation (section 2.5.4). In particular, since there is no evaporation, no corrections on the drag coefficients are needed.

⁹This reference is suitable for injected blobs but once the parent parcel has suffer previous atomization, the reference must look at its actual mass.

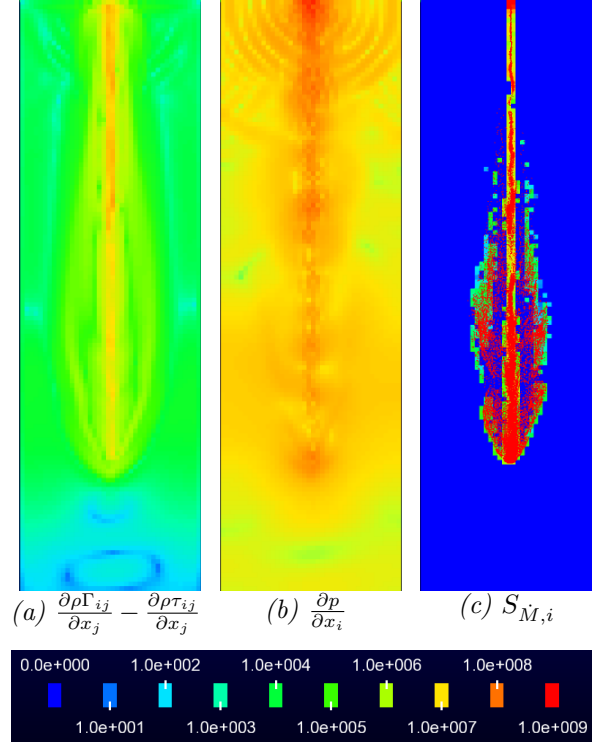


Figure 3.7: Momentum terms contribution [$kg/(m^2s^2)$] (RANS k- ε , $\Delta z \approx 0.5\text{mm}$, $t = 0.0015\text{s}$ ASOI, red dots are parcels).

In order to assess the particular contribution of the spray source term, Figure 3.7 displays the contour plots of the terms of the eq. 2.2. For a quantitative comparison, Figure 3.8 collects the values at the spray axis. Note, the logarithmic scale at both the contour plot and the graph. In the case of the contour plot, each change in color depicts a significant variation (i.e. an order of magnitude). From now on, we will use ASOI as acronym for After Start Of Injection to indicate an starting point for the time axis.

The contribution of the turbulent term and the spray source are in the same order of magnitude at the spray axis. As expected, the spray source term only provides values located at the cells where parcels are present.

It is worthy to mention how the contribution of viscous stress tensor (Γ_{ij}) is, at least, three orders of magnitude lower than Reynolds stresses (τ_{ij}). In the

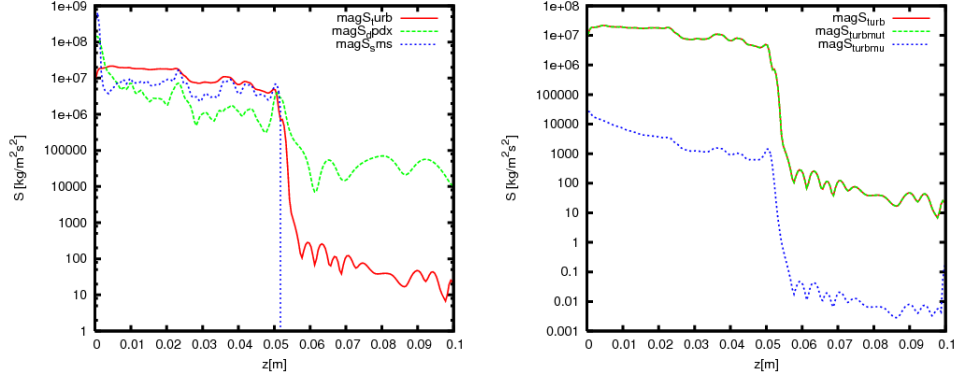


Figure 3.8: Momentum contribution along the spray axis (RANS $k-\varepsilon$, $\Delta z \approx 0.5\text{mm}$, $t = 0.0015\text{s}$ ASOI)

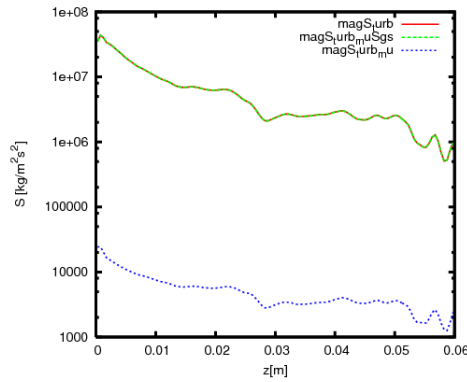


Figure 3.9: Momentum contribution along the spray axis (LES, $\Delta z \approx 0.5\text{mm}$, $t = 0.0015\text{s}$ ASOI).

case of our LES cases, when the viscous stress is compared with the modeled sub-grid stresses, the same trend is observed. In addition the values of RANS Reynolds stresses and LES sub-grid stresses are in the same order of magnitude at the spray axis.

In this regard, few considerations from chapter 2 explain this behavior. First, resolved terms of LES represent locally filtered values which are not *mean* or *ensemble averaged* values. Although we are using the same notation for RANS and LES, the properties of LES terms are different. In addition to that, flow structures do not come from the turbulence model but from

non-linear terms (i.e. $\frac{\partial \rho u_i u_j}{\partial x_j}$). Generally speaking, these flow structures are likely to develop under dense grids and low dissipative turbulence models. On the contrary, the meshes proposed are selected under RANS criteria (coarse meshes) and LES spatial filtering increases sub-grid dissipation as the number of cells in the grid decreases. As stated at the introduction, the challenge is to find the minimum space discretization that allows non-linear terms to function sufficiently.

Consistent with Figure 3.9, results at chapter 4 show how RANS-like cell sizes allow non-linear interactions and a sufficient range of length scales even though the dissipation modeled has the same levels as RANS calculations.

3.3.5 Turbulent dispersion

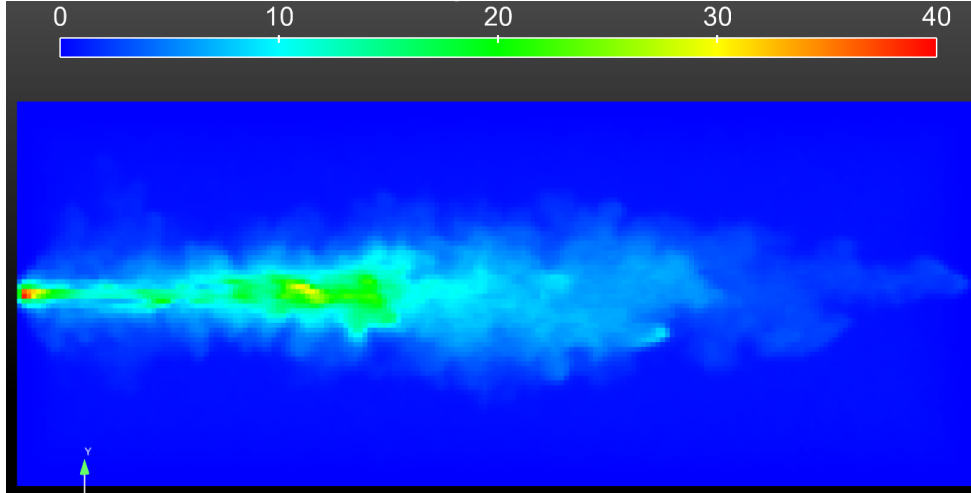
Regarding turbulence dispersion velocity (u_d), OpenFOAM has that term already implemented for RANS calculations but it had to be adapted by the author for LES. Also, the addition of turbulence velocity to the relative velocity (eq. 2.48) is subject to a correlation time for RANS that was not taken into account for LES due to the different nature of turbulent modeling (i.e. filtered VS ensemble averaged).

Figure 3.10 shows the simulated relative velocity and the sigma field set apart. Consistent with eq. 2.74, dispersion velocity is calculated as a function of sigma field (i.e. $u_d = C_{\text{turb}}\sigma$). Note as well the differences on the color scales. On one hand, the linear scale for σ contour plot and on the other the logarithmic scale used for the parcels. The range of values of the logarithmic scale was selected to depict a $\sim 100\%$ increase on the field with every color change.

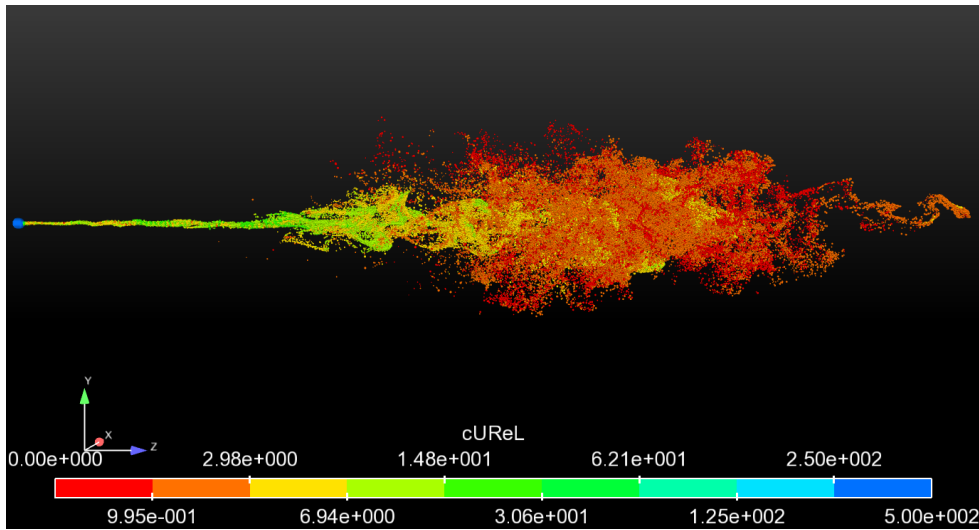
As clearly depicted, within the first third of the spray, the values of dispersion velocity may be¹⁰ in the same order of magnitude than the simulated relative velocity seen by the parcels. Hence, it is specially critic to account for its influence in this part of the spray.

A new value of u_d is modeled every Lagrangian time step (dt) for LES. The study of a correlation time in order to include u_d to the calculation of relative velocity and the different types of Gaussian distributions to be used

¹⁰Remember between dispersion velocity and sigma field there is a random number in the range of 0-1.



(a) Sigma field ($\sigma = \sqrt{\frac{2}{3}k}$) (m/s)



(b) Simulated relative velocity ($u_{p,i} - \tilde{u}$) (m/s)

Figure 3.10: Turbulent dispersion magnitude compared to relative velocity (DS, $\Delta z \approx 0.5\text{mm}$, $C_k = 0.3$ and $C_\epsilon = 0.05$, $t = 0.003\text{s}$ ASOI).

are out of the scope of the present study, but some .

Finally, keep in mind that the relative gas velocity seen by a 'droplet' (u_d

included) is used in the Lagrangian calculations of all the spray processes (i.e. drag, both primary and secondary break-up, evaporation) and for k at the DS turbulent model.

3.4 Evaporative case (*Spray-A*)

For the evaporative conditions, the experimental data comes from *Spray-A*. Details of the experiments and related scientific publications can be found at the ECN website¹¹. In particular, boundary conditions set up have been taken from *Spray-A* experiment series performed by CMT¹².

Pickett et al. [Pic+13] ($\bar{M}_0 = 1.5N$)	
Fuel	$C_{12}H_{26}$
Chamber	N_2
P_{inj} / P_a (MPa)	150 / 6
T_f / T_{ch} (k)	363 / 900
ρ_f / ρ_{ch}	713.13/22.8
\bar{u}_0 (m/s)	~ 600
d_{inlet} (μm)	89.4
d_{eq} (μm)	500

Table 3.3: Physical conditions of *spray-A*

Note, following equation 2.10, *Spray-A* is equivalent to both the simulated under non-evaporative conditions and the diesel-like gas jet ($d_{eq} = 516 \mu\text{m}$).

3.4.1 Injection rate

As shown by Pickett et al. [Pic+13], the accuracy of CFD model predictions used to optimize the combustion process depends upon the accuracy of the rate of injection (ROI). Figure 3.11 shows the improved rate used as the inlet boundary condition. Note the smoothness when compared with the ROI imposed to the non-evaporative case (Figure 3.1).

¹¹<http://www.sandia.gov/ecn/>

¹²Available as well at: <http://www.cmt.upv.es/ECN.aspx>

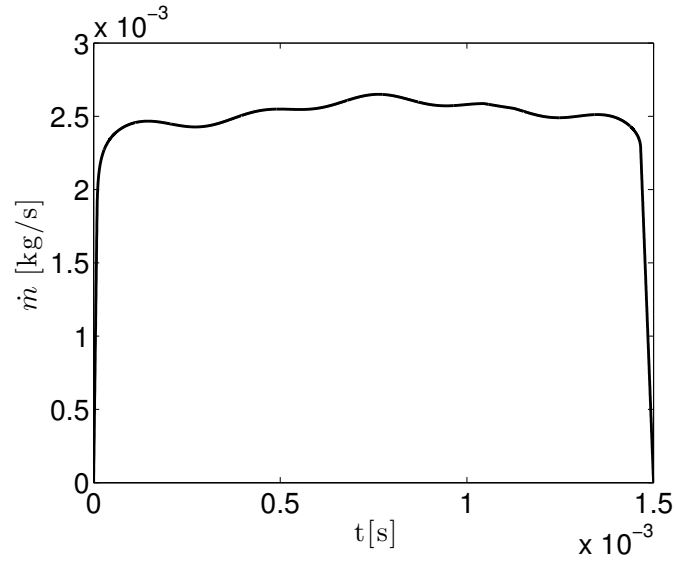


Figure 3.11: Spray-A injection rate.

Finally, atomization, break-up, collision and momentum transfer sub-models are exactly the same as those used under non evaporative conditions. In this regard, there is no correction applied on the C_D calculation to model the evaporation effects on the droplet drag 2.5.4 as suggested by referred studies.

Finally, Table 3.4 summarizes the numerical schemes used for the different terms in Navier-Stokes equations as well as turbulent models for both RANS and LES approaches.

Operator/term	Variable field	Setup
$\frac{\partial \phi}{\partial t}$	All	Euler and backward
$\frac{\partial \phi}{\partial x_i}$	Pressure	Gauss linear
$\frac{\partial(\phi \cdot u_i)}{\partial x_i}$	$\rho, \varepsilon, k, k_{sgs}$ u h	Gauss limitedLinear Gauss limitedLinearV Upwind
$\frac{\mu \partial^2 \phi}{\partial x_i^2}$	All	Gauss linear corrected

Table 3.4: numerical schemes

Chapter 3 bibliography

- [Bau06] C Baumgarten. *Mixture Formation in Internal Combustion Engines*. Ed. by D Mewes and F Mayinger. Springer, 2006, p. 311. ISBN: 978-3540308355 (cit. on pp. 53, 57–59, 101).
- [BR10b] Nidheesh Bharadwaj and Christopher J Rutland. “Droplet–ambient sub-grid interaction modelling in large eddy simulation of diesel sprays”. In: May. Cincimmati, 2010 (cit. on pp. 42, 100).
- [BR99] Jennifer C. Beale and Rolf D Reitz. “Modeling Spray Atomization with the Kelvin-Helmholtz/Rayleigh-Taylor Hybrid Model”. In: *Atomization and Sprays* 9.6 (1999), pp. 623–650 (cit. on p. 101).
- [Cha13] Mariany de J. Chavez. “Modelado CFD Euleriano-Lagrangiano del Chorro Diesel y evaluacion de su combinacion con modelos fenomenologicos y unidimensionales.” PhD thesis. Universidad Politecnica de Valencia, 2013, p. 203 (cit. on pp. 29, 34, 47, 101).
- [Cor98] D Correas. “Estudio teórico-experimental del chorro libre Diesel isoterma”. PhD thesis. Valencia: E.T.S. Ingenieros Industriales. Universidad Politécnica de Valencia, 1998 (cit. on pp. 54, 99).

- [Des+03] J M Desantes, R Payri, F J Salvador, and J Gimeno. “Measurements of Spray Momentum for the Study of Cavitation in Diesel Injection Nozzles”. In: *SAE paper 2003-01-0703* (2003). DOI: 10.4271/2003-01-0703 (cit. on p. 98).
- [Des+07] J M Desantes, R Payri, José M García-Oliver, and F J Salvador. “A contribution to the understanding of isothermal diesel spray dynamics”. In: *Fuel* 86.7-8 (2007), pp. 1093–1101. ISSN: 0016-2361. DOI: 10.1016/j.fuel.2006.10.011 (cit. on pp. 6, 8, 23, 28, 97, 102, 168).
- [Gim08] J Gimeno. “Desarrollo y aplicación de la Medida del flujo de cantidad de movimiento de un chorro Diesel.” PhD thesis. Universidad Politécnica de Valencia, 2008 (cit. on pp. 50, 92, 93).
- [Pay+05] R. Payri, García J., Salvador F., and J. Gimeno. “Using spray momentum flux measurements to understand the influence of diesel nozzle geometry on spray characteristics”. In: *Fuel* 84.5 (Mar. 2005), pp. 551–561. ISSN: 00162361. DOI: 10.1016/j.fuel.2004.10.009 (cit. on pp. 93, 98).
- [Pay+08a] R Payri, F J Salvador, J Gimeno, and G Bracho. “A New Methodology For Correcting The Signal Cumulative Phenomenon On Injection Rate Measurements”. In: *Experimental Techniques* 32.1 (2008), pp. 46–49. ISSN: 1747-1567. DOI: 10.1111/j.1747-1567.2007.00188.x (cit. on pp. 92–94, 100).
- [Pic+13] Lyle M. Pickett, Julien Manin, Raul Payri, Michele Bardi, and J Gimeno. *Transient Rate of Injection Effects on Spray Development*. Tech. rep. Sept. 2013. DOI: 10.4271/2013-24-0001 (cit. on pp. 93, 107).
- [PR02] Eric Pomraning and Christopher J Rutland. “Dynamic One-Equation Nonviscosity Large-Eddy Simulation Model”. In: *AIAA* 40.4 (2002) (cit. on pp. 41, 92).
- [RD87] Rolf D Reitz and Ramachandra Diwakar. “Structure of High-Pressure Fuel Sprays”. In: *SAE Technical Paper 870598* 96 (1987), pp. 492–509. DOI: 10.4271/870598 (cit. on pp. 56, 57, 101, 102).
- [SA10] Sibendu Som and Suresh K Aggarwal. “Effects of primary breakup modeling on spray and combustion characteristics of compression ignition engines”. In: *Combustion and Flame* 157.6 (June 2010),

- pp. 1179–1193. ISSN: 00102180. DOI: 10.1016/j.combustflame.2010.02.018 (cit. on pp. 56, 101).
- [SR00] David P Schmidt and Christopher J Rutland. “A New Droplet Collision Algorithm”. In: *Journal of Computational Physics* 164.1 (2000), pp. 62–80. ISSN: 0021-9991. DOI: 10.1006/jcph.2000.6568 (cit. on pp. 47, 102).
- [YH85] Akira Yoshizawa and Kiyosi Horiuti. “A Statistically-Derived Subgrid-Scale Kinetic Energy Model for the Large-Eddy Simulation of Turbulent Flows”. In: *Journal of the Physics Society Japan* 54.8 (Aug. 1985), pp. 2834–2839. ISSN: 0031-9015. DOI: 10.1143/JPSJ.54.2834 (cit. on pp. 40, 100).

Chapter 4

Results and Discussion

Contents

4.1	Introduction	114
4.2	LES of diesel-like gas jets	114
4.3	Non-evaporating diesel sprays	161
4.4	Evaporating diesel sprays	173
	Chapter 4 bibliography	178

4.1 Introduction



NCE we have described the state of the art in Diesel spray simulation and the numerical set-up needed to perform one simulation. This chapter is devoted to show the strengths of our approach and to validate the results coming from the aforementioned configuration. As we will show a correct set-up is a must for an adequate result, but BC are critical for obtain the right solution.

4.2 LES of diesel-like gas jets

In the previous sections (section 2.3.3) we have described several LES models. In order to understand the differences between these viscous and non- viscous models, simulations injecting gas into a constant volume chamber have been performed. First, mesh size dependency of macroscopic behavior has been explored, maintaining the value of turbulent coefficients. First and second order temporal schemes as well as the inlet boundary condition (both temporal and spatial set up) are analyzed in an attempt to asses their effect on the transient evolution of the gas phase.

4.2.1 Mesh size and temporal schemes independency

Locally refined mesh

Figure 4.1 shows the comparison of penetration for the different turbulent models for two different levels of mesh refinement. Here the location of the gas jet tip is placed for the isosurface depicted at Figure 4.2 ($Y_{fuel} = 0.01$). Also, note experimental results include both average and standard deviation. Besides the match in experimental trend for all the turbulent models with 0.25 mm mesh, the way mesh refinement affects DS turbulent model is clearly different to the rest of explored models. The refinement gradually changes the temporal evolution of penetration whereas DS concentrates them on the early stages of the gas jet evolution. It is also noticeable how DS maintains fairly the same penetration by the end of the injection process. For the so called viscous models, this temporal behavior can be explained by the isotropic way to model turbulence already mentioned 2.3.3.5 where, in the case of DS, the

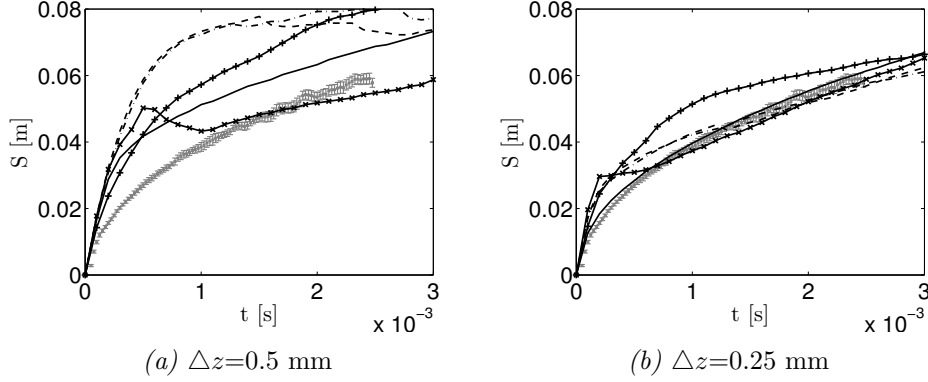


Figure 4.1: Turbulent model penetration comparison (vanDriest filter, improved mesh. \square Experimental results, $---$ Sm, $---$ SA, $+$ OEE, \times DS, $—$ $k - \varepsilon$ (RANS))

dynamic formulation (i.e. Leonard tensor) is suffering from a lack of spatial resolution near the nozzle exit. The fact that the DS matches experimental trend right after initial discrepancy is an evidence of the performance of dynamic formulation under non-isotropic flow conditions. Note, both Figure 4.1 and Figure 4.2 show results calculated with first order temporal scheme and the improved mesh for DS.

As mentioned above, Figure 4.2 depicts the $Y_{fuel} = 0.01$ iso-surface colored by velocity magnitude by the end of the injection event. The range of the velocity magnitude has been modified to turn the contrast up but the value at the inlet BC fluctuates around $\sim 373m/s$. Although symmetric shape is expected in RANS calculations, turbulent inlet boundary condition generates asymmetry at the outer region of the jet and a fluctuating distribution for gas velocity over that surface and the first part of the gas jet. Regarding gas jets simulated by LES, the viscous models requires a physical length to fully develop turbulence, given that the BC only applies a random perturbation on the reference field value $\bar{U} = (0, 0, 373.27)m/s$. In this case, the fluctuation scale is $(0.05, 0.05, 0.1)$, $\alpha = 0.0001$ (an actual temporal evolution of the inlet can be seen at Figure 4.17). Note this is not a synthetic boundary condition, where consistent eddies are introduced in the domain, being able to naturally travel and evolve from the very beginning. From Figure 4.2, the length for turbulence to develop is a function of cell size, time step, and temporal scheme (Figure 4.6) and it has a significant impact on the penetration

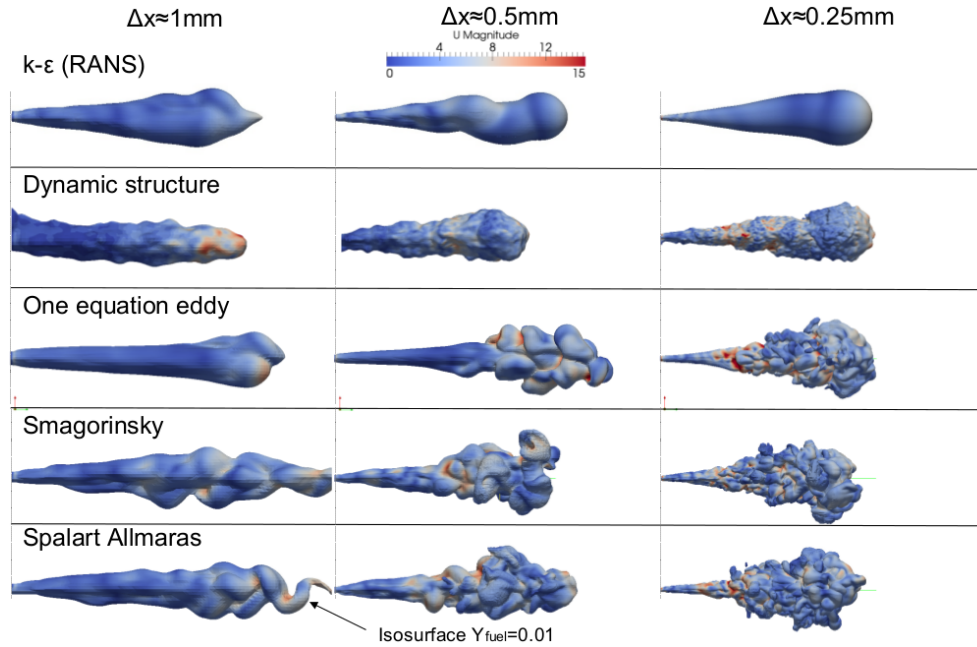


Figure 4.2: Iso-surface of $Y_{fuel} = 0.01$ colored by velocity magnitude ($t = 3\text{ms ASOI}$)

(Figure 4.8). Also, the laminar-like initial region is dependent on the temporal scheme (Figure 4.5 and Figure 4.6)

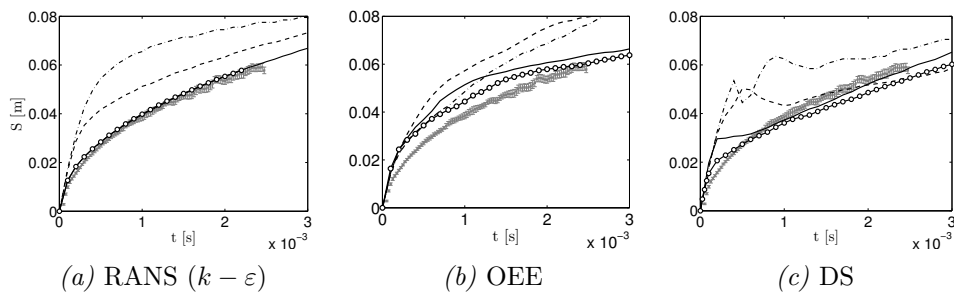


Figure 4.3: Mesh size independence study. I Experimental results, $---$ $\Delta z = 1\text{mm}$, $---$ $\Delta z = 0.5\text{mm}$, $---$ $\Delta z = 0.25\text{mm}$, \circ $\Delta z = 0.125\text{mm}$

Among compressible viscous models available in OpenFOAM, it has been already discuss the completeness and simplicity of OEE over the rest of the

models. Regardless of the loss of accuracy in the prediction of penetration¹ (Figure 4.3(b)) OEE includes an extra transport equation for k_{sgs} . Besides associated advantages to this transport equation, DS comparable formulation helps further analysis and result comparison. Therefore, from now on the study focuses on the differences between OEE and DS.

Unlike viscous models, where DS was used, this lack of turbulent consistency at the inlet boundary condition did not require an extra length to develop turbulence (once the plume has grown), showing a greater independence from the inlet boundary condition (Figures 4.1, 4.3(c), 4.17). Hence the dynamic formulation shows a higher capacity to generate consistent eddies from a non-consistent input randomness. This unique performance of DS does not prevent from the use of a turbulent BC. Like the others turbulent models, the gas jet did not generate any turbulent motion in the calculated domain when simulated with a non-perturbed constant value (Figure 4.20). As expected, a minimum level of perturbation is required for LES simulations². In addition, cell size and time step have a lower impact on penetration, regardless of the increase of turbulent scales seen with smaller cell size mesh. Compare with viscous models, this independence includes the increase of the temporal schemes (Figure 4.5 and Figure 4.6).

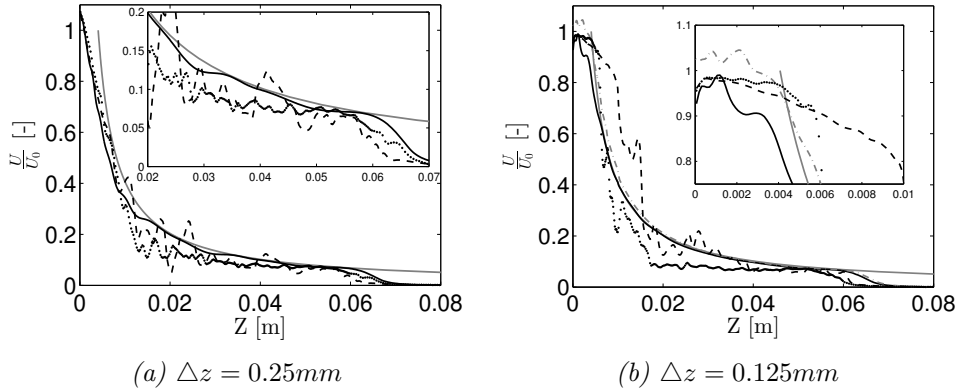


Figure 4.4: Gas jet axis velocity decay ($\bar{U}_0 = 373.27\text{m/s}$, $t = 3\text{ms}$ ASOI, first ddt).
— Theoretical decay, — $k - \varepsilon$ (RANS), --- OEE, ... DS, -·- $k - \varepsilon$ (RANS
 $\Delta z = 0.0625\text{mm}$)

¹Penetration trend can be fixed by tuning OEE turbulent coefficients.

²Discussed in greater detail at the following section.

Results about axis velocity decay are shown in Figure 4.4 for different mesh sizes. The abscissa has been defined as velocity divided by a constant value (i.e. the average inlet velocity). Note how inlet velocity has been randomly modified ($I_z=10\%$ at $Z = 0$) by the boundary condition and it can be higher or lower than the average ($1 \leq U(0) \leq 1$). Each marker on the DS result gives the value at the axis cell center so that the increase on mesh resolution can be appreciated. An increment in frequency content on the instantaneous axis velocity as a consequence of the increase of simulated eddies was found as we refined the mesh from $\Delta z = 1mm$ to $\Delta z = 0.25mm$. Remember $\Delta z = 0.125mm$ refinement step is performed only for the first 10mm and no significant changes can be appreciated after this point for DS velocity decay results. Regarding the $\Delta z = 0.125mm$ refined area, DS turbulent model matches better the end of the averaged non-perturbed zone than RANS and OEE approaches. It is worthy to note that, for the $\Delta z = 0.125mm$ refinement, there are 4 cell elements in X and Y coordinate directions at the nozzle surface, which is the minimum suggested for RANS transient jets [Abr97]. However, 0.25mm is the refinement chosen for the improved hexaedral mesh following penetration results. In addition $\Delta z = 0.25mm$ mesh provides a consistent mesh size and topology to compare with the L-E cases.

Grid-dependence of diesel-like gas jets using RANS (Figure 4.3(a)) follows the common CFD rule of decreasing as the number of cells is increased. In the case of LES the same trend must be found although the asymptotic limit for the cell size would be set by the DNS requirements under the specific flow simulation. Since the goal is to keep the same computational cost of RANS calculations the mesh will be set by the RANS grid-independent cell size. From this point LES should approach the most realistic behavior possible by means of improved turbulent models. As shown by Figure 4.3(a) no change in penetration is appreciated between 0.25 mm and 0.125 mm mesh. Therefore, 0.25 mm cell size fixes the threshold for OEE and DS results to match experimental trends in order to set a comparable computational performance.

As previously mentioned Euler temporal schemes (first order) calculations were run with an adjustable time step based on a $CFL = 0.5$. In contrast, cases calculated with backward temporal scheme (second order) needed a smaller CFL (i.e. $CFL=0.125$) to avoid instabilities. As it can be seen, for OEE (figure 4.5(a)) not only the reduction of time step required by the temporal scheme affects the penetration evolution, but the temporal scheme itself. In contrast, there is no substantial improvement when DS is used with $\Delta z = 0.25mm$

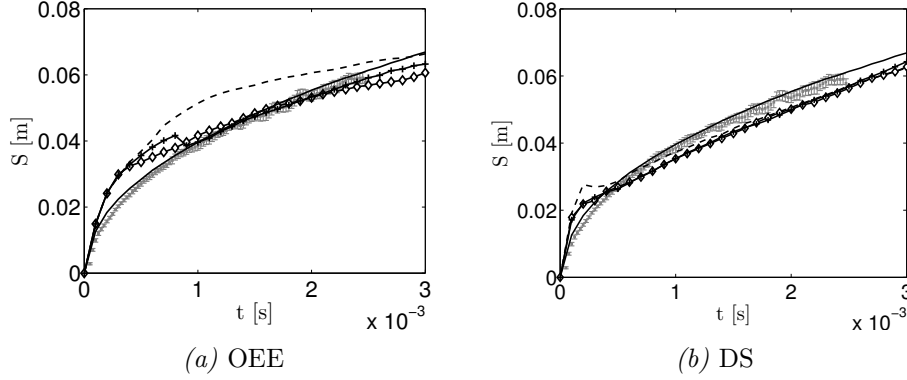


Figure 4.5: Time step and temporal scheme effect on penetration ($\Delta z = 0.25\text{mm}$, reference mesh). \square Experimental results, $—$ $k - \varepsilon$ (RANS), $- -$ $-1^{st} ddt$ CFL = 0.5, \diamond $-1^{st} ddt$ CFL = 0.125, $+ +$ $2^{nd} ddt$ CFL = 0.125

mesh (Figure 4.5(b)). Also both parameters have a smaller impact on the DS than the OEE by the end of the calculation. This argument supports the superiority of DS formulation based on the fact that Leonard tensor may need initial time to generate consistent anisotropic turbulence, but have no further macroscopic consequences on jet development after that (Figure 4.7). Regarding OEE, initial penetration is the same independently on numerical scheme or dt (Figure 4.5(a)) as a consequence of the required physical length to generate turbulence (i.e. not because of a better or a more robust turbulent modelling). Afterwards changes in penetration appear

As explained at section 3.2 variations on the morphology of the cells combined with different filter definitions were performed to analyze their impact on LES models. Figure 4.8 shows the penetration of different mesh topology calculated with maxDelta filter size. The percentage differences of penetration based on the filter utilized is included.

As mention in section 3.2.2, vanDriest is the by default filter used for previous results (Figures 4.1 - 4.7) For instance, the penetration difference in dash dotted blue, compares penetration curves with $\Delta z = 0.25\text{mm}$ results of Figure 4.3. In particular, a negative percentage means a lower penetration for the case with vanDriest filter.

Regarding DS results, when compared with square inlet meshes, roundInlet

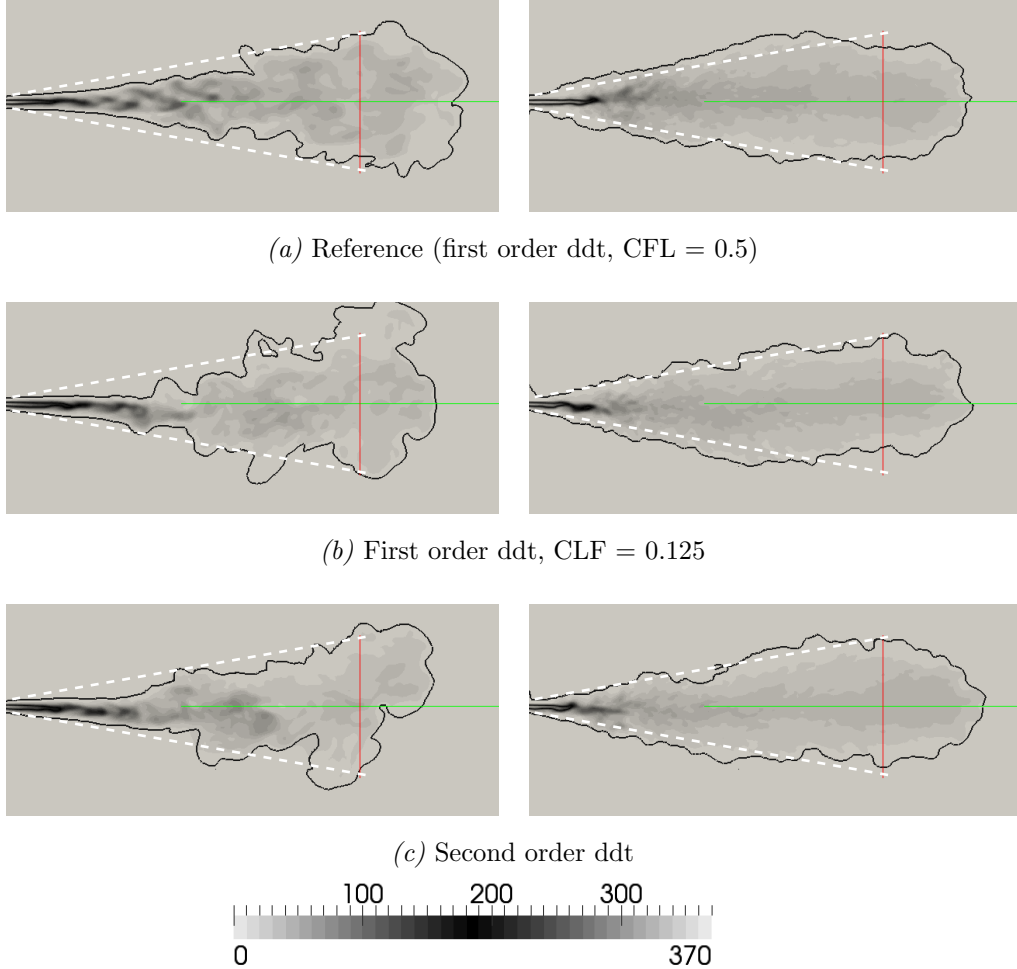


Figure 4.6: Contour plots of velocity magnitude (Reference mesh, $\Delta z = 0.25\text{mm}$; $t=0.003\text{s}$ ASOI). Left column: One equation eddy. Right column: Dynamic structure.

reduces the first part discrepancy with experimental measurements of penetration. Also, vanDriest filter initially *worsens*³ jet inception (i.e. before the slope changes) but it has very little impact afterwards.

³Although is a small percentage ($\leq 5\%$) over a small magnitude.

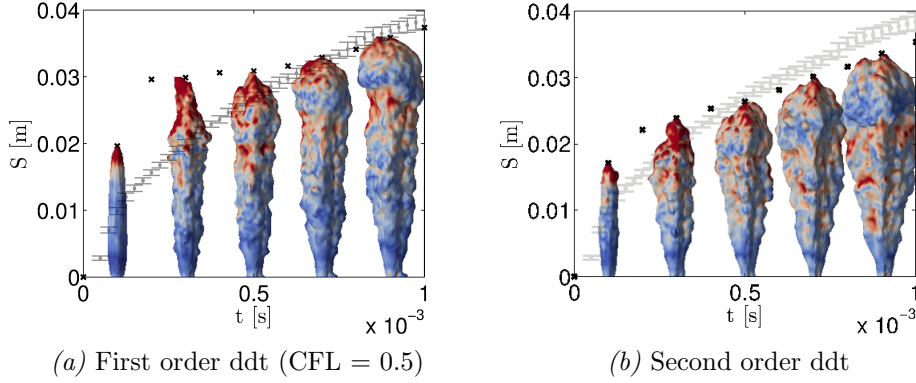


Figure 4.7: Gas jet first instants. Isosurface $Y_{fuel} = 0.01$ colored by velocity (DS, $\Delta z = 0.25$ mm, reference mesh)

In order to analyze velocity decay evolution, bear in mind that same axial mesh resolution is applied to all topologies. The only difference between square and round- like inlet is the discretization within the nozzle diameter in XY direction (i.e. along the axis). Compared with square inlet meshes, roundInlet mesh better displays the theoretical non perturbed zone (i.e. a *constant* axis magnitude within this region). In this regard, the fact of having a greater axial velocity close to the nozzle does not increase penetration significantly⁴ (Figure 4.14(b)). In the same sense, the initial evolution of penetration (i.e. $t \leq 0.0005s$) is lower than the square inlet. The increase of turbulent description enhances mixture and compensates for the actual values of axial velocity.

In the case of OEE, it may seem that the worst mesh leads to the better jet evolution. However, Initial separation between simulated and experimental penetration responds to the initial length required to develop turbulence⁵. In the same sense the decrease on the slope produced by vanDriest filter can not be considered an improvement, even if it means a match with the experimental penetration by the end of the injection event. In this regard, OEE turbulent model has a higher dependency on the inlet boundary condition and the filter effect may be assessed afterwards . Regarding the change in slope for round inlet after 60mm, remember the mesh refinement limits.

⁴Contrary to what one would expect.

⁵This idea will be further explained in following sections. As a provisional prove check velocity decay, as well as, Figures 4.2 and 4.17.

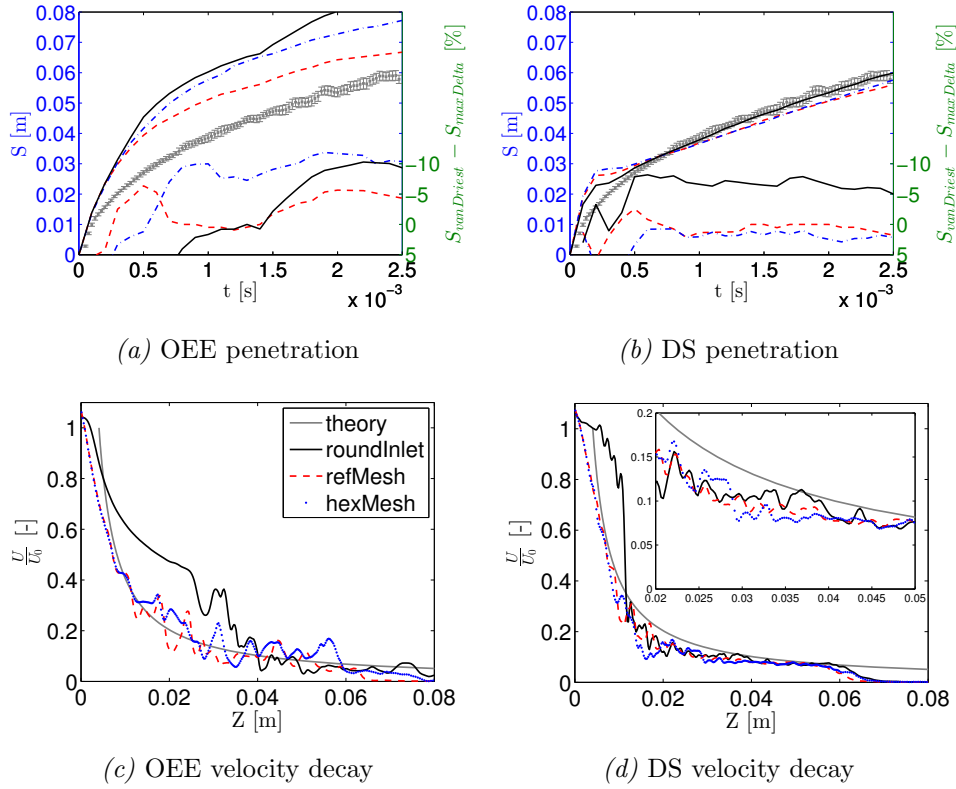


Figure 4.8: Mesh shape and filter effect on gas jet ($\Delta z = 0.25\text{mm}$, filter maxDelta).
 —Round inlet, -.- Improved mesh, - - - Reference mesh

Axis velocity decay (Figure 4.8(c)) shows the initial length required to develop turbulence. Note the extended delay on the generation of turbulence depicted by roundInlet mesh. Also, once turbulent behavior appears (0.025-0.04s) it further increases the velocity decay (seen also at Figure 4.10(a)).

Figure 4.9 shows the temporal evolution of axial velocity decay for the three topologies. As used in Figure 4.9(c) lines from 0.5ms (light gray) to 3ms (black) are drawn each 0.5ms. Note how for the first time the penetration for the three topologies coincide (Figure 4.14(b)). However, the velocity decay varies and only the round inlet mesh consistently shows a realistic evolution of the non perturbed zone. Macroscopic parameters such penetration are clearly insufficient to assess LES. Also, round inlet mesh achieves a higher turbu-

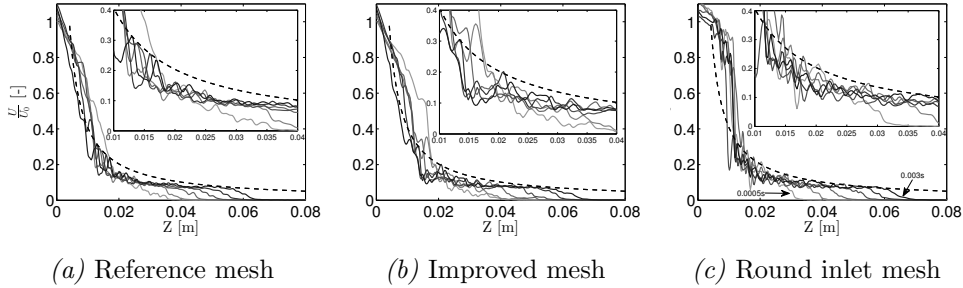


Figure 4.9: Temporal evolution of velocity decay (DS, $\Delta z = 0.25mm$, filter maxDelta) ---Theoretical decay.

lent amplitude. Notice, filter can not be blamed since the longest distance (i.e. in Z direction) at the axis is the same for all three configurations (same physical discretization). Hence, it has to be related with the radial improved discretization. Since the solution obtained with OEE is not realistic (Figure 4.14(a) and 4.8(c)) there is no need to analyze temporal evolution. In following sections improved inlet boundary conditions will reproduce reasonable macroscopic evolution of the gas jet simulated with OEE turbulent model.

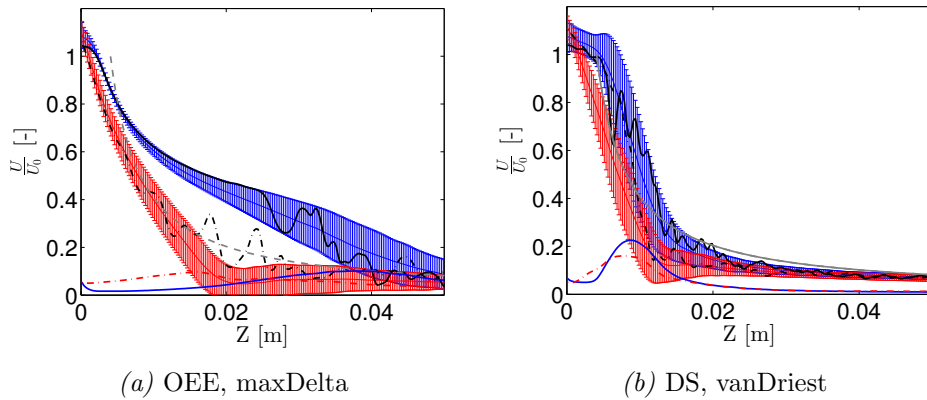


Figure 4.10: Average velocity decay ($\Delta z = 0.25mm$). █ Round inlet, █ Reference mesh.

Velocity field shown in Figure 4.10 have been time averaged from 0.003s to 0.009s. In interest of clarity, only two mesh results are included in each graph: reference mesh and roundInlet mesh. Note, the bars show both average and

standard deviation. Also, the blue and red line at the bottom of the graph depicts the actual value of the standard deviation. The black line represents the velocity decay at $t=0.003s$.

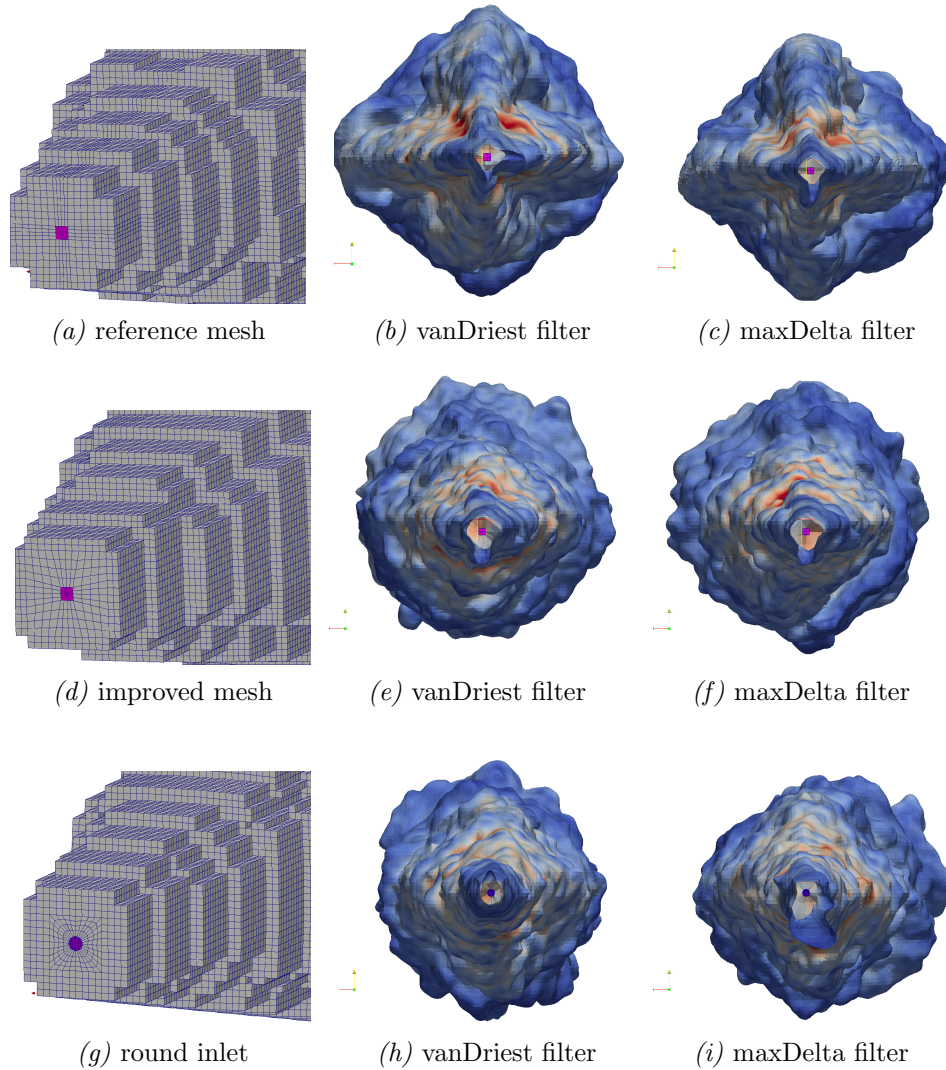


Figure 4.11: Mesh shape effect on E-E gas jet (DS, $\Delta z = 0.25mm$).

As seen at the DS velocity decay temporal evolution (Figure 4.9), turbulent amplitude is greater for round inlet than for the square inlet meshes. Note as

well, the averaged inlet is greater than 1. *TurbulentInlet* randomly modifies the reference value (i.e. $\vec{u} = (0, 0, 373)$) but does not take into account that for the magnitude, X and Y components always add their values, no matter what their sign is. Hence, the average of vector fields magnitude is always greater than the reference value imposed at the boundary condition⁶.

In the case of OEE, besides necessary improvements in the inlet BC, mesh inhomogeneity is a turbulent precursor. For this particular case it is greater than the random inlet itself. As explained in the following section, this is not the case when consistent turbulence is introduced by means of mapped inlet.

In summary there is a less overall effect on DS, from mesh topology and the type of filter for the range of cell sizes studied. The main differences are limited to the penetration first instants, for both parameters.

The last isosurfaces at Figure 4.7 (i.e. reference mesh) show a lack of axial symmetry. The biased shape of the gas jet case can be a consequence of mesh shape affecting resolved or sub-grid scales. There are two different inlet B.C (i.e. square and octagon) and two mesh procedures within the square shaped inlet B.C as shown at Figure 4.11 (gas jet as seen from the inlet). In this way we should be able to analyze the effect of inlet shape, cells morphology and the lack of hanging nodes.

Following filter definitions⁷ neighbor cells with half volume (i.e. the ones shown near the nozzle at Figure 4.11(a)) have half of the vanDriest filter length. Whereas maxDelta has an homogeneous filter length since $\Delta z = 0.25mm$ is a constant in the region of interest. Consequently the same biased shape for both filter with the reference mesh dismiss the filter as the cause of asymmetry. In addition, the fact that the improved mesh and round inlet mesh partially recover the symmetry supports the previous statement. Therefore, the asymmetry is a consequence of the effect of the mesh on the resolved scales. Keep in mind that the shape of Leonard stress tensor is based on the simulated scales. Hence the effect on resolved scales is transferred to sub-grid scales magnifying the tendency.

Figure 4.12 shows a X plane contour plot of jets from Figure 4.11. Note the apparent increase in spread angle of reference mesh due to cell shaped pref-

⁶This circumstance does not apply to scalar fields.

⁷vanDriest is the cube root of the cell volume, and maxDelta uses the maximum length between the cell centre and its faces as the filter length.

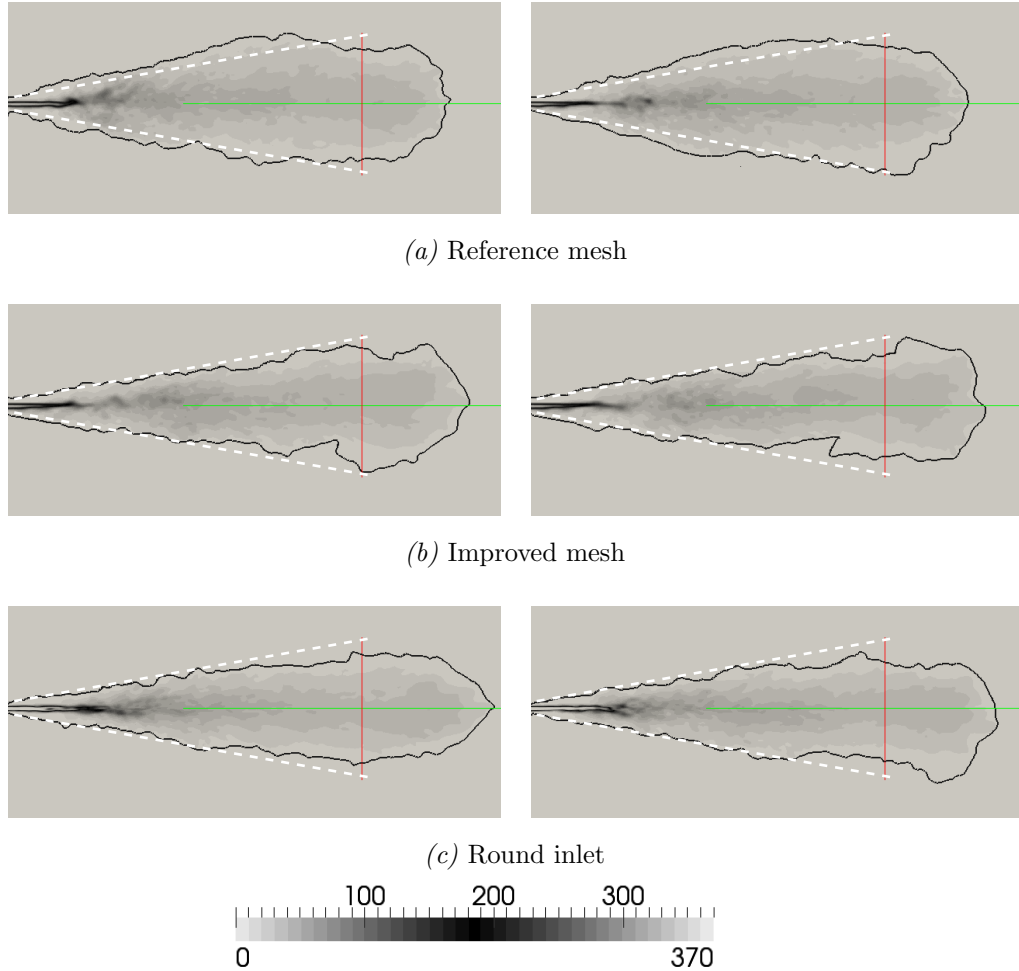


Figure 4.12: Mesh shape and filter effect on gas jet spreading angle ($\Delta z = 0.25\text{mm}$, $t=0.003\text{s}$ ASOI). Left column: vanDriest filter. Right column: maxDelta filter.

erential spread directions. Also, images confirm the extended non-perturbed zone at the round inlet meshes (i.e. high velocity region limited by white shape triangle from nozzle exit). Hence, at the end of the injection event, the small differences in penetration come from an artificially enhanced spreading rate.

In order to categorically state the effect of mesh topology on the DS turbulent model, time or ensemble averaged results must be analyzed. In this

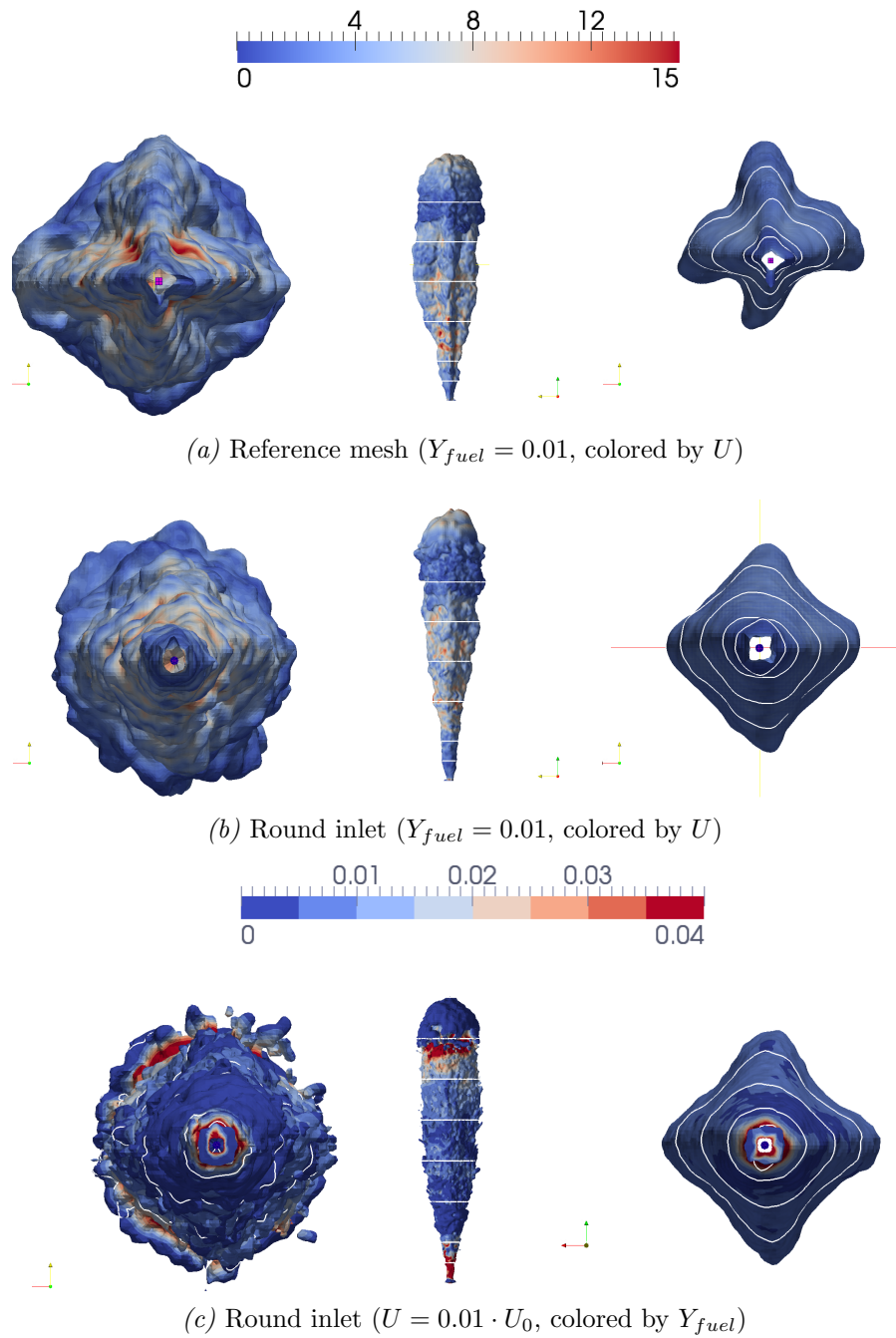


Figure 4.13: Mesh topology effect on averaged gas jet (DS, $\Delta z = 0.25\text{mm}$).

regard average velocity decay graphs have been already discussed (Figure 4.10). Figure 4.13 shows the average surface of the first 40mm. Left and center images represent the jet at 0.003s as seen from the inlet and the side. The white cuts on the jet side view are placed as a reference⁸. The same cuts appear at the averaged surface. The averaging process begins at the end of the injection event ($t=0.003s$) when the flow has already passed twice by the further section of study (i.e. $Z=40mm$). The average is run for 0.006s. Hence by the end of the averaging the pass flow time (pft) at $Z=40mm$ is ~ 5 .

Although instant images of roundInlet iso-surfaces may look axisymmetric, the average of the field reveals a preferential spread direction. As expected, this behavior is not only related to the transport scalar of injected fuel, but applies to velocity field as well. Figure 4.13(c) displays the iso-surface of 1% of U_0 . Note this surface should be equivalent to the $Y_{fuel} = 0.01$ iso-surface if the rate of momentum equals mass transport ($Sc = 1$). Also the range of velocity magnitude (0-15m/s) and Y_{fuel} (0-0.04) are equivalents under this hypothesis. Velocity and Y_{fuel} snapshots at 0.003s are not very similar but the surfaces for the averaged fields are very close⁹. Non-axisymmetric isosurface of average velocity advises against the analysis of radial profiles. Instead they will be displayed at the following section with the improved inlet BC.

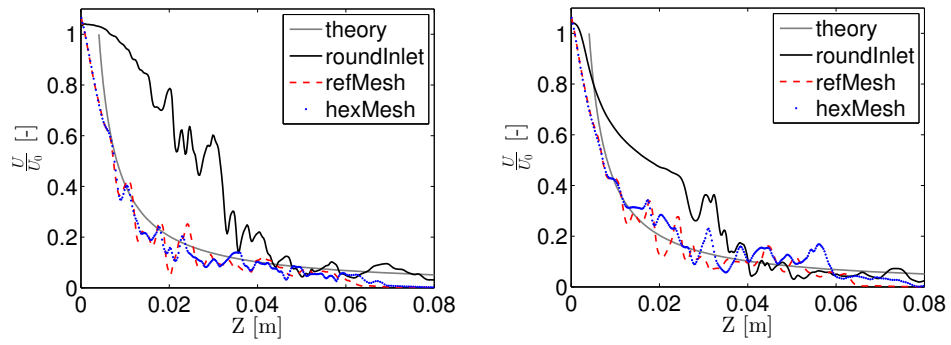
As already mentioned, OEE results are pending on a proper inlet BC. As a qualitative reference, following graphs and figures are consistent with the analysis performed for DS. First, the effect of mesh topology and filter on the velocity decay is displayed at Figure 4.14. Consistent with Figure 4.14(a) the greater differences appear for both filters with the round inlet mesh. Also, the difference in initial length to develop turbulence clearly appears at the contour plots. The closer to the nozzle the lower penetration is achieved by the jet.

Surfaces and lines at Figure 4.15 are colored with a range of magnitude velocity within (0-15[m/s]). Apparently there are not marked preferential directions and Iso-surface images does not offer a clear view (i.e. too much information). In order to distinguish the shape of the jet, several cuts along the axis have been performed (i.e. 5, 10, 20, 30 and 40mm).

The isosurface of the average field for the reference mesh and the roundInlet mesh can be found at Figure 4.16. When compared with Figure 4.13 OEE calculations need a longer period of time to average results. Since the only

⁸Figure 4.15 displays only the cuts at the same locations.

⁹For this particular case, the averaged $Sc \neq 1$.

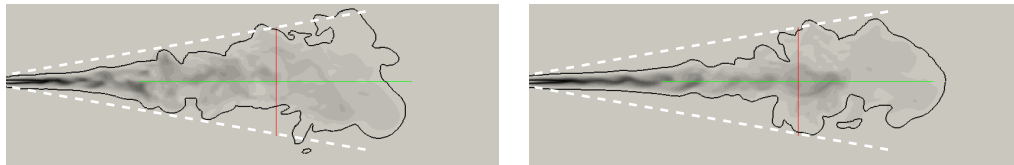


(a) VanDriest

(b) MaxDelta



(c) Reference mesh



(d) Improved mesh



(e) Round inlet

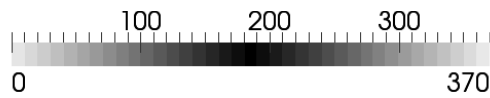
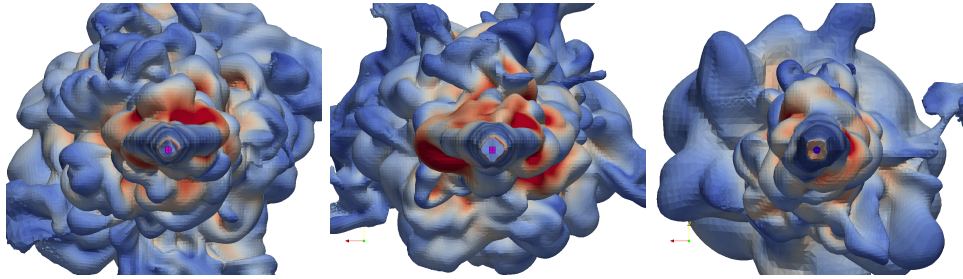
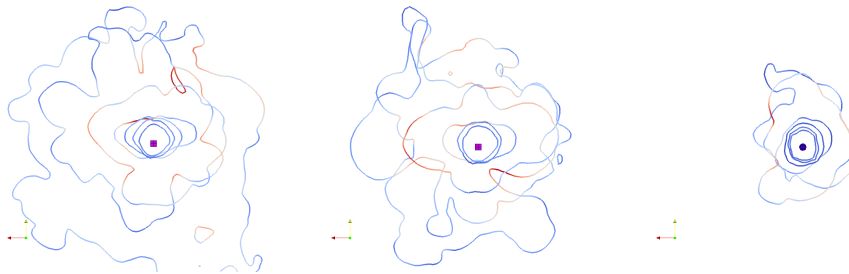


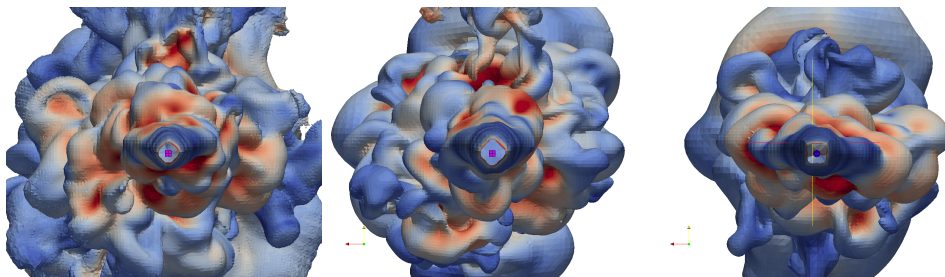
Figure 4.14: Mesh topology and filter effect on OEE gas jet ($\Delta z = 0.25\text{mm}$, $t=0.003\text{s}$ ASOI).



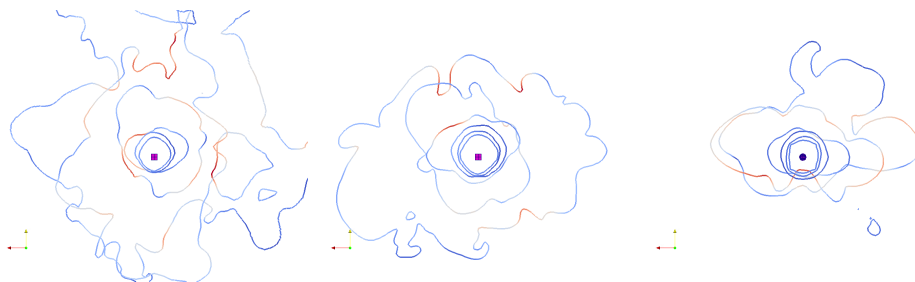
(a) vanDriest filter (Isosurface)



(b) vanDriest filter, cuts



(c) maxDelta filter (Isosurface)



(d) maxDelta filter, cuts

Figure 4.15: Mesh shape effect on E-E OEE spray evolution (DS, $\Delta z = 0.25mm$, $t=0.003s$ ASOI). From left to right: reference mesh, improved mesh and round inlet.

variable changing here is the mesh topology. One may state that cells inhomogeneity is a turbulent precursor. As analyzed at following sections, its weight becomes significant when non consistent eddies are introduced in the domain. In any case, the fact that inlet BC is key for OEE sets any further comment to the following section.

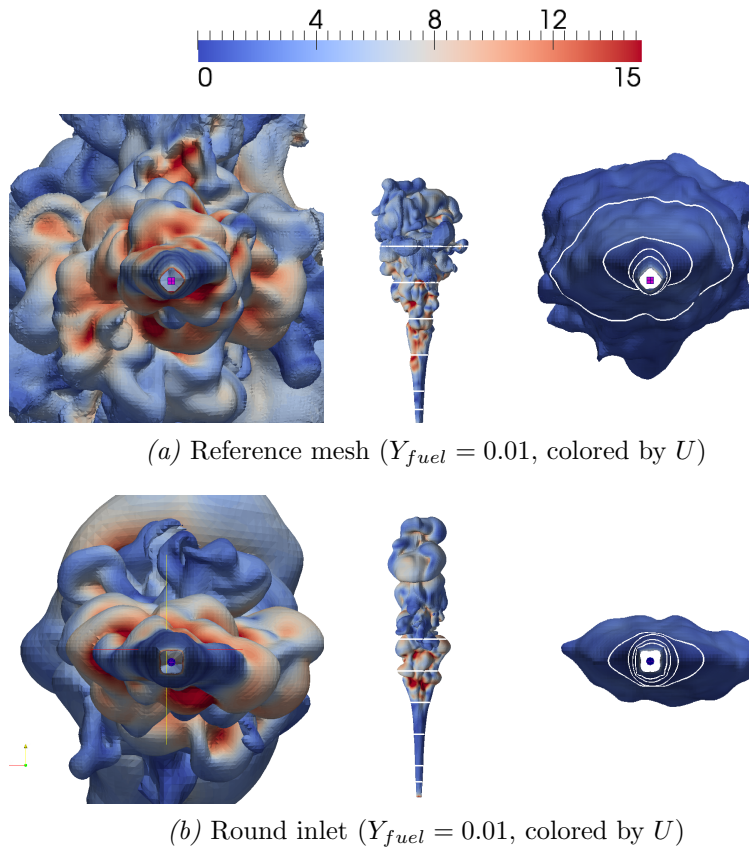


Figure 4.16: Mesh topology effect on averaged OEE gas jet ($\Delta z = 0.25mm$, $\max\Delta t$).

Finally, turbulent content of the flow can be seen at Figure 4.17. Note the inlet signal has exactly the same turbulent content for both DS and OEE. Inside the zoom region of DS graph we can appreciate the differences on the amplitude of the flow imposed and the amplitude of the closest signal to the nozzle (5mm). Bear in mind that this probe is right at the end of the non-perturbed zone, where the axis velocity should be very close to the injected

one and the interaction with the surrounding low velocity flow increases the turbulence. DS allows such patterns where OEE axis velocity decays (with $\sim 1/x$) and keeps the same turbulent content as the injection 2cm downstream the nozzle.

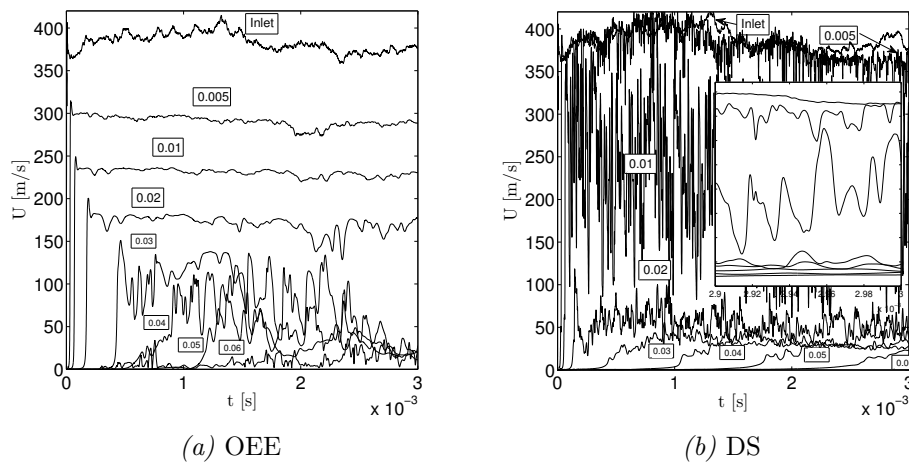


Figure 4.17: Axis velocity probes ($\Delta z = 0.25mm$, roundInlet, maxDelta filter)
 Ordinate range in zoom region is the same as the originating graph.

Grading mesh

As stated at section 3.2.2 the domain covers the first 0.07m after the end of the non-perturbed zone (Figure 3.4). At this location, the average radial profile of velocity and mass fraction follows the Gaussian distributions described in section 2.2 (eq. 2.12 and 2.13). Hence, both profiles are imposed as the reference for the *turbulentInlet* BC.

Figure 4.18 compares the penetration temporal evolution of both locally refined¹⁰ and grading mesh. Note the penetration of the locally refined mesh starts at (0,0) where the grading mesh penetration starts at $\sim 0.004m$. Also, a delay time is applied to account for the time needed by the spray to reach that location ($\sim 2.5 \cdot 10^{-5}s$)

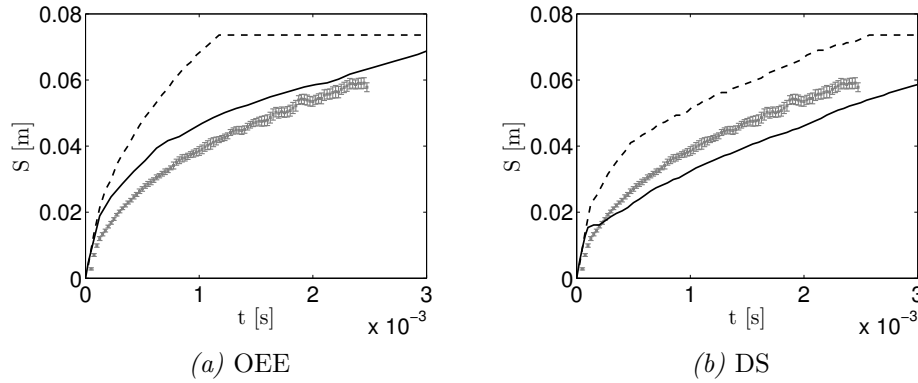


Figure 4.18: Penetration ($\Delta z = 0.0625mm$). I Experimental data, — Improved mesh, --- Grading mesh.

In agreement with the previous section, results of penetration for OEE ask for an improvement on the injection temporal evolution (i.e. the inlet BC). On one side, there is very little difference between the penetration of Figure 4.3(b) ($\Delta z = 0.125mm$, improved mesh) and the following refinement iteration depicted at Figure 4.18(a). On the other, OEE is unable to generate any turbulent structure on the gradMesh domain(Figure 4.19(a)) nor to approach the theoretical velocity decay.

From Figure 4.19(a) it is worthy to mention the improvement of the hex-

¹⁰Remember local refinement to achieve $\Delta z = 0.0625mm$ cell size is applied within the first 7.5mm.

aedral mesh on the velocity decay. A local refinement on the first 7.5mm improves, not only the match of the non-perturbed zone but the rest of the $\sim 1/x$ axial decay.

Regarding DS, the local refinement reduces the initial deviation with penetration seen at Figure 4.3(c) ($\Delta z = 0.125mm$, improved mesh). Although grading mesh penetration shows a shift from the experimental data, it reproduces the characteristic change of slope and the second stretch has the same gradient as the experimental penetration.

As expected the relevance of the BC increases with spatial discretization. Both OEE and DS require a better inlet BC to further analyze jet behavior as simulated on grading mesh.

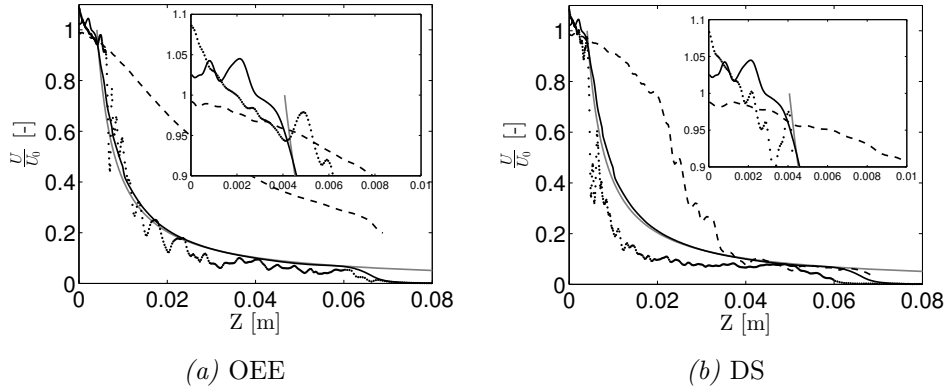


Figure 4.19: Gas jet axis velocity decay ($\bar{U}_0 = 373.27m/s$, $\Delta z = 0.0625mm$, $t = 3ms$ ASOI). — Theoretical decay, — $k - \varepsilon$ (RANS), \cdots Improved mesh, ---Grading mesh.

4.2.2 Boundary conditions sensitivity

This sections offers the record of successive improved inlet fields to simulate the reference case for both the locally refined mesh and the grading mesh.

Locally refined mesh

Besides *turbulentInlet* BC already described, there are basically two procedures to improve the turbulence of the imposed inlet fields. On one hand, fields

from previous simulations or experiments can be mapped on the inlet BC. In this way, by assuring sufficient temporal and spatial discretization, consistent turbulence is introduced on the domain. On the other, consistent eddies can be artificially generated (i.e. synthesize) at the BC. Synthetic BC has been developed for OpenFOAM and applied to exhaust LES by Montorfano et al [Mon+11]. However, the lack of resolution of the inlet BC in the present study (i.e. up to 4 elements for 0.25 mm cell) reduces its impact on the solution (related to the increase of complexity associated) and therefore advised against the use of this BC. Nevertheless, in light of the present results the study of this synthetic BC on the simulation of diesel-like gas jets is proposed as future works.

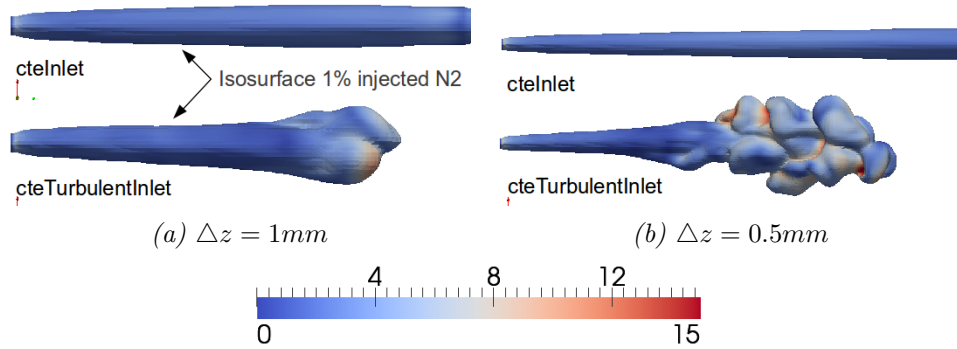


Figure 4.20: Gas jet shape as a function of inlet BC type (OEE, $t=3\text{ms ASOI}$)

On a first approach, both constant and turbulent BC were tested. As already mentioned, the behavior displayed at Figure 4.20 is consistent with any of the turbulent models previously used. Once confirmed a minimum level of perturbation is required for LES simulations, the goal is to delimit that *minimum* in terms of inlet quality.

Figure 4.21 shows the experimental injection rate and the temporal evolution of the inlet velocity. As already mentioned, the signal of a probe from one of the calculations is used to reproduce consistent turbulence. The case selected is calculated with DS on a roundInlet domain. As Figure 4.8(d) shows, this case reproduces the behavior of the non-perturbed zone, and it has the closer trend to the theoretical velocity decay.. .

It is worthy to note the 1mm difference between the probe of Figure 4.21(b) and 4.21(c). Although there are only four cells between them, conceptually

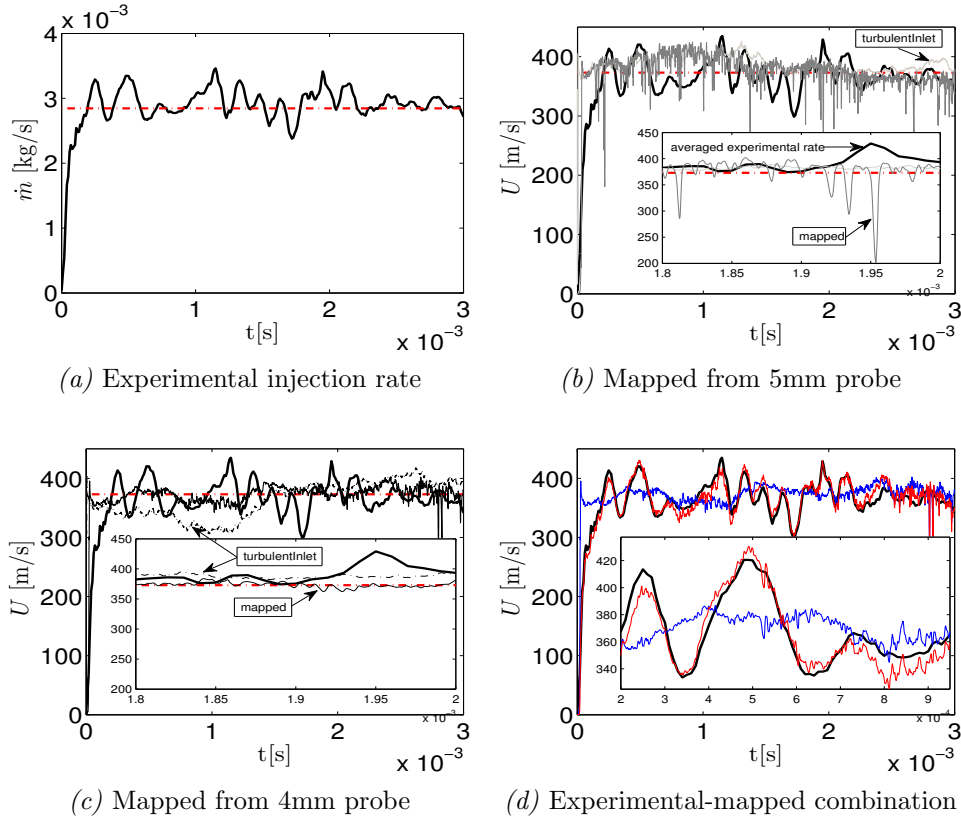


Figure 4.21: Evolution of the inlet BC

they belong to two different regions of the gas jet (i.e. right before and after the end of the non-perturbed zone). The difference in turbulent content is clear and it has already been analyzed¹¹.

Finally, experimental injection rate (Figure 4.21(a)) is an averaged profile from mass flow rate measurements. Therefore, turbulence is removed by the average process and the fluctuations shown by the injection rate are due to the flow dynamics inside the nozzle. Hence, by adding a consistent turbulent signal to the experimental velocity profile we are reproducing a singular injection event (Figure 4.21(d)). With this strategy we try to improve the simulation

¹¹The increase in turbulence of 0.005mm probe is due to the interaction of the injected gas (high velocity) with the surrounding gas (low velocity).

of the jet first instants (e.g. the first part of the penetration). . Note from now on the term *turbulent experimental rate* will refer to the combination of the experimental rate with the 4mm probe signal (i.e. red line at Figure 4.21(d)).

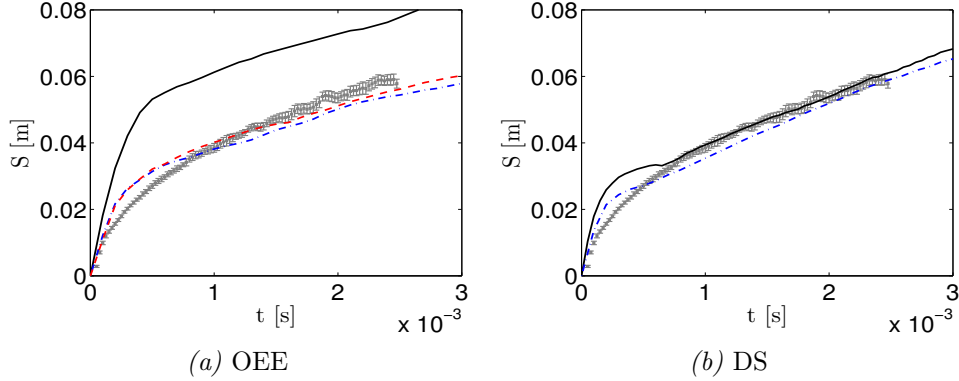


Figure 4.22: Penetration. Effect of consistent turbulence. (vanDriest, roundInlet mesh). —*turbulentInlet*, -.- mapped (5mm probe), - - - OEE $c_\varepsilon = 0.916$, $c_k = 0.067$ (mapped from 5mm probe),

Figure 4.22 shows the effect of the improvement in the physical description of the turbulence at the inlet. By including consistent eddies OEE penetration experiences a drastic reduction. The main improvement is located at the initial penetration due to a reduction of the initial length required to develop turbulence. Afterwards, the second slope of both *turbulentInlet* and mapped penetration are very similar. Hence, there is a limited influence on the second penetration stretch. A OEE case with modified turbulent coefficients is included to show the relative effect when compared with the inlet BC. In contrast with the BC, the turbulent coefficients affect the second part of the penetration.

We have verified as well how mapped roundInlet and improved mesh differ very little (even with slightly modified turbulent coefficients). Hence It is clear how OEE needs consistent turbulent eddies even for poor physical discretization.

Regarding the DS, imposed mapped fields have similar qualitative effect. The inlet BC improves the initial penetration and has no influence on the second part. However the BC has a lower impact on the DS which confirms the robustness of the model.

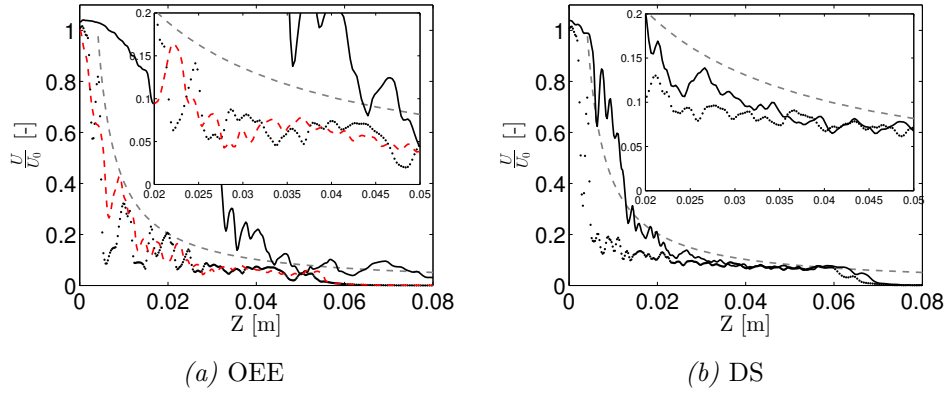


Figure 4.23: Velocity decay. Effect of consistent turbulence. (vanDriest, roundInlet mesh). —*turbulentInlet*, ··· mapped (5mm probe), - - - OEE $c_\epsilon = 0.916$, $c_k = 0.067$ (mapped from 5mm probe).

Changes previously described can be seen reflected on the velocity decay of the jets (Figure 4.23). In both cases (i.e. OEE and DS) the non-perturbed zone is reduced moving the axis velocity field underneath the theoretical decay. The explanation of this behavior can be found on the average fields shown at Figure 4.24.

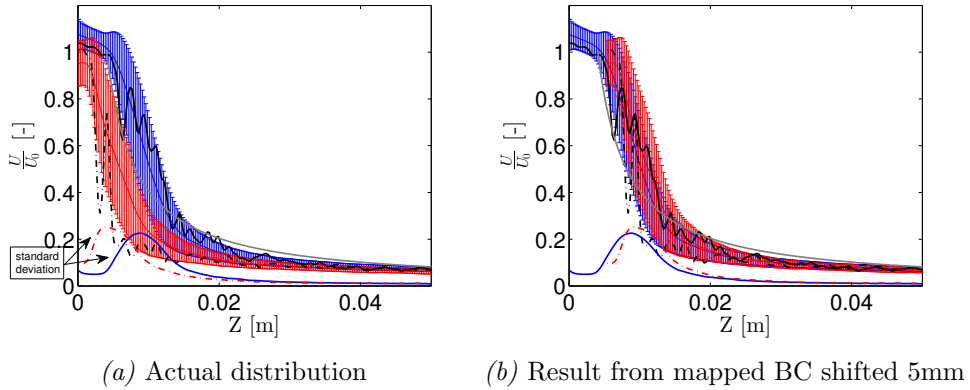


Figure 4.24: Average velocity decay. Effect of consistent turbulence. (DS, vanDriest, roundInlet mesh). ▮ *turbulentInlet*, ▮ mapped (5mm probe), —*turbulentInlet* (3ms ASOI), - - -mapped (3ms ASOI).

Note how the end of the non-perturbed zone can be characterized by an increase of velocity variance. Hence at the mapped BC case, the non-perturbed zone nearly disappears. This behavior is consistent with the turbulent characteristics of the inlet BC. The mapped values come from a probe at (0, 0, 0.00525)m where the flow is already a mixture of the injection and the surrounding.

As expected, when averaged mapped velocity decay is shifted towards $Z=0.00525\text{m}$ (i.e. the position where inlet data was acquired) averaged inlet velocity matches with *turbulentInlet* solution. In this regard, it is worthy to mention how after the initial discrepancies (Figure 4.24(b)) both average and standard deviation match ($Z > 0.5 + 1.5\text{cm}$)

In order to be consistent, the fields imposed should be mapped within the non-perturbed zone ($Z < 0.407\text{m}$). In order to let turbulence develop, the probe must be placed at the cell in front of the beginning of the theoretical decay line. As we have seen, this happens to be the location where turbulent inlet variance increases for the source case (i.e. DS, *roundInlet*) setting the end of the non-perturbed zone.

Following results compare mapped inlet BC with different turbulent nature (i.e. flow influenced by surrounding fluid or not). As it has already shown, an inlet mapped from 5mm probe represents an upgrade with respect to the openFOAM default *turbulentInlet*. However, there is a margin of improvement as it can be deduced from Figures 4.21(b) and 4.21(c).

Regarding penetration, Figure 4.25 shows a minor change on OEE jet and even smaller for DS. In the case of OEE, the increase of penetration when mapped with the 4mm-probe signal is due to the lower turbulence and the consequent mixing descent. In the case of DS, turbulent content has a lower impact as it has been demonstrated.

Velocity decay graphs (Figure 4.25(b)) show a greater improvement than penetration. Note how, besides the enhance simulation of the non-perturbed zone, and despite the differences on the initial velocity decay, penetration is almost the same for both DS and OEE. Instantaneous values of both OEE and DS show a better evolution within the non-perturbed zone and a decay closer to the theoretical trend.

As in the previous section, average velocity fields reveal a greater extent of the improvement achieved. Note, the drastic difference between mapping with

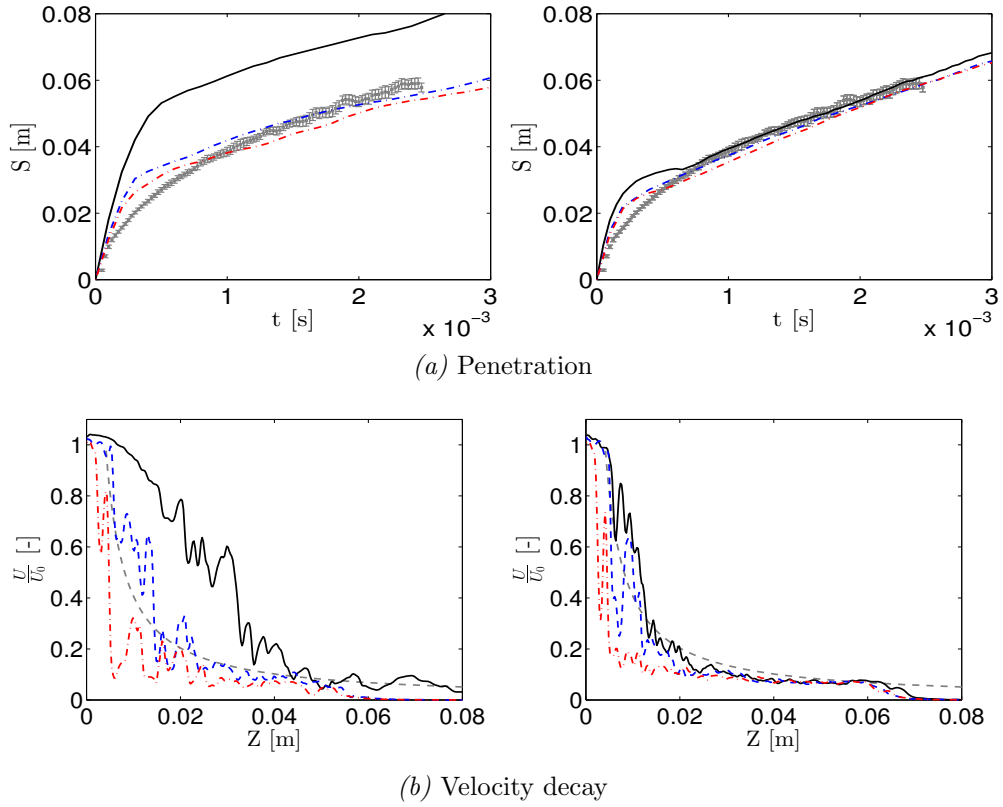


Figure 4.25: Effect of probe location (vanDriest, roundInlet mesh). Left column: OEE, right column: DS. — *turbulentInlet*, - - - mapped (4mm probe), - · - · - mapped (5mm probe).

1mm of difference in the probes location. It is key to have the fields before the injected flow mixes with the chamber gas.

In both cases, *turbulentInlet* and 4mm-mapped field cases increase the variance towards the vicinity of the theoretical end of non-perturbed zone. Also, the maximum variance happen to meet in magnitude and axial position.

Also, looking at the non-perturbed zone. *turbulentInlet* stochastic eddies neutralizethemselves reducing both the effective velocity magnitude imposed and the variance closer to the nozzle exit. On the contrary, when mapping consistent turbulent fields velocity magnitude show a sustained initial value

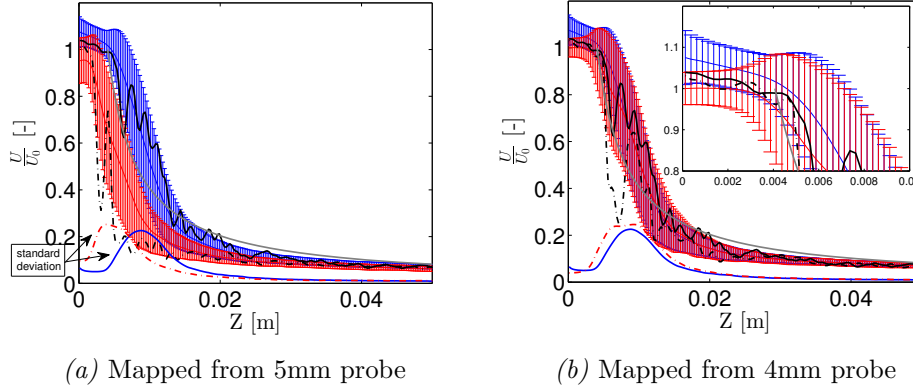


Figure 4.26: Average velocity decay. Effect of inlet turbulent content. (DS, vanDriest, roundInlet mesh). \mathbf{I} *turbulentInlet*, \mathbf{I} mapped, — *turbulentInlet* (3ms ASOI), - - - mapped (3ms ASOI)

and a reduced growth on the variance.

Note, at the end of the signal acquired by the 4mm probe (Figure 4.21(c)) there are 2 eddies with similar turbulent content than the 5mm probe. They can be easily identified since the inlet velocity magnitude suddenly drops under 300m/s. During that particular time the non-perturbed zone is momentarily shortened leaving the 4mm probe exposed to the mixture flow where velocity decays $\sim 100m/s$. Note, the standard deviation previous to those eddies is 11m/s which makes the unexpected eddy an order of magnitude greater.

In all fairness with the data measured they were not tone down when the signal was repeated for averaging process. As a consequence certain bump before the maximum variance can be seen. Also, those eddies were kept when the 4mm-probe signal was combined with the experimental average injection rate.

Figure 4.27 compares the average velocity decay of OEE and DS. Note, the eddies of unusual lower velocity introduced at the end of the injection rate affects the initial increase of OEE variance as well.

Axis velocity is very similar until the theoretical start of velocity decay (i.e. end of non-perturbed zone). At that very moment the variances over the mean increase for both as well as the differences on the actual and average

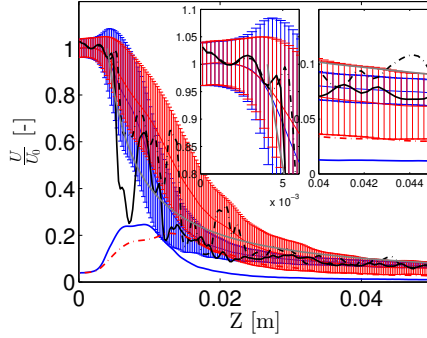


Figure 4.27: Average velocity decay. Effect of consistent turbulence on LES model. (vanDriest, roundInlet mesh, mapped from 4mm probe). $\color{blue}{\rule{0.5pt}{1.5pt}}$ DS, $\color{red}{\rule{0.5pt}{1.5pt}}$ OEE, — DS (3ms ASOI), - - - OEE (3ms ASOI)

velocity between them. In particular, OEE depicts greater eddies at the axis (higher variance) . This, combined with the lower axis averaged velocity after 3cm, increases the residence time of eddies which require longer periods for averaging . Consequently, OEE calculations require higher number of PFT (pass flow time) than DS to get the same quality of averaged fields (.

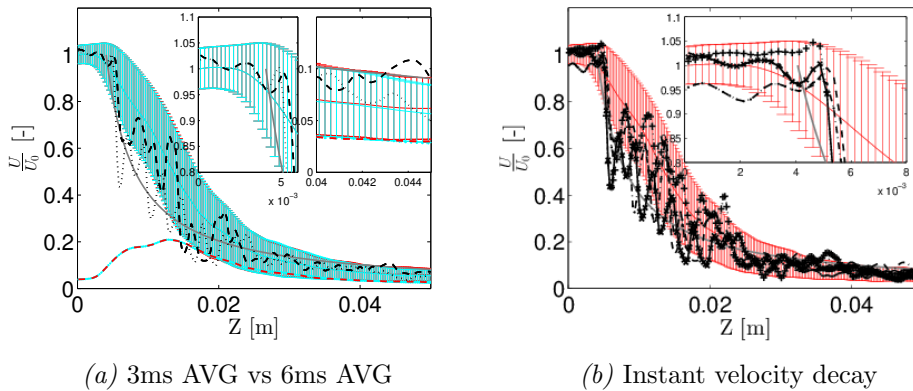


Figure 4.28: Velocity decay. Extended averaging time and instant values. (OEE, vanDriest, roundInlet mesh). $\color{blue}{\rule{0.5pt}{1.5pt}}$ 6ms averaged, $\color{red}{\rule{0.5pt}{1.5pt}}$ 3ms averaged, --- 3ms ASOI, + \cdot + 5ms ASOI, \cdot \cdot \cdot 6ms ASOI, - \cdot - 7ms ASOI, - \times - 9ms ASOI.

In order to check the adequacy of the average time used (i.e. 3ms) Figure 4.28 shows the averaged velocity profiles for both 3ms and 6ms time windows.

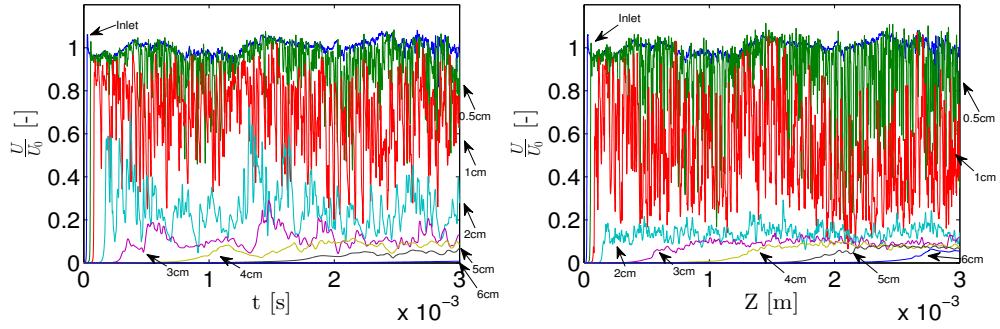
A insignificant difference can be appreciated at the end of the range plotted (i.e. from 0.04m in advance). Also, since the first 3ms are mimic in order to get statistics, the instant velocity field imposed at 3ms, 6ms and 9ms, as well as previous temporal evolution of the inlet are exactly the same. In this regard it is interesting to notice how axis velocity profile matches right until the end of the non-pert zone.

Fields shown at Figures 4.26, 4.27 and 4.28 have been time averaged by OpenFOAM. In contrast, the velocity shown in Figure 4.29(a) has been acquire with probes at the given locations (i.e. inlet, 5mm, 10mm, 20mm, 30mm, 40mm, 50mm, 60mm). The average time window is 3ms and the *Average consistency* is the ratio between the average at a given time and the last value (i.e. at 6ms).

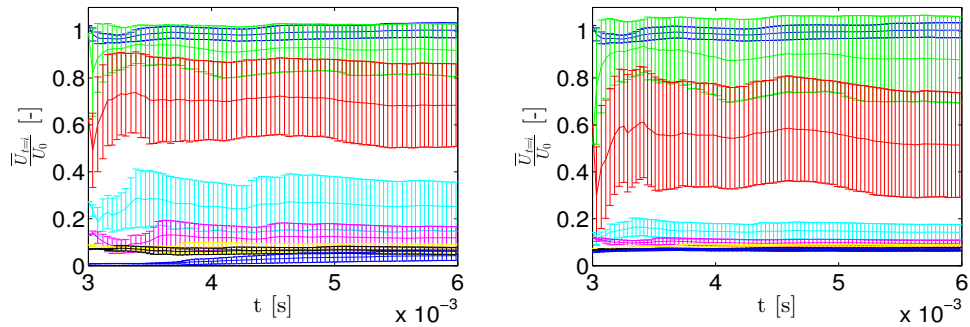
Consistent with results seen at Figure 4.27 the DS shows a higher amplitude for probes close to the nozzle (i.e. 5mm and 10mm) where OEE probes $> 20mm$ show a greater amplitude. In this regard, notice how the velocity field 5mm downstream the nozzle can be higher than the injected (DS at Figure 4.29(a)).

Also, the 20mm probe for OEE results clearly shows a lower frequency associated with the highest eddies. As confirmed with further analysis on the isosurfaces, velocity big fluctuations (i.e. big eddies) require longer averaging periods, even if the average velocity is higher. Note as well, how 30mm downstream the inlet, the velocity field for OEE requires more time than DS to reach a stationary state. This happens even if the initial increase in velocity for this probe, happens before its counterpart at the DS case. As a consequence, for a 3ms average window, OEE 60mm probe can not be taken into account. In the same sense, 50mm does not show a well established field at 4.29(a) nor a steady average value at Figure 4.29(c).

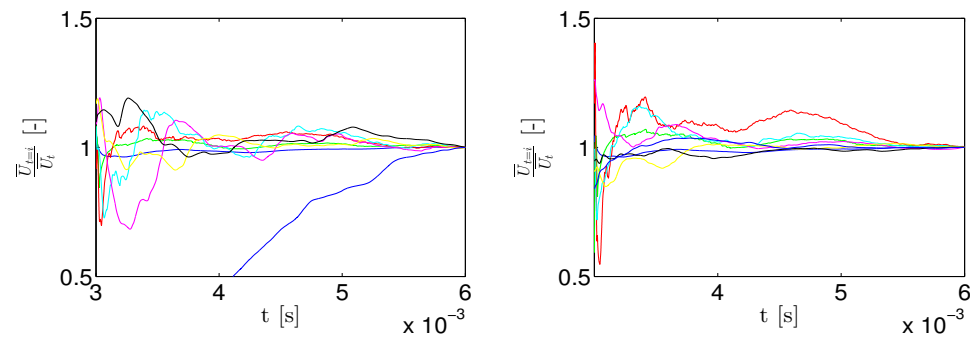
Figure 4.30 shows the contour plots of the cases compared at Figure 4.25. As already seen at the instantaneous velocity decay, turbulence is developed closer to the nozzle when using a mapped inlet. In addition, the initial angle for the 5mm probe is greater than the 4mm probe, for both OEE and DS. This behavior concurs with the difference in variance of Figure 4.26. Note the field plotted there is the velocity magnitude, but the increase of variance applies to the components perpendicular to the axis direction (i.e. X and Y). Hence, the



(a) Instantaneous values



(b) Average evolution



(c) Average consistency

Figure 4.29: Axis probes. (3ms average window, vanDriest, roundInlet mesh). Left column: OEE. Right column DS.

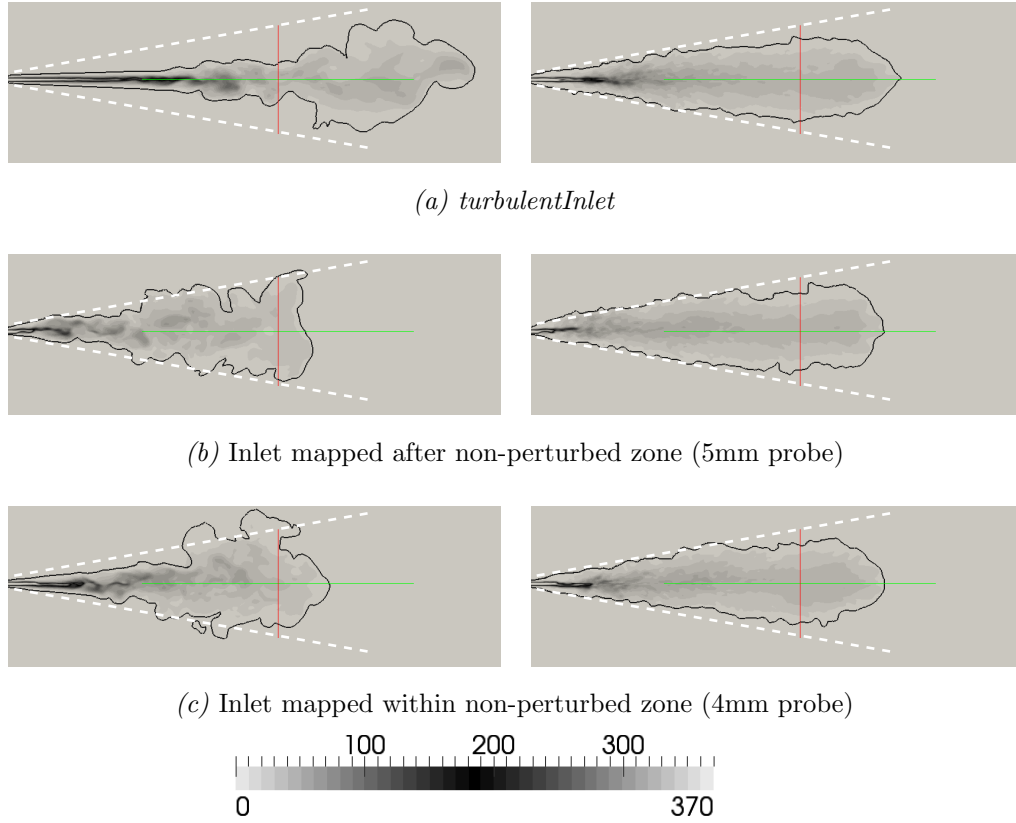


Figure 4.30: Inlet turbulent content effect on gas jet velocity field ($\Delta z = 0.25mm$, $t=0.003s$ ASOI). Left column: OEE. Right column: DS.

solid angle covered by the 5mm probe signal¹² is greater than the 4mm probe. Note as well, the inlet mapped is the same for both turbulent models, but the turbulence developed and the consequent jet shape is particular to each one.

Also, now that consistent turbulence is imposed both turbulent models show similar robustness and the local differences (i.e. increased in the non-perturbed zone, initial jet angle) have to be addressed by specific post-process and compared with experimental measurements.

Figures 4.31 and 4.33 show the $Y_{fuel} = 0.01$ isosurfaces, colored by velocity

¹²Inlet flow and chamber gas have been already mixed.

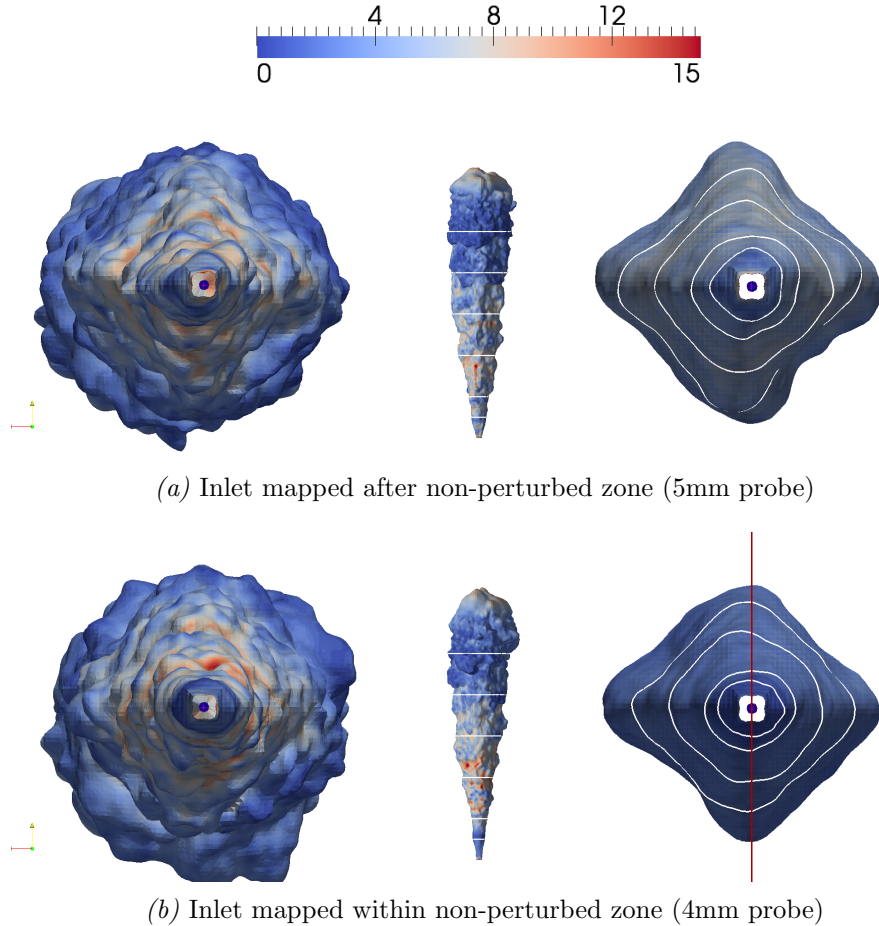


Figure 4.31: Inlet turbulent content effect on averaged DS gas jet. $Y_{fuel} = 0.01$, colored by U ($\Delta z = 0.25mm$, $t=3ms$ ASOI).

magnitude for both instant and average fields. Considering eddies are transported at the average velocity. If the jet limit is defined by the 1% of U_0 ¹³ and around ($Z \sim 3cm$) the average axis velocity is a 10% of U_0 , the surface at this location may need 10 more times to achieve the same average quality than the axis. In addition to that, there is the previous consideration of the frequency associated to the biggest eddies. OEE turbulent model generates bigger instabilities than DS, associated to lower transition times. Hence for

¹³Equivalent to $Y_{fuel} = 0.01$.

a given time window (i.e. 3ms) the quality of the average surface for DS is greater than the one achieved by OEE (Figure 4.33).

Although there is no doubt of the improvement that the 4mm probe represents, Figures 4.31 still shows preferential directions from 30mm onward. Since previous sections exhibit axisymmetric contours, the velocity field is not biased and the only parameter left is the mesh topology.

For both OEE and DS, average images show not only an initial higher angle but a greater overall spreading rate when inlet BC is mapped from 5mm probe. This confirms the fact that when the jet is initialize from a given section the rest tends to behave as a follow up from that point. In our case the jet performs as if it had been displaced the difference in penetrations of Figure 4.25(a) ($\sim 3mm$ for the OEE case).

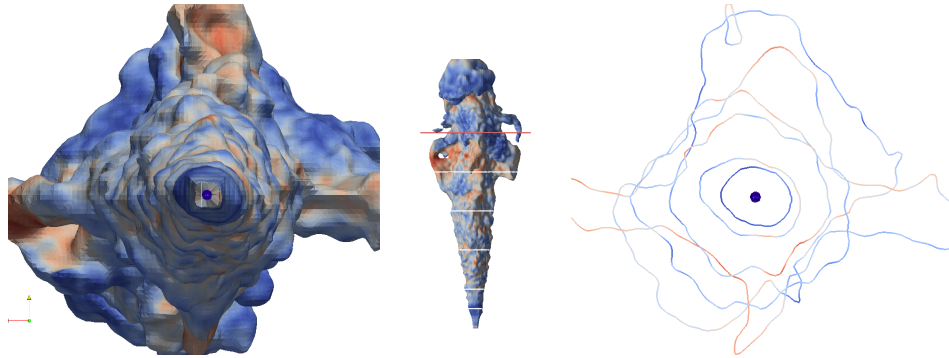


Figure 4.32: Temporal scheme effect on DS gas jet. $Y_{fuel} = 0.01$, colored by U (backward scheme, $\Delta z = 0.25mm$, $t=3ms$ ASOI).

Now the inlet BC is proved to satisfy the basic requirements, the temporal scheme issue can be resumed. Hence the question is whether a second order scheme such backward may get rid of the preferential directions or enhances the effect of the mesh topology. Figure 4.32 shows a clear deterioration and no further average is needed.

As seen in Figure 4.34(b) experimental rate needs $\sim 0.2ms$ to reach average injection velocity. By that time simulated and experimental penetration happen to reach their maximum difference. Consequently a combination of the mapped inlet from 4mm probe and the experimental rate is expected to improve the initial penetration slope. Since the rest of the experimental fluctuation is a consequence of the flow dynamics inside the nozzle, the new inlet

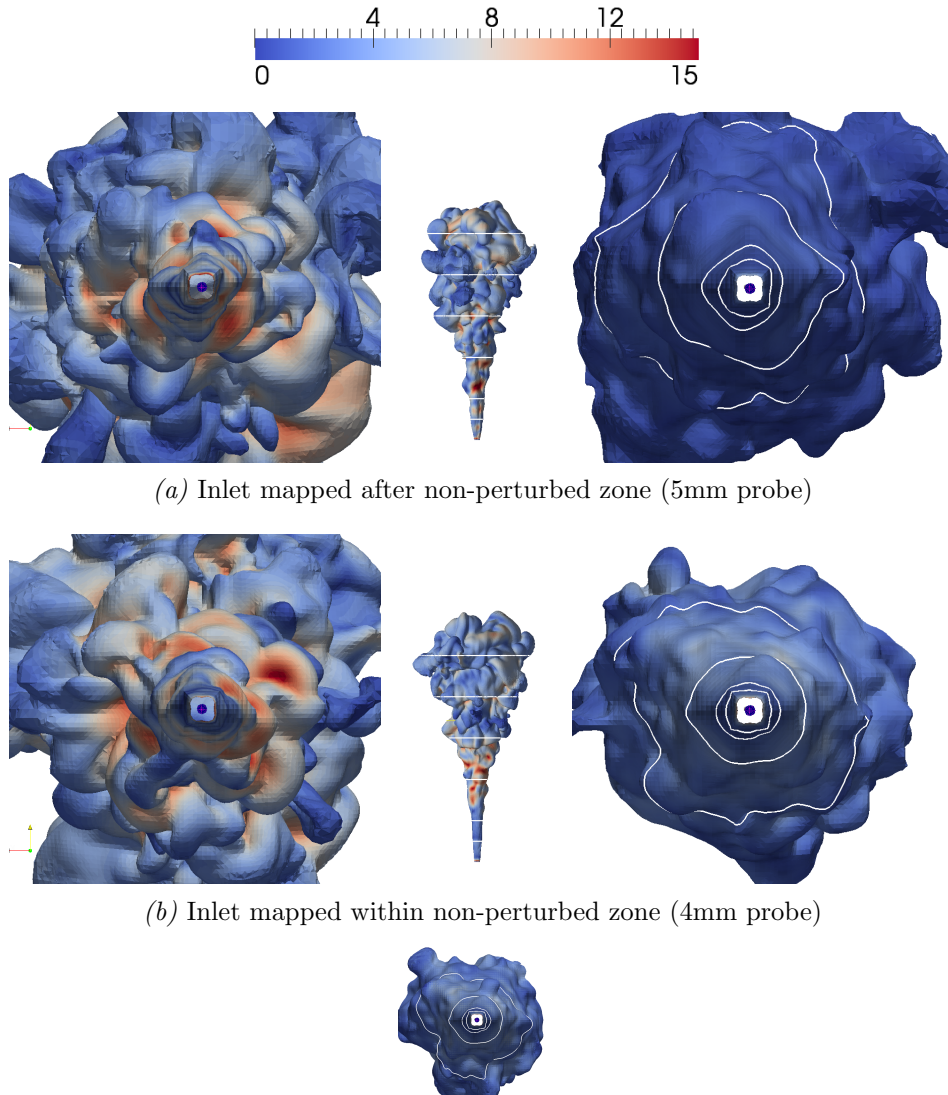


Figure 4.33: Inlet turbulent content effect on averaged OEE gas jet. $Y_{fuel} = 0.01$, colored by U ($\Delta z = 0.25mm$, $t=3ms$ ASOI).

BC should be reproduce the fluctuations of the experimental penetration.

Figure 4.35 compares the penetration and velocity decay obtained with the mapped inlet and the combination with the experimental rate. Regarding

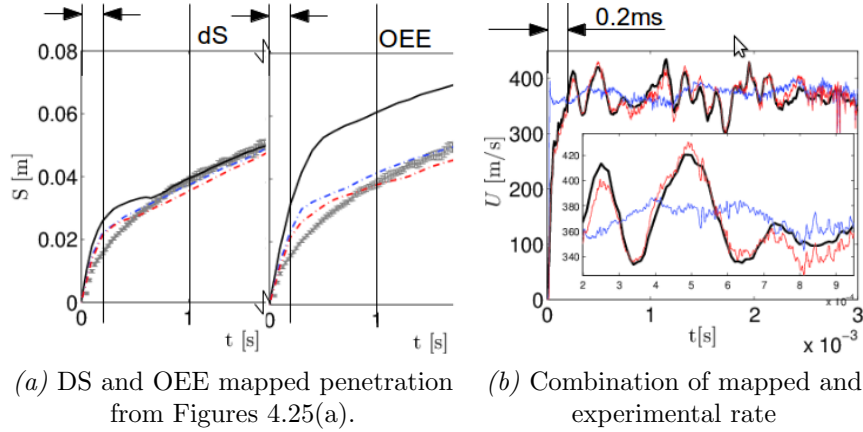


Figure 4.34: Initial deviation from experimental results (vanDriest, roundInlet mesh).

penetration (Figure 4.35(a)), the turbulent experimental rate¹⁴ suppose an improvement during the first 0.15ms but does not have an impact on the required length to develop turbulence (OEE) nor on the transition of the slope between the first and the second stretch of penetration (DS).

At this stage of inlet BC development, the progress in simulated penetration comes by an increase in the initial physical discretization and the a fine tune of turbulent coefficients.

Regarding velocity decay results (Figure 4.35(b)) OEE eddies for the turbulent experimental rate match mapped ones beyond the first 20mm ($\sim 39 \times d_{eq}$). Also, note this happens regardless of the difference in velocity magnitude at the non-perturbed zone. In addition, the simulated decay develops within the theoretical trend.

Similar patterns can be observed for the DS turbulent model. The eddies for both inlet BC match but along a shorten distance than OEE ($\sim 30 \times d_{eq}$). Consistent with previous simulations, the simulated decay develops slightly below the theoretical trend towards the far field.

Finally, Figure 4.36 shows the final improvement between *turbulentInlet*

¹⁴The combination of the 4mm probe with the experimental rate is called in this way from now on.

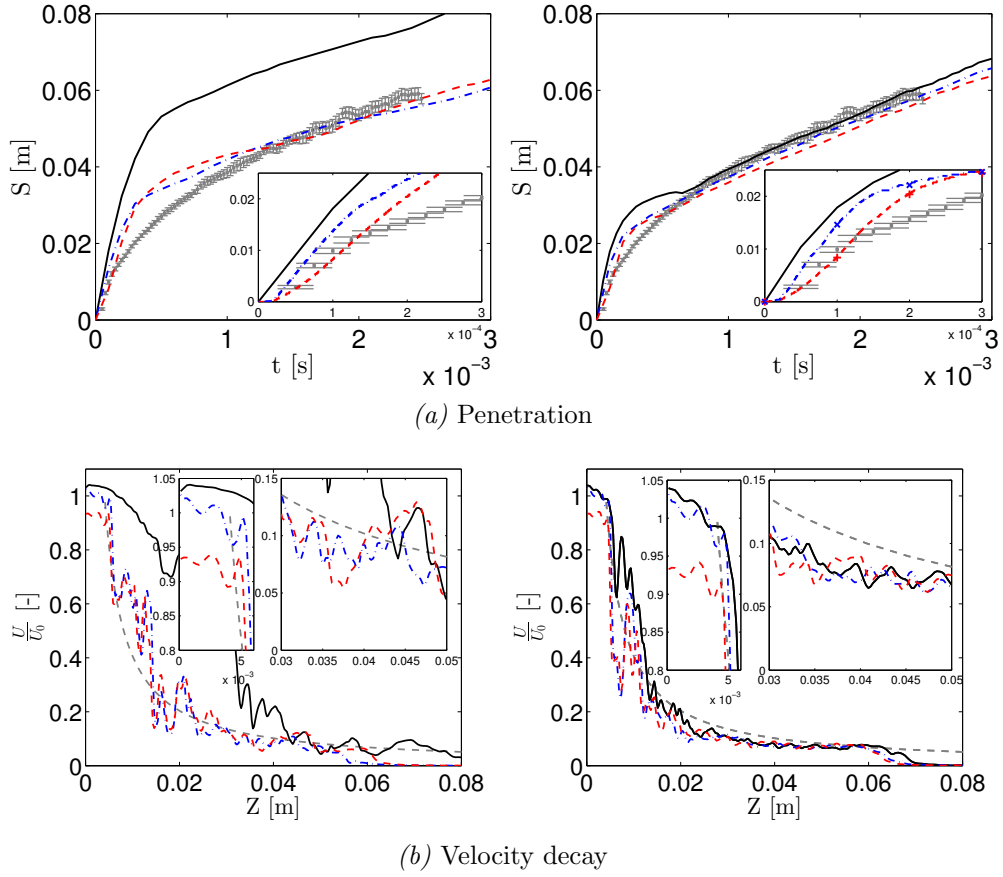


Figure 4.35: Effect of experimental injection rate (vanDriest, roundInlet mesh). Left column: OEE, right column: DS. \square Experimental data, — *turbulentInlet*, - · - mapped (4mm probe), - - - turbulent experimental rate.

and the best inlet BC cases. As a reference, the red line marks the domain midpoint (i.e. 50mm). In accordance with velocity decay trends (4.35(b)) OEE contours look alike within the first quarter of the domain. Also, the similarity extends to the jet contours far from the nozzle (e.g. notice the way jet curls at both sides of the red mark).

On the contrary, the characteristic smoothness of DS makes harder to identify the resemblance. The treatment of DS tends to homogenize eddies due to the way it models the eddies exchange momentum.

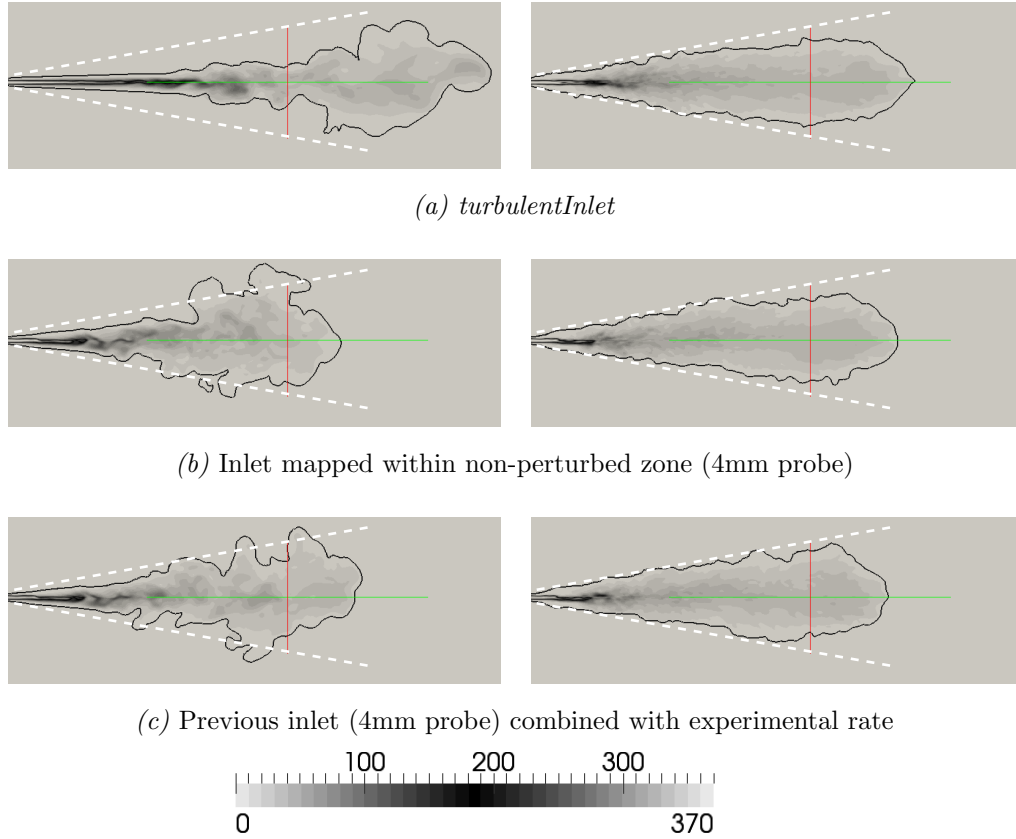


Figure 4.36: Inlet turbulent content effect on gas jet velocity field ($\Delta z = 0.25mm$, $t=0.003s$ ASOI). Left column: OEE. Right column: DS.

Note both inlet BC produce similar results but the turbulent experimental rate includes more physical description. Hence, the surface at $Z=0.004m$ (e.g. perpendicular to the jet axis) of this last case has been mapped in order to imposed the inlet at the grading mesh cases. Also, it has already been proved how, regardless of the turbulent model of the source case, each one (i.e. OEE or DS) develops its own patterns. Therefore, only the DS case has been mapped to both OEE ad DS grad-mesh cases.

Grading mesh

Fields from previous DS calculations have been mapped at the inlet in

order to have similar conditions and reduce uncertainties when comparing cases. Note, inlet BC now covers both the inlet and the wall from Figure 3.4. Hence between the grading mesh and the source case there is no significant difference on the velocity fields at 4mm. From that point the flow sees a more refined domain within the area of interest¹⁵ and a slightly modified topology¹⁶

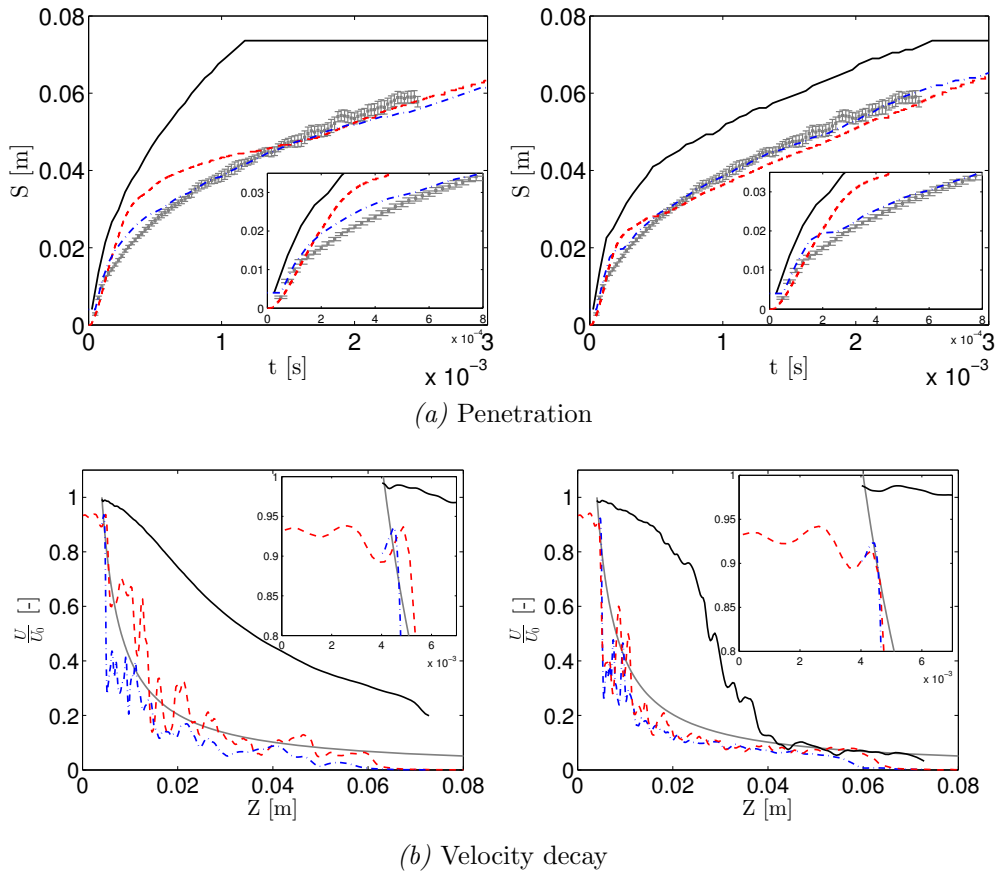


Figure 4.37: Effect of experimental injection rate (vanDriest, grading mesh). Left column: OEE, right column: DS. \square Experimental data, — theoretical decay, — grading mesh (*turbulentInlet*), - · - grading mesh (turbulent experimental rate), - - - roundInlet mesh ($\Delta z = 0.25\text{mm}$, turbulent experimental rate).

Figure 4.37 displays both the penetration and the velocity decay when the

¹⁵And more coarse in the vicinities.

¹⁶Keep in mind the core of the grading mesh domain is not axis-symmetric.

fields are mapped as explained (red line). As a reference, the evolution of local refined mesh that share the same injection rate and cases of grading mesh with a standard *turbulentInlet*. Also, both penetration and velocity decay are offset by 4mm^{17} (i.e. the location of the mapped field).

Regarding penetration, the improvement of the last set up is evident. Both turbulent models match the experimental trend for the most part of the curve and the initial discrepancy is reduced. Since DS penetration oscillates within the range of experimental deviation, the singular result has the same validity for this macroscopic parameter. On the other hand, OEE penetration slopes slightly differ from those experimental. The correction needed in terms of turbulent coefficients is as fine.

As expected, the very first part of velocity decay coincide for DS (Figure 4.37(b)). Note grading mesh with the turbulent injection rate mapped suddenly drops the axial velocity for both turbulent models. The characteristics of the velocity field mapped behaves as the injected flow is already mixed with the surroundings . Also, OEE generates greater eddies at the axis than DS, confirming its particular turbulent development independently of injection field.

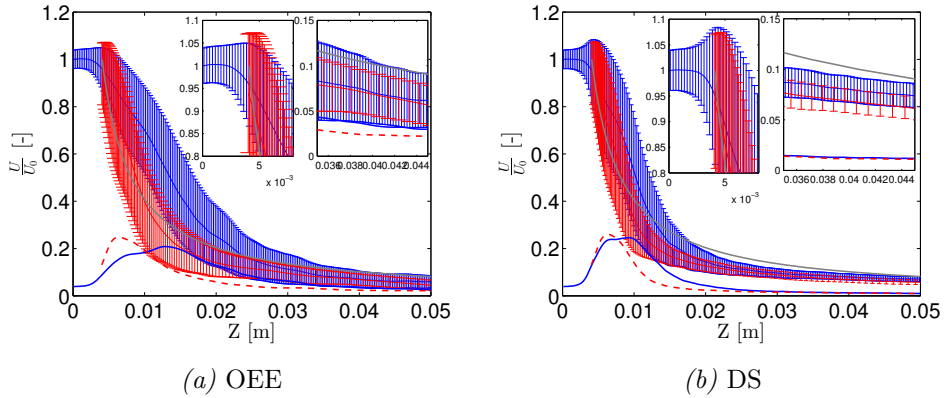


Figure 4.38: Average velocity decay (vanDriest). **I** 4mm mapped (roundInlet, $\Delta z = 0.25\text{mm}$), **I** turbulent experimental rate (gradMesh, $\Delta z = 0.0625\text{mm}$),

The differences between the two meshes in terms of average velocity decay can be seen in Figure 4.38. In addition to the information given by instan-

¹⁷Consistent with the procedure followed for the previous studies of grading mesh.

taneous fields, a greater decay is produced at the grading mesh for OEE and DS. Also OEE eddies in the far field are smaller for the grading mesh than the locally refined mesh. On the contrary, they keep the same amplitude for DS. Finally, the average velocity in the far field is the same for OEE for both meshes but slightly lower for DS (i.e. upper right zoom view).

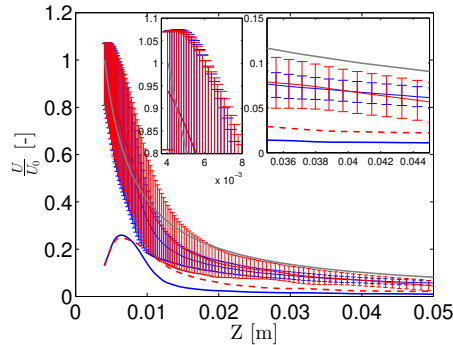


Figure 4.39: Average velocity decay (vanDriest, grading mesh). — OEE, — DS.

The more refined the mesh¹⁸ and the better the inlet BC the more similarities appear between OEE and DS. Figure 4.39 depicts the degree of similarity achieved at the present configuration of grad mesh and turbulent experimental rate. Average velocity decay first slope is higher for DS but far-field values coincide (i.e. upper right zoom view). Note this happens in a region with no influence of the BC and despite the jet morphology seen at following studies. Also a close view on the eddies amplitude reveal a maximum value similar for both turbulent models (i.e. they happen to meet in magnitude and location). Afterwards, greater eddies are generated by OEE.

Extending the information to 2D images, Figure 4.40 shows contour plots of velocity magnitude for locally refined round inlet mesh and the grading mesh. Note the domain of grading images are moved to the end of the non-perturbed zone. Hence the vertical red line sets 50mm from the nozzle exit for both domains. It is clear how the steady state of the jets depicted has not reach this position¹⁹.

As with average velocity decay graphs, OEE instantaneous jet outline looks more like DS with a more refined mesh. In the process of generating turbulence

¹⁸See also Figure 4.2.

¹⁹See for instance definition given at Figure 2.3.

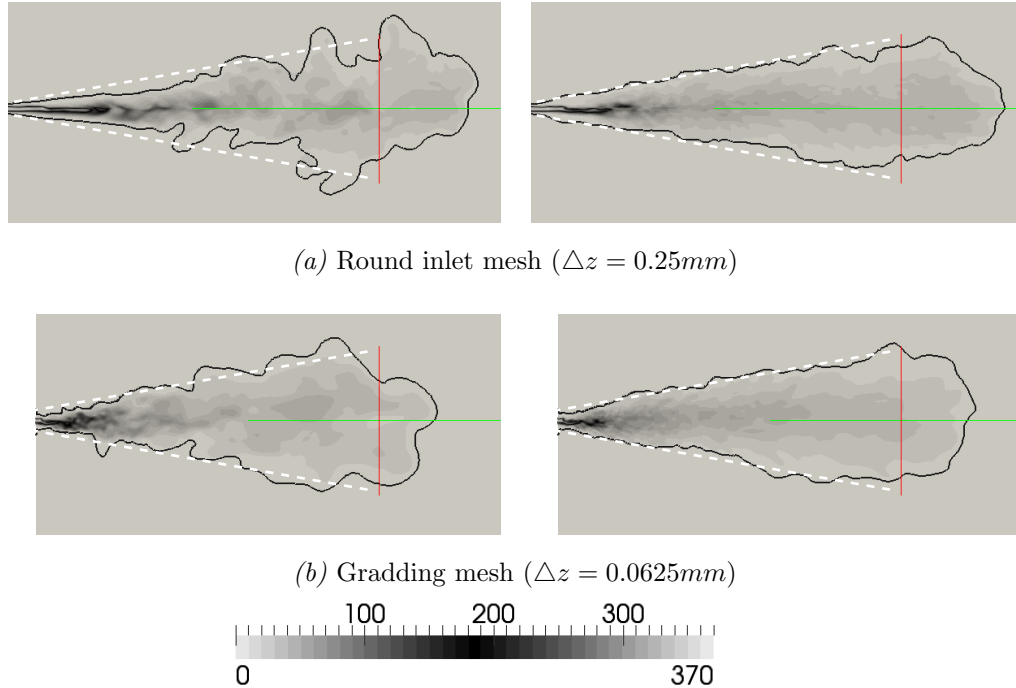


Figure 4.40: Turbulent experimental rate impact on gas jet velocity contours ($t=0.003s$ ASOI). Left column: OEE. Right column: DS.

with coarse meshes, OEE creates greater eddies than those strictly imposed by the physics. Hence by mesh convergence it is worthy to note the behavior of the more refined mesh is more physical. Also DS already provides consistent patterns with different cell sizes.

Remember both locally refined and grading mesh have a very restricted area with the $\Delta z = 0.0625mm$ cells (e.g. see Figure 3.5). Afterwards the cell size increase gradually. Hence, the “new” turbulent characteristics found in OEE are not due to the actual cell size where the fluid is located but to the way turbulence is initialized. OEE requires a higher physical discretization to initialize turbulence but not so much to transport the turbulent characteristics of the flow.

As with previous comparisons is worthy to highlight the DS model is able to consistently show similar trends within a wide range of cell sizes (e.g. as it

is for mesh topology, filter and inlet BC).

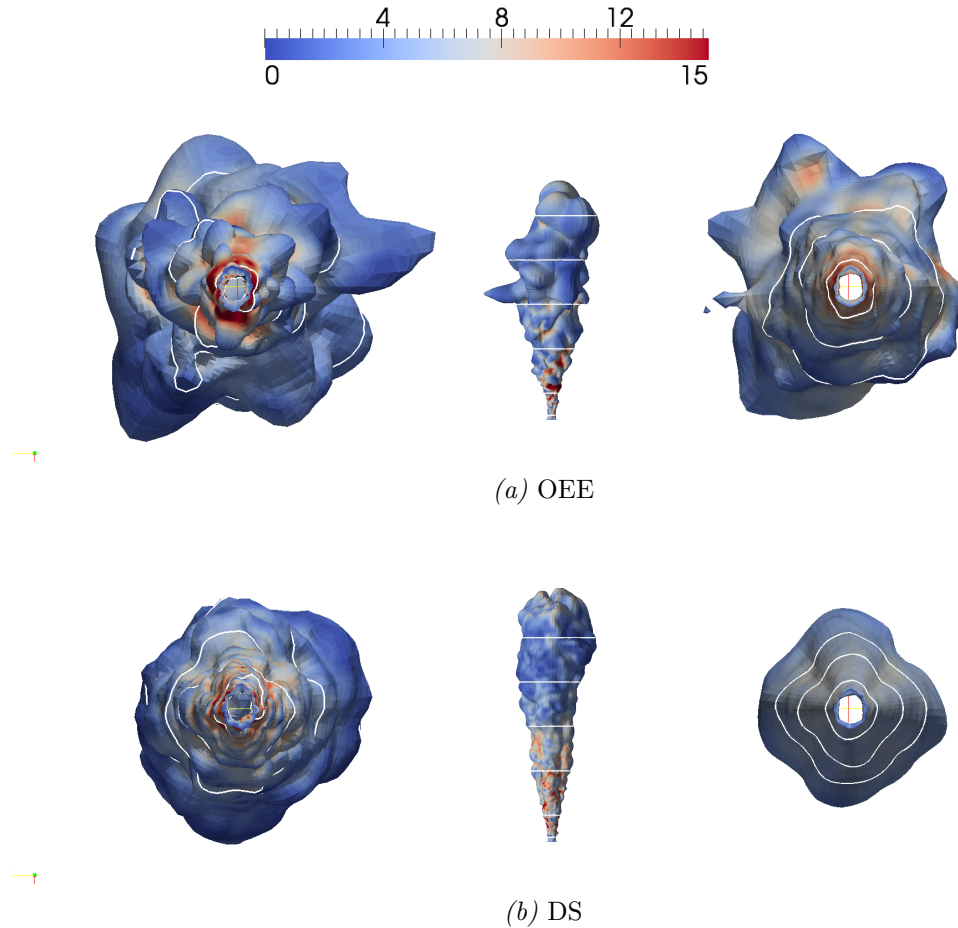


Figure 4.41: Turbulent model effect on averaged gas jet. $Y_{fuel} = 0.01$, colored by U (grading mesh, turbulent experimental rate, $\Delta z = 0.0625mm$, $t=3ms$ ASOI).

Figure 4.41 shows the iso-surfaces of $Y_{fuel} = 0.01$ for instantaneous values at 3ms ASOI and the averaged surface for a 3ms window time. By now is already clear that 3ms is enough averaging time for the axial velocity fields (0-40mm) but not so much for the periphery of the OEE jet. However, the time window is long enough to intuit no preferential directions on the OEE. On the contrary, smaller eddies of DS on the jet outline allow a clear image in order to see the biased shape. Although the construction of the grading mesh

domain was partially intended to remove such behavior²⁰ still an important part of the mesh within the jet core ($> 1/3$) is not axis-symmetric.

Since these last calculations are the ones that better match experiments in terms of macroscopic parameters, following a study on the radial profiles and the energy content of simulated eddies is included.

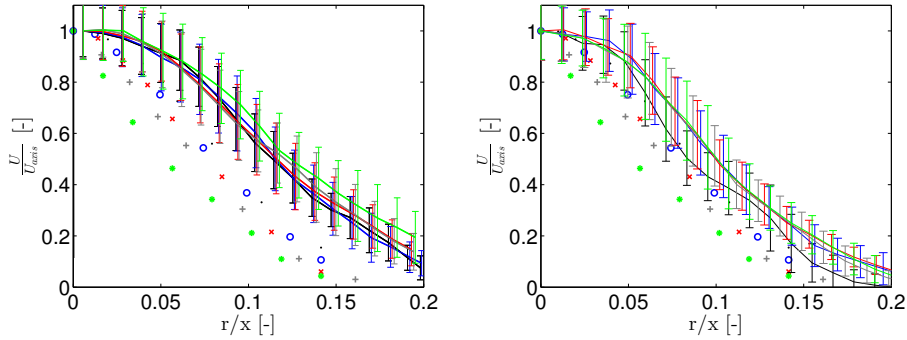


Figure 4.42: Radial profiles of axial velocity (DS, grading mesh, turbulent experimental rate, $\Delta z = 0.0625mm$). Left column: 0° radius. Right column: 45° radius. \blacksquare 50mm, \blacksquare 40mm, \blacksquare 35mm, \blacksquare 30mm, \blacksquare 25mm, symbols: experimental measurements coincide with locations color code.

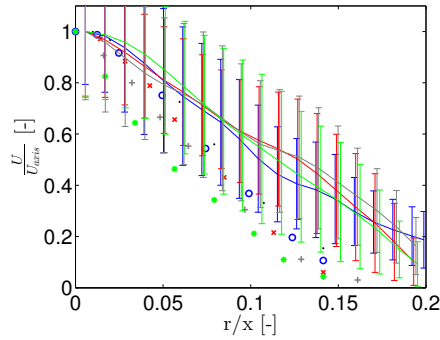


Figure 4.43: Radial profiles of axial velocity (OEE, grading mesh, turbulent experimental rate, $\Delta z = 0.0625mm$). \blacksquare 50mm, \blacksquare 40mm, \blacksquare 35mm, \blacksquare 30mm, \blacksquare 25mm, symbols: experimental measurements coincide with locations color code.

Regarding averaged velocity radial profiles, Figures 4.42 and 4.43 shows

²⁰The principal motivation was to optimize the cell number and reduce the computational cost as a consequence.

dimensionless profiles of axial velocity. Axial velocity (i.e. Z coordinate) is divided by the axis magnitude and radius by the axis location.

DS preferential directions can be seen at the radial profiles drawn for 0° and 45° . A radial collapse of the velocity field will provide a profile halfway between those depicted at Figures 4.42 but would mask the lack of symmetry.

In the case of OEE, simulated result behind $r/x = 0.1$ show lack of statistics. Also 50mm is not included since that location belonged to the transient part of the jet at 3ms. Even for the closer location plotted ($z=25\text{mm}$) the shape achieved by DS is better.

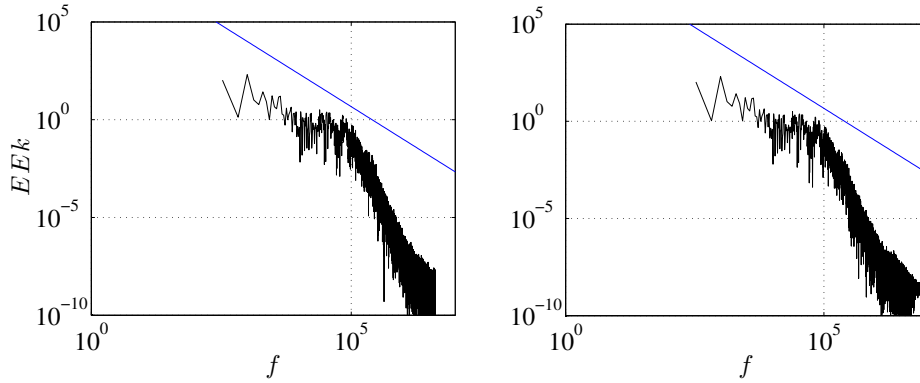


Figure 4.44: Energy content of inlet BC turbulent scales (roundInlet mesh, time window 3-6ms ASOI). Left column: OEE. Right column: DS. — $-5/3$ slope.

As an introduction to the frequency study the signal acquired at the first cell downstream the inlet BC is presented (Figure 4.44). The velocity field imposed refers to the 4mm probe of Figure 4.21(c). Although the source signal is exactly the same, the minimum dt imposed by the CFL condition is smaller for DS than OEE and so the maximum frequency seen is higher. The energy content is exactly the same for the significant scales but differ for the smaller ones. Note, the calculations have been run under a cte CFL number. As a consequence the dt varies slightly with iterations and so do change the probes time acquisition. In order to perform the frequency study the acquisition time must be constant. Hence the signal has been reconstructed using a cubic interpolation (i.e. Hermite polynomials) and the smallest dt . The bigger (more energetic) scales from the reconstructed signal are exactly the same. However, the interpolation generates eddies with the highest frequency that are clearly

visible at the following figures.

Figure 4.45 show the energy content of the axial component of the velocity for different locations at the jet axis. As with previous images of averaged fields the acquisition begins at 3ms and runs during the following 3ms.

In order to interpret the results the following keys are needed:

- Cell size: locations close to the inlet BC have a more refined cells for grading mesh. Hence, the simulation dt is smaller (i.e. for a given CFL number) and therefore the maximum frequency seen is higher. This can be identify by looking at the first two rows of the figure. The first row corresponds to locally refined mesh ($\Delta z = 0.25mm$ cells at 5mm from the nozzle) and the data plotted ends at lower frequencies than the second row ($\Delta z \sim 0.0625mm$) cells at 5mm from the nozzle)
- Cell size distribution: although grading mesh has a more refined mesh close to the inlet BC, the growth rate increase the cell sizes towards the end of the domain²¹. As a consequence the size of the smaller eddies (i.e. with the highest frequency and lower energy) being filtered increase towards the end of the domain for the grading mesh. This can be identified by the position of the lower peak at the graphs of the second and the fourth column. This explains also the constant line from the end of filtered eddies to the acquisition frequency.
- Velocity average and perturbation: as seen at Figure 4.29 inlet BC has a higher average velocity but smaller eddies than the axis flow at 5mm²². As a consequence, the energy of the very first frequency and the more energetic ones that follow are greater for 5mm probe than those imposed at the inlet (Figure 4.44 and 4.45(a)). Something similar happens between 5mm and 10mm axis probes for both turbulent models. From that point both averaged magnitude and eddies decay with distance which can be seen reflected at the gradual separation from the reference line.

In agreement with the lat item, 20mm probes signal confirm the data shown for the averaged axis velocity decay. OEE produce greater amplitude

²¹For instance, cell sizes past 35mm are already bigger than the equivalent location at the locally refined mesh.

²²In fact, the maximum velocity at 5mm is greater than the maximum imposed at the inlet.

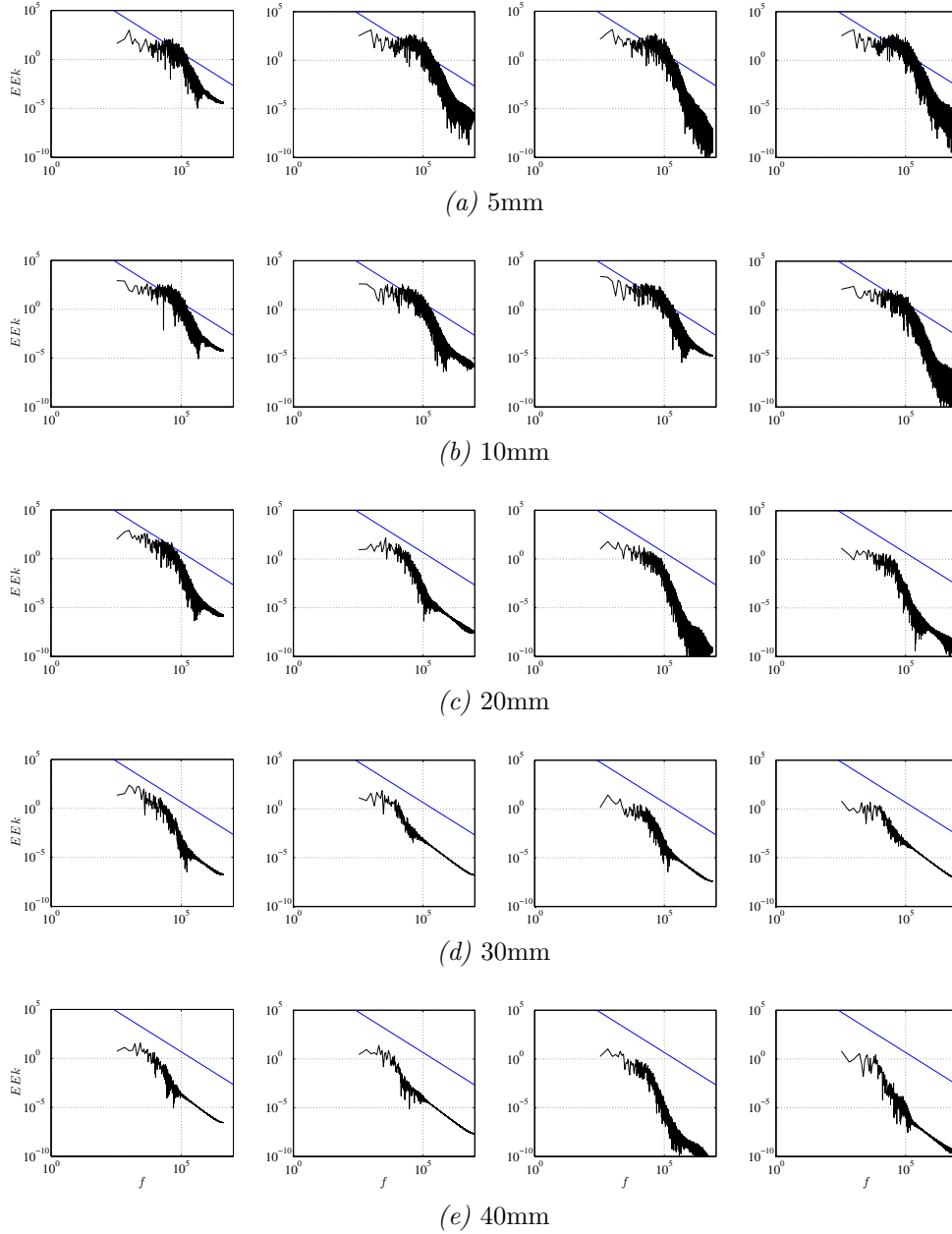


Figure 4.45: Energy content of turbulent scales (time window 3-6ms ASOI). First column: OEE roundInlet. Second column: OEE grading mesh. Third column: DS roundInlet. Fourth column: DS grading mesh. — $-5/3$ slope.

and therefore the trends are closer to the reference line (i.e. a greater energy content)

Finally, Figure 4.46 shows the axis probes at 50mm and 60mm. Most of the probes at 60mm and the 50mm probe for the OEE grading mesh case show how the jet was at its transitory part when probe acquisition was initiated²³. Compared with previous images the limit of use of this parameter is clear.

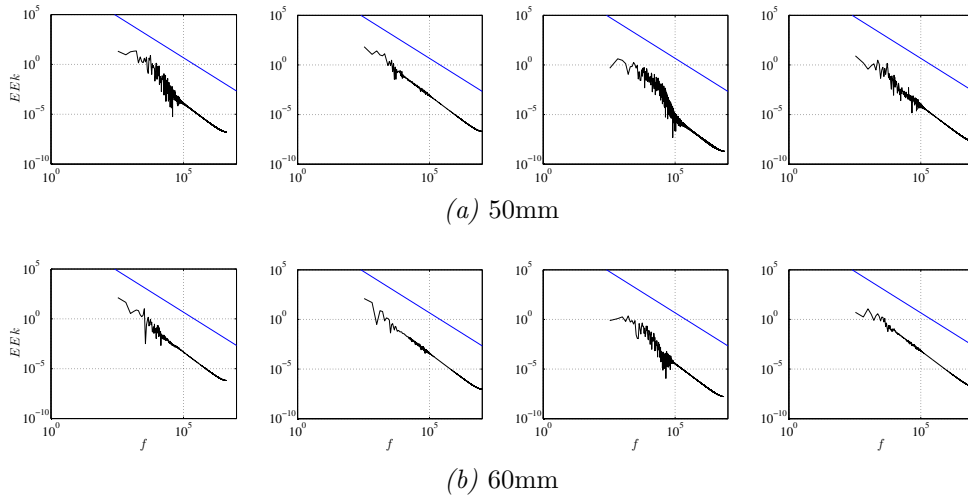


Figure 4.46: Energy content of turbulent scales (time window 3-6ms ASOI). First column: OEE roundInlet. Second column: OEE grading mesh. Third column: DS roundInlet. Fourth column: DS grading mesh. — $-5/3$ slope.

4.3 Non-evaporating diesel sprays

In this section spray cases are analyzed and compare with previous gas jets results.

4.3.1 Mesh size and temporal schemes independency

Turbulent model dependency on mesh refinement shows differences for studied turbulent models (Figure 4.47). For the same pair of turbulent constants,

²³Remember the chamber is initialized with a constant zero velocity field.

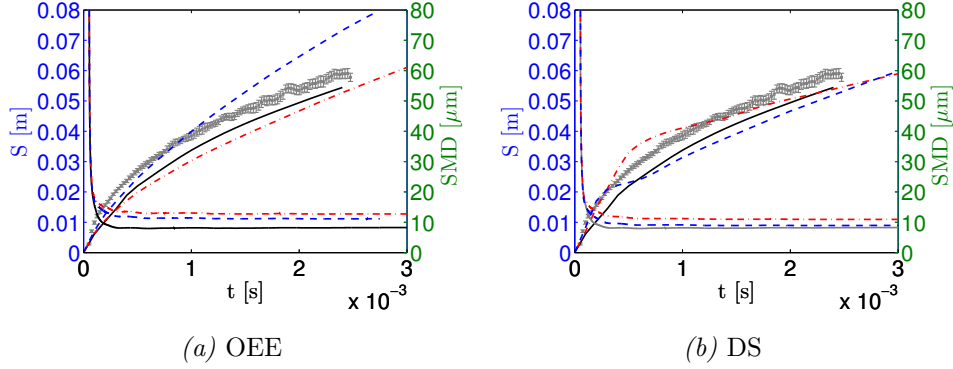


Figure 4.47: Turbulent model dependency on mesh refinement. \square Experimental data, — $k - \varepsilon$ (RANS), - · - 0.5 mm mesh, - - - 0.025 mm mesh.

OEE spray penetration progressively increases with time under a finer mesh. Beside the initial increase on momentum transfer with smaller cells, keeping the turbulent coefficients leads to a lower air entrainment.

Regarding the evolution for DS turbulent model, the initial difference in penetration is consistent with the inception of turbulence observed for the gas jet in the previous section. In both E-E and L-E cases the time required is reduced with smaller cells near the nozzle. Also, the slope of the second part of the penetration curve changes. In this sense, DS reduces air entrainment when being used in a finer mesh as seen for OEE turbulent model. In both cases E-E turbulent coefficients must be changed to correct the L-E coupling for finer meshes. In this regard, this represents the first difference in procedure with RANS calculations where a correct set of E-E turbulent coefficients provides an experimental-alike L-E air entrainment (and penetration).

The number of parcels in the system at 3ms for the 0.5 mm mesh RANS calculation is ~ 1.5 million. Therefore, the calculation of the Lagrangian part becomes the bottle neck compared with the number of cell elements (~ 0.5 million) for this mesh. It is also worthy to note the differences in number of parcels with LES (DS ~ 0.4 million and OEE ~ 0.2 million) at the end of the calculation. As explained in the numerical setup (section 3.3), this behavior is a consequence of the weight of turbulent velocity in the calculation of the gas-parcel relative velocity. Regarding DS and OEE discrepancy in total number of parcels, both gas-parcel interaction and the turbulent modelling of

DS increases relative velocity seen by the parcels. A clear example will be appreciated at the axis of the spray in figures 4.54(b) and 4.54(c) and can be as well infer from Figure 4.55.

Generally speaking, the number of parcels increases with smaller cells and so, for 0.25 mm mesh the parcels for DS raised up to ~ 0.8 million and OEE to ~ 0.4 million. In regards to RANS calculations, parcel generation due to KH had to be limited to 50 events in both atomization and breakup to avoid instabilities. With this restriction, the smaller parcels have, at least, decreased their mass 5 orders of magnitude (i.e. diameter reduced 2 orders of magnitude) and sum a total of ~ 1.2 million parcels by the end of the calculation.

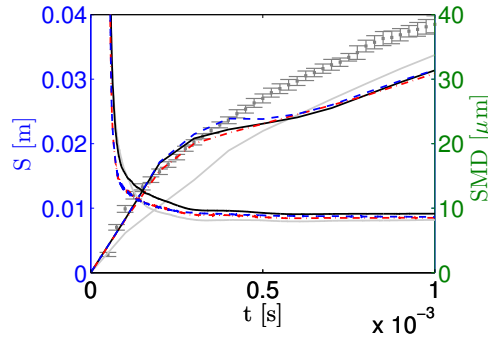


Figure 4.48: Effect of temporal scheme and δt on DS spray behavior (experimental injection profile) \square Experimental data, — $k - \epsilon$ (RANS), — first order ddt, - - second order ddt, - - - 0.125 CFL.

The study of numerical scheme and ddt focus on the DS turbulent model (Figure 4.48). The restriction on KH events had to be imposed as well to avoid instabilities. The effect of numerical scheme on the first part of parcel penetration was expected to be similar to E-E calculations. However, no significant influence was found on the reduction of penetration as a result of better turbulent generation. Consequently, there is no apparent advantage to the increase of calculation time required. A possible explanation may be the domination of the L-E coupling in the region close to the nozzle. In sum, temporal scheme reduces the time needed for initial turbulent development for E-E where in L-E calculation the initial turbulence is generated from the parcels-gas interaction.

Finally, different turbulent coefficients leading to a better agreement with

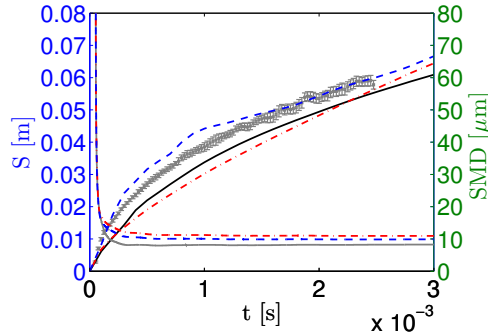


Figure 4.49: Improved turbulent coefficients for $t=3\text{ms}$ ASOI ($\Delta z = 0.25\text{mm}$) \perp Experimental data, — $k - \varepsilon$ (RANS), - · - OEE ($c_k = 0.6$, $c_\varepsilon = 0.05$), - - - DS ($c_k = 0.05$, $c_\varepsilon = 0.3$).

experiments are provided on Figure 4.57. The improved results at 3ms are depicted at figures appearing from now on.

Figure 4.50 only shows parcels located between $-0.5\text{mm} < x < 0.5\text{mm}$. Note the shadow does not take into account the parcel diameter (those changes can be seen in Figure 4.55). For the same turbulent model, no significant difference on parcel distribution was found between 0.5 mm and 0.25 mm mesh. From these images, first 0.02m are fairly similar. It can be argued that, depending on temperature (diesel vaporising conditions), spray liquid penetration can be stabilized within this length. Although, no value would be added on the L-E coupling once parcels are evaporated, the momentum transfer within this initial region is key to the generation of turbulence downstream (Figure 4.54). Moreover, it has been already shown the upgrade brought by DS on the gas phase in the previous section.

4.3.2 Injection profile sensitivity

Figure 4.51 shows the effect of the injection profile on the penetrations as well as to the SMD time evolution. In both figures RANS ($k - \varepsilon$) penetration (calculated with the experimental injection profile) is placed as a reference. It is worthy to note RANS penetration has proved negligible sensitivity on the injection profiles imposed (Figure 4.21(a)). Therefore only results of experimental profile are included here. Also, since the main changes are confined to

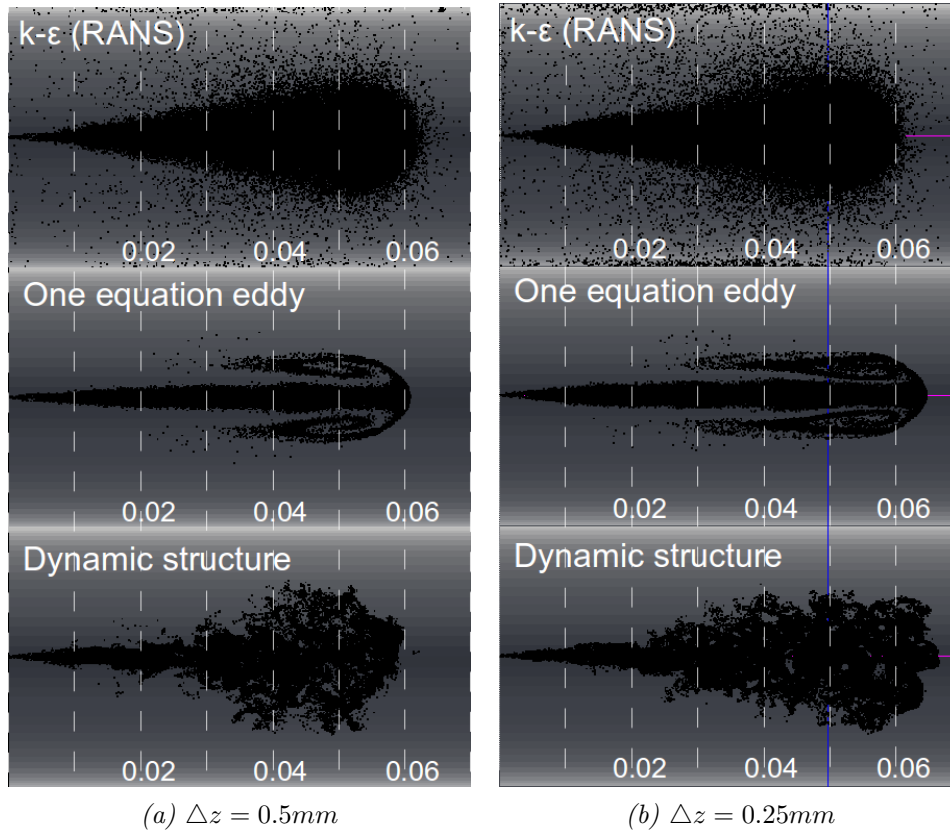


Figure 4.50: Parcels shadow ($t=3\text{ms ASOI}$)

the initial evolution of the spray only first instants of the calculation time is shown (i.e. 1ms). However, all cases have been run until 3ms.

Regarding SMD temporal evolution, the initial effect of atomization and breakup on the average diameter depends on the injection profile rather than the type of turbulent modelling. In terms of penetration noticeable differences are shown for DS (Figure 4.51(b)) compare with OEE.

In the early injection time the SMD evolution gives an idea of how fast the parcels are being atomized. The average injection profile enforces a constant injection velocity to the parcel ($U_{inj} \approx 373\text{m/s}$) against the chamber gas initialized with zero velocity. That huge relative velocity at the beginning of the

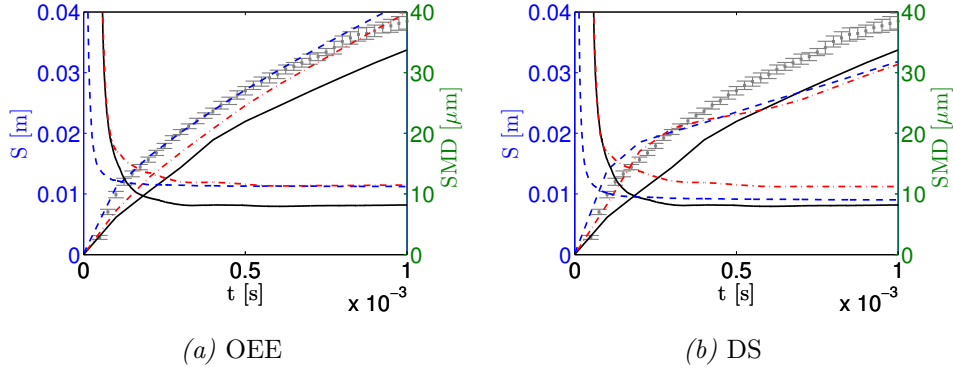


Figure 4.51: Penetration ($\Delta z = 0.25\text{mm}$). \square Experimental data, — $k - \varepsilon$ (RANS), - · - Experimental injection profile, - - - Average injection profile.

calculation time makes atomization and break up models to reduce the parcel diameter. In a following step, those injected and stripped/atomized parcels will transfer momentum to the gas phase, reducing the initial relative velocity. On the contrary, experimental injection profile gradually increases the velocity within the first 0.2ms ASOI so that relative velocity (and momentum transfer) and related atomization and break up effects build up progressively. In both cases, the SMD rapidly reaches an stable value, when the number of small diameter stripped parcels exceeds the contribution to the mean of the few big blobs ($D = 112\mu\text{m}$) been injected.

Regarding the differences in penetration, the greater initial velocities for the average injection increases the initial penetration as well as the effect of atomization and break up. Figure 4.51 shows this effect on both turbulent models although it has a greater impact on the DS. From this point OEE and DS penetration follows a different pattern. For DS turbulent model, the low velocity surrounding gas stems the parcels with smaller diameter (higher momentum transfer) and compensates the initial increase. After 0.2ms the parcels are injected at similar velocities for both average and experimental injection profiles. Once they reach the tip of the spray ($\sim 0.3\text{ms}$), they face likely gas velocity conditions and consequently penetration matches. Regarding OEE spray penetration, the subsequent adjustment does not lead to a shift of the penetration curves but to a gradual reduction of the initial gap.

4.3.3 Particle-gas phase interaction

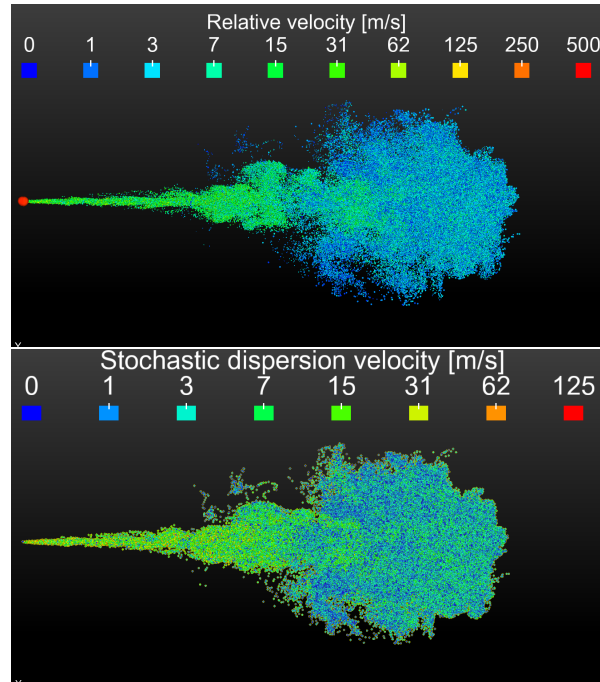
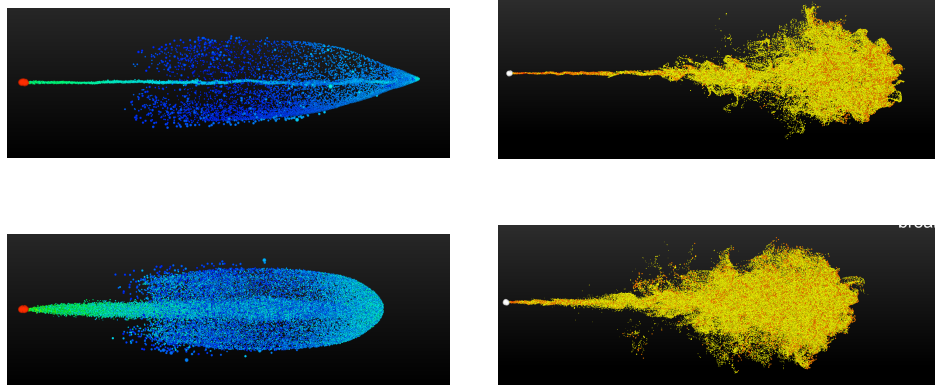


Figure 4.52: Axis velocity decay. ($U_0=373.27\text{m/s}$, $t=3\text{ms}$ ASOI, first ddt). Top: parcel scaled with droplet diameter. Bottom: fixed size.

Figure 4.52 resembles Figure 3.10 from previous chapter. Instead of the sigma Eulerian field, this shows the actual component of dispersion velocity for each parcel. The images confirm the hypothesis outlined based on sigma fields values: dispersion velocity is in fact the same order of magnitude as the simulated relative velocity even further than the first third of the spray.

Images at Figure 4.53 show the influence of turbulent dispersion velocity on turbulent models. In both cases, OEE and DS jet penetration increases when dispersion velocity is disconnected. in particular, OEE shows an arrow head, common to the other viscous models (i.e. Smagorinsky).



(a) OEE ($\Delta x = 0.1\text{mm}$, parcel droplet diameter, colored by relative velocity) (b) DS ($\Delta x = 0.5\text{mm}$, parcel droplet diameter, colored by atomization stage)

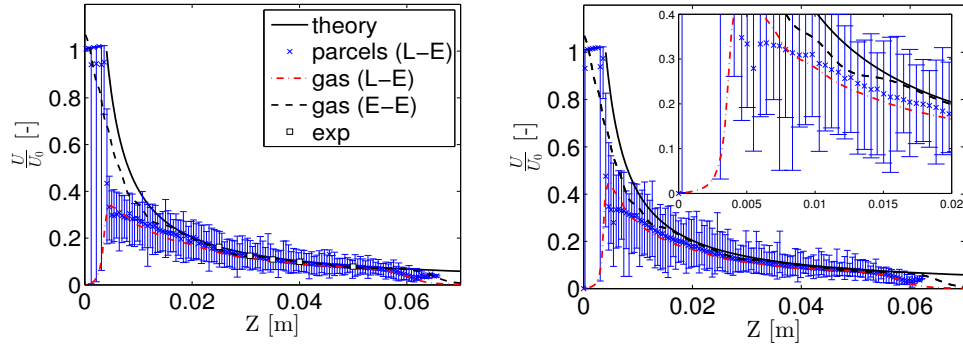
Figure 4.53: Turbulent dispersion sensitivity. ($t=3\text{ms}$ ASOI). Upper row: No dispersion velocity. Lower row: Dispersion velocity.

4.3.4 Comparison with E-E equivalent gas jet.

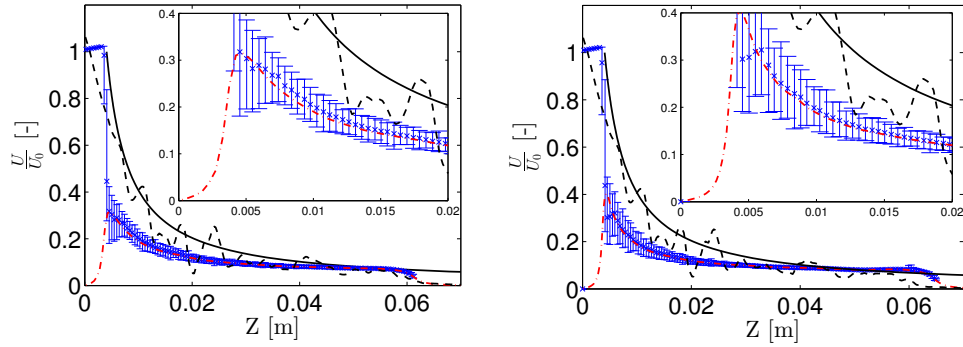
Figure 4.54 shows the axis velocity decay for both Lagrangian and Eulerian phase (from L-E calculations). As a reference, the theoretical velocity decay of a fully developed equivalent gas jet ([Des+07]) has been added. In addition, those results from equivalent E-E calculations from the previous section (only $\Delta x = 0.25\text{mm}$ mesh results) are included.

The calculation of the mean axis velocity is restricted to those parcels confined inside a 0.5 mm radius beam discretized every $\delta z=0.5$ mm. The range graphed corresponds to the maximum and minimum parcel velocity. RANS results (Figure 4.54(a)) is placed as a reference. Also the initial large parcels velocity width can be explained by reentrained parcels. Since experimental average velocity from PDA [Pay+08c] matches with the theoretical velocity decay, they have not been added in here to make graphs more clear.

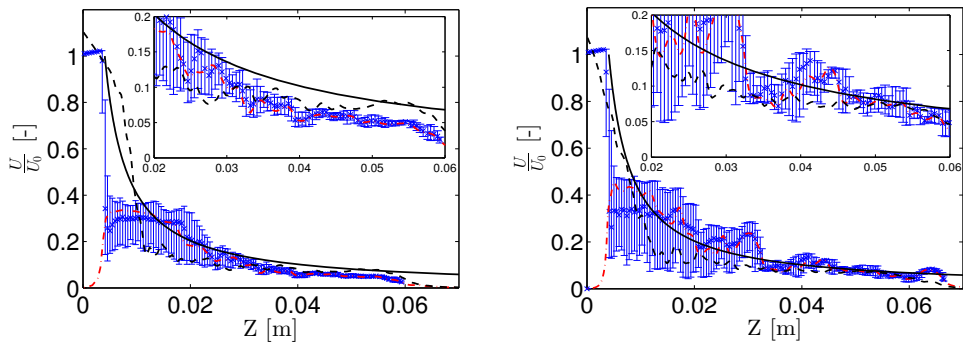
As in the gas jet section, axis velocity has been normalized with the average injection velocity. Note how liquid core length restrains breakup to happen after $7d_{eq}$ (user defined) when the creation of small diameter parcels increase momentum transfer. Until then, only stripped droplets from the injected blobs gradually lose their initial velocity by momentum transfer. There is a number



(a) RANS ($k - \epsilon$)



(b) OEE ($\Delta x = 0.25mm$ with $c_k = 0.6$, $c_\epsilon = 0.05$)



(c) DS ($\Delta x = 0.25mm$ with $c_k = 0.05$, $c_\epsilon = 0.3$)

Figure 4.54: Axis velocity decay. ($U_0=373.27m/s$, $t=3ms$ ASOI, first ddt). Left column: $\Delta x = 0.5mm$. Right column: $\Delta x = 0.25mm$.

of studies of more suitable atomization and break up models for LES. Here the focus is on the pros and cons of the DS turbulent model implemented versus the traditional OEE. Authors will carry a specific study of atomization and breakup models to achieve a more gradual momentum transfer in the next work.

The increase of axis velocity close to the nozzle (i.e. as we move away from it) is caused by the experimental injection profile. As mentioned before, injected parcels does not suffer from drag during the first $7d_{eq}$ and the injection velocity imposed decreases towards 0.3ms at Figure 4.21(a). Also, it is worthy to note the reduction on the dispersion of the parcels velocity as we move downstream. It is clear how LES simulations bring parcels into an equilibrium with the gas velocity closer to the nozzle than RANS calculations. Note how the cells at the end of the liquid core length determine the CFL number (e.g. for DS calculations, $CFL \approx 0.4$ for $\Delta z = 0.25mm$ mesh). Finally, authors noted how the higher number of parcels at 0.25 mm mesh increases the width of parcels velocity compared with 0.5 mm mesh results.

Now, focusing the analysis on the LES turbulent models. Compared with E-E results, OEE turbulent model entails a high reduction of the axis velocity perturbation (Figure 4.54(b)) till they are not noticeable anymore. In contrast, DS keeps perturbations in the same order of magnitude as seen for E-E gas jet . Note how initial axis velocity decay is better simulated by gas jet result where L-E velocity decay shows better agreement ones the axis velocity has crossed the theoretical line (Figure 4.54(c)). Also, between the maximum gas velocity and this switching point there is a higher number of parcels been dragged by the gas for DS.

It is worthy to mention the fact that mean parcel velocity is centered within the min-max velocity range for RANS and OEE where the distribution is moved towards faster parcels for DS. Take into account that the average is over the total number of parcels and has not been weighted by mass or any other factor. We have not find an explanation for such behavior and are committed to keep analyzing the data to find one.

In Figure 4.55 parcels sized by droplet diameter are superimpose to contour plots of U_y velocity within a range of $(\pm 5m/s)$. When switching from atomization to breakup, parcel diameter suffers an abrupt reduction of an order of magnitude. Besides the consideration of physical consistency, it is interesting to note its independency of the turbulent model approach. There

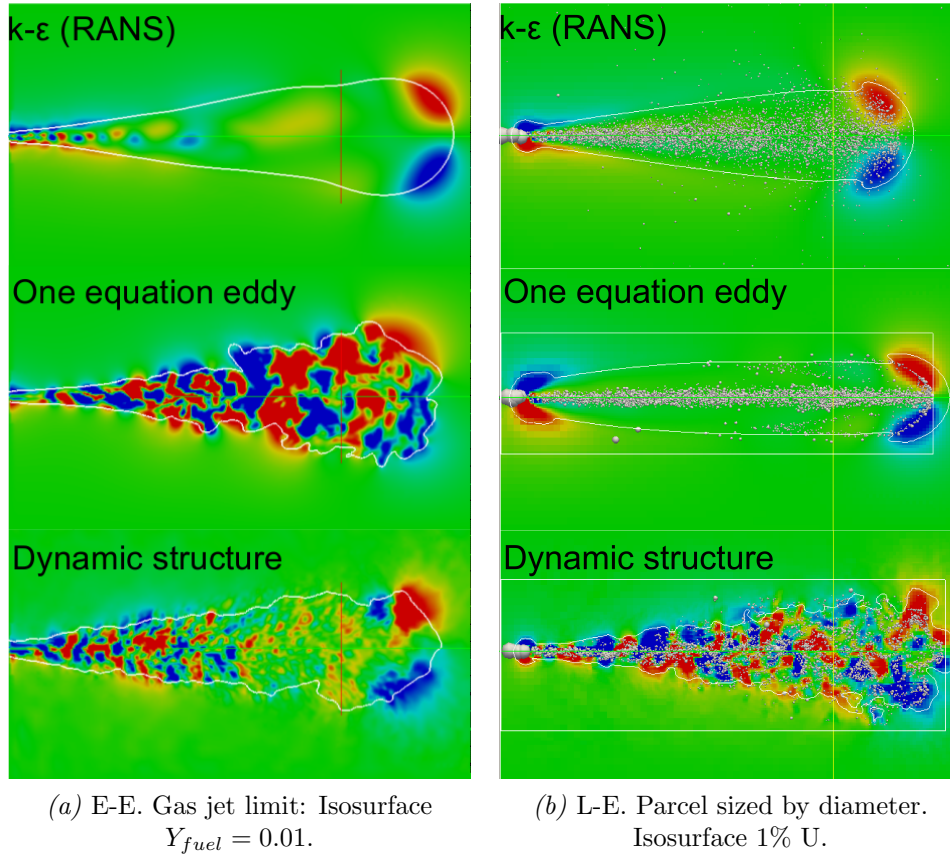


Figure 4.55: Contour plot of $U_y(\pm 5m/s)$ ($\Delta z = 0.25mm$; $t=3ms$ ASOI)

is a distinct big zone of air been entrained at the end of the liquid core length (i.e. velocity perpendicular to the main direction of the spray movement). This region happens to meet gas higher total velocity.

As expected, the other common region of higher U_y velocity is located at the tip. Here, OEE and RANS shows fairly similar portrayal despite of being different approaches where DS provides the turbulent description expected from LES. Previous results [Fuj+09] showed that the breakup model is significantly affected on the calculated spray shape, because the droplet diameter determined by breakup models affects on the transmittance of the droplet momentum into the ambient gas, the evolution of the vortex structure in the gas

phase and the droplet dispersion by the vortex structure. However, for the atomization and breakup models used here, DS clearly shows a much more realistic behavior. In addition to that, Figure 4.56(b) leaves no doubt on DS parcels distribution superiority at early stages of the spray evolution, even without a perfectly tuned set of turbulent coefficients.

A final remark on Figure 4.55; $Y_{fuel} = 0.01$ for E-E or 1% U for L-E are supposed to be equivalent. However, there is a difference between this iso-surface of 1% U and the penetration of the parcels (confined inside the white square). Therefore, penetration definitions for E-E and L-E cases are very close but not perfectly interchangeable.

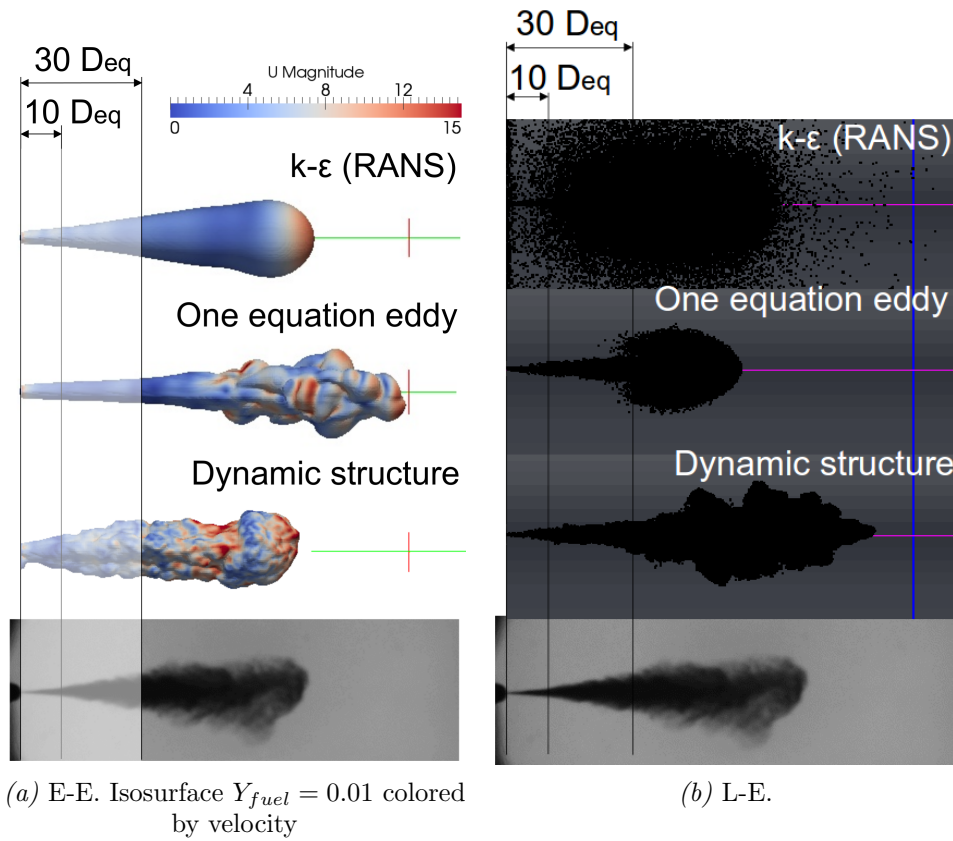


Figure 4.56: Comparison with shadowgraph pictures ($t = 0.9$ ms ASOI, $\Delta z = 0.25mm$)

4.4 Evaporating diesel sprays

Under evaporating conditions, liquid penetration may stabilize around the position were calculation still matches experimental measurement ($\sim 10 - 15\text{mm}$)

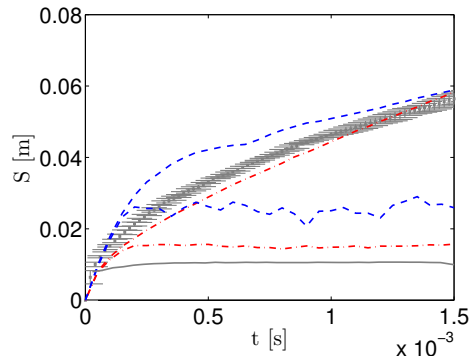
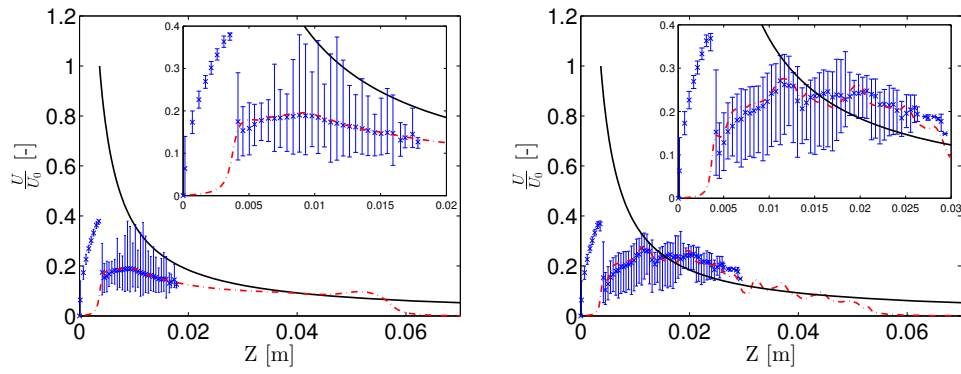


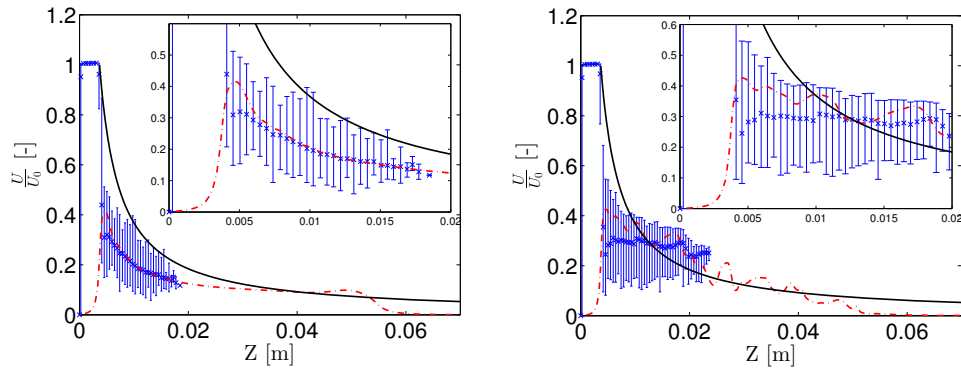
Figure 4.57: Penetration and LL for LES of sprayA for $t=3\text{ms}$ ASOI ($\Delta z = 0.25\text{mm}$), \perp Vapor penetration, — LL, - - - OEE ($c_k = 0.4$, $c_\varepsilon = 0.05$), - - - DS.

Figure 4.57 shows the vapor penetration and the LL for both OEE and DS turbulent models. Experimental results from CMT in collaboration with the ECN as well as the complete methodology can be consulted in [Pas+12]. Note, the coefficient of DS are kept the same where OEE have been modified to achieve similar penetration by the end of injection event. Non-evaporating OEE coefficients are ($c_k = 0.6$, $c_\varepsilon = 0.05$) as seen at Figure 4.57. Note as well, experimental results are averaged and no turbulent features appear at the LL. Hence, although OEE presents macroscopic trends closer to experimental measurements, there is a clear lack of turbulence. As expected from non-evaporative results, DS shows a initial discrepancy (i.e. until vapor penetration and LL separates. From that point, consistent with E-E calculations, there is a initial space required to develop turbulence at the gas phase (see temporal evolution at Figure 4.60(b)). This initialization of turbulence is more critical due to the short injection time (i.e. half of the non-evaporating case).

Regarding the velocity decay Figure 4.58 shows the simulations at 1.4 and 1.5ms ASOI. Images at $t=1.4\text{ms}$ are included to avoid the confusion that the velocity of the parcels close to the nozzle may create at $t=1.5\text{ms}$. Also, it



(a) $t=1.5\text{ms}$ ASOI



(b) $t=1.4\text{ms}$ ASOI

Figure 4.58: Axis velocity decay of evaporative cases ($\Delta x = 0.25\text{mm}$). Left column: OEE. Right column: DS. —Theoretical decay, \perp liquid phase (parcels), - · - gas phase.

allows to see how the atomization model maintains parcel velocity until the end of the theoretical non-perturbed zone. In this regard, there has been no modifications on the coefficients of the atomization model from the non-evaporating cases.

Besides the fact that parcels disappear at some point, the patterns shown here are parallel to those shown at Figure 4.54 for both liquid and gas phase. Hence, same comments may apply to evaporating cases. In addition to those, it is interesting to confirm that, while there is injection of parcels, the gas phase velocity is higher than the average for liquid parcels. However, the difference is reduced after the end of the injection event so that they stay on a buoyant state. This confirms that momentum transfer is sustained by the injection event.

Figure 4.59 shows contour plots of velocity magnitude (gray scale) and the tangential component (i.e. color plot of $U_y(\pm 5m/s)$). In addition to the gas phase, the region occupied by liquid parcels is depicted with a transparent shade. In this way it is easy to identify the turbulence inception patterns at the DS image (Figure 4.59(b)) and to differentiate them from the ones that are freely evolving downstream. Looking at the OEE image, parcels do not impose a tangential component but no turbulence arises from that interaction. Hence, very little (if any) difference with a classic RANS calculation is generated.

Finally, Figure 4.60 shows the temporal evolution of $Y_{fuel} = 0.01$ iso-surface, colored by velocity magnitude. As with previous images, the position of the parcels is included by a shadow. Note the length required to initiate the gas iso-surface is the same for both turbulent models. Due to the lack of momentum transfer of the atomization model, the velocities of the parcels are the same as well as the conditions of temperature drop between the parcels and the gas chamber. Hence the evaporation time to reach a certain mass fraction must be similar. The only difference may appear due to the contribution of the turbulent dispersion velocity. This effect will be visible when the temperature drop allows the evaporation to occur far from the non-perturbed zone artificial limit.

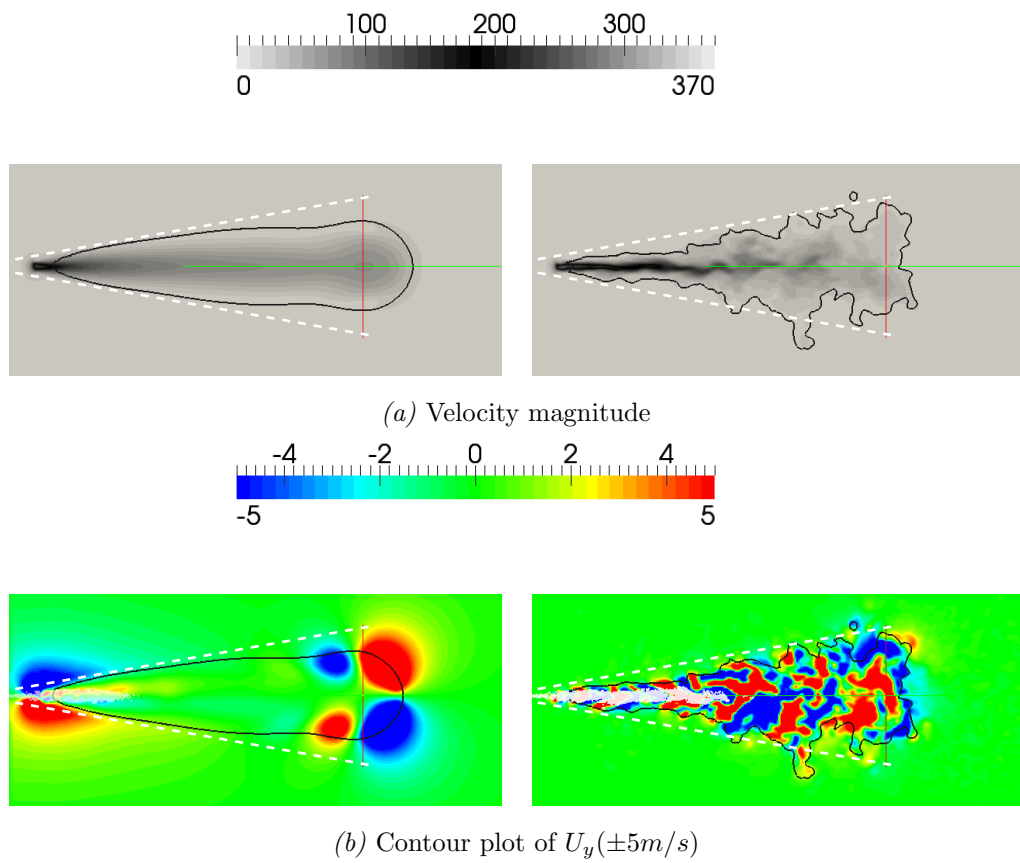
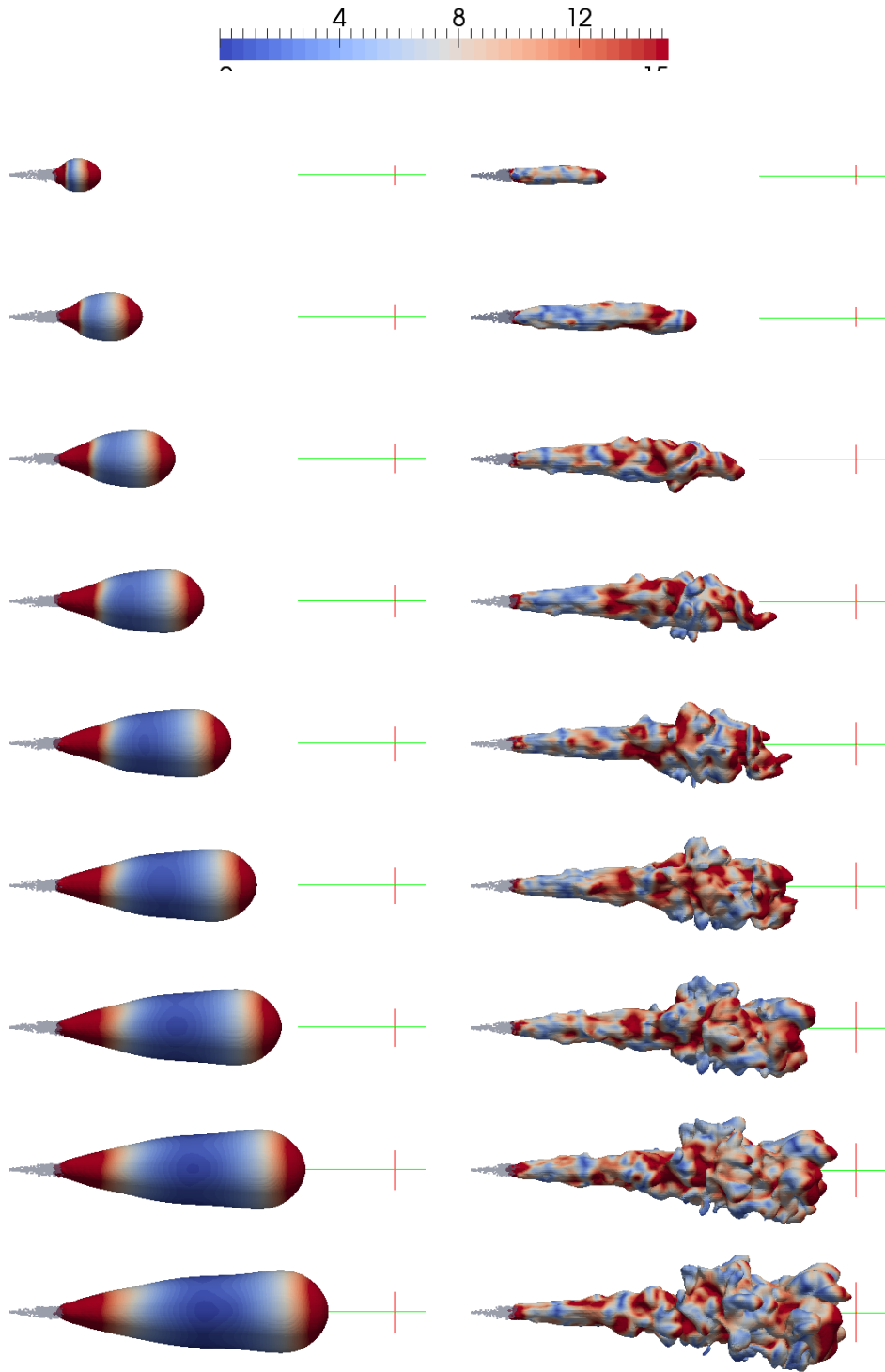


Figure 4.59: Turbulent development of evaporative cases ($\Delta x = 0.25mm$, gas jet limit: $Y_{fuel} = 0.01$, $t=1.4ms$ ASOI). Left column: OEE. Right column: DS.



177

(a) OEE ($\Delta x = 0.1\text{mm}$, parcel droplet diameter, colored by relative velocity) (b) DS ($\Delta x = 0.5\text{mm}$, parcel droplet diameter, colored by atomization stage)

Figure 4.60: Spray temporal evolution. ($t=1-9\text{ms}$). Left column: OEE. Right column: DS.

Chapter 4 bibliography

- [Abr97] J Abraham. “What is adequate resolution in the numerical computations of transients jets?” In: *SAE paper 970051* 106 (1997), pp. 141–155 (cit. on pp. 46, 118).
- [Des+07] J M Desantes, R Payri, José M García-Oliver, and F J Salvador. “A contribution to the understanding of isothermal diesel spray dynamics”. In: *Fuel* 86.7-8 (2007), pp. 1093–1101. ISSN: 0016-2361. DOI: 10.1016/j.fuel.2006.10.011 (cit. on pp. 6, 8, 23, 28, 97, 102, 168).
- [Fuj+09] Hajime Fujimoto, Tsukasa Hori, and Jiro Senda. *Effect of Breakup Model on Diesel Spray Structure Simulated by Large Eddy Simulation*. Tech. rep. Sept. 2009. DOI: 10.4271/2009-24-0024 (cit. on pp. 44, 171).
- [Mon+11] A Montorfano, F Piscaglia, and G Ferrari. “Inlet boundary conditions for incompressible LES: A comparative study”. In: *Mathematical and Computer Modelling* (2011). DOI: 10.1016/j.mcm.2011.10.077 (cit. on p. 135).
- [Pas+12] JV Pastor, R. Payri, and Nerva JG Garcia-Oliver JM and. “Schlieren Measurements of the ECN-Spray A Penetration under Inert and Reacting Conditions.” In: *SAE Technical Paper* 01 (2012), p. 0456 (cit. on p. 173).
- [Pay+08c] R Payri, B Tormos, F J Salvador, and L Araneo. “Spray droplet velocity characterization for convergent nozzles with three different diameters”. In: *Fuel* 87.15-16 (Nov. 2008), pp. 3176–3182. ISSN: 00162361. DOI: 10.1016/j.fuel.2008.05.028 (cit. on pp. 25, 168).

Chapter 5

Conclusions and future works

Contents

5.1	Conclusions	180
5.2	Future works	182
	Chapter 5 Bibliography	183

5.1 Conclusions



THREE DIMENSIONAL LES of diesel-like gas jets and liquid sprays under diesel conditions are performed in a constant volume vessel using OpenFOAM®. Provided viscous turbulent models are compared with a non-viscous model implemented in the code.

To limit computational cost, mesh independence study limits the cell size to 0.25 mm for RANS cases. This size is enough to fulfill macroscopic evolution (i.e. penetration), although local refinement near the nozzle is required to see the non-perturbed zone and the following expected velocity decay. In terms of LES, mesh convergence (instead of “independency”) is fulfilled for cell sizes around 0.0625 mm near the nozzle (i.e. a local discretization near the nozzle). However, the study assess the configuration, turbulent model and inlet BC needed to get the more realistic results for LES with the 0.25 mm cell size.

From gas jet mesh studies, there is a less overall effect on DS, from mesh topology and the type of filter for the range of cell sizes studied. The main differences are limited to the penetration first instants, for both parameters. In contrast, OEE is very sensible to an increase in the near nozzle resolution when *turbulentInlet* is the inlet BC used. Under this configuration, the *best* mesh leads to the *worst* results since the mesh discrepancies and inlet sharp angles act as a precursors of turbulence that otherwise (i.e. for the roundInlet mesh) needs more time and space to develop.

From temporal scheme and *dt* studies, a local mesh refinement seems to have greater impact on the evolution of the gas jet with an equivalent (or less) effect on computational cost.

When mapped inlet BC is applied to OEE cases with the roundInlet and the improved mesh (i.e. homogeneous hexaedral cells close to the jet axis) results differ very little (even with slightly modified turbulent coefficients). Hence It is clear how OEE needs consistent turbulent eddies even for poor physical discretization. Regarding the DS, imposed mapped fields have similar qualitative effect. A proper inlet BC improves the initial penetration and has no influence on the second part. However, the BC has a lower impact on the DS which confirms the robustness of the model.

These behavior was confirmed with the optimized grading mesh. In fact, the gas jet simulated with OEE and the more complex/realistic BC produced

jet shape and field values (not only for macroscopic scales) closer to the DS. Remember both locally refined and grading mesh have a very restricted area with the $\Delta z = 0.0625mm$ cells (e.g. see Figure 3.5). Afterwards the cell size increase gradually. Hence, the “new” turbulent characteristics found in OEE are not due to the actual cell size where the fluid is located but to the way turbulence is initialized. OEE requires a higher physical discretization to initialize turbulence but not so much to transport the turbulent characteristics of the flow. That said, the results of grading mesh and turbulent inlet for OEE where completely un-physical, confirming that the greater physical discretization of the inlet BC the more important/critical is the turbulent consistency of the field imposed.

As with previous comparisons with local refined meshes, is worthy to highlight the ability of DS model to consistently show similar trends within a wide range of cell sizes (e.g. as it is for mesh topology, filter and inlet BC).

In summary, despite mesh shape dependency shown by DS turbulent model for diesel-like gas jets, it shows: consistent simulated penetration at 3ms even for coarser meshes (i.e. 1mm cell size), likewise isosurfaces at this time, a lower dependency on inlet turbulent condition (restricted to initial turbulent inception) and more realistic portrayal on early stages (i.e. 0.9ms). Viscous models did not show shape cell dependency but neither they depict the advantages described by DS.

When no synthetic BC or experimental values are available DS provides a better simulation due to its proven robustness over turbulence initialization and the inlet BC. In the same sense, DS provides closer results with different cell sizes, specially valuable at low resolution simulations. Attention has to be payed to preferential directions specially when higher order temporal schemes are employed.

Regarding L-E calculations, turbulent coefficients need to be calibrated for a given mesh size for both viscous and non-viscous turbulent models. However, DS is less sensitive to initial turbulent inception with consecutive mesh refinements. Also, for this turbulent model no significant improvement is found for parcel distribution and mesh refinements. Nevertheless, enhances momentum transfer which happen to be key for downstream turbulent behavior. In regards of OEE, L-E simulations lose gas turbulent features shown by equivalent E-E calculations.

Atomization and breakup have a higher intensity in RANS calculations leading to a higher number of parcels. As a consequence, by the end of the calculations RANS cases are more computational (and time) consuming than LES. Also, atomization and breakup are enhanced by mesh refinement for any turbulent approach which have a clear impact on parcel velocity distribution. This effect is specially noticeable for DS calculations.

As expected from non-evaporating results, the lack of parcel turbulence inception on the gas phase of the OEE case has similar effect under evaporating conditions. Although macroscopic parameters such vapor penetration and LL are closer to experiments for the best set of turbulent coefficients, in terms of turbulent description there is no added value to RANS calculations. In the contrary, the turbulence generated within the LL for DS generates consistent eddies that evolve downstream. This is the important add on expected from LES (key to further combustion modelling) and a fine tune of turbulent coefficients will bring macroscopic features closer to experiments.

In the light of above non-viscous DS turbulent model seems a better choice for Engineering LES of diesel sprays.

5.2 Future works

Several studies have been proposed within previous chapters. Some are very specific, targeting a specific problem or question arisen from the analysis of the data. Within this group, authors proposed¹ a study of axisymmetric types of mesh to overcome the biased shape shown by the E-E phase calculated under DS turbulent model.

Also, the synthetic BC on the simulations of E-E seems compulsory for OEE (or the other viscous) turbulent model even under low mesh refinement levels. The DS shows an improvement on the jet first instants when coherent turbulence is introduced, so it should be included as the default set up unless temporal high fidelity fields are available to map at the inlet.

The interaction of atomization and break up model coefficients and the turbulent model used can be analysed in greater depth. In particular, the liquid core length coefficient is known to have a great impact on the initial

¹Mainly to themselves.

momentum transfer and on the spray evolution as a consequence. Moreover, cavitating conditions may be studied and specific atomization models referred at the literature review should be assessed.

The last of the “specific” improvements to be tested would be to implement in OEE a source term for the gas-liquid interaction equivalent to the one developed for DS

Finally, as shown in this thesis, E-E and L-E approach have both advantages and disadvantages in the various regions of spray (i.e. the dense zone close to the nozzle and the downstream dilute zone). Eulerian-Lagrangian spray Atomization (ELSA) model is -on the contrary- an integrated model for capturing the whole spray evolution, already tested in RANS calculations [Des+10b; Des+10a; Hoy+13]. Consequently, LES of atomization by means of ELSA model seems to be a necessary step forward.

Chapter 5 bibliography

- [Des+10a] A Desportes, M Zellat, G Desoutter, Y Liang, and F Ravet. “Application of the Eulerian-Lagrangian spray atomization (ELSA) model for the Diesel injection simulation”. In: *Conference on Thermo- and Fluid Dynamic Processes in Diesel Engines* (2010) (cit. on p. 183).
- [Des+10b] A Desportes, M Zellat, G Desoutter, D.Abouri, and Y Liang. “Validation and Application of the Eulerian-Lagrangian spray atomization (ELSA) model for the Diesel injection simulation”. In: *SAE Technical* (2010) (cit. on p. 183).
- [Hoy+13] Sergio Hoyas, Antonio Gil, Xandra Margot, Dung Khuong-Anh, and Frederic Ravet. “Evaluation of the Eulerian-Lagrangian Spray Atomization (ELSA) model in spray simulations: 2D cases”. In: *Mathematical and Computer Modelling* 57.7-8 (Apr. 2013), pp. 1686–1693. ISSN: 08957177. DOI: 10.1016/j.mcm.2011.11.006 (cit. on p. 183).

Global bibliography

- [Abr97] J Abraham. “What is adequate resolution in the numerical computations of transients jets?” In: *SAE paper 970051* 106 (1997), pp. 141–155 (cit. on pp. 46, 118).
- [Ado+07] P. Adomeit, O. Lang, S. Pischinger, R. Aym-anns, M. Graf, and G. Stapf. “Analysis of cyclic fluctuations of charge motion and mixture formation in a DISI engine in stratified operation.” In: *SAE paper 01* (2007), p. 1412 (cit. on p. 43).
- [Ame08] R. Amengual. *Bielas y Álabes*. Oficina Española de Patentes y Marcas, 2008 (cit. on p. 3).
- [Ams+89] Anthony A Amsden, Peter J O’Rourke, and D T Butler. “KIVA-II: A computer program for chemically reactive flows with sprays.” In: *LA-11560-MS, Los Alamos National Laboratory (T3 group internal report, approved for public release)* (1989) (cit. on pp. 61, 70).
- [Apt+03] Sourabh V Apte, M Gorokhovski, and P Moin. “LES of atomizing spray with stochastic modeling of secondary breakup”. In: *International Journal of Multiphase Flow* 29.9 (2003), pp. 1503–1522. ISSN: 0301-9322. DOI: 10.1016/S0301-9322(03)00111-3 (cit. on p. 58).
- [Ara+07] J. Arai, N. Oshima, M. Oshima, H. Ito, and M. Kubota. “Large eddy simulation of spray injection to turbulent flows from a slit nozzle.” In: *SAE paper 2007-01-1403* (2007) (cit. on p. 43).
- [Arc+89] C Arcoumanis, J.H. Whitelaw, and K.Y. Wong. “Gaseous Simulation of Diesel-Type Sprays in a Motored Engine”. In: *SAE paper 890793* (Feb. 1989). DOI: 10.4271/890793 (cit. on p. 64).

- [Arc+97] C Arcoumanis, M. Gavaises, and B. French. *Effect of Fuel Injection Processes on the Structure of Diesel Sprays*. Tech. rep. Feb. 1997. DOI: 10.4271/970799 (cit. on p. 60).
- [Arr97] J Arrègle. “Análisis de la estructura y dinámica interna de chorros Diesel”. PhD thesis. Valencia: E.T.S. Ingenieros Industriales. Universidad Politécnica de Valencia, 1997 (cit. on pp. 54, 58, 59).
- [AS89] B Abramzon and W A Sirignano. “Droplet vaporization model for spray combustion calculations”. In: *International Journal of Heat and Mass Transfer* 32.9 (Sept. 1989), pp. 1605–1618. ISSN: 00179310. DOI: 10.1016/0017-9310(89)90043-4 (cit. on p. 62).
- [Asg11] N Asgriz. *Handbook of Atomization and Sprays*. Ed. by Nasser Ashgriz. Boston, MA: Springer US, 2011. ISBN: 978-1-4419-7263-7. DOI: 10.1007/978-1-4419-7264-4 (cit. on p. 52).
- [AT13] Lakshman Anumolu and Mario F. Trujillo. “Gradient augmented reinitialization scheme for the level set method”. In: *International Journal for Numerical Methods in Fluids* 73.12 (Aug. 2013), pp. 1011–1041. ISSN: 02712091. DOI: 10.1002/flid.3834 (cit. on p. 49).
- [Bae+02] Choongsik Bae, Jun Yu, Jinsuk Kang, Jangsik Kong, Roy Cruenca, and Kyung Ook Lee. “The Influence of Injector Parameters on Diesel Spray”. In: (2002) (cit. on p. 24).
- [Bar+80] J. Bardina, J. H. Ferziger, and 1980 Reynolds W. C. 1980-1357. “Improved subgrid-scale models for large eddy simulation”. In: *AIAA paper 1357* (1980), p. 0 (cit. on p. 44).
- [Bau06] C Baumgarten. *Mixture Formation in Internal Combustion Engines*. Ed. by D Mewes and F Mayinger. Springer, 2006, p. 311. ISBN: 978-3540308355 (cit. on pp. 53, 57–59, 101).
- [Bia+07] G. M Bianchi, F. Minelli, and 2007. Scardovelli R.. 2007-01-0244. “3D large scale simulation of the high-speed liquid jet atomization”. In: *SAE paper 01* (2007), p. 0244 (cit. on p. 43).
- [Bor+92] J P Boris, F F Grinstein, E S Oran, and R L Kolbe. “New insights into large eddy simulation”. In: *Fluid Dynamics Research* 10.4-6 (Dec. 1992), pp. 199–228. ISSN: 0169-5983. DOI: 10.1016/0169-5983(92)90023-P (cit. on pp. 36, 43).

- [BR10a] Nidheesh Bharadwaj and Christopher J Rutland. “A Large-Eddy Simulation Study of Sub-Grid Two-Phase Interaction in Particle-Laden Flows and Diesel Engine Sprays”. In: *Atomization and Sprays* 20.8 (2010), pp. 673–695. ISSN: 1044-5110. DOI: 10.1615/AtomizSpr.v20.i8.20 (cit. on pp. 41, 42, 52, 58, 68).
- [BR10b] Nidheesh Bharadwaj and Christopher J Rutland. “Droplet-ambient sub-grid interaction modelling in large eddy simulation of diesel sprays”. In: May. Cincimmati, 2010 (cit. on pp. 42, 100).
- [BR99] Jennifer C. Beale and Rolf D Reitz. “Modeling Spray Atomization with the Kelvin-Helmholtz/Rayleigh-Taylor Hybrid Model”. In: *Atomization and Sprays* 9.6 (1999), pp. 623–650 (cit. on p. 101).
- [BS+72] P. R. Brazier-Smith, S. G. Jennings, and J. Latham. “The Interaction of Falling Water Drops: Coalescence”. In: *Proceedings of the Royal Society A: Mathematical, Physical and Engineering Sciences* 326.1566 (Jan. 1972), pp. 393–408. ISSN: 1364-5021. DOI: 10.1098/rspa.1972.0016 (cit. on p. 59).
- [Cha13] Mariany de J. Chavez. “Modelado CFD Euleriano-Lagrangiano del Chorro Diesel y evaluacion de su combinacion con modelos fenomenologicos y unidimensionales.” PhD thesis. Universidad Politecnica de Valencia, 2013, p. 203 (cit. on pp. 29, 34, 47, 101).
- [Che+09] J. Chesnel, J Reveillon, T Menard, M Doring, A Berlemont, and F X Demoulin. “LES of atomization: From the resolved liquid surface to the subgrid scale spray”. In: *ILASS* (2009) (cit. on p. 14).
- [Cla+79] R. A. Clark, J. H. Ferziger, and W. C. Reynolds. “Evaluations of subgrid-scale models using an accurately simulated turbulent flow.” In: *J. Fluid Mechanics* 91 (1979), pp. 1–16 (cit. on p. 37).
- [Cli+78] R Clift, J R Grace, and M E Weber. *Bubbles, Drops and Particles*. Academic Press, 1978, p. 394 (cit. on p. 61).
- [Cor98] D Correas. “Estudio teórico-experimental del chorro libre Diesel isoterma”. PhD thesis. Valencia: E.T.S. Ingenieros Industriales. Universidad Politécnica de Valencia, 1998 (cit. on pp. 54, 99).
- [Cro+88] C.T. Crowe, J.N. Chung, and T.R. Troutt. “Particle mixing in free shear flows”. In: *Progress in Energy and Combustion Science* 14.3 (Jan. 1988), pp. 171–194. ISSN: 03601285. DOI: 10.1016/0360-1285(88)90008-1 (cit. on p. 69).

- [Cum89] L Cummins. “Internal fire”. In: *SAE International* (1989) (cit. on p. 3).
- [Cum93] L Cummins. *Diesel’s Engine*. Carnot press, 1993 (cit. on p. 3).
- [Dal98] B B Dally. “Flow and mixing fields of turbulent bluff-body jets and flames”. In: *Combust. Theory Model.* 2 (1998), pp. 193–219 (cit. on p. 34).
- [Del+05] E Delacourt, B Desmet, and B Besson. “Characterisation of very high pressure diesel sprays using digital imaging techniques”. In: *Fuel* 84.7-8 (May 2005), pp. 859–867. ISSN: 00162361. DOI: 10.1016/j.fuel.2004.12.003 (cit. on p. 24).
- [Des+03] J M Desantes, R Payri, F J Salvador, and J Gimeno. “Measurements of Spray Momentum for the Study of Cavitation in Diesel Injection Nozzles”. In: *SAE paper 2003-01-0703* (2003). DOI: 10.4271/2003-01-0703 (cit. on p. 98).
- [Des+05] J M Desantes, J. V. Pastor, R Payri, and J. M. Pastor. “Experimental characterization of internal nozzle flow and Diesel spray behavior. Part II: Evaporative conditions”. In: *Atomization and Sprays* 15.5 (2005), pp. 517–544. ISSN: 1045-5110. DOI: 10.1615/AtomizSpr.v15.i5.30 (cit. on p. 24).
- [Des+06] J M Desantes, R Payri, F J Salvador, and A Gil. “Development and validation of a theoretical model for diesel spray penetration”. In: *Fuel* 85 (2006), pp. 910–917. ISSN: 0016-2361. DOI: 10.1016/j.fuel.2005.10.023 (cit. on pp. 23, 24, 28).
- [Des+07] J M Desantes, R Payri, José M García-Oliver, and F J Salvador. “A contribution to the understanding of isothermal diesel spray dynamics”. In: *Fuel* 86.7-8 (2007), pp. 1093–1101. ISSN: 0016-2361. DOI: 10.1016/j.fuel.2006.10.011 (cit. on pp. 6, 8, 23, 28, 97, 102, 168).
- [Des+08] J M Desantes, J V Pastor, José M García-Oliver, and J M Pastor. “A 1D model for the description of mixing-controlled reacting diesel sprays”. In: *Combustion and Flame* 156.1 (2008), pp. 234–249. ISSN: 0010-2180. DOI: DOI : 10.1016/j.combustflame.2008.10.008 (cit. on p. 8).

- [Des+10a] A Desportes, M Zellat, G Desoutter, Y Liang, and F Ravet. “Application of the Eulerian-Lagrangian spray atomization (ELSA) model for the Diesel injection simulation”. In: *Conference on Thermo- and Fluid Dynamic Processes in Diesel Engines* (2010) (cit. on p. 183).
- [Des+10b] A Desportes, M Zellat, G Desoutter, D.Abouri, and Y Liang. “Validation and Application of the Eulerian-Lagrangian spray atomization (ELSA) model for the Diesel injection simulation”. In: *SAE Technical* (2010) (cit. on p. 183).
- [Des+12] Suraj S Deshpande, Lakshman Anumolu, and Mario F Trujillo. “Evaluating the performance of the two-phase flow solver interFoam”. In: *Computational Science & Discovery* 5.1 (Nov. 2012), p. 014016. ISSN: 1749-4699. DOI: 10.1088/1749-4699/5/1/014016 (cit. on p. 48).
- [Du+06] J. Du, B. Fix, J. Glimm, X. Jia, X. Li, Li Y., and L. Wu. “A simple package for front tracking.” In: *J. Comp. Phys.* 213 (2006.), pp. 613–628 (cit. on p. 49).
- [Duk80] John K Dukowicz. “A particle-fluid numerical model for liquid sprays”. In: *Journal of Computational Physics* 35.2 (Apr. 1980), pp. 229–253. ISSN: 00219991. DOI: 10.1016/0021-9991(80)90087-X (cit. on pp. 45, 69).
- [Dum08] Christophe Dumouchel. “On the experimental investigation on primary atomization of liquid streams”. In: *Experiments in Fluids* 45.3 (2008), pp. 371–422. ISSN: 0723-4864. DOI: 10.1007/s00348-008-0526-0 (cit. on p. 55).
- [Eis+67] P Eisenklam, S A Arunachlaman, and J A Weston. “Evaporation rates and drag resistances of burning drops”. In: *11th International Symposium on Combustion*. Pittsburgh, 1967, pp. 715–728 (cit. on pp. 61, 62).
- [ET83] S.H. El Tahry. “k-epsilon equation for compressible reciprocating engine flows”. In: *Journal of Energy* 7.4 (July 1983), pp. 345–353. ISSN: 0146-0412. DOI: 10.2514/3.48086 (cit. on p. 33).
- [EW+54] M.M. El Wakil, O.A. Uyehara, and P.S. Myers. “A theoretical investigation of the heating up period of injected fuel drops vaporizing in air”. In: *NACA* (1954), p. 3179 (cit. on p. 66).

- [Fae+95] G.M. Faeth, L.-P. Hsiang, and P.-K. Wu. “Structure and breakup properties of sprays”. In: *International Journal of Multiphase Flow* 21 (1995), pp. 99–127. ISSN: 0301-9322. DOI: 10.1016/0301-9322(95)00059-7 (cit. on p. 68).
- [Fae87] G M Faeth. “Mixing, transport and combustion in sprays”. In: *Prog. Energy and Combust. Sci.* 13 (1987), pp. 293–345 (cit. on pp. 59, 68).
- [Fae96] G M Faeth. “Spray combustion phenomena”. In: *Symposium (International) on Combustion* 26.1 (Jan. 1996), pp. 1593–1612. ISSN: 00820784. DOI: 10.1016/S0082-0784(96)80383-3 (cit. on pp. 54, 55).
- [Fed+99] R.P. Fedkiw, T. Aslam, B. Merriman, and S. Osher. “A non-oscillatory Eulerian approach to interfaces in multimaterial flows (the Ghost Fluid Method).” In: *J. Comput. Phys.* 152 (1999), pp. 457–492 (cit. on p. 49).
- [FM01] Zhi-Gang Feng and Efsthios E. Michaelides. “Drag Coefficients of Viscous Spheres at Intermediate and High Reynolds Numbers”. In: *Journal of Fluids Engineering* 123.4 (2001), p. 841. ISSN: 00982202. DOI: 10.1115/1.1412458 (cit. on p. 61).
- [Fuj+09] Hajime Fujimoto, Tsukasa Hori, and Jiro Senda. *Effect of Breakup Model on Diesel Spray Structure Simulated by Large Eddy Simulation*. Tech. rep. Sept. 2009. DOI: 10.4271/2009-24-0024 (cit. on pp. 44, 171).
- [Gav+96] M Gavaises, A Theodorakakos, G Bergeles, and G Brenn. “Evaluation of the effect of droplet collisions on spray mixing”. In: *ARCHIVE: Proceedings of the Institution of Mechanical Engineers, Part C: Journal of Mechanical Engineering Science 1989-1996 (vols 203-210)* 210.53 (June 1996), pp. 465–475. ISSN: 0954-4062. DOI: 10.1243/PIME\PROC\1996\210\220\02 (cit. on p. 59).
- [GC89] R.A. Gore and C.T. Crowe. “Effect of particle size on modulating turbulent intensity.” In: *Int. J. Multiphase Flow* 15 (1989), pp. 279–285. DOI: 10.1016/0301-9322(89)90076-1 (cit. on p. 68).

- [GC97] A D Gosman and D Clerides. “Diesel Spray Modelling: A Review”. In: *Proceedings of ILASS-Europe*. Florence, Italy, 1997. DOI: 10.1.1.45.6492 (cit. on p. 59).
- [Ger+91] Massimo Germano, Ugo Piomelli, Parviz Moin, and William H. Cabot. “A dynamic subgrid-scale eddy viscosity model”. In: *Physics of Fluids A: Fluid Dynamics* 3.7 (1991), p. 1760. ISSN: 08998213. DOI: 10.1063/1.857955 (cit. on pp. 37, 41).
- [GI83] A D Gosman and E Ioannides. “Aspects of computer simulation of liquid-fueled combustors”. In: *Journal Energy* (1983) (cit. on p. 70).
- [Gim08] J Gimeno. “Desarrollo y aplicación de la Medida del flujo de cantidad de movimiento de un chorro Diesel.” PhD thesis. Universidad Politécnica de Valencia, 2008 (cit. on pp. 50, 92, 93).
- [GO06] José M García-Oliver. *El proceso de combustión turbulenta de chorros diesel de inyección directa*. Editorial Reverté, S.A., 2006, p. 336. ISBN: 8429147098 (cit. on pp. 27, 64).
- [Gra+12] V Granet, O. Vermorel, C. Lacour, B. Enaux, V. Dugué, and T. Poinso. “Large-Eddy Simulation and experimental study of cycle-to-cycle variations of stable and unstable operating points in a spark ignition engine”. In: *Combustion and Flame* 159.4 (Apr. 2012), pp. 1562–1575. ISSN: 00102180. DOI: 10.1016/j.combustflame.2011.11.018 (cit. on p. 43).
- [HA90] H Hiroyasu and M Arai. “Structures of Fuel Sprays in Diesel Engines”. In: *SAE Technical Paper* (1990), p. 900475 (cit. on p. 23).
- [Hey88] J B Heywood. *Internal combustion engine fundamentals*. McGraw-Hill, Inc., 1988. ISBN: 0-07-028637-X (cit. on pp. 5, 21, 45).
- [HF92a] L-P Hsiang and G M Faeth. “Near-limit drop deformation and secondary breakup”. In: *International Journal of Multiphase Flow* 18.5 (Sept. 1992), pp. 635–652. ISSN: 03019322. DOI: 10.1016/0301-9322(92)90036-G (cit. on pp. 56, 61).
- [HF92b] L.-P. Hsiang and G.M. Faeth. “Near-limit drop deformation and secondary breakup”. In: *International Journal of Multiphase Flow* 18.5 (Sept. 1992), pp. 635–652. ISSN: 03019322. DOI: 10.1016/0301-9322(92)90036-G (cit. on p. 62).

- [HG91] K Y Huh and A D Gosman. “A phenomenological model of diesel sprays atomization”. In: *Proceedings of the International Conference on Multiphase Flows*. Tsukuba, Japan, 1991 (cit. on p. 56).
- [Hil72] B. J. Hill. “Measurement of local entrainment rate in the initial region of axisymmetric turbulent air jets”. In: *Journal of Fluid Mechanics* 51.04 (Mar. 1972), pp. 773–779. ISSN: 0022-1120. DOI: 10.1017/S0022112072001351 (cit. on p. 27).
- [Hin75] JO Hinze. *Turbulence*. McGraw-Hill, Inc., 1975. ISBN: 0-07-029037-7 (cit. on p. 28).
- [Hir+83] H Hiroyasu, T Kadota, and M Arai. “Development and use of spray combustion modelling to predict Diesel engine efficiency and pollutant emission”. In: *Bull. JSME* 26.214 (1983), pp. 569–575 (cit. on p. 21).
- [Hir91] H Hiroyasu. “Experimental and Theoretical studies on the structure of fuel sprays in Diesel engines”. In: *Proceedings of ICLASS-91*. Gaithersburg, MD, U.S.A, 1991 (cit. on p. 64).
- [HJ06] Sergio Hoyas and Javier Jiménez. “Scaling of the velocity fluctuations in turbulent channels up to $Re_{\tau}=2003$ ”. In: *Physics of Fluids* 18.1 (2006), p. 011702. ISSN: 10706631. DOI: 10.1063/1.2162185 (cit. on p. 31).
- [HM01] Donghee Han and M.G Mungal. “Direct measurement of entrainment in reacting/nonreacting turbulent jets”. In: *Combustion and Flame* 124.3 (Feb. 2001), pp. 370–386. ISSN: 00102180. DOI: 10.1016/S0010-2180(00)00211-X (cit. on p. 27).
- [HN81] C.W Hirt and B.D Nichols. “Volume of fluid (VOF) method for the dynamics of free boundaries”. In: *Journal of Computational Physics* 39.1 (Jan. 1981), pp. 201–225. ISSN: 00219991. DOI: 10.1016/0021-9991(81)90145-5 (cit. on p. 48).
- [HO99] Philip G. Hill and Patric Ouellette. “Transient Turbulent Gaseous Fuel Jets for Diesel Engines”. In: *Journal of Fluids Engineering* 121.1 (1999), p. 93. ISSN: 00982202. DOI: 10.1115/1.2822018 (cit. on p. 27).
- [Hor+06] Tsukasa Hori, Jiro Senda, Takahiro Kuge, and H. Gen Fujimoto. *Large Eddy Simulation of Non-Evaporative and Evaporative Diesel Spray in Constant Volume Vessel by Use of KIVALES*. Tech. rep. Oct. 2006. DOI: 10.4271/2006-01-3334 (cit. on pp. 44, 58).

- [Hor+07] Tsukasa Hori, Takahiro Kuge, Jiro Senda, and Hajime Fujimoto. *Large Eddy Simulation of Diesel Spray Combustion with Eddy-Dissipation Model and CIP Method by Use of KIVALES*. Tech. rep. Apr. 2007. DOI: 10.4271/2007-01-0247 (cit. on p. 44).
- [Hor+08] Tsukasa Hori, Takahiro Kuge, Jiro Senda, and Hajime Fujimoto. *Effect of Convective Schemes on LES of Fuel Spray by Use of KIVALES*. Tech. rep. Apr. 2008. DOI: 10.4271/2008-01-0930 (cit. on p. 44).
- [Hor93] Kiyosi Horiuti. “A proper velocity scale for modeling subgrid-scale eddy viscosities in large eddy simulation”. In: *Physics of Fluids A: Fluid Dynamics* 5.1 (1993), p. 146. ISSN: 08998213. DOI: 10.1063/1.858800 (cit. on p. 37).
- [Hoy+13] Sergio Hoyas, Antonio Gil, Xandra Margot, Dung Khuong-Anh, and Frederic Ravet. “Evaluation of the Eulerian-Lagrangian Spray Atomization (ELSA) model in spray simulations: 2D cases”. In: *Mathematical and Computer Modelling* 57.7-8 (Apr. 2013), pp. 1686–1693. ISSN: 08957177. DOI: 10.1016/j.mcm.2011.11.006 (cit. on p. 183).
- [HS06] Shuhai Hou and David P. Schmidt. “Adaptive collision meshing and satellite droplet formation in spray simulations”. In: *International Journal of Multiphase Flow* 32.8 (Aug. 2006), pp. 935–956. ISSN: 03019322. DOI: 10.1016/j.ijmultiphaseflow.2006.02.013 (cit. on p. 59).
- [Hu+07] B. Hu, R. Jhavar, S. Singh, and R. Reitz. “Combustion Modeling of Diesel Combustion with Partially Premixed Conditions”. In: *SAE Technical Paper* 01 (2007), p. 0163. DOI: doi:10.4271/2007-01-0163 (cit. on p. 44).
- [Ina+04] T. Inamuro, T. Ogata, S. Tajima, and N. Konishi. “A Lattice Boltzmann method for incompressible two-phase flows with large density differences”. In: *Journal of Computational Physics* 198 (2004), pp. 628–644 (cit. on p. 49).
- [Ing56] R.D. Ingebo. *Drag Coefficients for Droplets and Solid Spheres in Clouds Accelerating in Airstreams*. Tech. rep. National Advisory Committee for Aeronautics, Technical Note 3762, 1956 (cit. on p. 61).

- [Ish75] M. Ishii. *Thermo-Fluid Dynamic Theory*. Paris: Editorial Eyrolles, 1975 (cit. on p. 48).
- [Jim03] Javier Jiménez. “Computing high-Reynolds-number turbulence: will simulations ever replace experiments?” In: *Journal of Turbulence* 4.022 (June 2003). ISSN: 1468-5248. DOI: 10.1088/1468-5248/4/1/022 (cit. on p. 31).
- [JL10] W P Jones and C Lettieri. “Large eddy simulation of spray atomization with stochastic modeling of breakup”. In: *Physics of Fluids* 22.11 (2010), p. 115106. ISSN: 10706631. DOI: 10.1063/1.3508353 (cit. on pp. 14, 58).
- [Joe+08] T. Joelsson, R. Yu, X. S. Bai, A. Vressner, and 2008. Johansson B. 2008-01-1668. “Large eddy simulation and experiments of the auto-ignition process of lean ethanol/air mixture in HCCI engines.” In: *SAE paper* 01 (2008), p. 1668 (cit. on p. 44).
- [Jon+10] W P Jones, S. Lyra, and A.J. Marquis. “Large Eddy Simulation of evaporating kerosene and acetone sprays”. In: *International Journal of Heat and Mass Transfer* 53.11-12 (May 2010), pp. 2491–2505. ISSN: 00179310. DOI: 10.1016/j.ijheatmasstransfer.2010.01.028 (cit. on p. 37).
- [JP82] J Janicka and N Peters. “Prediction of turbulent jet diffusion flame lift-off using a PDF transport equation”. In: *Symposium International on Combustion* 19 (1982), pp. 367–374 (cit. on p. 34).
- [JR06] R. Jhavar and C. Rutland. “Using Large Eddy Simulations to Study Mixing Effects in Early Injection Diesel Engine Combustion”. In: *SAE Technical Paper* 01 (2006), p. 0871. DOI: doi:10.4271/2006-01-0871 (cit. on p. 44).
- [Kaa+03] Ossi Kaario, H Pokela, L Kjaldman, J Tiainen, and Martti Larmi. “LES and RNG turbulence modeling in DI diesel engines.” In: *SAE paper 2003-01-1069* (2003) (cit. on p. 44).
- [Kas+09] Alan L. Kastengren, Christopher F. Powell, Yujie Wang, Kyoung-Su Im, and Jin Wang. “X-ray radiography measurements of diesel spray structure at engine-like ambient density”. In: *Atomization and Sprays* 19.11 (2009), pp. 1031–1044. DOI: 10.1615/AtomizSpr.v19.i11.30 (cit. on p. 25).

- [KB88] T Kamimoto and MH Bae. “High combustion temperature for the reduction of particulate in diesel engines”. In: *SAE Technical Paper 880423* (1988). DOI: 10.4271/880423. (cit. on p. 5).
- [Kem07] Andreas M. Kempf. “LES Validation from Experiments”. In: *Flow, Turbulence and Combustion* 80.3 (Dec. 2007), pp. 351–373. ISSN: 1386-6184. DOI: 10.1007/s10494-007-9128-9 (cit. on pp. 10, 35).
- [KM95] Won-Wook Kim and Suresh Menon. “A new dynamic one-equation subgrid-scale model for large eddy simulations”. In: *33rd Aerospace Sciences Meeting and Exhibit*. Reston, Virginia: American Institute of Aeronautics and Astronautics, Jan. 1995. DOI: 10.2514/6.1995-356 (cit. on p. 40).
- [Kon+99] S. C. Kong, P. K. Senecal, and Rolf D Reitz. “Developments in Spray Modeling in Diesel and Direct-Injection Gasoline Engines”. In: *Oil & Gas Science and Technology* 54.2 (Mar. 1999), pp. 197–204. ISSN: 1294-4475. DOI: 10.2516/ogst:1999015 (cit. on p. 57).
- [Kra95] Cedimir Kralj. “Numerical Simulation Of Diesel Spray Processes”. PhD thesis. Imperial College, 1995 (cit. on p. 65).
- [Leb+09] R Lebas, T Menard, P.A. Beau, A Berlemont, and F.X. Demoulin. “Numerical simulation of primary break-up and atomization: DNS and modelling study”. In: *International Journal of Multiphase Flow* 35.3 (Mar. 2009), pp. 247–260. ISSN: 03019322. DOI: 10.1016/j.ijmultiphaseflow.2008.11.005 (cit. on pp. 32, 33).
- [Lef89] A H Lefebvre. *Atomization and Sprays*. Hemisphere Publishing Corporation, 1989. ISBN: 0-89116-603-3 (cit. on pp. 24, 51, 53, 62, 63).
- [Lip+05] Andreas M Lippert, Shengming Chang, Sasanka Are, and David P. Schmidt. *Mesh Independence and Adaptive Mesh Refinement For Advanced Engine Spray Simulations*. Tech. rep. Apr. 2005. DOI: 10.4271/2005-01-0207 (cit. on p. 20).
- [Liu+93] Alex B. Liu, Daniel Mather, and Rolf D Reitz. *Modeling the Effects of Drop Drag and Breakup on Fuel Sprays*. Tech. rep. Mar. 1993. DOI: 10.4271/930072 (cit. on pp. 61, 62).

- [Lop05] J J Lopez. *Estudio teórico-experimental del chorro libre diesel no evaporativo y de su interacción con el movimiento del aire*. Reverté, S.A., 2005, p. 378. ISBN: 8429147039 (cit. on p. 27).
- [LS74] B E Launder and D B Spalding. “The numerical computation of turbulent flows”. In: *Computer Methods in Applied Mechanics and Engineering* 3.2 (1974), pp. 269–289. ISSN: 0045-7825. DOI: DOI:10.1016/0045-7825(74)90029-2 (cit. on p. 33).
- [M+06] T. Ménard, P. A. Beau, S. Tanguy, F. X. Demoulin, and A. Berlemont. “Numerical Jet Atomization: Part I â DNS Simulation of Primary Break Up”. In: *Volume 1: Symposia, Parts A and B*. Vol. 2006. ASME, 2006, pp. 547–554. ISBN: 0-7918-4750-0. DOI: 10.1115/FEDSM2006-98165 (cit. on p. 32).
- [Mar+10] Lionel Martinez, Adlene Benkenida, and Benedicte Cuenot. “A model for the injection boundary conditions in the context of 3D simulation of Diesel Spray: Methodology and validation”. In: *Fuel* 89.1 (2010), pp. 219–228. ISSN: 0016-2361. DOI: 10.1016/j.fuel.2009.06.012 (cit. on p. 46).
- [ME51] R. A. Mugele and H. D. Evans. “Droplet Size Distribution in Sprays”. In: *Industrial & Engineering Chemistry* 43.6 (June 1951), pp. 1317–1324. ISSN: 0019-7866. DOI: 10.1021/ie50498a023 (cit. on p. 30).
- [Mon+11] A Montorfano, F Piscaglia, and G Ferrari. “Inlet boundary conditions for incompressible LES: A comparative study”. In: *Mathematical and Computer Modelling* (2011). DOI: 10.1016/j.mcm.2011.10.077 (cit. on p. 135).
- [Mor11] J de la Morena. “Estudio de la influencia de las caractersticas del flujo interno en toberas sobre el proceso de inyección Diesel en el campo próximo”. PhD thesis. Universidad Politécnica de Valencia, 2011 (cit. on p. 50).
- [MR07] A Munnannur and Rolf D Reitz. “Droplet Collision Modeling in Multi-Dimensional Spray Computations”. In: *International Multidimensional Engine Modeling User’s Group Meeting at the SAE Congress*. Detroit, MI, 2007 (cit. on p. 59).
- [NA00] A Nishimura and Dennis N Assanis. “A Model for Primary Diesel Fuel Atomization Based on Cavitation Bubble Collapse Energy”. In: *ILASS*. 2000 (cit. on p. 56).

- [Nin07] Wei Ning. “Development of a Next-generation Spray and Atomization Model Using an Eulerian-Lagrangian Methodology”. PhD thesis. University of Wisconsin-Madison, 2007 (cit. on pp. 34, 49).
- [NS80] T Newcomb and R Spurr. *A Technical history of the motorcar*. 1980 (cit. on p. 3).
- [NS96] J D Naber and Dennis L Siebers. “Effects of gas density and vaporization on penetration and dispersion of Diesel sprays”. In: *SAE paper 960034* (1996) (cit. on pp. 24, 25).
- [NT39] S Nukiyama and Y Tanasawa. “Experiments on the atomization of liquids in an air stream, Report 3, On the droplet size distribution in an atomized jet”. In: *Trans. Soc. Mech. Eng. Jpn.* 5.18 (1939), pp. 62–67 (cit. on p. 51).
- [OA87] Peter J O’Rourke and Anthony A Amsden. *The Tab Method for Numerical Calculation of Spray Droplet Breakup*. Tech. rep. Nov. 1987. DOI: 10.4271/872089 (cit. on p. 56).
- [OB80] Peter J O’Rourke and F V Bracco. “Modeling of drop interactions in thick sprays and a comparison with experiments”. In: *Proceedings of the Institution of Mechanical Engineers* 9 (1980), pp. 101–106 (cit. on pp. 59, 61, 62).
- [Obe91] F Obermeier. *Modeling of nozzle flow*. 1991 (cit. on p. 51).
- [PA02] Scott L Post and John Abraham. “Modeling the outcome of drop-drop collisions in Diesel sprays”. In: *International Journal of Multiphase Flow* 28.6 (June 2002), pp. 997–1019. ISSN: 03019322. DOI: 10.1016/S0301-9322(02)00007-1 (cit. on p. 59).
- [Par+08] Su Han Park, Hyun Kyu Suh, and Chang Sik Lee. “Effect of Cavitating Flow on the Flow and Fuel Atomization Characteristics of Biodiesel and Diesel Fuels”. In: *Energy & Fuels* 22.1 (2008), pp. 605–613. DOI: 10.1021/ef7003305 (cit. on pp. 50, 51).
- [Pas+00] J V Pastor, Emilio Encabo, and Santiago Ruiz. *New Modelling Approach For Fast Online Calculations In Sprays*. Tech. rep. Mar. 2000. DOI: 10.4271/2000-01-0287 (cit. on p. 28).
- [Pas+08] J M Pastor, J J Lopez, and José M García-Oliver. “A 1D model for the description of mixing-controlled inert diesel sprays”. In: *Fuel* 87.13-14 (2008), pp. 2871–2885. ISSN: 0016-2361. DOI: 10.1016/j.fuel.2008.04.017 (cit. on pp. 8, 11, 21).

- [Pas+12] JV Pastor, R. Payri, and Nerva JG Garcia-Oliver JM and. “Schlieren Measurements of the ECN-Spray A Penetration under Inert and Reacting Conditions.” In: *SAE Technical Paper* 01 (2012), p. 0456 (cit. on p. 173).
- [Pay+05] R. Payri, García J., Salvador F., and J. Gimeno. “Using spray momentum flux measurements to understand the influence of diesel nozzle geometry on spray characteristics”. In: *Fuel* 84.5 (Mar. 2005), pp. 551–561. ISSN: 00162361. DOI: 10.1016/j.fuel.2004.10.009 (cit. on pp. 93, 98).
- [Pay+08a] R Payri, F J Salvador, J Gimeno, and G Bracho. “A New Methodology For Correcting The Signal Cumulative Phenomenon On Injection Rate Measurements”. In: *Experimental Techniques* 32.1 (2008), pp. 46–49. ISSN: 1747-1567. DOI: 10.1111/j.1747-1567.2007.00188.x (cit. on pp. 92–94, 100).
- [Pay+08b] R Payri, F J Salvador, J Gimeno, and J de la Morena. *Macroscopic Behavior of Diesel Sprays in the Near-Nozzle Field*. Tech. rep. 1. Apr. 2008, pp. 528–536. DOI: 10.4271/2008-01-0929 (cit. on p. 24).
- [Pay+08c] R Payri, B Tormos, F J Salvador, and L Araneo. “Spray droplet velocity characterization for convergent nozzles with three different diameters”. In: *Fuel* 87.15-16 (Nov. 2008), pp. 3176–3182. ISSN: 00162361. DOI: 10.1016/j.fuel.2008.05.028 (cit. on pp. 25, 168).
- [PD11] F Payri and J M Desantes. *Motores de combustión interna alternativos*. Ed. by F Payri and J.M. Desantes. Ed. Reverté, 2011, p. 1002. ISBN: 978-84-291-4802-2 (cit. on p. 3).
- [Pic+13] Lyle M. Pickett, Julien Manin, Raul Payri, Michele Bardi, and J Gimeno. *Transient Rate of Injection Effects on Spray Development*. Tech. rep. Sept. 2013. DOI: 10.4271/2013-24-0001 (cit. on pp. 93, 107).
- [PM96] U Petersen and S A MacGregor. “Jet mixing in a model direct injection Diesel engine with swirl”. In: *Journal of Mechanical Engineering Science, IME C07394* 210 (1996), pp. 69–78 (cit. on p. 28).
- [Pop00] S Pope. *Turbulent Flows*. Cambridge University Press, 2000, p. 771. ISBN: 978-0-521-59886-6 (cit. on pp. 7, 12, 21, 26, 33, 36).

- [PR02] Eric Pomraning and Christopher J Rutland. “Dynamic One-Equation Nonviscosity Large-Eddy Simulation Model”. In: *AIAA* 40.4 (2002) (cit. on pp. 41, 92).
- [QL97] J. Qian and C. K. Law. “Regimes of coalescence and separation in droplet collision”. In: *Journal of Fluid Mechanics* 331 (Jan. 1997), pp. 59–80. ISSN: 00221120. DOI: 10.1017/S0022112096003722 (cit. on p. 59).
- [Ran58] W E Ranz. “Some experiments on orifice sprays”. In: *The Canadian Journal of Chemical Engineering* (Aug. 1958), pp. 175–181 (cit. on p. 24).
- [Ray78] Lord Rayleigh. “On The Instability Of Jets”. In: *Proceedings of the London Mathematical Society* s1-10.1 (Nov. 1878), pp. 4–13. ISSN: 0024-6115. DOI: 10.1112/plms/s1-10.1.4 (cit. on p. 53).
- [RB79] Rolf D Reitz and F. B. Bracco. *On the Dependence of Spray Angle and Other Spray Parameters on Nozzle Design and Operating Conditions*. Tech. rep. Feb. 1979. DOI: 10.4271/790494 (cit. on p. 24).
- [RB82] Rolf D Reitz and F. B. Bracco. “Mechanism of atomization of a liquid jet”. In: *Physics of Fluids* 25.10 (1982), p. 1730. ISSN: 00319171. DOI: 10.1063/1.863650 (cit. on pp. 53, 54).
- [RD87] Rolf D Reitz and Ramachandra Diwakar. “Structure of High-Pressure Fuel Sprays”. In: *SAE Technical Paper 870598* 96 (1987), pp. 492–509. DOI: 10.4271/870598 (cit. on pp. 56, 57, 101, 102).
- [Rei87] Rolf D Reitz. “Modeling atomization processes in high-pressure vaporizing sprays.” In: *Atomization and Spray Technology* 3.4 (1987), pp. 309–337 (cit. on pp. 56, 61).
- [RI00] Henrik Rusche and R I Issa. “The Effect of Void age on the Drag Force on Particles, Droplets and Bubbles in Dispersed Two-Phase Flow.” In: *Japanese European Two-Phase Flow Meeting*. Tshkuba, Japan, 2000 (cit. on pp. 61, 62).
- [RM52] W.E. Ranz and W.R. Marshal. “Evaporation from drops”. In: *Chem. Eng. Prog.* 3 (1952), pp. 141–146 (cit. on pp. 65, 66).
- [RR33] P Rosin and E Rammler. “The laws governing the fineness of powdered coal”. In: *J. Inst. Fuel* 7.31 (1933), pp. 29–36 (cit. on p. 51).

- [RS61] F. P. Ricou and D. B. Spalding. “Measurements of entrainment by axisymmetrical turbulent jets”. In: *Journal of Fluid Mechanics* 11.1 (1961), pp. 21–32. ISSN: 0022-1120. DOI: 10.1017/S0022112061000834 (cit. on p. 27).
- [Run+03] T. Rung, U. Bunge, M. Schatz, and F. Thiele. “Restatement of the Spalart-Allmaras Eddy-Viscosity Model in Strain-Adaptive Formulation”. In: *AIAA Journal* 41.7 (July 2003), pp. 1396–1399. ISSN: 0001-1452. DOI: 10.2514/2.2089 (cit. on p. 39).
- [Rut11] Christopher J Rutland. “Large-eddy simulations for internal combustion engines - a review”. In: *International Journal of Engine Research* 12.5 (Aug. 2011), pp. 421–451. ISSN: 1468-0874. DOI: 10.1177/1468087411407248 (cit. on pp. 9, 35, 36).
- [SA10] Sibendu Som and Suresh K Aggarwal. “Effects of primary breakup modeling on spray and combustion characteristics of compression ignition engines”. In: *Combustion and Flame* 157.6 (June 2010), pp. 1179–1193. ISSN: 00102180. DOI: 10.1016/j.combustflame.2010.02.018 (cit. on pp. 56, 101).
- [SA94] P R Spalart and S R Almaras. “A one-equation turbulence model for aerodynamic flows”. In: *Recherche aerospatiale* 1 (1994), pp. 5–21 (cit. on pp. 38, 39).
- [SAE97] SAE. *The automobile. A century of progress*. 1997 (cit. on p. 3).
- [Saf+10] Khadidja Safer, Abdelhamid Bounif, Mériem Safer, and Iskender Gökalp. “Free Turbulent Reacting Jet Simulation Based on Combination of Transport Equations and PDF”. In: *Engineering Applications of Computational Fluid Mechanics* 4.2 (2010), pp. 246–259 (cit. on p. 33).
- [Sal03] F J Salvador. “Estudio teorico experimental de la influencia de la geometria de toberas de inyeccion Diesel sobre las caracteristicas del flujo interno y del chorro.” PhD thesis. Universidad Politécnica de Valencia, 2003 (cit. on p. 50).
- [San+99] K. Sankaranarayanan, X. Shan, Kevrekidis I. G., and S. Sundaresan. “Bubble flow simulations with the Lattice Boltzmann method”. In: *Chemical Engineering Science* 54 (1999), pp. 4817–4823 (cit. on p. 49).

- [Sch07] François G. Schmitt. “About Boussinesq’s turbulent viscosity hypothesis: historical remarks and a direct evaluation of its validity”. In: *Comptes Rendus Mécanique* 335.9-10 (Sept. 2007), pp. 617–627. ISSN: 16310721. DOI: 10.1016/j.crme.2007.08.004 (cit. on p. 33).
- [Sco+93] Alberto Scotti, Charles Meneveau, and Douglas K. Lilly. “Generalized Smagorinsky model for anisotropic grids”. In: *Physics of Fluids A: Fluid Dynamics* 5.9 (1993), p. 2306. ISSN: 08998213. DOI: 10.1063/1.858537 (cit. on p. 37).
- [Sen+13a] P. K. Senecal, E. Pomraning, K. J. Richards, and Sibendu Som. *An Investigation of Grid Convergence for Spray Simulations using an LES Turbulence Model*. Tech. rep. Apr. 2013. DOI: 10.4271/2013-01-1083 (cit. on pp. 44, 58).
- [Sen+13b] P. K. Senecal, Eric Pomraning, K. J. Richards, and Sibendu Som. “Grid-Convergent Spray Models for Internal Combustion Engine Computational Fluid Dynamics Simulations”. In: *Journal of Energy Resources Technology* 136.1 (Sept. 2013), p. 012204. ISSN: 0195-0738. DOI: 10.1115/1.4024861 (cit. on p. 47).
- [Sen+13c] Peter K. Senecal, Eric Pomraning, Q Xue, Sibendu Som, Shid-dhartha Banerjee, B Hu, K Liu, and J M Deur. “Large eddy simulation of vaporizing sprays considering multi- injection averaging and grid-convergent mesh resolution”. In: *Proceedings of the ASME 2013 Internal Combustion Engine Division Fall Technical Conference (2013)* (cit. on p. 58).
- [Set99] J. A. Sethian. *Level set methods and fast marching methods*. second ed. Cambridge, U.K: Cambridge University Press, 1999. ISBN: 9780521645577 (cit. on p. 48).
- [Sho+07] Babak Shotorban, K.K.Q. Zhang, and Farzad Mashayek. “Improvement of particle concentration prediction in large-eddy simulation by defiltering”. In: *International Journal of Heat and Mass Transfer* 50.19-20 (Sept. 2007), pp. 3728–3739. ISSN: 00179310. DOI: 10.1016/j.ijheatmasstransfer.2007.02.033 (cit. on p. 42).
- [Sie99] Dennis L Siebers. “Scaling Liquid-Phase Fuel Penetration in Diesel Sprays Based on Mixing-Limited Vaporization”. In: *SAE paper 1999-01-0528* (Mar. 1999). DOI: 10.4271/1999-01-0528 (cit. on p. 64).

- [Sir99] W A Sirignano. *Fluid Dynamics and Transport of Droplets and Sprays*. Cambridge University Press, 1999 (cit. on pp. 61, 64).
- [Sma63] J Smagorinsky. “General circulation experiments with the primitive equations”. In: *Monthly Weather Review* 91.3 (1963), pp. 99–164. DOI: 10.1175/1520-0493(1963)091<0099:GCEWTP>2.3.CO;2 (cit. on p. 36).
- [Som+12] Sibendu Som, Douglas E. Longman, Zhaoyu Luo, Max Plomer, Tianfeng Lu, Peter K. Senecal, and Eric Pomraning. “Simulating Flame Lift-Off Characteristics of Diesel and Biodiesel Fuels Using Detailed Chemical-Kinetic Mechanisms and Large Eddy Simulation Turbulence Model”. In: *Journal of Energy Resources Technology* 134.3 (2012), p. 032204. ISSN: 01950738. DOI: 10.1115/1.4007216 (cit. on p. 44).
- [SP00] Mark Sussman and Elbridge Gerry Puckett. “A Coupled Level Set and Volume-of-Fluid Method for Computing 3D and Axisymmetric Incompressible Two-Phase Flows”. In: *Journal of Computational Physics* 162.2 (2000), pp. 301–337. ISSN: 0021-9991. DOI: 10.1006/jcph.2000.6537 (cit. on p. 48).
- [SR00] David P Schmidt and Christopher J Rutland. “A New Droplet Collision Algorithm”. In: *Journal of Computational Physics* 164.1 (2000), pp. 62–80. ISSN: 0021-9991. DOI: 10.1006/jcph.2000.6568 (cit. on pp. 47, 102).
- [SS03] J. A. Sethian and Peter Smereka. “Level set methods for fluid interfaces”. In: *Annual Review of Fluid Mechanics* 35.1 (Jan. 2003), pp. 341–372. ISSN: 0066-4189. DOI: 10.1146/annurev.fluid.35.101101.161105 (cit. on p. 48).
- [Sti03] Gunnar Stiesch. *Modeling Engine Spray and Combustion Processes*. Heat and Mass Transfer. Berlin, Heidelberg: Springer Berlin Heidelberg, 2003, p. 282. ISBN: 978-3-642-05629-1. DOI: 10.1007/978-3-662-08790-9 (cit. on pp. 46, 47, 56).
- [Su+96] T. F. Su, M. A. Patterson, Rolf D Reitz, and P. V. Farrell. *Experimental and Numerical Studies of High Pressure Multiple Injection Sprays*. Tech. rep. Feb. 1996. DOI: 10.4271/960861 (cit. on p. 58).
- [Suz97] T Suzuki. *The romance of engines*. 1997 (cit. on p. 3).

- [Tak+00] N. Takada, M. Misawa, A. Tomiyama, and Fujiwara. “Numerical simulation of two- and three-dimensional two-phase fluid motion by Lattice Boltzmann method”. In: *Computer Physics Communications* 129 (2000), pp. 233–246 (cit. on p. 49).
- [Tay50] G I Taylor. “The Instability of Liquid Surfaces when Accelerated in a Direction Perpendicular to their Planes. I”. In: *Proceedings of the Royal Society A: Mathematical, Physical and Engineering Sciences* 201.1065 (Mar. 1950), pp. 192–196. ISSN: 1364-5021. DOI: 10.1098/rspa.1950.0052 (cit. on p. 56).
- [Tay63] G I Taylor. *Generation of ripples by wind blowing over a viscous fluid*. 1963 (cit. on p. 56).
- [Til+13] J. Tillou, J.-B. Michel, C. Angelberger, C. Bekdemir, and D. Veynante. “Large-Eddy Simulation of Diesel Spray Combustion with Exhaust Gas Recirculation”. In: *Oil & Gas Science and Technology à Revue dâIFP Energies nouvelles* (Nov. 2013). ISSN: 1294-4475. DOI: 10.2516/ogst/2013139 (cit. on p. 46).
- [Ton+06] S Tonini, M Gavaises, C Arcoumanis, and A Theodorakakos. *Prediction of Liquid and Vapor Penetration of High Pressure Diesel Sprays*. Tech. rep. Apr. 2006. DOI: 10.4271/2006-01-0242 (cit. on p. 61).
- [Try+01] G. Tryggvason, B. Bunner, A. Esmaceli, D. Juric, N. Al-Rawahi, W. Tauber, J. Han, S. Nas, and Y.J. Jan. “A front tracking method for the computations of multiphase flow.” In: *J. Comp. Phys.* 169 (2001.), pp. 708–759 (cit. on p. 49).
- [Tur00] S.R. Turns. *An introduction to combustion*. McGraw-Hill, 2000 (cit. on p. 67).
- [Val+01] Ariane Vallet, A A Burluka, and R Borghi. “Development of a Eulerian model for the atomization of a liquid jet”. In: *Atomization and sprays* 11 (2001), pp. 619–642 (cit. on p. 49).
- [Vil+04] E de Villiers, A.D. Gosman, and H.G. Weller. “Large Eddy Simulation of Primary Diesel Spray Atomization”. In: *SAE Technical* (Mar. 2004). DOI: 10.4271/2004-01-0100 (cit. on pp. 14, 44, 49).

- [Vit+12] Oldrich Vitek, Jan Macek, Reinhard Tatschl, Zoran Pavlovic, and Peter Priesching. “LES Simulation of Direct Injection SI-Engine In-Cylinder Flow”. In: *SAE Technical Paper 2012-01-0138* (2012). DOI: 10.4271/2012-01-0138 (cit. on pp. 6, 58).
- [VM95] H. K. Versteeg and W. Malalsekera. *An introduction to computational fluid dynamics - the finite volume method*. Longman Scientific and Technical, 1995, p. 267. ISBN: 978-0-13-127498-3 (cit. on pp. 21, 33).
- [Vre+08] A. Vressner, R. Egnell, and B. Johansson. “Combustion chamber geometry effects on the performance of an ethanol fueled HCCI engine”. In: *SAE paper 1* (2008), p. 1656 (cit. on p. 44).
- [Vuj+09] M. Vujanovic, W. Edelbauer, E. von Berg, R. Tatschl, and N. Duic. “Numerical modeling of Diesel sprays with an Eulerian-Eulerian Approach”. In: *9th ERCOFTAC AHS Pilot Centre Meeting*. AVL List GmbH Austria, 2009 (cit. on p. 48).
- [Vuo+08] Ville Vuorinen, Martti Larimi, and Laszlo Fuchs. *Large-Eddy Simulation on the Effect of Droplet Size Distribution on Mixing of Passive Scalar in a Spray*. Tech. rep. Apr. 2008. DOI: 10.4271/2008-01-0933 (cit. on pp. 43, 46).
- [Vuo10] Ville Vuorinen. “LES of certain droplet size effects in fuel sprays”. PhD thesis. Aalto University, 2010 (cit. on pp. 46, 50).
- [Web31] Constantin Weber. “Zum Zerfall eines Flüssigkeitsstrahles (Disintegration of Liquid Jets)”. In: *ZAMM - Zeitschrift für Angewandte Mathematik und Mechanik* 11.2 (1931), pp. 136–154. ISSN: 00442267. DOI: 10.1002/zamm.19310110207 (cit. on p. 53).
- [Wie90] A. Wierzbna. “Deformation and breakup of liquid drops in a gas stream at nearly critical Weber numbers”. In: *Experiments in Fluids* 9.1-2 (1990), pp. 59–64. ISSN: 0723-4864. DOI: 10.1007/BF00575336 (cit. on p. 56).
- [Wil85] F.A. Williams. *Combustion Theory*. Ed. by MA Reading. 2nd Editio. Addison-Wesley Publishing Co., 1985 (cit. on p. 45).
- [Wu+84] K Wu, C C Su, R L Steinberger, D Santavicca, and F V Bracco. “Measurements of the spray angle of atomizing jets”. In: *Journal of fluids engineering* 105.4 (1984), pp. 406–413 (cit. on p. 24).

- [Xue+13] Qingluan Xue, Sibendu Som, Peter Senecal, and Eric Pomraning. “Large Eddy Simulation of Fuel Spray under Non-reacting IC Engine Conditions”. In: *Atomization and Sprays* 23.10 (2013), pp. 925–955. ISSN: 1044-5110. DOI: 10.1615/AtomizSpr.2013008320 (cit. on pp. 43, 47, 50, 58).
- [Yak+89] A. Yakhot, S. A. Orszag, Victor Yakhot, and M. Israeli. “Renormalization group formulation of large-eddy simulations”. In: *Journal of Scientific Computing* 4.2 (June 1989), pp. 139–158. ISSN: 0885-7474. DOI: 10.1007/BF01061499 (cit. on p. 37).
- [Yan+00] Xiaofeng Yang, Yoshihisa Takamoto, and Atsushi Okajima. *Improvement of Three-Dimensional Diesel Spray Modeling in Near Region with Coarse Mesh*. Tech. rep. Mar. 2000. DOI: 10.4271/2000-01-0274 (cit. on p. 47).
- [YC76] M C Yuen and L W Chen. “On Drag of Evaporating Liquid Droplets”. In: *Combustion Science and Technology* 14.4-6 (Oct. 1976), pp. 147–154. ISSN: 0010-2202. DOI: 10.1080/00102207608547524 (cit. on pp. 61, 62).
- [YH85] Akira Yoshizawa and Kiyosi Horiuti. “A Statistically-Derived Subgrid-Scale Kinetic Energy Model for the Large-Eddy Simulation of Turbulent Flows”. In: *Journal of the Physics Society Japan* 54.8 (Aug. 1985), pp. 2834–2839. ISSN: 0031-9015. DOI: 10.1143/JPSJ.54.2834 (cit. on pp. 40, 100).
- [YO86] Victor Yakhot and Steven Orszag. “Renormalization-Group Analysis of Turbulence”. In: *Physical Review Letters* 57.14 (Oct. 1986), pp. 1722–1724. ISSN: 0031-9007. DOI: 10.1103/PhysRevLett.57.1722 (cit. on p. 33).
- [Yu+06] R. Yu, X. S. Bai, H. Lehtiniemi, S. S. Ahmed, F. Mauss, M. Richter, M. Alden, L. Hildings-son, B. Johansson, and A. Hultqvist. “Effect of turbulence and initial temperature inhomogeneity on homogeneous charge compression ignition combustion”. In: *SAE paper* 01 (2006), p. 3318 (cit. on p. 44).
- [Yu+07] R. Yu, X. S. Bai, A. Vressner, A. Hultqvist, B. Johansson, J. Olofsson, H. Seyfried, J. Sjolholm, M. Richter, and M. Alden. “Effect of turbulence on HCCI combustion. 2007- 01-0183”. In: *SAE paper* 01 (2007), p. 0183 (cit. on p. 44).

- [Yu+08] R. Yu, Bai X. S. Joellsson T., and B. Johansson. “Effect of temperature stratification on the auto- ignition of lean ethanol / air mixture in HCCI engine.” In: *SAE paper* 01 (2008), p. 1669 (cit. on p. 44).
- [Yue+01] Yong Yue, Christopher F. Powell, Ramesh Poola, Jinn Wang, and Johannes K. Schaller. “Quantitative measurements of diesel fuel spray characteristics in the near-nozzle region using x-ray absorption”. In: *Atomization and Sprays* 11.4 (2001), pp. 471–490 (cit. on p. 25).
- [Zuo+00] B. Zuo, A. M. Gomes, and C. J. Rutland. “Modelling superheated fuel sprays and vaporization”. In: *International Journal of Engine Research* 1 (2000), pp. 321–336. DOI: 10.1243/1468087001545218 (cit. on p. 64).
- [Fab+08] Fabian Peng Kärrholm, Feng Tao, and P A Niklas Nordin. “Three-Dimensional Simulation of Diesel Spray Ignition and Flame Lift-Off Using OpenFOAM and KIVA-3V CFD Codes.” In: *SAE paper 2008-01-0961* (2008). DOI: 10.4271/2008-01-0961 (cit. on pp. 47, 50).
- [Koj+12] Koji Kitaguchi, Soichi Hatori, Tsukasa Hori, and Jiro Senda. “Optimization of breakup model using LES of diesel spray”. In: *Atomization and Sprays* 22.1 (2012), pp. 57–77 (cit. on pp. 14, 58).
- [Ope10] OpenCFD Limited. *OpenFOAM-The Open-source CFD toolbox*. 2010 (cit. on p. 8).
- [von+99] Christopher von Kuensberg Sarre, Song-Charng Kong, and Rolf D Reitz. *Modeling the Effects of Injector Nozzle Geometry on Diesel Sprays*. Tech. rep. Mar. 1999, pp. 1–14. DOI: 10.4271/1999-01-0912 (cit. on p. 51).